OLFACTORY SUBSYSTEMS IN MAMMALS: MORPHOLOGY, GENETIC AND EVOLUTION

EDITED BY: Ignacio Salazar and Pablo Chamero
PUBLISHED IN: Frontiers in Neuroanatomy

frontiers Research Topics

frontiers

ISSN 1664-8714
ISBN 978-2-88919-554-1
DOI 10.3389/978-2-88919-554-1

About Frontiers

Frontiers is more than just an open-access publisher of scholarly articles: it is a pioneering approach to the world of academia, radically improving the way scholarly research is managed. The grand vision of Frontiers is a world where all people have an equal opportunity to seek, share and generate knowledge. Frontiers provides immediate and permanent online open access to all its publications, but this alone is not enough to realize our grand goals.

Frontiers Journal Series

The Frontiers Journal Series is a multi-tier and interdisciplinary set of open-access, online journals, promising a paradigm shift from the current review, selection and dissemination processes in academic publishing. All Frontiers journals are driven by researchers for researchers; therefore, they constitute a service to the scholarly community. At the same time, the Frontiers Journal Series operates on a revolutionary invention, the tiered publishing system, initially addressing specific communities of scholars, and gradually climbing up to broader public understanding, thus serving the interests of the lay society, too.

Dedication to Quality

Each Frontiers article is a landmark of the highest quality, thanks to genuinely collaborative interactions between authors and review editors, who include some of the world's best academicians. Research must be certified by peers before entering a stream of knowledge that may eventually reach the public - and shape society; therefore, Frontiers only applies the most rigorous and unbiased reviews.
Frontiers revolutionizes research publishing by freely delivering the most outstanding research, evaluated with no bias from both the academic and social point of view.
By applying the most advanced information technologies, Frontiers is catapulting scholarly publishing into a new generation.

What are Frontiers Research Topics?

Frontiers Research Topics are very popular trademarks of the Frontiers Journals Series: they are collections of at least ten articles, all centered on a particular subject. With their unique mix of varied contributions from Original Research to Review Articles, Frontiers Research Topics unify the most influential researchers, the latest key findings and historical advances in a hot research area! Find out more on how to host your own Frontiers Research Topic or contribute to one as an author by contacting the Frontiers Editorial Office: **researchtopics@frontiersin.org**

OLFACTORY SUBSYSTEMS IN MAMMALS: MORPHOLOGY, GENETIC AND EVOLUTION

Topic Editors:
Ignacio Salazar, University of Santiago de Compostela, Spain
Pablo Chamero, University of Saarland, Germany

The nasal cavity and the elements it comprises are lined by mucosa. This mucosa contains olfactory sensory neurons, which are organized into four different territories: main olfactory epithelium, septal organ, vomeronasal epithelium and ganglion of Grünemberg. From a morphological point of view, these territories could initially be considered as isolated olfactory subsystems, which -as a whole or independently- have been addressed in the contributions enclosed in this Topic.

Citation: Salazar, I., Chamero, P., eds. (2015). Olfactory Subsystems in Mammals: Morphology, Genetic and Evolution. Lausanne: Frontiers Media. doi: 10.3389/978-2-88919-554-1

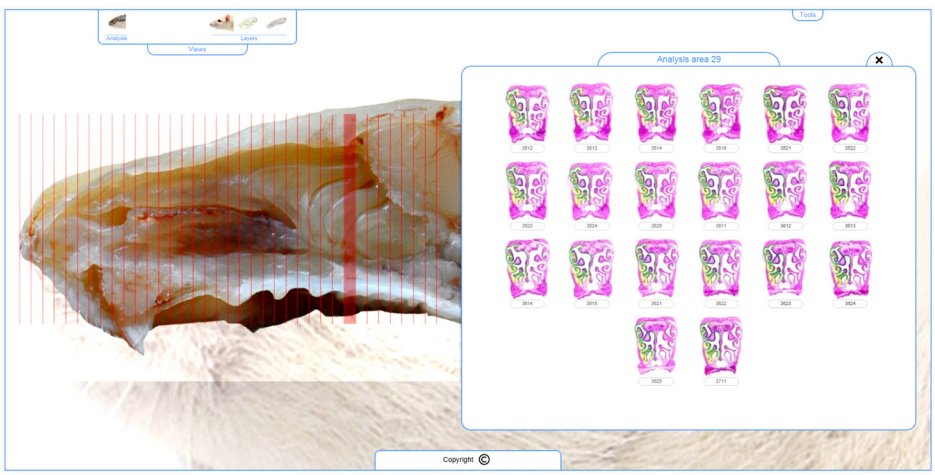

Inside the nasal cavity of mice, the medial view of the nasal conchae and ethmoturbinates are shown after the removal of the nasal septum. The whole nasal cavity is organized in thirty-six transverse segments, one of which is represented on the right side. The presumptive olfactory subsystems can be identified in detail by observing the corresponding sections.
Taken from: Anatomy, histochemistry, and immunohistochemistry of the olfactory subsystems in mice. Front. Neuroanat. doi:10.3389/fnana.2014.00063, Supplementary Material

Table of Contents

04 ***The nasal cavity and its olfactory sensory territories***
Ignacio Salazar

07 ***Possible functional role of olfactory subsystems in monitoring inhalation and exhalation***
Kensaku Mori, Hiroyuki Manabe and Kimiya Narikiyo

10 ***Anatomy, histochemistry, and immunohistochemistry of the olfactory subsystems in mice***
Arthur W. Barrios, Gonzalo Núñez, Pablo Sánchez Quinteiro and Ignacio Salazar

20 ***Dog and mouse: toward a balanced view of the mammalian olfactory system***
Arthur W. Barrios, Pablo Sánchez-Quinteiro and Ignacio Salazar

27 ***Morphological and physiological species-dependent characteristics of the rodent Grueneberg ganglion***
Julien Brechbühl, Magali Klaey, Fabian Moine, Esther Bovay, Nicolas Hurni, Monique Nenniger-Tosato and Marie-Christine Broillet

41 ***Physiological characterization of formyl peptide receptor expressing cells in the mouse vomeronasal organ***
Tobias Ackels, Benoît von der Weid, Ivan Rodriguez and Marc Spehr

54 ***Signaling mechanisms and behavioral function of the mouse basal vomeronasal neuroepithelium***
Anabel Pérez-Gómez, Benjamin Stein, Trese Leinders-Zufall and Pablo Chamero

61 ***Lacrimal gland removal impairs sexual behavior in mice***
Rosa Maria Cavaliere, Filippo Ghirardi and Roberto Tirindelli

68 ***The molecular evolutionary dynamics of the vomeronasal receptor (class 1) genes in primates: a gene family on the verge of a functional breakdown***
Anne D. Yoder and Peter A. Larsen

frontiers in Neuroanatomy

EDITORIAL
published: 18 March 2015
doi: 10.3389/fnana.2015.00031

The nasal cavity and its olfactory sensory territories

Ignacio Salazar *

Unit of Anatomy and Embryology, Department of Anatomy and Animal Production, Faculty of Veterinary, University of Santiago de Compostela, Santiago de Compostela, Spain

Keywords: main olfactory epithelium, vomeronasal epithelium, ganglion of Grüneberg

The sense of smell is more complex than previously believed. For different reasons, the receptors traditionally thought of having the ability to identify chemical olfactory signals were exclusively confined to the epithelium of the mucosa lining both the posterior part of the walls of the nasal cavity and the ethmoturbinates. However, at the end of the nineteenth century, the vomeronasal organ (VNO) was demonstrated to have its own sensory epithelium, able to perform a similar function (Retzius, 1894). In later years, a small and isolated area of olfactory epithelium was detected in the nasal septum (Rodolfo-Masera, 1943); this structure was denominated septal organ. Later evidence showed than a group of cells located on the superior and anterior part of the nasal vestibuli (Grüneberg, 1973) also had a functional role within the olfactory system (Fuss et al., 2005). These findings led to being currently accepted that in certain macrosmatic animals the olfactory sensory receptors are located in four different regions of the nasal cavity: the main olfactory epithelium (MOE), the vomeronasal epithelium (VnE), the septal organ (SO), and the ganglion of Grüneberg (GG). Besides, a subdivision of both the MOE and the VnE can be done into four and two areas respectively. Following a morphological criterion four/eight structures integrate the olfactory subsystems (OSbS) (Breer et al., 2006). However, the axonal projections of those structures onto the olfactory bulb have been observed to show overlapping (Munger et al., 2009), and the concept of OSbS should be limited to the morphological location of the mentioned structures. That point of view has been used in this Research topic.

To begin to understand the sense of smell as a whole in the mammalian class, one of the biggest challenges we are confronted with is to find answers to some basic and critical questions as, for instance: what are exactly the GG, the VNO and the SO, and what are their precise functions? How are the connections between them and how does each of them interact with the MOE? What happens if one or more than one of such structures is absent in a particular species? From an evolutionary perspective, it is reasonable to assume that partial or total response to these questions and others can be found, but it would require having the genome of the species, and a deep knowledge of the morphological characteristics of each structure.

Many recent studies have contributed to the progress in the knowledge of the sense of smell, and one of the most relevant is the work of Buck and Axel (1991), where the authors laid the molecular foundations for odor recognition (see also Axel, 2005; Buck, 2005). Another recent and significant work concerns the implication of the main olfactory subsystem (MOS) in the recognition of pheromonal signals, performed by three different laboratories and published in the same year (Boehm et al., 2005; Mandiyan et al., 2005; Yoon et al., 2005; see also Baum and Larriva-Sahd, 2014). These papers not only demonstrated the important role MOS plays in sexual and aggressive behavior, but also revealed an anatomical projection from the MOE to LHRH neurons in the neuroendocrine hypothalamus, which regulate gonadal hormone release (Keverne, 2005). Such findings have revolutionized our understanding over how the sense of smell controls the neuroendocrine brain. The classical belief that common odors are perceived through the olfactory pathway and pheromones by the VNO is dead. Each pathway must be assessed for a putative pheromone on its own evidence (Shepherd, 2006).

OPEN ACCESS

Edited and reviewed by:
Javier DeFelipe, Cajal Institute, Spain

***Correspondence:**
Ignacio Salazar, ignacio.salazar@usc.es

Received: *17 February 2015*
Accepted: *27 February 2015*
Published: *18 March 2015*

Citation:
Salazar I (2015) The nasal cavity and its olfactory sensory territories. Front. Neuroanat. 9:31. doi: 10.3389/fnana.2015.00031

This Research Topic includes, as an introduction, an interesting opinion article (Mori et al., 2014) where the authors establish a new and appealing relationship between the olfactory perception and the respiratory rhythm, being involved different regions of the central olfactory system like the olfactory bulb and some areas of the olfactory cortex. The morphology of the OSbS as a whole has been addressed by Salazar's group in two articles. The first of them presents an on-line atlas of the murine nasal cavity, freely available at http://www.usc.es/anatembriol/ (Barrios et al., 2014a); in the second, one of the most relevant results points out that the dog lacks two of the olfactory areas of the mouse, the SO and the GG (Barrios et al., 2014b).

The SO, when present, is a small patch of olfactory sensory epithelium forming an island in the respiratory epithelium, near the inferior part of the nasal septum. This organization shows resemblance with the typical distribution of both epithelia in humans (Escada et al., 2009), and is therefore the structure of the OSbS to which less attention is paid, in exact opposition to what occurs with the GG. In a nice paper Brechbühl et al. (2014), using different procedures, show the presence of the GG in the rat, hamster and gerbil, and found that those species had morphological and physiological differences.

Finally, five articles are devoted to various aspects of the VNO. Ackels et al. (2014) study the characterization of the recently discovered formyl peptide receptor family and suggest the use of the transgenic mouse strain model they employed to carry out future research about the subject. A mini review of the basal vomeronasal neuroepithelium is the contribution of Pérez-Gómez et al. (2014). In this work, the authors highlight the critical role of this part of the epithelium in different ranges of instinctive behaviors. Also in mice, as the previous reference, Cavaliere et al. (2014) establish a direct relationship between the orbital glands and the vomeronasal system by means of the detection of the exocrine gland-secreting peptides. The last two contributions deal with the genetic and evolutionary approach. In an elegant paper Hohenbrink et al. (2014) present the expression patterns of vomeronasal receptors of a species of primate, and at the same time demonstrate that a substantial number of such receptors were expressed in the MOE. Therefore, the chemosensory system in primates indicates greater functional overlap between the VNO and MOE, a very interesting finding. The contribution of Yoder and Larsen (2014) is mainly focused on the molecular-evolutionary dynamics of vomeronasal receptor genes1 in primates; the authors review and update this interesting issue, closely related to the goal of the present Research Topic.

References

Ackels, T., von der Weid, B., Rodriguez, I., and Spehr, M. (2014). Physiological characterization of formyl peptide receptor expressing cells in the mouse vomeronasal organ. *Front. Neuroanat.* 8:134. doi: 10.3389/fnana.2014.00134

Axel, R. (2005). Scents and sensibility: a molecular logic of olfactory perception (Nobel lecture). *Angew. Chem. Int. Ed Engl.* 44, 6110–6127. doi: 10.1002/anie.200501726

Barrios, W. A., Nuñez, G., Sánchez-Quinteiro, P., and Salazar, I. (2014a). Anatomy, histochemistry and immunohistochemistry of the olfactory subsystems in mice. *Front. Neuroanat.* 8:63. doi: 10.3389/fnana.2014.00063

Barrios, W. A., Sánchez-Quinteiro, P., and Salazar, I. (2014b). Dog and mouse: Towards a balanced view of the mammalian olfactory system. *Front. Neuroanat.* 8:106. doi: 10.3389/fnana.2014.00106

Baum, M., and Larriva-Sahd, J. A. (2014). Interactions between the mammalian main and accessory olfactory systems. *Front. Neuroanat.* 8:45. doi: 10.3389/fnana.2014.00045

Boehm, U., Zou, Z., and Buck, L. B. (2005). Feedback loops link odor and pheromone signaling with reproduction. *Cell* 123, 683–695. doi: 10.1016/j.cell.2005.09.027

Brechbühl, J., Klaey, M., Moine, F., Bovay, E., Hurni, N., Tosato, M. N., et al. (2014). Morphological and physiological species-dependent characteristics of the rodent Grueneberg ganglion. *Front. Neuroanat.* 8:87. doi: 10.3389/fnana.2014.00087

Breer, H., Fleischer, J., and Strotmann, J. (2006). The sense of smell: multiple olfactory subsystems. *Cell Mol. Life Sci.* 63, 1465–1475. doi: 10.1007/s00018-006-6108-5

Buck, L., and Axel, R. (1991). A novel multigene family may encode odorant receptors: a molecular basis for odor recognition. *Cell* 65, 175–187. doi: 10.1016/0092-8674(91)90418-X

Buck, L. B. (2005). Unraveling the sense of smell (Nobel lecture). *Angew. Chem. Int. Ed. Engl.* 44, 6128–6140. doi: 10.1002/anie.200501120

Cavaliere, R. M., Ghirardi, F., and Tirindelli, R. (2014). Lacrimal gland removal impairs sexual behavior in mice. *Front. Neuroanat.* 8:101. doi: 10.3389/fnana.2014.00101

Escada, P. A., Lima, C., and da Silva, J. M. (2009). The human olfactory mucosa. *Eur. Arch. Otorhinolaryngol.* 266, 1675–1680. doi: 10.1007/s00405-009-1073-x

Fuss, S. H., Omura, M., and Mombaerts, P. (2005). The Grüneberg ganglion of the mouse projects axons to glomeruli in the olfactory bulb. *Eur. J. Neurosci.* 22, 2649–2654. doi: 10.1111/j.1460-9568.2005.04468.x

Grüneberg, H. (1973). A ganglion probably belonging to the N. terminalis system in the nasal mucosa of the mouse. *Z. Anat. Entwicklungsgesch.* 140, 39–52. doi: 10.1007/BF00520716

Hohenbrink, P., Dempewolf, S., Zimmermann, E., Mundy, N. I., and Radespiel, U. (2014). Functional promiscuity in a mammalian chemosensory system: extensive expression of vomeronasal receptors in the main olfactory epithelium of mouse lemurs. *Front. Neuroanat.* 8:102. doi: 10.3389/fnana.2014.00102

Keverne, E. B. (2005). Odor here, odor there: chemosensation and reproductive function. *Nature Neurosci.* 8, 1637–1638. doi: 10.1038/nn1205-1637

Mandiyan, V. S., Coats, J. K., and Shah, N. M. (2005). Deficits in sexual and aggressive behaviors in *Cnga2* mutant mice. *Nature Neurosci.* 8, 1660–1662. doi: 10.1038/nn1589

Mori, K., Manabe, H., and Narikiyo, K. (2014). Possible functional role of olfactory subsystems in monitoring inhalation and exhalation. *Front. Neuroanat.* 8:107. doi: 10.3389/fnana.2014.00107

Munger, S. D., Leinders-Zufall, T., and Zufall, F. (2009). Subsystem organization of the mammalian sense of smell. *Annu. Rev. Physiol.* 71, 115–140. doi: 10.1146/annurev.physiol.70.113006.100608

Pérez-Gómez, A., Stein, B., Leinders-Zufall, T., and Chamero, P. (2014). Signaling mechanisms and behavioral function of the mouse basal vomeronasal neuroepithelium. *Front. Neuroanat.* 8:135. doi: 10.3389/fnana.2014.00135

Retzius, G. (1894). Die Riechzellen der Ophidier in der Riechschleimhaut und im Jacobson'schen Organ. *Biol. Untersuch. Neue Folge* 6, 48–51.

Rodolfo-Masera, T. (1943). Sur l'esistenza di un particolare organo olfacttivo nel setto nasale della cavia e di altri roditori. *Arch. Ital. Anat. Embryol.* 48, 157–212.

Shepherd, G. M. (2006). Behaviour: smells, brains and hormones. *Nature* 439, 149–151. doi: 10.1038/439149a

Yoder, A. D., and Larsen, P. A. (2014). The molecular evolutionary dynamics of the vomeronasal receptor (Class 1) genes in primates: a gene family on the verge of a functional breakdown. *Front. Neuroanat.* 8:153. doi: 10.3389/fnana.2014.00153

Yoon, H., Enquist, L. W., and Dulac, C. (2005). Olfactory inputs to the hypothalamic neurons controlling reproduction and fertility. *Cell* 123, 669–682. doi: 10.1016/j.cell.2005.08.039

Conflict of Interest Statement: The authors declare that the research was conducted in the absence of any commercial or financial relationships that could be construed as a potential conflict of interest.

frontiers in
NEUROANATOMY

OPINION ARTICLE
published: 29 September 2014
doi: 10.3389/fnana.2014.00107

Possible functional role of olfactory subsystems in monitoring inhalation and exhalation

***Kensaku Mori*[1,2]*, *Hiroyuki Manabe*[1,2] *and Kimiya Narikiyo*[1,2]**

[1] *Department of Physiology, Graduate School of Medicine, The University of Tokyo, Tokyo, Japan*
[2] *CREST, Japan Science and Technology Agency, Tokyo, Japan*
**Correspondence: moriken@m.u-tokyo.ac.jp*

Edited by:
Ignacio Salazar, University of Santiago de Compostela, Spain

Reviewed by:
Peter Brennan, University of Bristol, UK

Keywords: respiration phase, Grueneberg ganglion, CO_2-detection, cool sensor, necklace glomeruli

In parallel with progress in understanding the canonical main olfactory system, a recent advance has accelerated elucidation of the structural organization and functional properties of the olfactory subsystems. These include the ganglion of Grueneberg, septal organ, and specific subsets of olfactory sensory neurons in the main olfactory epithelium. The emerging concept of the olfactory subsystems is that each subsystem expresses distinct classes of chemoreceptors and signal transduction molecules, and thereby detects distinct categories of odor or pheromone molecules. The chemical signals detected by the subsystems are sent via their axons to subsystem-specific domains in the glomerular map of the main olfactory bulb (Mori and Sakano, 2011).

For example, a small subset of olfactory sensory neurons in the main olfactory epithelium of mice expresses a second class of odorant receptors, trace amine-associated receptors (TAARs) (Liberles and Buck, 2006), and detects amine compounds (Zhang et al., 2013) that are released from male urine, predators, spoiled foods or dead animals. TAAR-expressing olfactory sensory neurons project axons to glomeruli clustered in a specific region in the dorsal domain of the glomerular map (Johnson et al., 2012; Pacifico et al., 2012). Another example is a subset of neurons in the Grueneberg ganglion that detects an alarm pheromone, 2-*sec*-butyl-4, 5-dihydrothiazole (SBT), which is released from conspecific mice under a threatening situation (Brechbuhl et al., 2013). This subset of Grueneberg ganglion neurons mediates the alarm pheromone-induced innate fear response and sends axons to the glomeruli at the dorso-posterior part of the main olfactory bulb.

In this opinion article, we argue for the notion that on top of their major role as detectors of distinct categories of chemical signals, some of the olfactory subsystems play important roles in detecting the timing of the inhalation phase and exhalation phase of respiration. Olfactory perception occurs in discrete breaths (sniffs). Therefore, respiration rhythm plays a key role orchestrating the information processing mode across a number of regions in the central olfactory system, which includes the olfactory bulb and numerous areas of the olfactory cortex (Mori and Manabe, 2014).

Each respiration cycle consists of an inhalation phase followed by an exhalation phase (**Figure 1**). During the inhalation phase, odorants in the external world are drawn, together with external cool air, into the nasal cavity and thereby activate olfactory sensory neurons in the olfactory epithelium. Therefore, the central olfactory system is engaged in the processing of olfactory sensory inputs from the external world during the inhalation phase. During the exhalation phase, warm lung air flows through the pharynx into the nasal cavity via the retronasal pathway. The air stream then flows outwardly through the nostrils, preventing external odors from reaching the nasal cavity. The central olfactory system is thus temporarily isolated from the external odor world, and typically process olfactory information off-line during the exhalation phase. However, a unique mode of olfactory sensory neuron stimulation occurs during eating: the central olfactory system receives retronasal odor stimulation from foods in the mouth during the exhalation phase (Gautam and Verhagen, 2012). Thus, in awake behaving states, the central olfactory system appears subject to respiration phase-paced changes in information processing mode. In agreement with this idea, a recent study showed that mice can behaviorally discriminate the sniff phase of optogenetically driven activation of olfactory sensory neurons (Smear et al., 2011).

We speculate that in order for the central olfactory system to perform respiration phase-specific changes in the mode of information processing, it should receive signals regarding the timing of inhalation and exhalation. Here, we hypothesize that some of the olfactory subsystems function as monitors of the inhalation and exhalation phases of respiration. Specifically, we propose that these olfactory subsystems convey information on dynamic change in the direction of respiratory air flow to the central olfactory system.

The Grueneberg ganglion is an olfactory subsystem located at the entrance of the nose, a strategically important place for immediately detecting the inhalation of external chemical cues and air. As stated above, a subset of sensory neurons in the ganglion respond to alarm pheromone SBT (Brechbuhl et al., 2013), while other subsets of ganglion neurons respond to other chemical cues. Interestingly, Grueneberg ganglion cells express thermosensitive potassium channel TREK-1 (Stebe et al., 2014) and

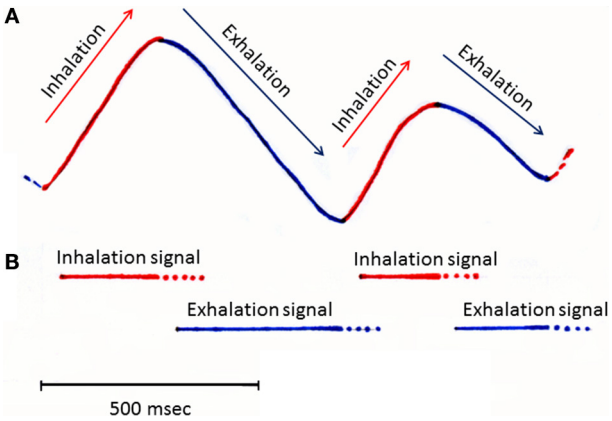

FIGURE 1 | A schematic diagram illustrating the respiration rhythms and possible timing of inhalation and exhalation signals. Inhalation and exhalation phases of slow respirations recorded from a rat during awake resting. Upper swing of trace **(A)** (output from a thermocouple placed in the nasal cavity) indicates the inhalation phase (shown red), while a downswing indicates the exhalation phase (shown blue). Bars in **(B)** indicate the possible timing of inhalation (red bars) and exhalation signals (blue bars) which might be detected by specific subsets of olfactory sensory neurons and sent to the olfactory bulb.

respond to cool ambient temperature (Mamasuew et al., 2008). Because an inhalation of external cool air is a good stimulus for these sensory neurons, we speculate that the additional function of Grueneberg ganglion neurons is to monitor the timing of inhalation, especially when mice sniff in a cool environment. At relatively warm environmental temperature, however, Grueneberg ganglion neurons may not be a reliable monitor of inhalation (Mamasuew et al., 2008), and hitherto unknown olfactory or trigeminal subsystems might contribute to signal the inhalation phase.

Axons of Grueneberg ganglion cells project to glomeruli at the dorso-posterior part of the main olfactory bulb, forming a semicircle around the anterior part of the accessory olfactory bulb (Fuss et al., 2005; Koos and Fraser, 2005; Fleischer et al., 2006; Roppolo et al., 2006; Storan and Key, 2006). It should be noted that these glomeruli are distinct from guanylyl cyclase-D (GC-D)-positive necklace glomeruli, which receive axons from CO_2-sensitive olfactory sensory neurons in the main olfactory epithelium (Fuss et al., 2005).

A small subset of olfactory sensory neurons in the olfactory epithelium express GC-D and cAMP-stimulated phosphodiesterase-2A (PDE2A). Because these olfactory sensory neurons project axons to the necklace glomeruli located at the posterior-most part of the glomerular map, they are called necklace olfactory neurons (Luo, 2008). These necklace olfactory neurons detect atmospheric carbon dioxide (CO_2) with high sensitivity (Hu et al., 2007). We speculate that during the exhalation phase, the CO_2-sensitive necklace olfactory neurons are exposed to and activated by the air from the lung, which contains a high concentration of CO_2. We therefore hypothesize that the necklace glomerular system may have an additional functional role, namely monitoring the exhalation phase of respiration. However, the CO_2 levels will not be raised in the anatomical dead space air in which gas exchange has not occurred. Therefore, the CO_2-sensitive necklace olfactory neurons may not reliably signal the start of exhalation and may signal the latter phase of exhalation. It is possible that hitherto unknown olfactory or trigeminal subsystems also might contribute the detection of the exhalation phase.

The septal organ is an island of olfactory epithelium located at the ventral base of the nasal septum. About 70% of olfactory sensory neurons in the septal organ respond to both odor stimulation and to mechanical stimulation, suggesting that they respond with spike discharges in synchrony with the nasal air flow even without odor input (Grosmaitre et al., 2007). The olfactory sensory neurons in the septal organ project axons to a subset of glomeruli in the medioventral part of the posterior olfactory bulb (Ma et al., 2003). In addition, about 50% of olfactory sensory neurons show mechanosensitivity in the main olfactory epithelium. On these bases, the mechanosensitive neurons in the septal organ and main olfactory epithelium may respond to air flow in the nasal cavity during both inhalation and exhalation, and drive synchronization of the activity of olfactory bulb neurons with inhalation and exhalation. Of interest, olfactory sensory neurons in the cyclic nucleotide-gated channel (CNGA2) knockout mice lose mechanosensitivity, and olfactory bulb activity does not synchronize with respiration cycle (Grosmaitre et al., 2007).

The above discussions argue for the idea that at least some of the olfactory subsystems have an important role in detecting the timing of inhalation, exhalation, and air flow in the nasal cavity. Further experiments are needed to determine the functional role of each olfactory subsystem in detecting distinct phases of the respiration cycle. The timing of inhalation and exhalation plays a pivotal role in information processing in the central olfactory system (Mori et al., 2013; Nagayama et al., 2014). Thus, our understanding of the dynamics of information processing in the large-scale networks of the central olfactory system is critically dependent on a better understanding of neuronal mechanisms for detecting respiratory phases, and for sending breath cycle signals to specific glomeruli in the olfactory bulb.

REFERENCES

Brechbühl, J., Moine, F., Klaey, M., Nenniger-Tosato, M., Hurni, N., Sporkert, F., et al. (2013). Mouse alarm pheromone shares structural similarity with predator scents. *Proc. Natl. Acad. Sci. U.S.A.* 110, 4762–4767. doi: 10.1073/pnas.12142 49110

Fleischer, J., Hass., N., Schwarzenbacher, K., Besser, S., and Breer, H. (2006). A novel population of neuronal cells expressing the olfactory marker protein (OMP) in the anterior/dorsal region of the nasal cavity. *Histochem. Cell Biol.* 125, 337–349. doi: 10.1007/s00418-005-0077-x

Fuss, S. H., Omura, M., and Mombaerts, P. (2005). The Grueneberg ganglion of the mouse projects axons to glomeruli in the olfactory bulb. *Eur. J. Neurosci.* 22, 2649–2654. doi: 10.1111/j.1460-9568.2005.04468.x

Gautam, S. H., and Verhagen, J. V. (2012). Retronasal odor representations in the dorsal olfactory bulb of rats. *J. Neurosci.* 32, 7949–7959. doi: 10.1523/JNEUROSCI.1413-12.2012

Grosmaitre, X., Santarelli, L. C., Tan, J., Luo, M., and Ma, M. (2007). Dual functions of mammalian olfactory sensory neurons as odor detectors and mechanical sensors. *Nat. Neurosci.* 10, 348–354. doi: 10.1038/nn1856

Hu, J., Zhong, C., Ding, C., Chi, Q., Walz, A., Mombaerts, P., et al. (2007). Detection of near-atmospheric concentrations of CO2 by an olfactory subsystem in the mouse. *Science* 317, 953–957. doi: 10.1126/science.1144233

Johnson, M. A., Tsai, L., Roy, D. S., Valenzuela, D. H., Mosley, C., Magklara, A., et al. (2012). Neurons expressing trace amine-associated receptors project to discrete glomeruli and constitute an olfactory subsystem. *Proc. Natl. Acad. Sci. U.S.A.* 109, 13410–13415. doi: 10.1073/pnas.1206724109

Koos, D. S., and Fraser, S. E. (2005). The Grueneberg ganglion projects to the olfactory bulb. *Neuroreport* 16, 1929–1932. doi: 10.1097/01.wnr.0000186597.72081.10

Liberles, S. D., and Buck, L. B. (2006). A second class of chemosensory receptors in the olfactory epithelium. *Nature* 442, 645–650. doi: 10.1038/nature05066

Luo, M. (2008). The necklace olfactory system in mammals. *J. Neurogenet.* 22, 229–238. doi: 10.1080/01677060802340228

Ma, M., Grosmaitre, X., Iwema, C. L., Baker, H., Greer, C. A., and Shepherd, G. M. (2003). Olfactory signal transduction in the mouse septal organ. *J. Neurosci.* 23, 317–324.

Mamasuew, K., Breer, H., and Fleischer, J. (2008). Grueneberg ganglion neurons respond to cool ambient temperatures. *Eur. J. Neurosci.* 28, 1775–17785. doi: 10.1111/j.1460-9568.2008.06465.x

Mori, K., and Manabe, H. (2014). "Unique characteristics of the olfactory system," in *The Olfactory System*, ed K. Mori (Tokyo: Springer Japan), 1–18.

Mori, K., Manabe, H., Narikiyo, K., and Onisawa, N. (2013). Olfactory consciousness and gamma oscillation couplings across the olfactory bulb, olfactory cortex, and orbitofrontal cortex. *Front. Psychol.* 4:743. doi: 10.3389/fpsyg.2013.00743

Mori, K., and Sakano, H. (2011). How is the olfactory map formed and interpreted in the mammalian brain? *Annu. Rev. Neurosci.* 34, 467–499. doi: 10.1146/annurev-neuro-112210-112917

Nagayama, S., Igarashi, K. M., Manabe, H., and Mori, K. (2014). "Parallel tufted cell and mitral cell pathways from the olfactory bulb to the olfactory cortex," in *The Olfactory System*, ed K. Mori (Tokyo: Springer Japan), 133–160.

Pacifico, R., Dewan, A., Cawley, D., Guo, C., and Bozza, T. (2012). An olfactory subsystem that mediates high-sensitivity detection of volatile amines. *Cell Rep.* 2, 76–88. doi: 10.1016/j.celrep.2012.06.006

Roppolo, D., Ribaud, V., Jungo, V. P., Luscher, C., and Rodriguez, I. (2006). Projection of the Gruneberg ganglion to the mouse olfactory bulb. *Eur. J. Neurosci.* 23, 2887–2894. doi: 10.1111/j.1460-9568.2006.04818.x

Smear, M., Shusterman, R., O'Connor, R., Bozza, T., and Rinberg, D. (2011). Perception of sniff phase in mouse olfaction. *Nature* 479, 397–400. doi: 10.1038/nature10521

Stebe, S., Schellig, K., Lesage, F., Breer, H., and Fleischer, J. (2014). The thermosensitive potassium channel TREK-1 contributes to coolness-evoked responses of Grueneberg ganglion neurons. *Cell. Mol. Neurobiol.* 34, 113–122. doi: 10.1007/s10571-013-9992-x

Storan, M. J., and Key, B. (2006). Septal organ of Gruneberg is part of the olfactory system. *J. Comp. Neurol.* 494, 834–844. doi: 10.1002/cne.20858

Zhang, J., Pacifico, R., Cawley, D., Feinstein, P., and Bozza, T. (2013). Ultrasensitive detection of amines by a trace amine-associated receptor. *J. Neurosci.* 33, 3228–32239. doi: 10.1523/JNEUROSCI.4299-12.2013

Conflict of Interest Statement: The authors declare that the research was conducted in the absence of any commercial or financial relationships that could be construed as a potential conflict of interest.

Received: 05 August 2014; accepted: 11 September 2014; published online: 29 September 2014.
Citation: Mori K, Manabe H and Narikiyo K (2014) Possible functional role of olfactory subsystems in monitoring inhalation and exhalation. Front. Neuroanat. ***8****:107. doi: 10.3389/fnana.2014.00107*
This article was submitted to the journal Frontiers in Neuroanatomy.

frontiers in
NEUROANATOMY

ORIGINAL RESEARCH ARTICLE
published: 14 July 2014
doi: 10.3389/fnana.2014.00063

Anatomy, histochemistry, and immunohistochemistry of the olfactory subsystems in mice

Arthur W. Barrios[1], Gonzalo Núñez[2], Pablo Sánchez Quinteiro[1] and Ignacio Salazar[1]*

[1] *Unit of Anatomy and Embryology, Department of Anatomy and Animal Production, Faculty of Veterinary, University of Santiago de Compostela, Lugo, Spain*
[2] *ICT Department, Hospital Polusa, Lugo, Spain*

Edited by:
Pablo Chamero, University of Saarland, Germany

Reviewed by:
Alino Martinez-Marcos, Universidad de Castilla, Spain
Carla Mucignat, University of Padova, Italy

***Correspondence:**
Ignacio Salazar, Unit of Anatomy and Embryology, Department of Anatomy and Animal Production, Faculty of Veterinary, University of Santiago de Compostela, Av. Carballo Calero s/n, 27002 Lugo, Spain
e-mail: ignacio.salazar@usc.es

The four regions of the murine nasal cavity featuring olfactory neurons were studied anatomically and by labeling with lectins and relevant antibodies with a view to establishing criteria for the identification of olfactory subsystems that are readily applicable to other mammals. In the main olfactory epithelium and the septal organ the olfactory sensory neurons (OSNs) are embedded in quasi-stratified columnar epithelium; vomeronasal OSNs are embedded in epithelium lining the medial interior wall of the vomeronasal duct and do not make contact with the mucosa of the main nasal cavity; and in Grüneberg's ganglion a small isolated population of OSNs lies adjacent to, but not within, the epithelium. With the exception of Grüneberg's ganglion, all the tissues expressing olfactory marker protein (OMP) (the above four nasal territories, the vomeronasal and main olfactory nerves, and the main and accessory olfactory bulbs) are also labeled by *Lycopersicum esculentum* agglutinin, while *Ulex europaeus* agglutinin I labels all and only tissues expressing $G_{\alpha i2}$ (the apical sensory neurons of the vomeronasal organ, their axons, and their glomerular destinations in the anterior accessory olfactory bulb). These staining patterns of UEA-I and LEA may facilitate the characterization of olfactory anatomy in other species. A 710-section atlas of the anatomy of the murine nasal cavity has been made available on line.

Keywords: nasal cavity, morphology, digital atlas, olfactory epithelium, subdivisions, mouse

INTRODUCTION

Though between-species differences are notorious, the olfactory systems of mammals are in general able to recognize thousands of odorant molecules that vary in shape, size, charge, and function. These molecules are captured by the odorant receptors that populate the terminal dendritic trees of olfactory sensory neurons (OSNs) located in up to four areas of the epithelium lining the nasal cavities (Buck and Axel, 1991; Buck, 1996). The major such area is the main olfactory sensory epithelium (MOE) (Graziadei, 1971); the other nasal structures with OSN-bearing epithelium that may be present are the vomeronasal organ (VNO) (Jacobson, 1813; Doving and Trotier, 1998; Zancanaro, 2014), the septal organ (SO) (Broman, 1921; Rodolfo-Masera, 1943), and the ganglion of Grüneberg (GG) (Grüneberg, 1973). All these territories have been identified in mice (Breer et al., 2006; Storan and Key, 2006).

Of the four territories mentioned above, the GG was largely overlooked until its "rediscovery" a decade ago (Fuss et al., 2005; Koos and Fraser, 2005; Roppolo et al., 2006; Storan and Key, 2006), since when it has attracted considerable interest (Brechbühl et al., 2008; Schmid et al., 2010; Mamasuew et al., 2011; Matsuo et al., 2012). The other three have often been hypothesized as having distinct olfactory functions, an idea that in the case of the VNO and MOE is supported by the fact that whereas MOE OSNs project to the main olfactory bulb (MOB), the OSNs of the sensory epithelium of the VNO (the VNsE) project to the accessory olfactory bulb (AOB). Indeed, in both these cases more detailed correspondences have been distinguished: the apical and basal regions of the VNsE project to the anterior and posterior AOB, respectively (Jia and Halpern, 1996; Salazar and Sánchez-Quinteiro, 2003), while four MOE zones have been reported to correspond to four MOB regions defined along an anterodorsomedial-caudoventrolateral axis (Ressler et al., 1993; Vassar et al., 1993). However, more exact MOE-MOB relationships are based on types of OSN rather than the MOE area they occupy (Munger et al., 2009; Ma, 2010; Mori and Sakano, 2011; Murthy, 2011); and, more importantly, the anatomical and functional independence of the vomeronasal and main olfactory systems is questioned by a number of findings (Boehm et al., 2005; Mandiyan et al., 2005; Yoon et al., 2005), notably the feedback from higher centers. Much remains to be known about the interactions of these two systems with each other (Keverne, 2005; Brennan and Zufall, 2006; Shepherd, 2006; Mucignat-Caretta et al., 2012) and with the GG and SO (Levai and Strotmann, 2003; Ma et al., 2003; Kaluza et al., 2004; Tian and Ma, 2008).

Abbreviations: AOB, accessory olfactory bulb; Bn, Bouin fixative; Fr, buffered formalin fixative; GG, ganglion of Grüneberg; HE, haematoxylin-eosin; LEA, *Lycopersicum esculentum* agglutinin; MOB, main olfactory bulb; MOE, main olfactory epithelium; NBo, main olfactory nerve bundles; NBv, vomeronasal nerve bundles; OMP, olfactory marker protein; OR, olfactory receptor; OSbS, olfactory subsystems; OSNs, olfactory sensory neurons; PB, phosphate buffer; SO, septal organ; TAARs, trace-amine-associated receptors; UEA-I, *Ulex europaeus* agglutinin I; VNa, apical vomeronasal sensory epithelium; VNb, basal vomeronasal sensory epithelium; VNO, vomeronasal organ; VNsE, vomeronasal sensory epithelium.

In view of the above, the MOE, VNsE, SO and GG can be considered as the entry points of four olfactory subsystems (OSbS), the integration of which at higher levels has yet to be determined. To consolidate and possibly refine the structural basis of this approach in a way that would be readily applicable to other mammals, in the work described here we documented the morphology of the entire nasal cavity of the mouse and studied selected territories histochemically (using the lectins *Ulex europaeus* agglutinin-I and *Lycopersicum esculentum* agglutinin) and immunohistochemically [using antibodies against olfactory marker protein (OMP) and the G-protein subunits $G_{\alpha i2}$ and $G_{\alpha 0}$]. OMP is considered to be a marker of all olfactory neurons; $G_{\alpha i2}$ and $G_{\alpha 0}$ differentiate vomeronasal OSNs projecting to different AOB territories (Wekesa and Anholt, 1999); and the two lectins used have coherent staining patterns in the olfactory bulbs (Salazar et al., 2001).

Our morphological material is available on-line as a 710-section digital atlas of the murine nasal cavity (see Supplementary Material below). As far as we know, this is the first time that the anatomies of all four olfactory territories have been presented together in relation to the cavity as a whole.

MATERIALS AND METHODS

ANIMALS

Fourteen male or female healthy BALB/c mice aged at least 10 months, reared in the animal care facilities of the University of Santiago de Compostela (Registry No. 15003AE), were euthanized and decapitated in the Department of Pharmacology for use as control animals in pharmacological research; housing and handling followed the guidelines of the USC Biethical Committee. The intact heads were kindly donated to the authors.

PROCESSING OF SAMPLES AND TISSUE SECTIONS

Eight heads were fixed by immersion in 10% buffered formalin (Fr) and stored in 4% Fr. The other six heads were fixed by immersion in Bouin's fixative (Bn), and after 24 h were transferred to 70% alcohol.

For examination of the entire nasal cavity, two Fr-fixed heads were decalcified in Shandon TBD-1 rapid decalcifier (Thermo, Pittsburgh, PA), oriented so that the hard palate was horizontal, embedded in paraffin wax, and cut in transverse sections 8-10 μm thick perpendicular to the hard palate. Alternate sections (710) were transferred to slides and stained with haematoxylin-eosin (HE).

From two Fr- and two Bn-fixed heads, the brain was removed and transferred again to Fr or Bn. The remaining pieces of the these heads, and the other eight heads (four Fr- and four Bn-fixed), were decalcified, oriented as above, and embedded, and serially cut transverse sections were transferred to slides. In the light of the information obtained from the entire nasal cavity series (see above), selected sections at seven different levels intersecting the GG, VNO, and SO, and at four levels of the posterior MOE, were stained with HE, and the remainder were used in histochemical and immunohistochemical protocols.

Fr- and Bn-fixed olfactory bulbs were used as controls for the histochemical and immunohistochemical procedures described below.

LECTIN HISTOCHEMISTRY

The lectins *Ulex europaeus* agglutinin I (UEA-I) and *Lycopersicum esculentum* agglutinin (LEA) were obtained as biotin conjugates from Sigma (St. Louis, MO, USA). Tissue sections were (1) incubated for 30 min at room temperature with 2% bovine serum albumin in 0.1 M phosphate buffer (PB, pH 7.2); (2) incubated for 24 h at 4°C with lectin at concentrations ranging from 20 to 60 μg/mL in 0.1 M Tris buffer containing 0.5% bovine serum albumin; (3) washed for 2 × 10 min in PB; (4) incubated for 90 min at room temperature with Vectastain ABC reagent (1:250 in PB); and (5) incubated in 0.2 M Tris–HCl buffer (pH 7.6) containing 0.05% 3,3-diaminobenzidine and 0.003% H_2O_2. Controls were run without lectin or with preabsorption of lectin by an excess amount of the corresponding sugar.

IMMUNOHISTOCHEMISTRY

Immunohistochemical studies were performed using antibodies against olfactory marker protein (OMP) (Wako Chemicals, 1:500 dilution) and the G-proteins $G_{\alpha i2}$ (Santa Cruz Biotechnology, 1:100) and $G_{\alpha 0}$ (Santa Cruz Biotechnology and Medical & Biological Lab Co., 1:100). Sections were dewaxed in xylene, rehydrated, and successively incubated (1) for 30 min at room temperature in PB containing 5% normal horse serum and 2% bovine serum albumin, (2) for 24 h at 4°C in primary antibody solution, (3) for 1 h in biotinylated secondary antibody solution, and (4) for 2 h in a solution of avidin-biotin-horseradish peroxidase complex (ABC Vectastain reagent); after which standard procedures for visualization of the horseradish peroxidase complex with 3,3-diaminobenzidine were followed, and the sections were dehydrated through alcohols, cleared in xylene, and coverslipped.

IMAGE ACQUISITION AND PROCESSING

Digital images were captured using a Karl Zeiss Axiocam MRc5 digital camera. When necessary, Adobe Photoshop CS4 (Adobe Systems, San Jose, CA) was used to adjust contrast and brightness to equilibrate light levels, and/or to crop, resize and rotate the images for presentation; no additional digital image manipulation was performed.

IMPLEMENTATION OF THE ON-LINE ATLAS (SUPPLEMENTARY MATERIAL)

The on-line atlas was developed using the languages HTML5, CSS3, JavaScript, PHP5 and XML, the libraries/frameworks JavaScript jQuery (v1.10.1) and Normalize.css (v2.1.3), and the scripts/plug-ins PhpThumb (v3.0), JQuery Sketch.js, Zoomooz (v1.1.6), ColorBox (v1.3.31), waitForImages, FitText (v1.1), qTip2 (v2.1.1), and Image Power Zoomer (v1.1). It consists of a front end comprising the content and associated functionality (accessible in any current web browser, including the latest versions of Mozilla Firefox, Google Chrome, Opera, Safari and Internet Explorer) and a back end PHP-based area for merging and managing the data, images and texts.

RESULTS

ANATOMY

Figures 1A, **2** (see also the Supplementary Material) show the locations of the MOE, SO, VNO and GG, which occupy the mucosal lining of most of the nasal cavity except the ventral concha (for turbinate numbering, see **Figures 1**, **3**).

The MOE features three major cell types: neurons, supporting cells, and the basal stem cells that generate olfactory neurons throughout life (**Figure 4A**). Three regions may be distinguished on the basis of whether the MOE tissue is locally, on average, (i) 3–5, (ii) 6–10, or (iii) 11 or more cells thick (**Figures 4B–D**, **5**). In general, the MOE is thicker in dorsal regions than in the corresponding ventral regions, and there are similar thick-thin differences in the medial-lateral and posterior-anterior directions (see Supplementary Material).

The SO is an independent structure with the same characteristics as MOE region (i) (**Figure 6A**).

The VNO occupies a thin cylindrical lamina of bone located on the floor of the nasal cavity adjacent to the vomer. It comprises the vomeronasal duct (a blind epithelial tube with a single small rostral orifice connecting it with the main nasal cavity) together with surrounding glands, vessels, nerves, and connective tissue. The VNsE is limited to the central levels of the medial wall of the duct (**Figure 6B**).

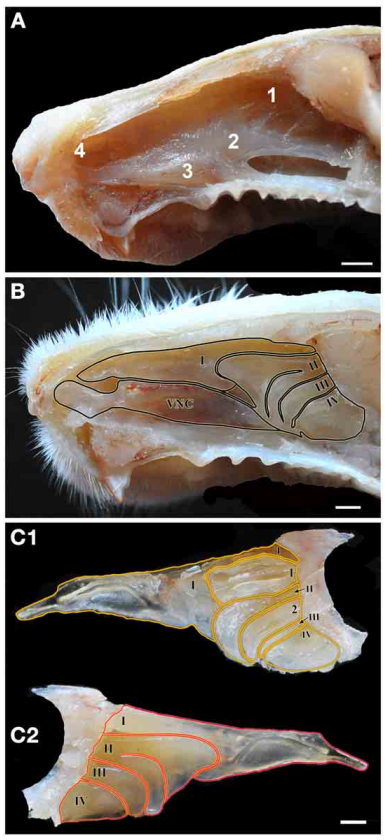

FIGURE 1 | Views of the nasal cavity. (A) The nasal septum, showing the location of the main olfactory epithelium (1), the septal organ (2), the vomeronasal organ (3) and Grüneberg's ganglion (4). **(B)** Medial view of the nasal conchae and ethmoturbinates following removal of the nasal septum, with endoturbinates numbered by Roman numerals (VNC, ventral nasal concha). **(C)** Lateral **(C1)** and medial **(C2)** views of the isolated dorsal nasal concha and ethmoturbninates, with ectoturbinates numbered by Arabic numerals and endoturbinates as in **(B)**. Scale bars: **(A)** 2 mm; **(B,C)** 1 mm.

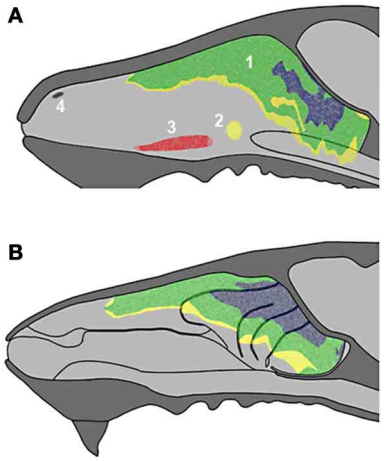

FIGURE 2 | Schematic drawings of the nasal septum (A) and the medial aspect of the nasal cavity (B), showing the locations of the main olfactory epithelium (1), septal organ (2), vomeronasal organ (3) and Grüneberg ganglion (4) with indication of epithelial thickness (yellow, thin; green, medium; blue, thick). See supplementary material.

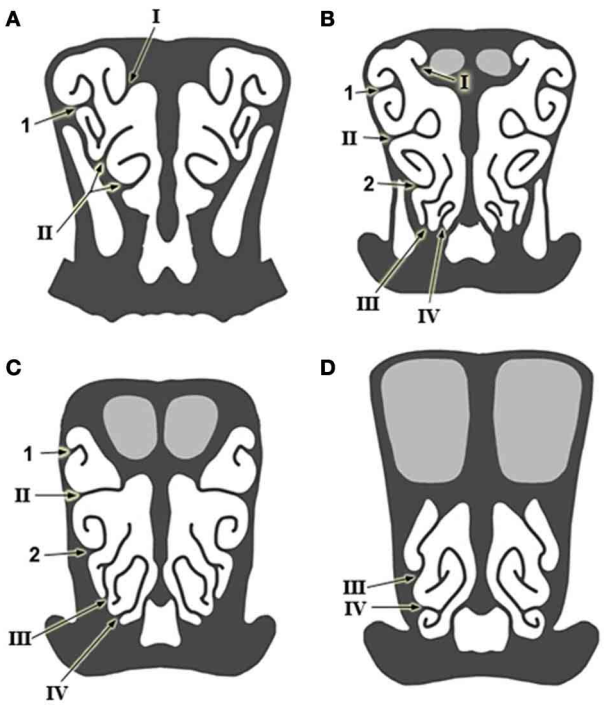

FIGURE 3 | Schematic drawings of transverse sections of the head, from anterior to posterior levels (A–D), showing the arrangement of the ethmoturbinates at several levels in the posterior part of the nasal cavity. Numbering as in **Figure 1**.

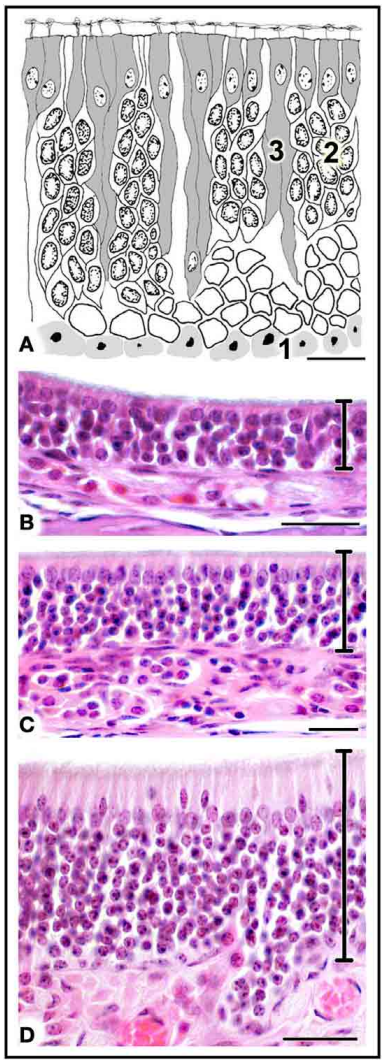

FIGURE 4 | (A) Diagrammatic reconstruction of main olfactory epithelium, showing basal cells (1), mature neurons (2) and supporting cells (3) (modified after Graziadei, 1971). **(B,C)** Haematoxylin-eosin-stained sections of areas of epithelium with different thicknesses (see text). Scale bars: **(A)** 10 μm; **(B)** 20 μm; **(C,D)** 25 μm.

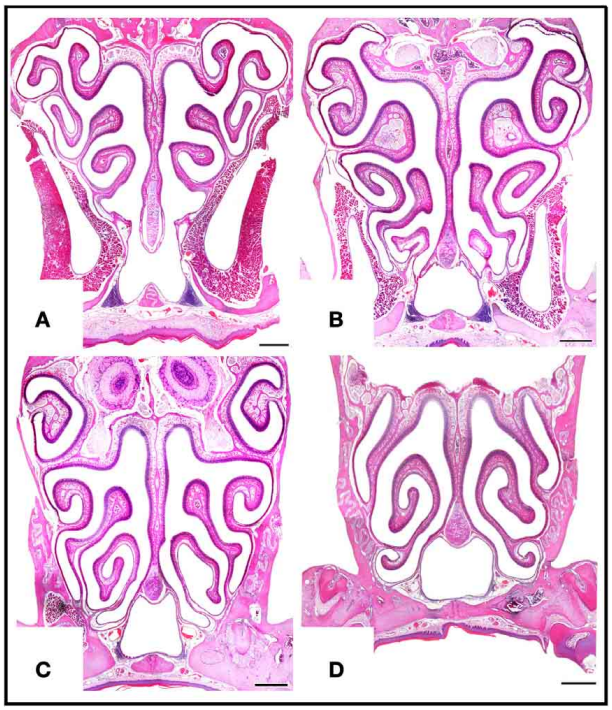

FIGURE 5 | Haematoxylin-eosin-stained transverse sections at four levels of the posterior nasal cavity, from anterior to posterior levels (A–D), where most of the MOE is located. Scale bars: 500 μm.

In the GG, located in the nasal vestibule adjacent to the nasal septum and the dorsolateral nasal cartilage (**Figure 6C**), a small isolated group of OSNs are embedded in connective tissue under a dense network of blood vessels, adjoining but not within the epithelium. Among adult mice there is significant between-individual variation in GG anatomy; for example, symmetry between the right and left sides is not universal.

HISTOCHEMISTRY AND IMMUNOHISTOCHEMISTRY

Main olfactory epithelium

We first applied all the histochemical and immunohistochemical stains to sections in which both main olfactory and vomeronasal nerves run adjacent to the septum. Though with different intensities, anti-OMP and LEA stained the MOE and both the main olfactory and vomeronasal nerves bundles (NBo and NBv, respectively); anti-$G_{\alpha 0}$ strongly labeled all nerve bundles; and UEA-I and anti-$G_{\alpha i2}$ bound only to NBv (**Figure 7**). The results of staining for OMP (**Figure 8**) and $G_{\alpha 0}$ (**Figure 9**) at six different transverse levels of the nasal cavity were in agreement with these findings.

Vomeronasal organ, septal organ, and the ganglion of Grüneberg

The staining behavior of UEA-I, anti-$G_{\alpha 0}$ and anti-$G_{\alpha i2}$ in the VNsE distinguished apical and basal layers, UEA-I and anti-$G_{\alpha i2}$ staining the apical VNsE (VNa), and anti-$G_{\alpha 0}$ the basal VNsE (VNb) (in this case mainly at the edges of the sensory epithelium) (**Figures 10B,D,E**). Anti-OMP and LEA stained both layers (**Figures 10A,C**). The staining pattern of the SO was essentially identical to that of the MOE (**Figure 10F1** shows OMP positivity in an SO section). GG cells were also clearly OMP-positive, but accepted no other stain (**Figure 10F2**).

Olfactory bulbs

The staining patterns of the olfactory bulbs used as controls are shown in **Figure 11**. Note that like anti-OMP, LEA stains both the nervous and glomerular layers of both the MOB and the AOB.

DISCUSSION

The above results clearly identify four different olfactory sensory areas in the nasal cavities, and accordingly justify the use of OSbS terminology. In regard to the anatomy of the VNO, it is perhaps worth stressing that vomeronasal OSNs do not make

FIGURE 6 | Haematoxylin-eosin-stained transverse sections showing the locations of the septal organ (A), the vomeronasal organ (B), and Grüneberg's ganglion (C), together with an enlarged view of each in the corresponding inset. Topography of the rüneberg's ganglion cells (arrows heads). Scale bars: **(A–C)**, 500 μm; insets, 50 μm.

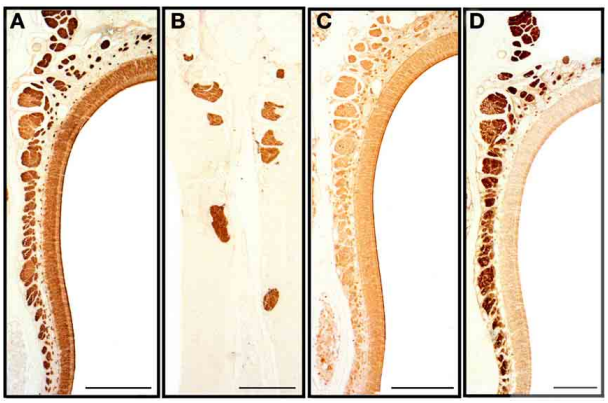

FIGURE 7 | Transverse sections of the nasal septum stained with anti-OMP (A), UEA-I (B), LEA (C) and anti-$G_{\alpha 0}$ (D), showing the olfactory sensory epithelium and the olfactory and vomeronasal nerve bundles. Scale bars: **(A,C)** 150 μm; **(B,D)** 100 μm.

contact with the mucosa of the main nasal cavity. For them to bind the semiochemicals to which they respond, these latter must therefore be pumped into the vomeronasal duct in some way, probably by vascular constriction (Meredith et al., 1980; Salazar et al., 2008). Thus, the non-epithelial components of the VNO do not merely provide mechanical and physiological support for the sensory epithelium, but must play an active role in olfaction. This raises a question as to the triggering of this pumping mechanism, which if vascular is presumably not of itself a voluntary action. One possibility is that it may be part of some general scent-seeking behavioral pattern; another, that it may be triggered by the detection of an olfactory signal of broad significance by one of the three olfactory territories of the main nasal cavity.

The possibility of further defining subdivisions of the olfactory epithelial territories on the basis of the receptor types borne by OSNs appears to depend on both the OSbS and the broad class of receptor types in question. The VNsE is clearly divisible into an apical stratum with OSNs bearing receptors of type V1R, and a basal stratum with V2R-bearing OSNs (Wagner et al., 2006). The axons of these apical and basal strata respectively project to the anterior and posterior regions of the AOB. Further, the upper and lower sublayers of the basal VNsE respectively project to the anterior and posterior parts of the posterior AOB, in correlation with whether the V2R OSNs do not or do express *H2-mv* genes (Salazar and Sánchez-Quinteiro, 2003; Ishii and Mombaerts, 2008). However, these divisions appear to be crossed by OSNs bearing formyl peptide receptors, which seem to be widely dispersed in either the entire VNsE (Liberles et al., 2009) or, with a rostrocaudal gradient that is more pronounced in juveniles than adults, in its apical layer (Rivière et al., 2009; Dietschi et al., 2013). Moreover, the functional significance of these subdivisions is unknown, and its elucidation will require more extensive investigation of the ligands recognized by the vomeronasal system (Chamero et al., 2012; Francia et al., 2014).

In the MOE, the first reports of zonal organization of OSNs bearing the multiple varieties of "canonical" G-protein-coupled olfactory receptor (OR), made possible by the cloning of odorant receptor genes (Buck and Axel, 1991), spoke of each receptor-defined OSN type being distributed at random in just one of three or four zones (Ressler et al., 1993; Vassar et al., 1993). Subsequently, a more refined scheme emerged that related to the distinction between phylogenetically older (class I) and younger (class II) OR types: while almost all OSNs with a class I OR type or belonging to a subset of class II OR types are randomly located in a dorsomedial region (D), each of the multiple other class II types is borne exclusively by OSNs occupying a type-specific antero-posterior swathe in the remainder of the MOE (V), with the centerline of one swathe displaced dorsoventrally just slightly from that of the next, so that each swathe overlaps multiple others (Miyamichi et al., 2005). The projection of the OSNs defined by a given OR type to just a single pair of MOB glomeruli, confirmed by experiments with P2-IRES-tau-lacZ mice (Mombaerts et al., 1996), makes the detailed map of the MOE in the MOB discrete (Luo and Flanagan, 2007), but this map nevertheless respects the zonal organization described above: OR OSNs in MOE region D project to the dorsal MOB (Kobayakawa et al., 2007; Bozza et al., 2009), and the dorsoventral

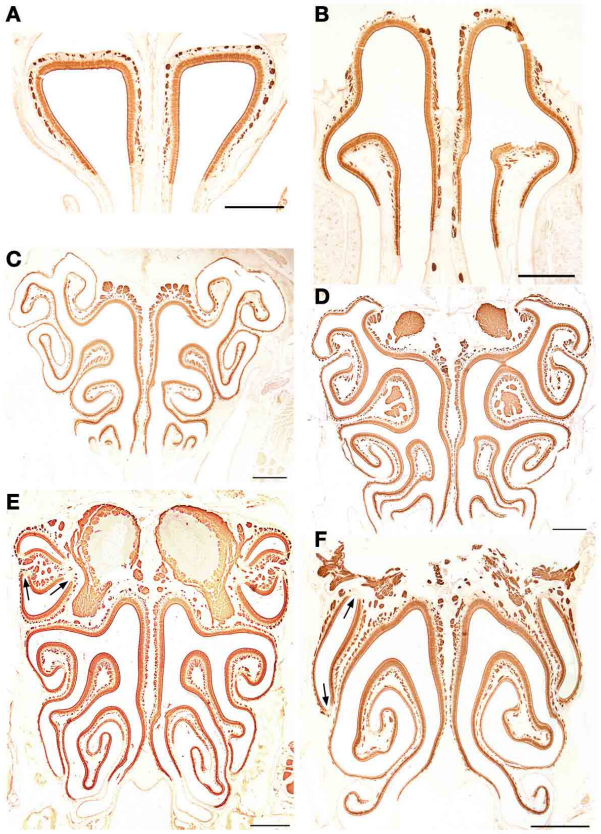

FIGURE 8 | Anti-OMP-stained transverse sections of the nasal cavity at the central levels of the vomeronasal organ (A) and septal organ (B), and at the same levels as in Figure 4 (C–F). Note the similar reactivities of epithelium and axon bundles. In **(E,F)**, arrows indicate small areas devoid of immunoreactivity. Scale bars: 500 μm.

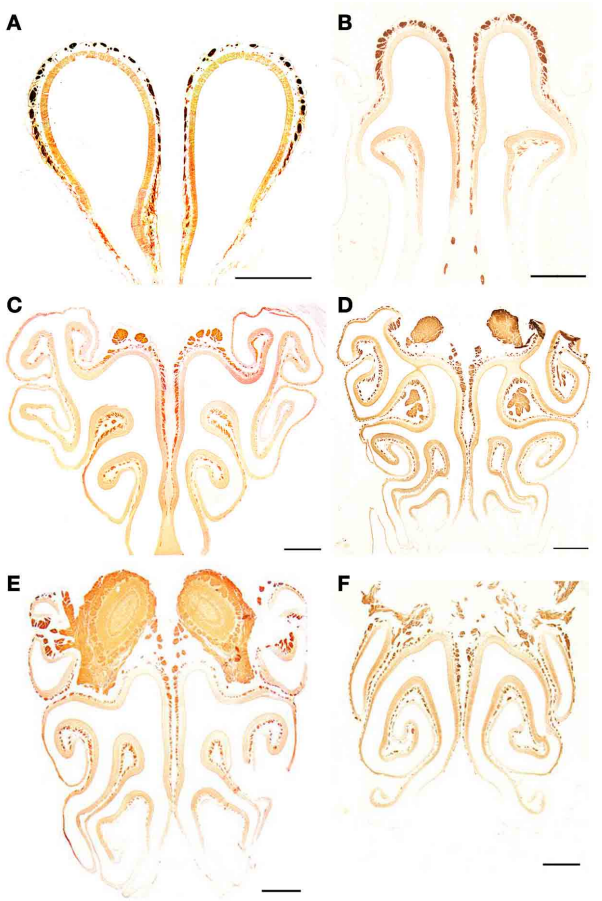

FIGURE 9 | Anti-$G_{\alpha 0}$-stained transverse sections of the nasal cavity at the same levels (A–F) as in Figure 8. Note the different reactivities of epithelium and axon bundles. Scale bars: 500 μm.

order of OR types in region V is faithfully reproduced by the glomeruli to which their OSNs project in the ventral MOB. Also, the more recently discovered subset of OR OSNs that express TRPM5, which are mainly located in the ventrolateral MOE, mainly project to glomeruli in the ventral MOB (Lin et al., 2007); and a similar degree of topographical correspondence is seen in regard to OSNs bearing trace-amine-associated receptors (TAARs, one of the two known types of non-OR olfactory receptor in the MOE; Liberles and Buck, 2006), TAAR OSNs located in the dorsal MOE projecting to two or three glomeruli in a well-defined dorsal area of the MOB (Pacifico et al., 2012). However, topographicness is less evident in the mapping of OSNs with guanylyl cyclase D receptors, the other non-OR MOE receptor type. These OSNs, which are found in clusters in a limited MOE zone (mostly in the dorsal recesses of the nasal cavity), project to a number of the "necklace glomeruli" surrounding the caudal end of the MOB (Gibson and Garbers, 2000; Walz et al., 2007).

In the present study we found that the MOE is in general thicker in the dorsal zone than the ventral, thicker in the medial zone than the lateral, and thicker in the posterior zone than the anterior. The relevance of these findings to the zonal organization described above is unclear, but they should be taken into account in future work, among other reasons because they are consistent with inspiratory airflow paths (Schoenfeld and Cleland, 2005).

The olfactory bulbs were initially included in this study merely as control tissues, since in previous work they have reacted very well with the lectins employed in the present study, exhibiting consistent, anatomically coherent patterns: although staining uniformity depends upon the age of the animal (Salazar and Sánchez-Quinteiro, 2003), LEA labels the glomeruli and incoming nerves of both the AOB and the MOB, while UEA-I binds only to the vomeronasal nerves and AOB structures (Salazar et al., 2001). Our present results confirm these findings and extend them to the corresponding sensory epithelia. UEA-I thus emulates anti-$G_{\alpha i2}$ in its specificity (under the conditions of this study) for the olfactory subsystem entered via the apical VNsE; while LEA, except for its failure to stain the Grüneberg ganglion, emulates the neuron-staining behavior of anti-OMP, which is specific for the olfactory nervous system as a whole (Margolis, 1972) (in **Figures 8E,F**, note the absence of stain in acute angles

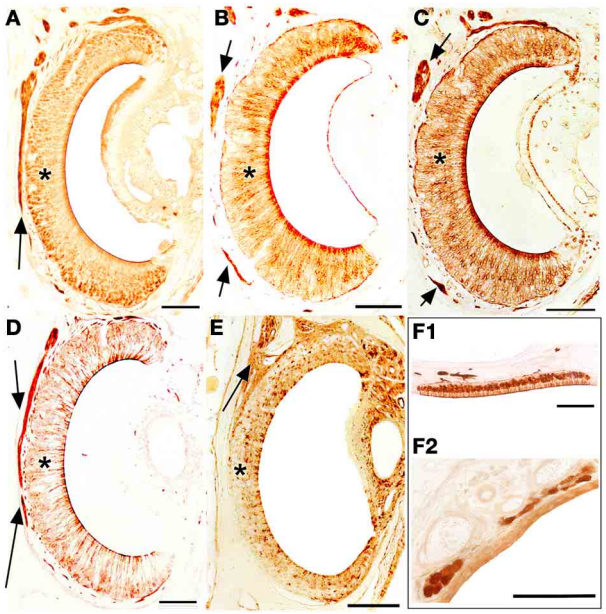

FIGURE 10 | Transverse sections of the vomeronasal duct stained with anti-OMP (A), UEA-I (B), LEA (C), anti-$G_{\alpha 0}$ (D) and anti-$G_{\alpha i2}$ (E), and of the septal organ (F_1) and Grüneberg ganglion (F_2) stained with anti-OMP. Arrows indicate vomeronasal nerve axons medial to the vomeronasal sensory epithelium (asterisk). Scale bars: 100 μm.

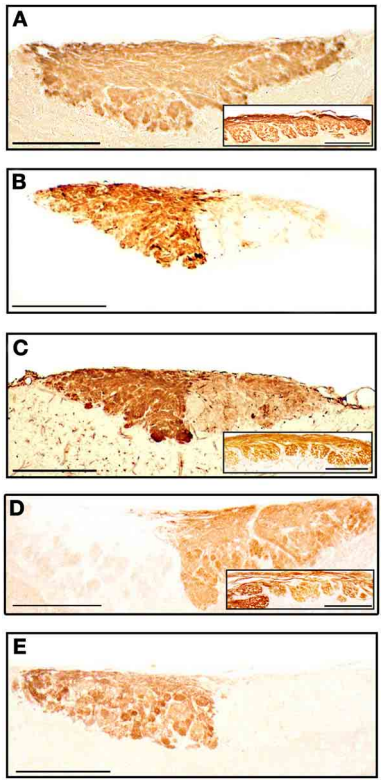

FIGURE 11 | Parasagittal sections of the olfactory bulb through the AOB (left anterior, right posterior) stained with anti-OMP (A), UEA-I (B), LEA (C), anti-$G_{\alpha 0}$ (D) and anti-$G_{\alpha i2}$ (E). Insets show the nervous and glomerular layers of the MOB. Scale bars: **(A)** 250 μm; **(B–E)** and insets, 200 μm.

of the turbinates, where neural cells are lacking; Suzuki et al., 2000). Although LEA, unlike anti-OMP, also stains glands, vessels and other tissues adjoining neurons, and is also prone to non-specific staining, this mimicry of anti-OMP by LEA and of anti-$G_{\alpha i2}$ by UEA-I, which is also found in a number of other species (see Salazar and Sánchez-Quinteiro, 2009), allows the use of these inexpensive lectins to obtain prima facie evidence concerning the structure of the VNsE in hitherto unstudied species. Although the molecular basis of this mimicry, i.e., the identity of the sugar-bearing molecules to which UEA-I and LEA bind in the olfactory system, is not totally clear, it appears to involve the role of cell surface blood group antigens in the wiring of the olfactory system (see, for example, St John et al., 2006).

In this study, neither UEA-I nor anti-$G_{\alpha i2}$ bound to the MOE, the septal organ, or Grüneberg's ganglion. The absence of binding to the MOE appears to contradict a report that $G_{\alpha i2}$ is expressed in olfactory neurons located near the dorsal septum and in the dorsal recess of the nasal cavity, and in MOB glomeruli concentrated mainly on the medial side (Wekesa and Anholt, 1999); it seems possible that the neurons stained by Wekesa and Anholt in the nasal cavity may have been vomeronasal nerves, although this would not explain their observations in the MOB. Our results are in keeping with those of Wekesa and Anholt (1999) in that expression of $G_{\alpha o}$ was restricted to the basal VNsE and to the glomeruli and incoming axons of the MOB and posterior AOB. That Grüneberg's ganglion was stained by anti-OMP but by neither anti-$G_{\alpha o}$ nor anti-$G_{\alpha i2}$ is in keeping with the findings of Roppolo et al. (2006), who observed mRNA for OMP but not for then known ORs, V1Rs or V2Rs, but not with studies that have detected several TAARs (Fleischer et al., 2007) and the novel vomeronasal receptor V2r83 (Fleischer et al., 2006), which is apparently co-expressed with the guanylyl cyclase GC-G (Matsuo et al., 2012).

CONCLUDING REMARKS

The discovery of novel genes involved in the initial stages of olfaction has renewed interest in this sensory system, which is evidently more complex than was previously imagined. Even at the grossest level, it is clear that any division into subsystems must define more than just the main and accessory olfactory systems, and at least three sets of criteria are available for refinement of this earlier conception: (i) division into four subsystems in accordance with the four spatially separated areas of sensory epithelium (MOE, SO, VNsE, and GG); (ii) division as above together with further division in accordance with axon targets, giving six subsystems (MOE OSNs projecting to necklace glomeruli, MOE OSNs projecting to non-necklace glomeruli, the SO, apical VNsE OSNs, basal VNsE OSNs, and GG); (iii) division of OSNs in accordance with their receptor type (which affords subsystems with epithelial domains that are both overlapping and fragmented, but is nevertheless a feasible option). However, there is an often overlooked problem in that the more complex

Table 1 | Summarizes the histochemical and immunohistochemical results.

	OMP	UEA-I	LEA	Gαo	Gαi2
GG	+	−	−	−	−
VNa	+	+	+	−	+
VNb	+	−	+	+	−
SO	+	−	+	−	−
MOE	+	−	+	−	−
NBv	+	+	+	+	+
NBo	+	−	+	+	−
AOBa	+	+	+	−	+
AOBp	+	−	+	+	−
MOB	+	−	+	+	−

Reactivities of the Grüneberg ganglion (GG), apical vomeronasal sensory epithelium (VNa), basal vomeronasal sensory epithelium (VNb), septal organ (SO), main olfactory epithelium (MOE), vomeronasal nerve bundles (NBv), main olfactory nerve bundles (NBo), anterior accessory olfactory bulb (AOBa), posterior accessory olfactory bulb (AOBp) and main olfactory bulb (MOB) with anti-OMP, UEA-I, LEA, anti-$G_{\alpha o}$ and anti-$G_{\alpha i2}$.

the classification, the more difficult it will be to corroborate in larger species (e.g., if criteria require examination of transgenic animals), and the more difficult it will be to adapt to species with olfactory abilities differing from those of mice (Salazar and Sánchez-Quinteiro, 2009).

We suggest that the five-subsystem classification implicit in **Table 1** (MOE-NBo-MOB, SO, VNa-NBv-AOBa, VNb-NBv-AOBp, GG) constitutes a basic scheme, the validity of which for any other species can be easily investigated by the methods described in this paper, and which if necessary can be easily adapted in accordance with the results of these procedures. Although there is no doubt that progress in our understanding of the sense of smell will continue to be driven by molecular-genetic approaches (Axel, 2005), it is equally unquestionable that such studies should be consistent with the anatomy of the explored region (Schoenfeld and Cleland, 2005).

AUTHOR CONTRIBUTIONS

Ignacio Salazar designed the research and wrote the paper. Arthur W. Barrios, Gonzalo Núñez and Pablo Sánchez Quinteiro performed the work. Arthur W. Barrios Barrios, Gonzalo Núñez, Pablo Sánchez Quinteiro and Ignacio Salazar analyzed and discussed the data.

ACKNOWLEDGMENTS

We thank N. Vandenberghe and D. Salazar for intellectual support and helpful comments; L. Botana and A. Alonso for kindly providing mice; A. Outeiro and J. Castiñeira for technical assistance; and I.C. Coleman for revising the final English version. WAB thanks the Spanish Ministry of Foreign Affairs and Cooperation for an AECID grant. Private financial support is gratefully acknowledged. We apologize to the authors whose works have contributed to this field and could not be cited here.

SUPPLEMENTARY MATERIAL

The on-line atlas of the murine nasal cavity associated with this manuscript as Supplementary Material is available at http://www.usc.es/anatembriol/. It comprises transverse sections of the whole nasal cavity organized in thirty-five 20-section segments and a final 10-section segment. Clicking on Views and then on Analysis shows, superimposed on a lateral view of the nasal cavity, a grid defining the 31 transverse segments. Clicking on a segment opens a window with thumbnails of its 10 or 20 numbered sections; clicking on a thumbnail brings up the section. The **GG** is located in segments 4 and 5 (sections 0522-0626), the **VNO** in segments 12-20 (sections 1511-2416), the **SO** in segments 21-23 (sections 2531-2724), and the **MOE** in segments 12-35 (sections 1421-4621). The turbinates are located as follows: the **dorsal nasal concha** and **endoturbinate I** in segments 12-30 (sections 1421-3812), **endoturbinate II** in segments 20-31 (sections 2412-3926), **endoturbinate III** in segments 26-32 (sections 3031-4126), **endoturbinate IV** in segments 28-35 (sections 3421-4621), **ectoturbinate 1** in segments 23-31 (sections 2733-3923), and **ectoturbinate 2** in segments 26-31 (sections 3114-4016). Yellow indicates MOE with 3-5 rows of cells, green 6-10 rows, and blue 11 or more rows (see also **Figure 2**).

REFERENCES

Axel, R. (2005). Scents and sensibility: a molecular logic of olfactory perception (Nobel lecture). *Angew. Chem. Int. Ed. Engl.* 44, 6110–6127. doi: 10.1002/anie.200501726

Boehm, U., Zou, Z., and Buck, L. B. (2005). Feedback loops link odor and pheromone signaling with reproduction. *Cell* 123, 683–695. doi: 10.1016/j.cell.2005.09.027

Bozza, T., Vassalli, A., Fuss, S., Zhang, J. J., Weiland, B., Pacifico, R., et al. (2009). Mapping of class I and class II odorant receptors to glomerular domains by two distinct types of olfactory sensory neurons in the mouse. *Neuron* 61, 220–233. doi: 10.1016/j.neuron.2008.11.010

Brechbühl, J., Klaey, M., and Broillet, M. C. (2008). Grüneberg ganglion cells mediate alarm pheromone detection in mice. *Science* 321, 1092–1095. doi: 10.1126/science.1160770

Breer, H., Fleischer, J., and Strotmann, J. (2006). The sense of smell: multiple olfactory subsystems. *Cell. Mol. Life Sci.* 63, 1465–1475. doi 10.1007/s00018-006-6108-5

Brennan, P. A., and Zufall, F. (2006). Pheromonal communication in vertebrates. *Nature* 444, 308–315. doi: 10.1038/nature05404

Broman, I. (1921). Über die Entwicklung der konstanten grösseren Nasennebenhöhlendrüsen der Nagetiere. *Z. Anat. Entwickl. Gesch.* 60, 439–586. doi: 10.1007/BF02593654

Buck, L. (1996). Information coding in the vertebrate olfactory system. *Annu. Rev. Neurosci.* 19, 517–544. doi: 10.1146/annurev.ne.19.030196.002505

Buck, L., and Axel, R. (1991). A novel multigene family may encode odorant receptors: a molecular basis for odor recognition. *Cell* 65, 175–187. doi: 10.1016/0092-8674(91)90418-X

Chamero, P., Leinders-Zufall, T., and Zufall, F. (2012). From genes to social communication: molecular sensing by the vomeronasal organ. *Trends Neurosci.* 35, 597–606. doi: 10.1016/j.tins.2012.04.011

Dietschi, Q., Assens, A., Challet, L., Carleton, A., and Rodriguez, I. (2013). Convergence of FPR-rs3-expressing neurons in the mouse accessory olfactory bulb. *Mol. Cell. Neurosci.* 56, 140–147. doi: 10.1016/j.mcn.2013.04.008

Doving, K. B., and Trotier, D. (1998). Structure and function of the vomeronasal organ. *J. Exp. Biol.* 201, 2913–2925.

Fleischer, J., Schwarzenbacher, K., Besser, S., Hass, N., and Breer, H. (2006). Olfactory receptors and signalling elements in the Grueneberg ganglion. *J. Neurochem.* 98, 543–554. doi: 10.1111/j.1471-4159.2006.03894.x

Fleischer, J., Schwarzenbacher, K., and Breer, H. (2007). Expression of trace amine-associated receptors in the Grueneberg ganglion. *Chem. Senses* 32, 623–631. doi: 10.1093/chemse/bjm032

Francia, S., Pifferi, S., Menini, A., and Tirindelli, R. (2014). "Vomeronasal receptors and signal transduction in the vomeronasal organ of mammals," in *Neurobiology of Chemical Communication*, Chapter 10, ed C. Mucignat-Caretta (Boca Raton, FL: CRC Press), 297–324. doi: 10.1201/b16511-11

Fuss, S. H., Omura, M., and Mombaerts, P. (2005). The Grüneberg ganglion of the mouse projects axons to glomeruli in the olfactory bulb. *Eur. J. Neurosci.* 22, 2649–2654. doi: 10.1111/j.1460-9568.2005.04468.x

Gibson, A. D., and Garbers, D. L. (2000). Guanylyl cyclases as a family of putative odorant receptors. *Annu. Rev. Neurosci.* 23, 417–439. doi: 10.1146/annurev.neuro.23.1.417

Graziadei, P. P. P. (1971). "The olfactory mucosa of vertebrates", in *Handbook of Sensory Physiology.* Vol. IV. *Chemical Senses 1, Olfaction*, ed L. M. Beidler (Berlin: Springer-Verlag), 27–58.

Grüneberg, H. (1973). A ganglion probably belonging to the N. terminalis system in the nasal mucosa of the mouse. *Z. Anat. Entwicklungsgesch.* 140, 39–52. doi: 10.1007/BF00520716

Ishii, T., and Mombaerts, P. (2008). Expression of nonclassical class I major histocompatibility genes defines a tripartite organization of the mouse vomeronasal system. *J. Neurosci.* 28, 2332–2341. doi: 10.1523/JNEUROSCI.4807-07.2008

Jacobson, L. (1813). Anatomisk beskrivelse over et nyt organ I huusdyrenes nase. *Vet-Selskapets Skrifter* 2, 209–246.

Jia, C., and Halpern, M. (1996). Subclasses of vomeronasal receptor neurons: differential expression of G proteins (Gi2a and Goa) and segregated projections to the accessory olfactory bulb. *Brain Res.* 719, 117–128. doi: 10.1016/0006-8993(96)00110-2

Kaluza, J. F., Gussing, F., Bohm, S., Breer, H., and Strotmann, J. (2004). Olfactory receptors in the mouse septal organ. *J. Neurosci. Res.* 76, 442–452. doi: 10.1002/jnr.20083

Keverne, E. B. (2005). Odor here, odor there: chemosensation and reproductive function. *Nature Neurosci.* 8, 1637–1638. doi: 10.1038/nn1205-1637

Kobayakawa, K., Kobayakawa, R., Matsumoto, H., Oka, Y., Imai, T., Ikawa, M., et al. (2007). Innate versus learned odour processing in the mouse olfactory bulb. *Nature* 450, 503–508. doi: 10.1038/nature06281

Koos, D. S., and Fraser, S. E. (2005). The Grueneberg ganglion projects to the olfactory bulb. *Neuroreport* 16, 1929–1932. doi: 10.1097/01.wnr.0000186597.72081.10

Levai, O., and Strotmann, J. (2003). Projection pattern of nerve fibres from the septal organ: Dil-tracing studies with transgenic OMP mice. *Histochem. Cell Biol.* 120, 483–492. doi: 10.1007/s00418-003-0594-4

Liberles, S. D., and Buck, L. B. (2006). A second class of chemosensory receptors in the olfactory epithelium. *Nature* 442, 645–650. doi: 10.1038/nature05066

Liberles, S. D., Horowitz, L. F., Kuang, D., Contos, J. J., Wilson, K. L., Siltberg-Liberles, J., et al. (2009). Formyl peptide receptors are candidate chemosensory receptors in the vomeronasal organ. *Proc. Natl. Acad. Sci. U.S.A.* 106, 9842–9847. doi: 10.1073/pnas.0904464106

Lin, W., Margolskee, R., Donnert, G., Hell, S. W., and Restrepo, D. (2007). Olfactory neurons expressing transient receptor potential channel M5 (TRPM5) are involved in sensing semiochemicals. *Proc. Natl. Acad. Sci. U.S.A.* 104, 2471–2476. doi: 10.1073/pnas.0610201104

Luo, L., and Flanagan, J. G. (2007). Development of continuous and discrete neural maps. *Neuron* 56, 284–300. doi: 10.1016/j.neuron.2007.10.014

Ma, M. (2010). "Multiple olfactory subsystems convey various sensory signals," in *The Neurobiology of Olfaction,* Chapter 9, ed A. Menini (Boca Raton, FL: CRC Press), 225–240. doi: 10.1201/9781420071993-c9

Ma, M., Grosmaitre, X., Iwema, C. L., Baker, H., Greer, C. A., and Shepherd, G. M. (2003). Olfactory signal transduction in the mouse septal organ. *J. Neurosci.* 23, 317–324.

Mamasuew, K., Hofmann, N., Breer, H., and Fleischer, J. (2011). Grüneberg ganglion neurons are activated by a defined set of odorants. *Chem. Senses* 28, 271–282. doi: 10.1093/chemse/bjq124

Mandiyan, V. S., Coats, J. K., and Shah, N. M. (2005). Deficits in sexual and aggressive behaviors in *Cnga2* mutant mice. *Nature Neurosci.* 8, 1660–1662. doi: 10.1038/nn1589

Margolis, F. L. (1972). A brain protein unique to the olfactory bulb. *Proc. Natl. Acad. Sci. U.S.A.* 69, 1221–1224. doi: 10.1073/pnas.69.5.1221

Matsuo, T., Rossier, D. A., Kan, C., and Rodriguez, I. (2012). The wiring of Grueneberg ganglion axons is dependent on neuropilin 1. *Development* 139, 2783–2791. doi: 10.1242/dev.077008

Meredith, M., Marques, D. M., O'Connell, R. J., and Stern, F. L. (1980). Vomeronasal pump: significance for male hamster sexual behavior. *Science* 207, 1224–1226.

Miyamichi, K., Serizawa, S., Kimura, H. M., and Sakano, H. (2005). Continuous and overlapping expression domains of odorant receptor genes in the olfactory epithelium determine the dorsal/ventral positioning of glomeruli in the olfactory bulb. *J. Neurosci.* 25, 3586–3592. doi: 10.1523/JNEUROSCI.0324-05.2005

Mombaerts, P., Wang, F., Dulac, C., Chao, S. K., Nemes, A., Mendelsohn, M., et al. (1996). Visualizing an olfactory sensory map. *Cell* 87, 675–686. doi: 10.1016/S0092-8674(00)81387-2

Mori, K., and Sakano, H. (2011). How is the olfactory map formed and interpreted in the mammalian brain? *Annu. Rev. Neurosci.* 34, 467–499. doi: 10.1146/annurev-neuro-112210-112917

Mucignat-Caretta, C., Redaelli, M., and Caretta, A. (2012). One nose, one brain: contribution of the main and accessory olfactory system to chemosensation. *Front. Neuroanat.* 6:46. doi: 10.3389/fnana.2012.00046

Munger, S. D., Leinders-Zufall, T., and Zufall, F. (2009). Subsystem organization of the mammalian sense of smell. *Annu. Rev. Physiol.* 71, 115–140. doi: 10.1146/annurev.physiol.70.113006.100608

Murthy, V. N. (2011). Olfactory maps in the brain. *Annu. Rev. Neurosci.* 34, 233–258. doi: 10.1146/annurev-neuro-061010-113738

Pacifico, R., Dewan, A., Cawley, D., Guo, C., and Bozza, T. (2012). An olfactory subsystem that mediates high-sensitivity detection of volatile amines. *Cell Rep.* 2, 76–88. doi: 10.1016/j.celrep.2012.06.006

Ressler, K. J., Sullivan, S. L., and Buck, L. B. (1993). A zonal organization of odorant receptor gene expression in the olfactory epithelium. *Cell* 73, 597–609. doi: 10.1016/0092-8674(93)90145-G

Rivière, S., Challet, L., Fluegge, D., Spehr, M., and Rodriguez, I. (2009). Formyl peptide receptor-like proteins are a novel family of vomeronasal chemosensors. *Nature* 459, 574–577. doi: 10.1038/nature08029

Rodolfo-Masera, T. (1943). Sur l'esistenza di un particolare organo olfacttivo nel setto nasale della cavia e di altri roditori. *Arch. Ital. Anat. Embryol.* 48, 157–212.

Roppolo, D., Ribaud, V., Jungo, V. P., Lüscher, C., and Rodríguez, I. (2006). Projection of the Grüneberg ganglion to the mouse olfactory bulb. *Eur. J. Neurosci.* 23, 2887–2894. doi: 10.1111/j.1460-9568.2006.04818.x

Salazar, I., and Sánchez-Quinteiro, P. (2003). Differential development of binding sites for four lectins in the vomeronasal system of juvenile mouse: from the sensory transduction site to the first relay stage. *Brain Res.* 979, 15–26. doi: 10.1016/S0006-8993(03)02835-X

Salazar, I., and Sánchez-Quinteiro, P. (2009). The risk of extrapolation in neuroanatomy: the case of the mammalian vomeronasal system. *Front. Neuroanat.* 3:22. doi: 10.3389/neuro.05.022.2009

Salazar, I., Sánchez-Quinteiro, P., Alemañ, N., and Prieto, D. (2008). Anatomical, immunohistochemical and physiological characteristics of the vomeronasal vessels in cows and their possible role in vomeronasal reception. *J. Anat.* 212, 686–697.

Salazar, I., Sánchez-Quinteiro, P., Lombardero, M., and Cifuentes, J. M. (2001). Histochemical identification of carbohydrate moities in the accessory olfactory bulb of the mouse using a panel of lectins. *Chem. Senses* 26, 645–652. doi: 10.1093/chemse/26.6.645

Schmid, A., Pyrski, M., Biel, M., Leinders-Zufall, T., and Zufall, F. (2010). Grüneberg ganglion neurons are finely tuned cold sensors. *J. Neurosci.* 30, 7563–7568. doi: 10.1523/JNEUROSCI.0608-10

Schoenfeld, T. A., and Cleland, T. A. (2005). The anatomical logic of smell. *Trends Neurosci.* 28, 620–627. doi: 10.1016/j.tins.2005.09.005

Shepherd, G. M. (2006). Behaviour: smells, brains and hormones. *Nature* 439, 149–151. doi: 10.1038/439149a

St John, J. A., Claxton, C., Robinson, M. W., Yamamoto, F., Domino, S. E., and Key, B. (2006). Genetic manipulation of blood group carbohydrates alters development and pathfinding of primary sensory axons of the olfactory systems. *Dev. Biol.* 298, 470–484. doi: 10.1016/j.ydbio.2006.06.052

Storan, M. J., and Key, B. (2006). Septal organ of Grüneberg is part of the olfactory system. *J. Comp. Neurol.* 494, 834–844. doi: 10.1002/cne.20858

Suzuki, Y., Takeda, M., Obara, N., Suzuki, N., and Takeichi, N. (2000). Olfactory epithelium consisting of supporting cells and horizontal basal cells in the posterior nasal cavity of mice. *Cell Tissue Res.* 299, 313–325. doi: 10.1007/s004419900135

Tian, H., and Ma, M. (2008). Differential development of odorant receptor expression patterns in the olfactory epithelium: a quantitative analysis in the mouse septal organ. *Dev. Neurobiol.* 68, 476–486. doi: 10.1002/dneu.20612

Vassar, R., Ngai, J., and Axel, R. (1993). Spatial segregation of odorant receptor expression in the mammalian olfactory epithelium. *Cell* 74, 309–318. doi: 10.1016/0092-8674(93)90422-M

Wagner, S., Gresser, A. L., Torello, A. T., and Dulac, C. (2006). A multireceptor genetic approach uncovers an ordered integration of VNO sensory inputs in the accessory olfactory bulb. *Neuron* 50, 697–709. doi: 10.1016/j.neuron.2006.04.033

Walz, A., Feinstein, P., Khan, M., and Mombaerts, P. (2007). Axonal wiring of guanylate cyclase-D-expressing olfactory neurons is dependent on neuropilin 2 and semaphorin 3F. *Development* 134, 4063–4072. doi: 10.1242/dev.008722

Wekesa, K. S., and Anholt, R. R. (1999). Differential expression of G proteins in the mouse olfactory system. *Brain Res.* 837, 117–126. doi: 10.1016/S0006-8993(99)01630-3

Yoon, H., Enquist, L. W., and Dulac, C. (2005). Olfactory inputs to the hypothalamic neurons controlling reproduction and fertility. *Cell* 123, 669–682. doi: 10.1016/j.cell.2005.08.039

Zancanaro, C. (2014). "Vomeronasal organ: a short history of discovery and an account of development and morphology in the mouse", in *Neurobiology of Chemical Communication*, Chapter 9, ed C. Mucignat-Caretta (Boca Raton, FL: CRC Press), 285–296. doi: 10.1201/b16511-10

Conflict of Interest Statement: The authors declare that the research was conducted in the absence of any commercial or financial relationships that could be construed as a potential conflict of interest.

Received: 29 May 2014; accepted: 23 June 2014; published online: 14 July 2014.
Citation: Barrios AW, Núñez G, Sánchez Quinteiro P and Salazar I (2014) Anatomy, histochemistry, and immunohistochemistry of the olfactory subsystems in mice. Front. Neuroanat. ***8****:63. doi: 10.3389/fnana.2014.00063*
This article was submitted to the journal Frontiers in Neuroanatomy.

frontiers in
NEUROANATOMY

ORIGINAL RESEARCH ARTICLE
published: 25 September 2014
doi: 10.3389/fnana.2014.00106

Dog and mouse: toward a balanced view of the mammalian olfactory system

Arthur W. Barrios, Pablo Sánchez-Quinteiro and Ignacio Salazar*

Unit of Anatomy and Embryology, Department of Anatomy and Animal Production, Faculty of Veterinary, University of Santiago de Compostela, Lugo, Spain

Edited by:
Pablo Chamero, University of Saarland, Germany

Reviewed by:
Antonio Pereira, Federal University of Rio Grande do Norte, Brazil
Maud Rimbault, National Institutes of Health, USA

***Correspondence:**
Ignacio Salazar, Unit of Anatomy and Embryology, Department of Anatomy and Animal Production, Faculty of Veterinary, University of Santiago de Compostela, Av Carballo Calero s/n, 27002 Lugo, Spain
e-mail: ignacio.salazar@usc.es

Although the most intensively studied mammalian olfactory system is that of the mouse, in which olfactory chemical cues of one kind or another are detected in four different nasal areas [the main olfactory epithelium (MOE), the septal organ (SO), Grüneberg's ganglion, and the sensory epithelium of the vomeronasal organ (VNO)], the extraordinarily sensitive olfactory system of the dog is also an important model that is increasingly used, for example in genomic studies of species evolution. Here we describe the topography and extent of the main olfactory and vomeronasal sensory epithelia of the dog, and we report finding no structures equivalent to the Grüneberg ganglion and SO of the mouse. Since we examined adults, newborns, and fetuses we conclude that these latter structures are absent in dogs, possibly as the result of regression or involution. The absence of a vomeronasal component based on VR2 receptors suggests that the VNO may be undergoing a similar involutionary process.

Keywords: olfactory epithelium, olfactory subsystems, morphology, evolution, dog

INTRODUCTION

The dog is increasingly appreciated in biomedical research as a species that, unlike purpose-bred laboratory animals, shares the genetic, and clinical variety of human patients (Karlsson and Lindblad-Toh, 2008). Its nasal cavity has been studied from various points of view. Anatomically, Graeger's paper (Graeger, 1958) is considered the classical reference. Physiologically, attention has recently focused on nasal airflow patterns (Craven et al., 2007, 2010). Clinically, the presentation, diagnosis, prognosis, and treatment of tumors is a major current concern (McEntee, 2004; Turek and Lana, 2012; Mason et al., 2013), but the olfactory mucosa of the nasal cavity has also attracted clinical interest because of its unique maintenance of a population of basal cells supporting the continual regeneration of olfactory sensory neurons (OSNs) (Graziadei and Monti-Graziadei, 1979); the intraspinal implantation of cells derived from autologous olfactory mucosa cultures has in fact recently been successful in ameliorating the effects of spinal cord injuries in companion dogs (Granger et al., 2012).

In the mouse, the animal in which the mammalian olfactory system has been most intensively studied, the nasal mucosa features four separate olfactory areas: the main olfactory epithelium (MOE), the septal organ (SO), the ganglion of Grüneberg (GG), and the vomeronasal sensory epithelium [VNsE, not to be confused with the vomeronasal organ (VNO) of which it forms a part] (Breer et al., 2006; Munger et al., 2009; Ma, 2010; Barrios et al., 2014). These four sensory areas can be considered as the points of entry to four olfactory subsystems (OSbS), the integration of which at higher levels is a focus of current research. However, this four-subsystem scheme is by no means exhibited by all mammals, or even by all macrosmatic mammals (Salazar and Sánchez-Quinteiro, 2009). In the work described here we examined its validity for the dog, a notoriously macrosmatic animal. We found that the dog has no GG or SO, and that its VNO shows signs of similar involution.

MATERIALS AND METHODS

ANIMALS

The dogs studied were 31 male or female mesaticephalic adults, 17 newborn males or females from four different litters, and 16 fetuses obtained on days 30, 35, or 40 of gestation. Most were German Shepherds or mongrels derived therefrom, and all were mesaticephalic. All were obtained legally through the dissecting and post-mortem rooms and Department of Clinical Science of our faculty and were treated in accordance with Spanish and EU legislation for the care and handling of animals in research (RD 223/1998, 86/609/EEC) and with the guidelines of the University of Santiago de Compostela Bioethical Committee. The heads of all animals were intact and showed no clinical or post-mortem evidence of neurological disease; all were processed as specified below as soon after death as was possible.

PROCESSING OF SAMPLES AND TISSUE SECTIONS

Using traditional anatomical techniques, 22 adult heads were carefully prepared by dissection and micro-dissection—from outside to inside—to afford views of the lateral and medial walls of the nasal cavity and lateral and medial views of the turbinates. Views were systematically recorded in photographs and drawings, and the chromatic characteristics of the mucosa were noted. The separate components of the turbinate complex were then dissected and prepared.

Seven puppy heads were similarly prepared except for the final dissection of the turbinate complex.

Transverse sections of uniform thickness were cut on a polystyrene block from two adult heads that had been washed and frozen following appropriate cleaning, fixation by immersion in 10% formaldehyde for 96 h, and removal of the mandibles and associated structures.

Ten puppy heads were prepared for histological examination as follows. Eight heads (group 1) were fixed by immersion in neutral buffered formaldehyde, where they remained until use, and two (group 2) were immersed in Bouin's fixative for 24 h and then transferred to 70% alcohol. For examination of the whole nasal cavity (mainly with a view to delimiting the MOE), two group 1 heads were decalcified in Shandon TBD-1 rapid decalcifier (Thermo, Pittsburgh, PA) and embedded in one piece, appropriately oriented, in paraffin wax, after which serial transverse sections 8–10 μm thick were cut. 710 alternate sections from one of these heads, and 710 corresponding sections from the other, were transferred to slides and stained with hematoxylin-eosin (HE). The remaining eight heads (six from group 1 and the two group 2 heads) were prepared, sectioned and stained in the same way, except that before sectioning the nasal cavity was divided transversally into three blocks of more or less equal length.

All fetal heads were processed for histological examination in the same way as the puppy heads, with the main goal of scrutinizing the regions in which the GG and SO were expected to be found, if present. The posterior nasal cavity was also studied.

Owing to the difficulty of histological preparation of the whole adult nasal cavity, the following subregions of the remaining seven adult heads were excised, decalcified, and embedded in paraffin wax for sectioning and subsequent staining of the sections with HE or antibodies (see below): (i) four levels of the nasal septum; and (ii) the individual turbinates.

IMMUNOHISTOCHEMISTRY

Immunohistochemical studies were performed using antibodies against olfactory marker protein (OMP) (Wako Chemicals, 1:500 dilution) and the G-proteins $G_{\alpha i2}$ (Santa Cruz Biotechnology, 1:100) and $G_{\alpha o}$ (Santa Cruz Biotechnology and Medical & Biological Lab Co., 1:100). Sections were dewaxed in xylene, rehydrated, and successively incubated (1) for 30 min at room temperature in PBS containing 5% normal horse serum and 2% bovine serum albumin, (2) for 24 h at 4°C in primary antibody solution, (3) for 1 h in biotinylated secondary antibody solution, and (4) for 2 h in a solution of avidin-biotin-horseradish peroxidase complex (ABC Vectastain reagent); after which standard procedures for visualization of the horseradish peroxidase complex with 3,3-diaminobenzidine were followed, and the sections were dehydrated through alcohols, cleared in xylene, and coverslipped. Sections of formalin- or Bouin-fixed canine and murine olfactory bulbs were used as control tissues.

IMAGE ACQUISITION AND PROCESSING

Digital images were captured using a Karl Zeiss Axiocam MRc5 digital camera. When necessary, Adobe Photoshop 6.0 (Adobe Systems, San Jose, CA) was used to adjust contrast and brightness to equilibrate light levels, and/or to crop, resize, and rotate the images for presentation; no additional digital image manipulation was performed.

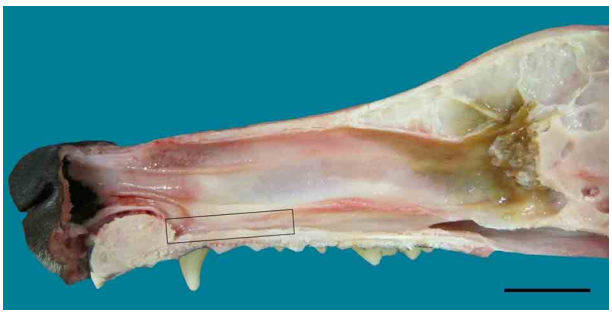

FIGURE 1 | Lateral view of the nasal septum of an adult dog, showing the difference in color between sensory (yellow-brown) and respiratory (red-orange) mucosa. The rectangle frames the vomeronarasal organ. Scale bar: 2 cm (see Figure S1).

RESULTS

The nasal cavities form a bilaterally symmetric pair flanking the nasal septum. **Figure 1** and Figure S1 show views of the lateral and medial cavity walls and of the turbinate complex within the cavity; **Figure 2** lateral and medial views of the turbinate complex without the walls of the cavity; and Figure S2 lateral and medial views of each separate component of the turbinate complex. This comprises six lateral ectoturbinates, four medial endoturbinates, and the ventral concha; the dorsal concha is a rostral projection of endoturbinate I, and the middle concha part of endoturbinate II. Parts of ectoturbinates 2 and 3 project to the frontal sinus. Transverse sections (**Figure 3** and Figure S3) clearly show the aptness of the term "complex."

In the mucosa lining the nasal cavity, color differentiates between the respiratory and olfactory epithelia, the former exhibiting shades of red or orange, the latter shades of yellow or brown (**Figure 1** and Figure S1). Histological examination of selected zones of the nasal septum and of the isolated turbinates 2, 3, II, and III (**Figure 4** and Figure S4) shows the transition between the two types of epithelia (**Figure 4A**), and also differences among different areas of sensory mucosa in regard to the thicknesses of epithelium and lamina propria and the relative thicknesses of the layers of the three epithelial cell types (sustentacular, basal, and neuronal) (**Figures 4B–E** and Figure S4). Immunohistochemically, the mature neurons and their apical projections of these zones were stained by anti-OMP, and the nerve bundles in the lamina propria by both anti-OMP and anti-$G_{\alpha 0}$, but anti-$G_{\alpha i2}$ stained nothing specifically (**Figure 5** and Figure S5). Staining consistent with these results was observed in the olfactory bulbs of dogs and mice used as controls (results not shown).

The VNO, enveloped in a cartilaginous lamina, lies adjacent to the nasal septum (**Figure 1**). Since the VNsE is located internally, forming the central levels of the medial wall of the VNO duct, its macroscopic display would be difficult, requiring a precise, somewhat curvilinear longitudinal section through the cartilage and its content (the duct and the other soft tissues that surround it). Histologically, the VNsE is composed of basal cells, receptor neurons and supporting cells, while the anterior part of the VNO duct features stratified squamous epithelium and the posterior

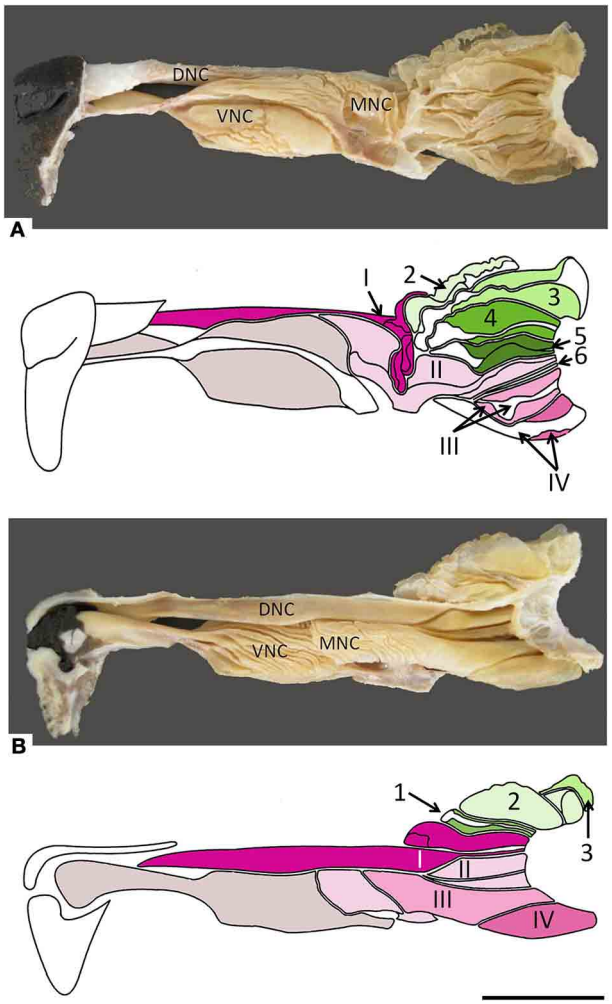

FIGURE 2 | Photographs and schematic drawings of the turbinate complex in lateral (A) and medial (B) views. DNC, dorsal nasal concha; MNC, middle nasal concha; VNC, ventral nasal concha. Ectoturbinates are identified in the drawings by Arabic numerals (1–6) and shades of green, endoturbinates by roman numerals (I–IV) and shades of pink. Scale bar: 2 cm (see Figure S2).

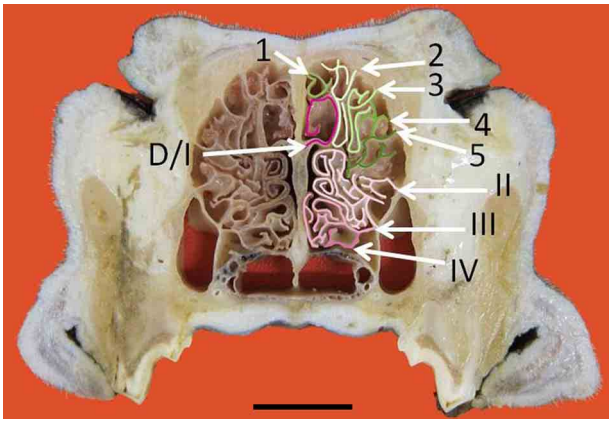

FIGURE 3 | Transverse frozen section of the nasal cavity. D, dorsal nasal concha. Ectoturbinates are identified by Arabic numerals (1–5) and endoturbinates by roman numerals (I–IV). Scale bar: 2 cm (see Figure S3).

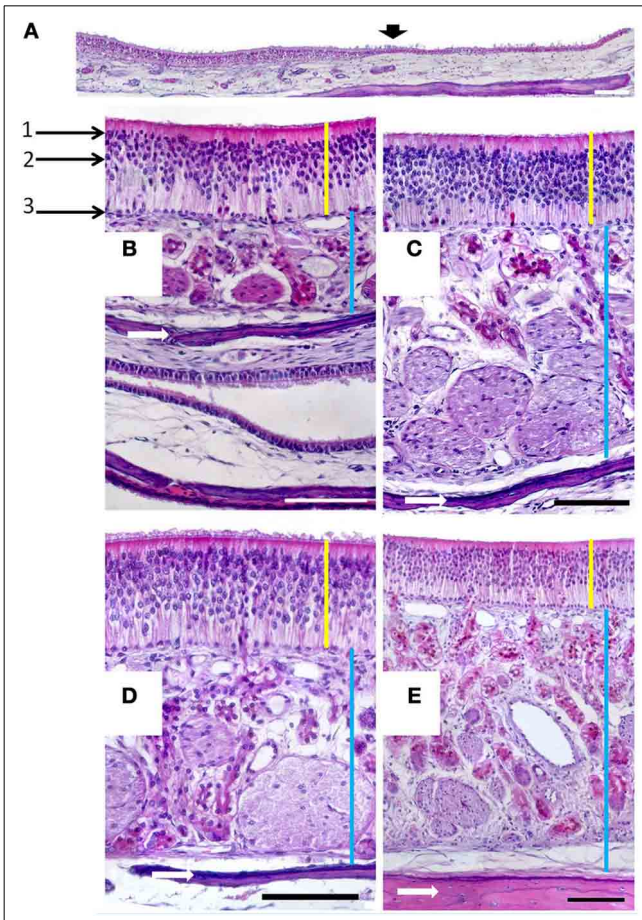

FIGURE 4 | (A) Hematoxylin-eosin-stained longitudinal section showing the transition (arrowed) from the respiratory to the sensory epithelium. **(B–E)** Hematoxylin-eosin stained transverse sections showing the mucosa of ectoturbinate 2 **(B)**, ectoturbinate 3 **(C)**, endoturbinate III **(D)**, and the nasal septum **(E)**. Yellow bars indicate sensory epithelium; blue bars, lamina propria; and white arrows, bone. 1, supporting cells; 2, neurons; 3, basal cells. Scale bars: **(A)** 2 mm; **(B–E)** 100 μm (see Figure S4).

part simple columnar epithelium (**Figure 6** and Figure S6). The immunohistochemical features of the VNsE have recently been reported elsewhere (Salazar et al., 2013) and are commented on below in the Discussion.

The above descriptions all refer to adult specimens. In newborns the frontal sinus and ectoturbinate 6 are missing, and ectoturbinate 1 is very small (**Figure 7**). The MOE cannot usually be distinguished chromatically from respiratory epithelium, and must be identified histologically. Figure S7 shows the territory it occupies as determined by examination of series of transverse sections, which also show the simplicity and small area of the neonatal turbinates in comparison with those of adults (Figure S8).

In neither adults nor newborns did we find any structure with the characteristics defining the SO and GG in mice (Barrios et al., 2014). Among our 16 fetal specimens (**Figure 8** shows sections

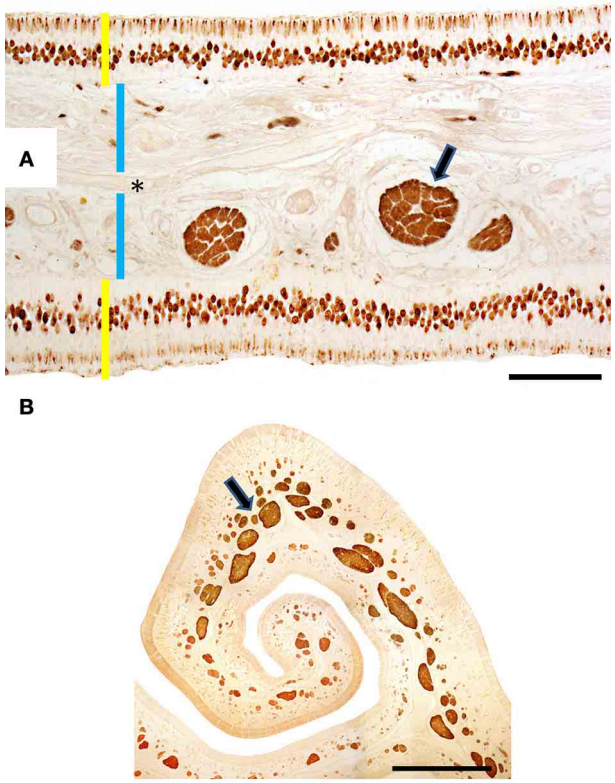

FIGURE 5 | Transverse sections of endoturbinate II stained with anti-OMP (A) and anti-$G_{\alpha o}$ (B), showing labeling of mature neurons (in A) and nerve bundles (arrowed) of the olfactory mucosa. Yellow bars indicate sensory epithelium; blue bars, lamina propria; the asterisk, bone. Scale bars: **(A)** 100 μm; **(B)** 1 mm (see Figure S5).

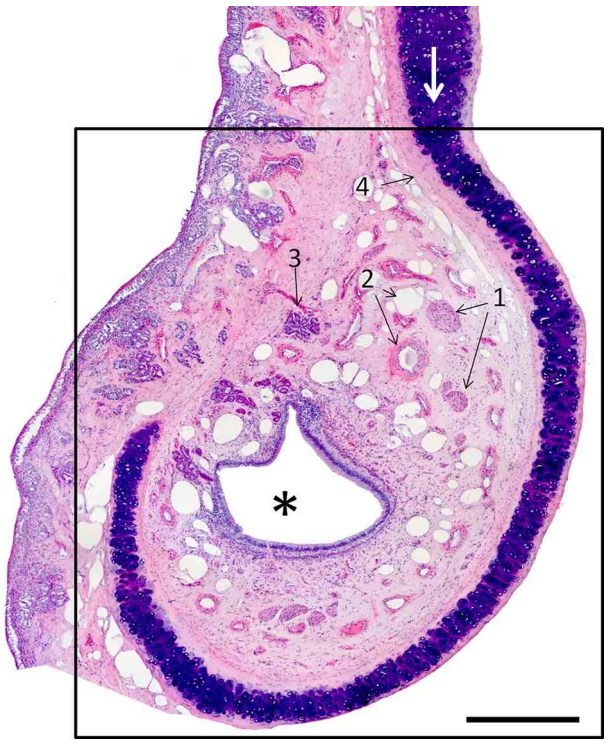

FIGURE 6 | Hematoxylin-eosin-stained transverse section of the vomeronasal organ (VNO, framed); left is lateral, up is dorsal. The asterisk indicates the lumen of the vomeronasal duct; (1) nerves; (2) vessels; and (3) a gland. The VNO is partially surrounded by connective tissue (4) and cartilage (white arrow). Scale bar: 500 μm (see Figure S6).

from one) there was one specimen in which the possible existence of GG cells was suggested by the presence of a nerve surrounded by vessels in the region homologous to the mouse GG, but OMP failed to label any cells in this area.

DISCUSSION

Among mammalian olfactory systems, the most extensively, and intensively studied has been that of the mouse—a circumstance it shares with many of the other characteristics of this animal (Paigen, 1995). It comprises four major subsystems (OSbS) stimulated via four different areas of the nasal mucosa: the MOE, the VNsE, the SO, and the GG (Barrios et al., 2014). A five-subsystem scheme emerges if the difference between vomeronasal subsystems based on semiochemical receptor types VR1 and VR2 is taken into account (Barrios et al., 2014). Although numerous studies of the canine nasal mucosa have been published (Lauruschkus, 1942; Müller, 1955; Neuhaus, 1955; Adams and Hotchkiss, 1983; Kavoi et al., 2010), we are unaware of any previous systematic search for these four or five OSbS in the dog. The findings reported above, together with our previous observation that the canine vomeronasal system binds anti-$G_{\alpha i2}$ but not anti-$G_{\alpha o}$ antibodies (Salazar et al., 2013), show that the dog has only the main and vomeronasal subsystems, and that the latter is in all probability entirely VR1-based.

Our observations of the MOE show different areas to differ considerably, especially as regards the thickness of the neuron layer and hence the surface density of neurons, even on a single turbinate. However, we were unable to organize the observed variation in a classification of mucosal types, or to relate our observations to the two-type classification proposed previously (Bock et al., 2009) on the basis of morphological characteristics, neuron turnover, and immunoreactivity.

Whereas the murine vomeronasal system expresses the VR1-associated protein $G_{\alpha i2}$ in the apical layer of the VNsE and the anterior half of the accessory olfactory bulb (AOB), and the VR2-associated protein $G_{\alpha o}$ in the basal layer of the VNsE and the posterior half of the AOB (Barrios et al., 2014), the canine system does not express $G_{\alpha o}$, and expresses $G_{\alpha i2}$ throughout the AOB as well as in the VNsE (Salazar et al., 2013). This behavior is in keeping with reported failure to find functional VR2 genes in the canine genome (Young and Trask, 2007). Given their presence in opossum (Young and Trask, 2007) and rodents (Ishii and Mombaerts, 2011), their absence from the dog (and cow and primates) (Young and Trask, 2007) must be the result of an involutionary process (Salazar and Sánchez-Quinteiro, 2009).

Regressive processes, whether evolutionary or ontogenic, seem also to have led to the absence of both SO and GG from the

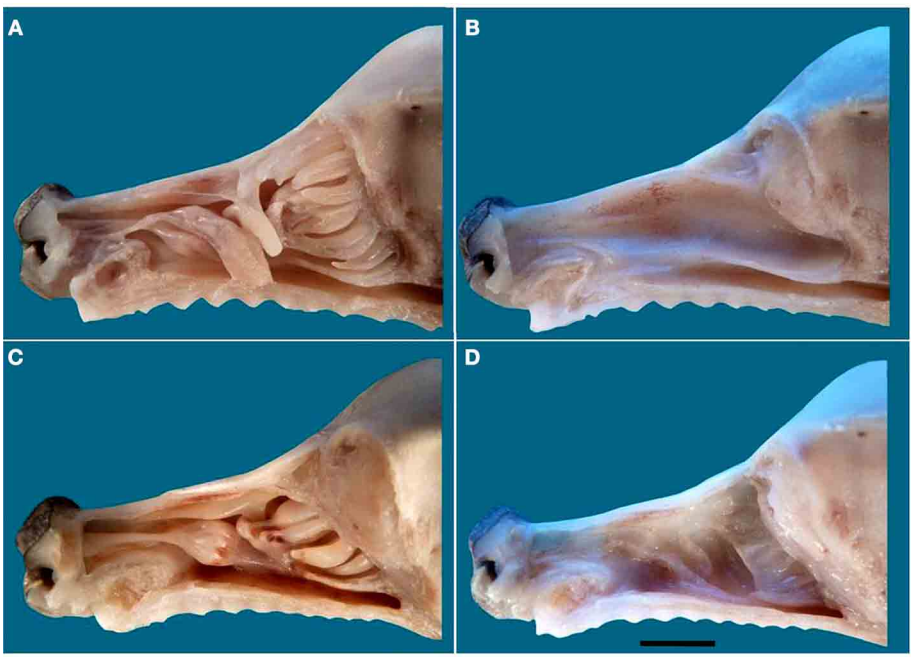

FIGURE 7 | The nasal cavity of the newborn dog. (A) Lateral view of the turbinate complex. **(B)** Lateral view of the nasal septum. **(C)** Medial view of the turbinate complex. **(D)** Medial view of the lateral wall. Scale bar: 1 cm (see Figure S7).

canine nasal cavity. Contrary to such frequently made assertions as that "the mammalian nose contains several distinct chemosensory organs, including the... MOE, the... VNO and the SO" (Tian and Ma, 2004), the SO, though present in marsupials, and in mice, rats, and rabbits, is absent from the ferret and the cat as well as the dog, (though reportedly present in fetal cat) (Breipohl et al., 1983; Kociánová et al., 2006; Ma, 2010). Similarly, statements to the effect that Grüneberg found the GG "in all mammals examined, including humans" (Tian and Ma, 2004) ignore the fact that he actually reported definitely observing it in only three of the 13 species he studied: mouse, rat, and hamster (Grüneberg, 1973). In four species (squirrel, guinea pig, shrew, and tarsier—note the two rodents) it seemed to be absent; and in the remaining six, including *Homo sapiens*, its presence was uncertain. Furthermore, he only studied two species as adults (mouse and shrew) and three more as newborns (rat, mole, and guinea-pig); all his other specimens were embryos or fetuses, and he specifically suggested that in many species the ganglion, though possibly present in these early stages, may regress during prenatal development—a process he definitely asserted of the raccoon on the basis of examination of four fetal stages.

That the dog lacks two of the olfactory epithelia of the mouse (SO and GG), and has an apparently less complex form of a third (the VNsE), may seem surprising in view of its notoriously macrosmatic nature. It may be the case that the larger size of the canine nasal cavity allows physical separation to play a larger part in the dog's discrimination among odors than is possible in the mouse (Schoenfeld and Cleland, 2005); in this respect, it must be borne in mind that our dogs were mainly German Shepherds or of German Shepherd descent, so the possibility that the SO and GG may be present in other breeds cannot be absolutely ruled out. Another possibility is that in spite of the sensitivity of the dog's sense of smell, and its ability to learn to detect unfamiliar substances by olfaction, its lifestyle prior to its domestication some 15,000 years ago (Leonard et al., 2002; Savolainen et al., 2002) required recognition of a smaller range of olfactory cues than did that of the mouse. In this regard, the dog is reported to have 811 functional olfactory receptor genes as against the 1035 of the mouse (Shi and Zhang, 2009; Niimura, 2012).

Since its domestication, the dog has of course been the object of intensive artificial selection processes that have variously pursued the enhancement of morphological, behavioral and physiological traits (regarding the mechanistic differences among these different types of modification, see Carroll, 2005, 2008; Liao et al., 2010). Creating the approximately 400 breeds of dog now estimated to exist (American Kennel Club, 2006) has altered the genome and its realization in many ways (Wayne and von Holdt, 2012), it is commonly thought that dogs collectively exhibit greater morphological variation than any other land mammal (Ostrander, 2012), and these alterations have been vigorously investigated, especially since the publication of the genome (Lindblad-Toh et al., 2005). Most of these studies have concerned the morphological traits that define breeds—body size, coat, leg length, and width, skull shape, etc. (Boyko et al., 2010; Parker et al., 2010; Schoenebeck and Ostrander, 2013), but others have addressed olfactory receptor genes, finding both marked uniformity at the gene family level, and significant variation at lower levels (Issel-Tarver and Rine, 1996; Olender et al., 2004;

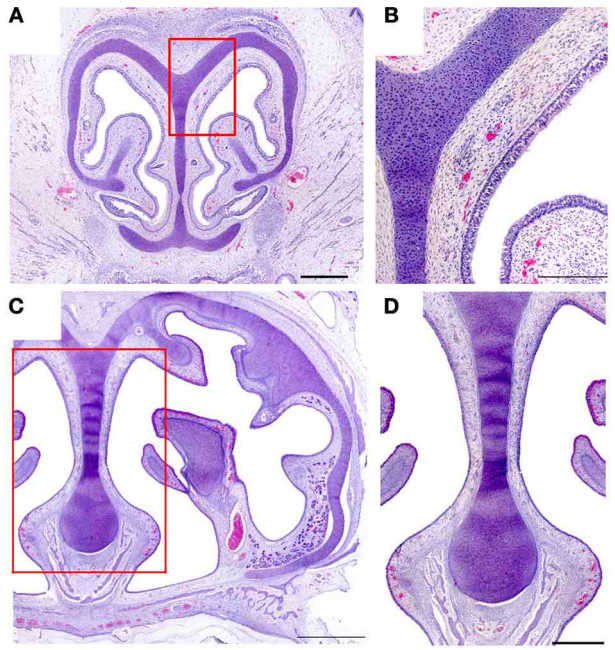

FIGURE 8 | Hematoxylin-eosin-stained transverse sections of the nasal cavity of a newborn, at the levels corresponding to the murine ganglion of Grüneberg (A) and septal organ (C). (B,D) Details of **(A,C)**, respectively. Scale bars: **(A)** 500 μm; **(B)** 250 μm; **(C)** 1000 μm; **(D)** 500 μm.

Tacher et al., 2005; Robin et al., 2009; Chen et al., 2012; Derrien et al., 2012; Quignon et al., 2012). This pattern suggests that our main results—the absence of SO, GG, and a VR2-based vomeronasal subsystem—seem likely to be generalizable to breeds other than German Shepherds, but confirmation is required. Light would also be thrown on this issue by a study of wolves to determine whether the absence of these subsystems is a result of domestication.

In the study of olfaction, as in other fields (Karlsson and Lindblad-Toh, 2008), the dog is proving to be a mine of information, and is leading to a much more balanced view of the mammalian olfactory system than was promoted by exclusive attention to the mouse model.

AUTHOR CONTRIBUTIONS

Ignacio Salazar designed the research and wrote the paper. Arthur W. Barrios, and Pablo Sánchez-Quinteiro performed the work. Arthur W. Barrios, Pablo Sánchez-Quinteiro, and Ignacio Salazar analyzed and discussed the data.

ACKNOWLEDGMENTS

We thank all the colleagues who participated in this work, especially to J. Rodriguez and L. Avedillo; J. Castiñeira for technical assistance; and I. C. Coleman for revising the final English version. Arthur W. Barrios thanks the Spanish Ministry of Foreign Affairs for an MAEC-AECID grant. Private financial support is gratefully acknowledged. We regret that we were not able to cite all of the papers that have contributed to this field.

SUPPLEMENTARY MATERIAL

The Supplementary Material for this article can be found online at: http://www.frontiersin.org/journal/10.3389/fnana.2014.00106/abstract

REFERENCES

Adams, D. R., and Hotchkiss, D. K. (1983). The canine nasal mucosa. *Anat. Histol. Embryol.* 12, 109–125. doi: 10.1111/j.1439-0264.1983.tb01008.x

American Kennel Club. (2006). *The Complete Dog Book*, *20th Edn*. New York, NY: Random House Publishing Group.

Barrios, W. A., Nuñez, G., Sánchez-Quinteiro, P., and Salazar, I. (2014). Anatomy, histochemistry and immunohistochemistry of the olfactory subsystems in mice. *Front. Neuroanat*. 8:63. doi: 10.3389/fnana.2014.00063

Bock, P., Rohn, K., Beineke, A., Baumgärtner, W., and Wewetzer, K. (2009). Site-specific population dynamics and variable olfactory marker protein expression in the postnatal canine olfactory epithelium. *J. Anat.* 215, 522–535. doi: 10.1111/j.1469-7580.2009.01147.x

Boyko, A. R., Quignon, P., Li, L., Schoenebeck, J. J., Degenhardt, J. D., Lohmueller, K. E., et al. (2010). A simple genetic architecture underlies morphological variation in dogs. *PLoS Biol.* 8:e1000451. doi: 10.1371/journal.pbio.1000451

Breer, H., Fleischer, J., and Strotmann, J. (2006). The sense of smell: multiple olfactory subsystems. *Cell. Mol. Life Sci.* 63, 1465–1475. doi: 10.1007/s00018-006-6108-5

Breipohl, W., Naguro, T., and Miragall, F. (1983). Morphology of the Masera organ in NMRI mice (combined morphometric, freeze-fracture, light- and scanning electron microscopic investigations). *Verh. Anat. Ges.* 77, 741–743.

Carroll, S. B. (2005). Evolution at two levels: on genes and form. *PLoS Biol.* 3:e245. doi: 10.1371/journal.pbio.0030245

Carroll, S. B. (2008). Evo-devo and an expanding evolutionary synthesis: a genetic theory of morphological evolution. *Cell* 134, 25–36. doi: 10.1016/j.cell.2008.06.030

Chen, R., Irwin, D. M., and Zhang, Y-P. (2012). Differences in selection drive olfactory receptor genes in different directions in dogs and wolf. *Mol. Biol. Evol*. 29, 3475–3484. doi: 10.1093/molbev/mss153

Craven, B. A., Neuberger, T., Paterson, E. G., Webb, A. G., Josephson, E. M., Morrison, E. E., et al. (2007). Reconstruction and morphometric analysis of the nasal airway of the dog (Canis familiaris) and implications regarding olfactory airflow. *Anat. Rec.* 290, 1325–1340. doi: 10.1002/ar.20592

Craven, B. A., Paterson, E. G., and Settles, G. S. (2010). The fluid dynamics of canine olfaction: unique nasal airflow patterns as an explanation of macrosmia. *J. R. Soc. Interface* 7, 933–943. doi: 10.1098/rsif.2009.0490

Derrien, T., Vaysse, A., André, C., and Hitte, C. (2012). Annotation of the domestic dog genome sequence: finding the missing genes. *Mamm. Genome* 23, 57–74. doi: 10.1007/s00335-011-9372-0

Graeger, K. (1958). Die Nasenhöhle und die Nasennebenhöhlen beim Hund unter Besonderer Berücksichtigung der Siebbeinmuscheln. *Dtsch. Tierärztl. Wschr.* 65, 425–429.

Granger, N., Blamires, H., Franklin, R. J., and Jeffery, N. D. (2012). Autologous olfactory mucosal cell transplants in clinical spinal cord injury: a randomized double-blinded trial in a canine translational model. *Brain* 135, 3227–3237. doi: 10.1093/brain/aws268

Graziadei, P. P., and Monti-Graziadei, G. A. (1979). Neurogenesis and neuron regeneration in the olfactory system of mammals. I. Morphological aspects of differentiation and structural organization of the olfactory sensory neurons. *J. Neurocytol.* 8, 1–18. doi: 10.1007/BF01206454

Grüneberg, H. (1973). A ganglion probably belonging to the N. Terminalis system in the nasal mucosa of the mouse. *Z. Anat. Entwicklungsgesch.* 140, 39–52. doi: 10.1007/BF00520716

Ishii, T., and Mombaerts, P. (2011). Coordinated coexpression of two vomeronasal receptor V2R genes per neuron in the mouse. *Mol. Cell. Neurosci.* 46, 397–408. doi: 10.1016/j.mcn.2010.11.002

Issel-Tarver, L., and Rine, J. (1996). Organization and expression of canine olfactory receptor genes. *Proc. Natl. Acad. Sci. U.S.A.* 93, 10897–10902. doi: 10.1073/pnas.93.20.10897

Karlsson, E. K., and Lindblad-Toh, K. (2008). Leader of the pack: gene mapping in dogs and other model organisms. *Nat. Rev. Genet.* 9, 713–725. doi: 10.1038/nrg2382

Kavoi, B., Makanya, A., Hassanali, J., Carlsson, H. E., and Kiama, S. (2010). Comparative functional structure of the olfactory mucosa in the domestic dog and sheep. *Ann. Anat.* 192, 329–337. doi: 10.1016/j.aanat.2010.07.004

Kociánová, I., Gorošová, A., Tichý, F., Čížek, P., and Machálka, M. (2006). Structure of Masera's septal olfactory organ in cat (*Felix silvestris* f. *catus)*. Light microscopy in selected stages of ontogeny. *Acta Vet. Brno* 75, 471–475. doi: 10.2754/avb200675040471

Lauruschkus, N. (1942). Über Riechfeldgrösse und Riechfeldkoeffizient bei einigen Hunderassen und der Katze. *Arch. Tierheilk.* 77, 473–497.

Leonard, J. A., Wayne, R. K., Wheeler, J., Valadez, R., Guillen, S., and Vila, C. (2002). Ancient DNA evidence for old world origin of new world dogs. *Science* 298, 1613–1616. doi: 10.1126/science.1076980

Liao, B-Y., Weng, M-P., and Zhang, J. (2010). Contrasting genetic paths to morphological and physiological evolution. *Proc. Natl. Acad. Sci. U.S.A.* 107, 7353–7358. doi: 10.1073/pnas.0910339107

Lindblad-Toh, K., Wade, C. M., Mikkelsen, T. S., Karlsson, E. K., Jaffe, D. B., Kamal, M., et al. (2005). Genome sequence, comparative analysis and haplotype structure of the domestic dog. *Nature* 438, 803–819. doi: 10.1038/nature04338

Ma, M. (2010). "Multiple olfactory subsystems convey various sensory signals," in *The Neurobiology of Olfaction*, chapter 9, ed A. Menini (Boca Raton, FL: CRC Press), 1–20.

Mason, S. L., Maddox, T. W., Lillis, S. M., and Blackwood, L. (2013). Late presentation of canine nasal tumours in a UK referral hospital and treatment outcomes. *J. Small Anim. Pract.* 54, 347–353. doi: 10.1111/jsap.12083

McEntee, M. C. (2004). "Neoplasms of the nasal cavity," in *Respiratory Disease in Dogs and Cats*, ed L. G. King (Philadelphia, PA: Saunders), 293–301. doi: 10.1016/B978-0-7216-8706-3.50041-4

Müller, A. (1955). Quantitative studies on olfactory epithelium of dogs. *Z. Zellforsch. Mikrosk. Anat.* 41, 335–350. doi: 10.1007/BF00340605

Munger, S. D., Leinders-Zufall, T., and Zufall, F. (2009). Subsystems organization of the mammalian sense of smell. *Annu. Rev. Physiol.* 71, 115–140. doi: 10.1146/annurev.physiol.70.113006.100608

Neuhaus, W. (1955). Die Form der Riechzellen des Hundes. *Naturwissenschaften* 42, 374–375. doi: 10.1007/BF00629028

Niimura, Y. (2012). Olfactory receptor multigene family in vertebrates: from the viewpoint of evolutionary genomics. *Curr. Genomics* 13, 103–114. doi: 10.2174/138920212799860706

Olender, T., Fuchs, T., Linhart, C., Shamir, R., Adams, M., Kalush, F., et al. (2004). The canine olfactory subgenome. *Genomics* 83, 361–372. doi: 10.1016/j.ygeno.2003.08.009

Ostrander, E. A. (2012). Introduction [to the special issue on advances in the canine system for genetic studies]. *Mamm. Genome* 23, 1–2. doi: 10.1007/s00335-012-9389-z

Paigen, K. (1995). A miracle enough: the power of mice. *Nat. Med.* 1, 215–220. doi: 10.1038/nm0395-215

Parker, H. G., Shearin, A. L., and Ostrander, E. A. (2010). Man's best friend becomes biology's best in show: genome analyses in the domestic dog. *Annu. Rev. Genet.* 44, 309–336. doi: 10.1146/annurev-genet-102808-115200

Quignon, P., Rimbault, M., Robin, S., and Galibert, F. (2012). Genetics of canine olfaction and receptor diversity. *Mamm. Genome* 23, 132–143. doi: 10.1007/s00335-011-9371-1

Robin, S., Tacher, S., Rimbault, M., Vaysse, A., Dréano, S., André, C., et al. (2009). Genetic diversity of canine olfactory receptors. *BMC Genomics* 10:21. doi: 10.1186/1471-2164-10-21

Salazar, I., Cifuentes, J. M., and Sánchez-Quinteiro, P. (2013). Morphological and immunohistochemical features of the vomeronasal system in dogs. *Anat. Rec.* 296, 146–155. doi: 10.1002/ar.22617

Salazar, I., and Sánchez-Quinteiro, P. (2009). The risk of extrapolation in neuroanatomy: the case of the mammalian vomeronasal system. *Front. Neuroanat.* 3:22. doi: 10.3389/neuro.05.022.2009

Savolainen, P., Zhang, Y. P., Luo, J., Lundeberg, J., and Leitner, T. (2002). Genetic evidence for an East Asian origin of domestic dogs. *Science* 298, 1610–1613. doi: 10.1126/science.1073906

Schoenebeck, J. J., and Ostrander, E. A. (2013). The genetic of canine skull shape variation. *Genetics* 193, 317–325. doi: 10.1534/genetics.112.145284

Schoenfeld, T. A., and Cleland, T. A. (2005). The anatomical logic of smell. *Trends Neurosci.* 28, 620–627. doi: 10.1016/j.tins.2005.09.005

Shi, P., and Zhang, J. (2009). Extraordinary diversity of chemosensory receptor gene repertoires among vertebrates. *Results Probl. Cell Differ.* 47, 1–23. doi: 10.1007/400_2008_4

Tacher, S., Quignon, P., Rimbault, M., Dreano, S., Andre, C., and Galibert, F. (2005). Olfactory receptor sequence polymorphism within and between breeds of dogs. *J. Hered.* 96, 812–816. doi: 10.1093/jhered/esi113

Tian, H., and Ma, M. (2004). Molecular organization of the olfactory septal organ. *J. Neurosci.* 24, 8383–8390. doi: 10.1523/JNEUROSCI.2222-04.2004

Turek, M. M., and Lana, S. E. (2012). "Canine nasosinal tumors," in *Small Animal Clinical Oncology*, eds S. J. Withrow and D. M. Vail (St. Louis, MO: Saunders), 525–540.

Wayne, R. K., and von Holdt, B. M. (2012). Evolutionary genomics of dog domestication. *Mamm. Genome* 23, 3–18. doi: 10.1007/s00335-011-9386-7

Young, J. M., and Trask, B. J. (2007). V2R gene families degenerated in primates, dog and cow, but expanded in opossum. *Trends Genet.* 23, 212–215. doi: 10.1016/j.tig.2007.03.004

Conflict of Interest Statement: The authors declare that the research was conducted in the absence of any commercial or financial relationships that could be construed as a potential conflict of interest.

Received: 30 June 2014; accepted: 09 September 2014; published online: 25 September 2014.

Citation: Barrios AW, Sánchez-Quinteiro P and Salazar I (2014) Dog and mouse: toward a balanced view of the mammalian olfactory system. Front. Neuroanat. ***8****:106. doi: 10.3389/fnana.2014.00106*

This article was submitted to the journal Frontiers in Neuroanatomy.

frontiers in
NEUROANATOMY

ORIGINAL RESEARCH ARTICLE
published: 27 August 2014
doi: 10.3389/fnana.2014.00087

Morphological and physiological species-dependent characteristics of the rodent Grueneberg ganglion

Julien Brechbühl, Magali Klaey, Fabian Moine, Esther Bovay, Nicolas Hurni, Monique Nenniger-Tosato and Marie-Christine Broillet*

Department of Pharmacology and Toxicology, Faculty of Biology and Medicine, University of Lausanne, Switzerland

Edited by:
Ignacio Salazar, University of Santiago de Compostela, Spain

Reviewed by:
Charles A. Greer, Yale University School of Medicine, USA
Joerg Fleischer, Universität Hohenheim, Germany

***Correspondence:**
Marie-Christine Broillet, Department of Pharmacology and Toxicology, Faculty of Biology and Medicine, University of Lausanne, Bugnon 27, CH-1005 Lausanne, Switzerland
e-mail: mbroille@unil.ch

In the mouse, the Grueneberg ganglion (GG) is an olfactory subsystem implicated both in chemo- and thermo-sensing. It is specifically involved in the recognition of volatile danger cues such as alarm pheromones and structurally-related predator scents. No evidence for these GG sensory functions has been reported yet in other rodent species. In this study, we used a combination of histological and physiological techniques to verify the presence of a GG and investigate its function in the rat, hamster, and gerbil comparing with the mouse. By scanning electron microscopy (SEM) and transmitted electron microscopy (TEM), we found isolated or groups of large GG cells of different shapes that in spite of their gross anatomical similarities, display important structural differences between species. We performed a comparative and morphological study focusing on the conserved olfactory features of these cells. We found fine ciliary processes, mostly wrapped in ensheating glial cells, in variable number of clusters deeply invaginated in the neuronal soma. Interestingly, the glial wrapping, the amount of microtubules and their distribution in the ciliary processes were different between rodents. Using immunohistochemistry, we were able to detect the expression of known GG proteins, such as the membrane guanylyl cyclase G and the cyclic nucleotide-gated channel A3. Both the expression and the subcellular localization of these signaling proteins were found to be species-dependent. Calcium imaging experiments on acute tissue slice preparations from rodent GG demonstrated that the chemo- and thermo-evoked neuronal responses were different between species. Thus, GG neurons from mice and rats displayed both chemo- and thermo-sensing, while hamsters and gerbils showed profound differences in their sensitivities. We suggest that the integrative comparison between the structural morphologies, the sensory properties, and the ethological contexts supports species-dependent GG features prompted by the environmental pressure.

Keywords: olfactory subsystem, Grueneberg ganglion, rodent, electron microscopy, calcium imaging, chemo-sensitivity, thermo-sensitivity, alarm pheromone

INTRODUCTION

In the nasal cavities of the mouse, close to the opening of the nares, a ganglion structure of unknown function was found in 1973 (Grüneberg, 1973). It was described as a heterogenic and compact structure situated between large blood vessels (BV). Histological investigations performed at the time allowed the identification of similar ganglion structures in other mammalian species (Grüneberg, 1973; Tachibana et al., 1990). It was rediscovered in 2005 (Fuss et al., 2005; Koos and Fraser, 2005; Fleischer et al., 2006a; Roppolo et al., 2006; Storan and Key, 2006) during inspection of whole-mount specimens from a particular gene-targeted OMP-GFP (olfactory marker protein-green fluorescent protein) mouse in which all mature olfactory neurons express GFP as a histological reporter under the control of the OMP promoter (Margolis, 1972; Mombaerts et al., 1996; Potter et al., 2001). This structure was further referred to as the Grüneberg ganglion or Grueneberg ganglion (GG) according to its first description (Grüneberg, 1973). The GG of OMP-GFP mice was found to start developing around embryonic day 16 and to be composed of two different cell types, neurons and glial cells. It appeared to be complete at birth and to persist throughout the mouse life (Fuss et al., 2005; Koos and Fraser, 2005; Fleischer et al., 2006a; Roppolo et al., 2006; Storan and Key, 2006; Brechbühl et al., 2008; Liu et al., 2009). Its localization in a water permeant epithelium that lacks direct contact with the nasal cavity and its general morphological aspect were further compared with the amphid neurons of the nematode *Caenorhabditis elegans* (*C. elegans*) (Brechbühl et al., 2008, 2013a) which respond both to chemo- and thermo-stimuli. The olfactory function of the GG was supported in the mouse by the expression of putative olfactory receptors (Fleischer et al., 2006b, 2007); the presence of numerous cilia (Brechbühl et al., 2008; Liu et al., 2009) and the direct connections to the necklace complex of the olfactory bulb of the brain (Koos and Fraser, 2005; Roppolo et al., 2006; Matsuo et al., 2012). Recently, we found the mouse GG to be involved in the recognition of volatile danger

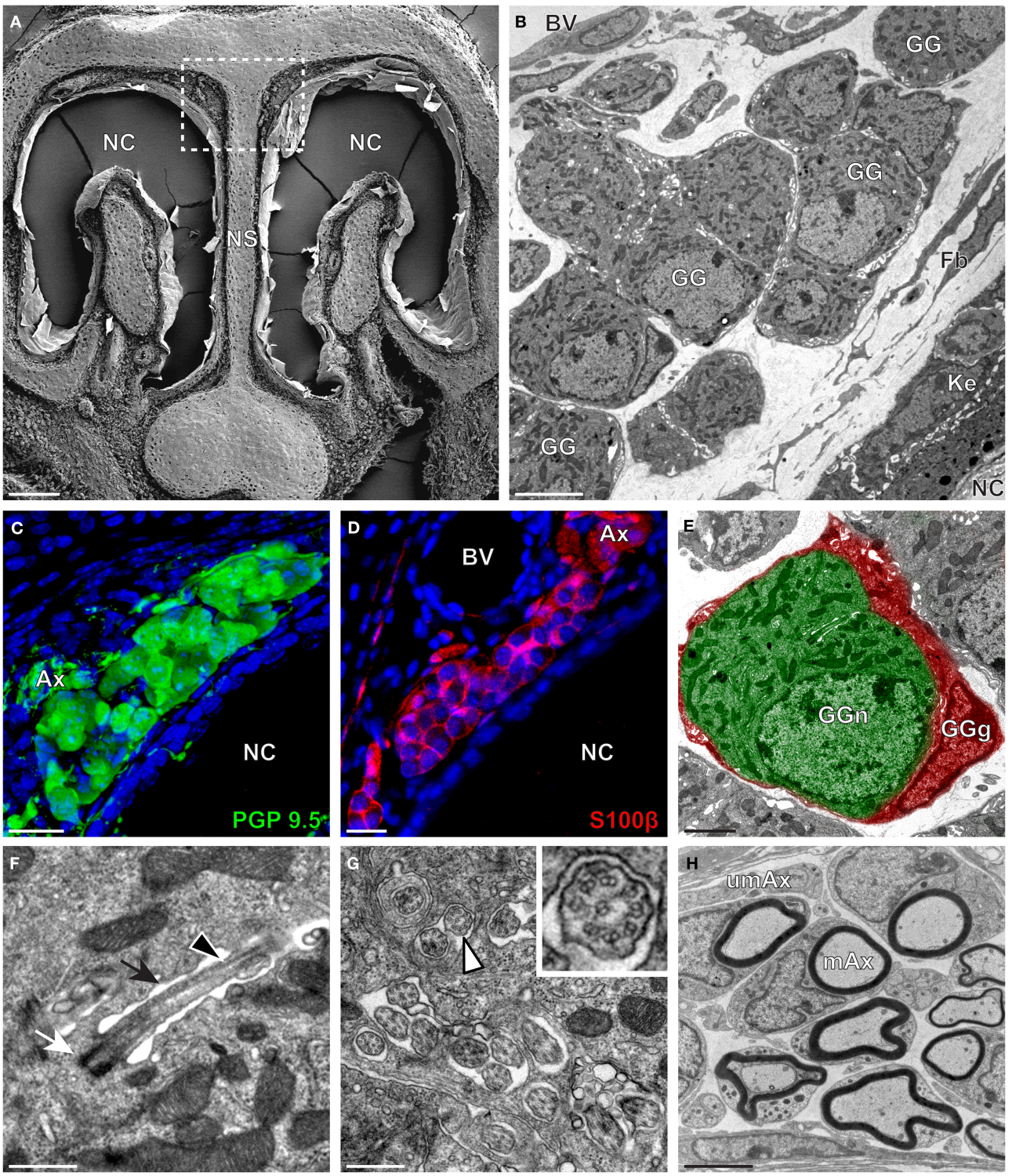

FIGURE 1 | Morphology and ultrastructural features of mouse GG. (A) General SEM view of a coronal slice performed in a mouse (P26) GG region. The nasal septum (NS) and the nasal cavities (NC) are shown. The white dashed rectangle highlights the GG region. **(B)** TEM observation of a group of mouse (P6) GG cells. The presence of a meshwork of fibroblasts (Fb) and a keratinized epithelium (Ke) separating the GG neurons from the NC, as well as the proximity of a blood vessel (BV) can be observed. **(C,D)** Immunohistochemistry observations demonstrating the presence of both neuronal (**C**, PGP 9.5 in green, P1) and glial cells (**D**, slice view of S100β in red, P17) in the mouse GG. **(E)** High power pseudocolorized TEM view of one mouse (P6) GG neuron (GGn, in green) completely wrapped in a GG glial cell (GGg, in red). **(F,G)** Ultrastructural TEM view of mouse GGn cilia.

FIGURE 1 | Continued
(F) Sagittal observation of one mouse (P6) GGn ciliary process with its basal body (white arrow) corresponding to the beginning of the cilium as well as part of its long axoneme (black arrowhead). The GGn cell membrane (black arrow) shows the invagination of the cilium. **(G)** Coronal observation of a group of deeply invaginated mouse (P15) GGn cilia. A zoomed view of a single cilium (white arrowhead) shows the distribution of the microtubular doublets (corresponding in mouse to 8 + 1 or 9 + 0). **(H)** Coronal section of a mouse (P15) GG axonal nerve bundles (Ax). Myelinated (mAx) and unmyelinated (umAx) fibers were observed. SEM, scanning electron microscopy; TEM, transmitted electron microscopy. A minimum of 3 animals (from P1 to P31) and 6 slices per conditions were used and observed for each SEM, TEM or immunohistochemistry observations. **(C,D)** Nuclei are shown in blue (DAPI counterstain). Scale bars are 100 μm in **(A)**, 5 μm in **(B)**, 20 μm in **(C,D)**, 2 μm **(E)**, 0.5 μm in **(F,G)**, and 3 μm in **(H)**

Table 1 | Morphological characteristics of the rodent GG.

Animal	General morphology			Ciliary processes per GGn			GG nerve
	GGn shape	Size of GGn [μm]	GGg/GGn	Nb of cilia	Diameter [nm]	Microtubular structures	GG axonal bundles
Mouse	Round-ovoid	9–14	1/(1–2)	(2–3) × (5–15)	150–250	(8 + 1); (9 + 0)	Myelinated ≅ Unmyelinated
Rat	Round	11–17	(1–2)/1	1 × (15–30)	200–300	(8 + 1); (9 + 0)	Myelinated ≅ Unmyelinated
Hamster	Flat-ovoid	12–18	1/1	(1–2) × (5–15)	150–300	(8 + 1); (9 + 0); (>9 + 0)	Myelinated > Unmyelinated
Gerbil	Ovoid	11–17	1/(2–3)	(1–3) × (10–15)	100–200	(8 + 1); (9 + 0)	Myelinated < Unmyelinated

Comparative table of the main morphological features observed in the GG of mouse, rat, hamster, and gerbil. For the general morphology, the size of each GG neuron as well as the ratio between the number of GG glial cells and the number of GG neurons are indicated (GGg/GGn). For the ciliary processes, the number of cilia per GG neuron [(n cluster) × (n cilia per cluster)], the diameter and the microtubular distribution (peripheral microtubular doublet + central microtubular doublet) are indicated. For the GG nerve, the proportion of myelinated and unmyelinated axonal bundles is listed (≅, > or <). GGn, Grueneberg ganglion neuron; GGg, Grueneberg ganglion glial cell. For each animal species and morphological criteria, a minimum of 45 GGn groups was observed.

cues such as mouse alarm pheromones and other structurally-related molecules found in predator scents (Brechbühl et al., 2008, 2013b). Different technical approaches demonstrated that both chemo- and thermo-stimuli could initiate neuronal responses in the mouse GG (Brechbühl et al., 2008, 2013a; Mamasuew et al., 2008, 2011a; Schmid et al., 2010) partially using cyclic guanosine monophosphate (cGMP)-dependent pathways (Fleischer et al., 2009; Liu et al., 2009; Mamasuew et al., 2010, 2011b; Schmid et al., 2010; Brechbühl et al., 2013a; Hanke et al., 2013; Stebe et al., 2013).

To our knowledge no evidence for the multisensory functions observed in the mouse GG has been reported yet in other rodent species. We here investigated and confirmed by ultrastructural and immunohistochemical approaches the presence of a GG in the rat, hamster, and gerbil. Their olfactory features were compared with those observed in the mouse. We found that both the morphology and the physiological responses, measured by calcium imaging experiments, were different between the investigated rodent species. Thus, chemo- and thermo-evoked neuronal responses were correlated with the structural morphology and with the signaling proteins expressed. Similar chemo- and thermo-responses were observed in mouse and rat GG neurons, while in the hamster and gerbil profound sensitivity differences existed. We thus propose that the environmental and evolutionary pressure could explain the interspecies sensitivities displayed by the rodential Grueneberg ganglia.

MATERIALS AND METHODS

ANIMALS AND TISSUE PREPARATION

Adults and pups C57BL/6J mice (*Mus musculus*), Wistar rats (*Rattus norvegicus*), Golden hamsters (*Mesocricetus auratus*), and Mongolian gerbils (*Meriones unguiculatus*) were used for experimental investigations and were ordered from Janvier Labs. Postnatal day is indicated as (P). Animals were euthanized by CO_2 or cervical dislocation. Animal care was in accordance with the Swiss legislation and the veterinary authorities. Nasal cavities were prepared in ice-cold artificial cerebrospinal fluid (ACSF; 118 mM NaCl, 25 mM $NaHCO_3$, 10 mM D-glucose, 2 mM KCl, 2 mM $MgCl_2$, 1.2 mM NaH_2PO_4, and 2 mM $CaCl_2$, pH 7.4) saturated with oxycarbon gas [95% O_2: 5% CO_2; (vol/vol)] under a dissecting microscope set-up (M165 FC; Leica).

SCANNING AND TRANSMITTED ELECTRON MICROSCOPY OBSERVATIONS

For scanning electron microscopy (SEM) and transmitted electron microscopy (TEM) procedures, coronal sections from GG regions were prepared according to Brechbühl et al. (2008). Briefly, animals were anesthetized with intraperitoneal injections of sodium pentobarbital. After fixation steps with 2% paraformaldehyde (PAF 2%; #158127, Sigma), 2.5% glutaraldehyde (Glut 2.5%; #16220, Electron Microscopy Sciences) in phosphate buffered saline (PBS; 138 mM NaCl, 2.7 mM KCl, 1.76 mM KH_2PO_4, and 10.0 mM Na_2HPO_4, pH 7.4), animal heads were delicately dissected and placed overnight in the same fixative solution at 4°C. They were then briefly rinsed in PBS, included in 5% agar (#A7002, Sigma) and fixed vertically with Roti® coll 1 cyanacrylat glue (#0258.1, Carl Roth) onto the holder of the vibroslicer (VT1200 S, Leica). 80–200 μm coronal sections were obtained and collected in 0.1 M cacodylate buffer (#20840, Sigma). These slices could be then used for SEM or TEM preparations. For SEM processing, selected sections were fixed in 0.2 M cacodylate buffer containing Glut 2.0% overnight at 4°C. After washing phases, samples were dehydrated at room

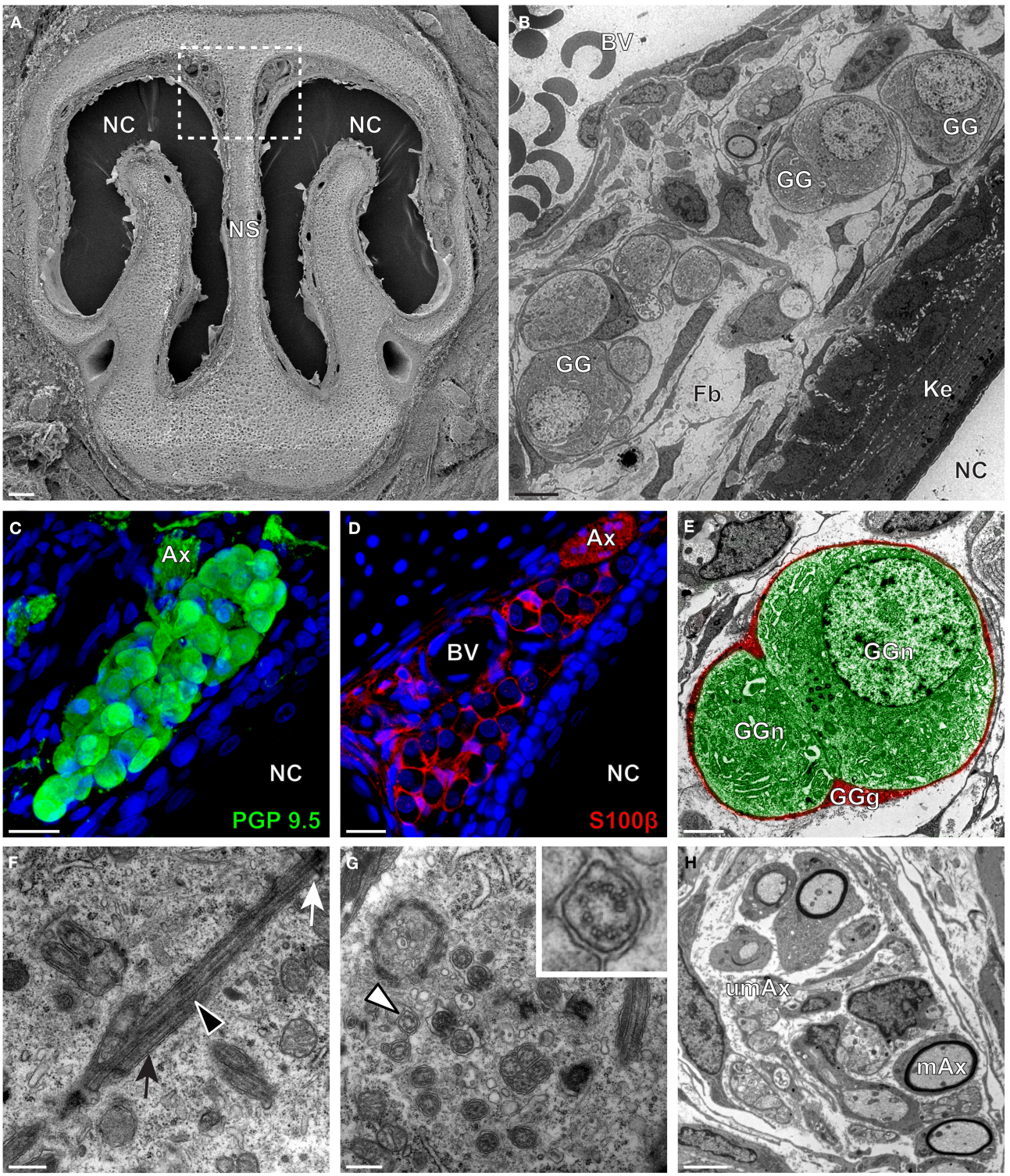

FIGURE 2 | Morphology and ultrastructural features of rat GG. (A) General SEM view of a coronal slice performed in a rat (P7) GG region. The nasal septum (NS) and the nasal cavities (NC) are shown. The white dashed rectangle highlights the GG region. **(B)** TEM observation of a group of rat (P7) GG cells. The presence of a meshwork of fibroblasts (Fb) and a keratinized epithelium (Ke) separating the GG neurons from the NC, as well as the proximity of a blood vessel (BV) can be observed. **(C,D)** Immunohistochemistry observations demonstrating the presence of both neuronal (**C**, PGP 9.5 in green, P1) and glial cells (**D**, slice view of S100β in red, P18) in the rat GG. **(E)** High power pseudocolorized TEM view of one rat (P7) GG neuron (GGn, in green) completely wrapped in a GG glial cell (GGg, in red). **(F,G)** Ultrastructural TEM view of rat GGn cilia.

FIGURE 2 | Continued
(F) Sagittal observation of one rat (P7) GGn ciliary process with its basal body (white arrow) corresponding to the beginning of the cilium as well as part of its long axoneme (black arrowhead). The GGn cell membrane (black arrow) shows the invagination of the cilium. **(G)** Coronal observation of a group of deeply invaginated rat (P7) GGn cilia. A zoomed view of a single cilium (white arrowhead) shows the distribution of the microtubular doublets (corresponding in rat to $8+1$ or $9+0$). **(H)** Coronal section of a rat (P7) GG axonal nerve bundles (Ax). Myelinated (mAx) and (umAx) unmyelinated fibers were observed. SEM, scanning electron microscopy; TEM, transmitted electron microscopy. A minimum of 3 animals (from P1 to P24) and 6 slices per conditions were used and observed for each SEM, TEM, or immunohistochemistry observations. **(C,D)** Nuclei are shown in blue (DAPI counterstain). Scale bars are 100 μm in **(A)**, 5 μm in **(B)**, 20 μm in **(C,D)**, 2 μm **(E)**, 0.5 μm in **(F,G)** and 3 μm in **(H)**.

temperature (RT; corresponded to 23–25°C) using increasing alcohol concentrations and dried by the critical point method. Finally, they were mounted on aluminum stubs, coated with platinum (12 nm) and examined with a scanning electron microscope (JSM-6300F, JEOL) operated at 5 to 15 kV accelerating voltage. For TEM processing, selected sections were placed in 1% osmium tetroxide in 0.1 M cacodylate buffer for 60 min at RT and then washed with distilled water. They were then transferred for 30 min of staining in 1% uranyl acetate and washed with distilled water. Sections were dehydrated in graded alcohol series and placed in propylene oxide. Embedding procedures were done in EPON®-DMP30 resin further replaced by fresh Durcapan® on glass slides and placed in an oven for 48 h at 65°C. 50–70 nm ultra-thin sections were prepared and membrane contrast was obtained by lead-citrate. Observations were made on a TEM microscope (CM 100 EDX, Philips).

IMMUNOHISTOCHEMISTRY

The floating immunohistochemistry procedure used was from Brechbühl et al. (2013a). Briefly, the tips of noses were transferred and dissected in PBS before being fixed in PAF 4% at 4°C for 3 h. Fixed tissue preparations were embedded in 5% agar (#A7002, Sigma) and 60-120 μm coronal sections were cut and collected in PBS. Slices were then blocked overnight at 4°C in a PBS solution containing 10% normal goat serum (NGS; #UP379030, Interchim) and 0.5% Triton® X-100 (#93420, Sigma). Primary antibodies were applied to the slices for 16 h at RT in NGS 5%, Triton® X-100 0.25%. Slices were washed in NGS 2% before incubation in the dark with the secondary antibody in NGS 2% for 1 h at RT. Finally, slices were washed and mounted in Vectashield® mounting medium (#H-1200, Vector Labs) containing 4′,6-diamidino-2-phenylindole (DAPI; for nuclear counterstaining). The protein gene product 9.5 (PGP 9.5; primary antibody 1:1000, Rabbit, #A01398, GenScript) was used as a neuronal marker. The S100 beta protein (S100β; primary antibody 1:500, Rabbit, #ab41548, Abcam) was used as a glial cell marker. The primary antibodies used for the detection of signaling proteins were for the particulate guanylyl cyclase G (GC-G; 1:300, Rabbit, #PGCG-701AP, FabGennix) and the cyclic nucleotide-gated channel A3 (CNGA3; 1:300, Rabbit, #LS-C14509, Lifespan Bioscience). The secondary antibody used was a Cy3-conjugated AffiniPure anti-Rabbit (Cy3; 1:200, Goat, #111-165-144, Jackson ImmunoResearch). Negative control experiments were performed by omitting primary antibodies and were also used for comparison in case of residual expression. Observations were done with LED-fluorescence microscopy (EVOS® *fl*, AMG) and acquisitions were made by confocal microscopy (SP5, Leica; LSM 710 Quasar, Zeiss) under the 40× objectives. Post-analysis and reconstructions were made with the software Imaris (Bitplane IMARIS 7.1.1).

CALCIUM IMAGING

Calcium imaging experiments were performed on acute tissue slices of GG according to Brechbühl et al. (2008, 2013b). Animals were dissected in fresh ACSF solution at 4°C. The tips of the noses were included in blocks of 4–5% agar at a temperature <41°C and directly placed on ice for solidification. Coronal slices from 60 to 80 μm were cut and collected in ACSF at 4°C with a vibroslicer (VT1200 S, Leica). They were selected under a stereomicroscope (M165 FC, Leica) based on their general morphology, loaded in a solution of 5 μM Fura-2 acetoxymethyl ester (Fura-2AM; #0103, TEFLabs) containing 0.1% of Pluronic® F-127 (#P-6867, Invitrogen) for a minimum of 45 min in an incubator (37°C, 5% CO_2). Slices were placed in a RC-26G bath chamber (#64-0235, Warner Instruments) and immobilized with a slice anchor. Observations were made under an inverted fluorescence microscope (Axiovert 135, Zeiss) with a 25× or 63× objective and a Cool SNAP-HQ camera. A bipolar temperature controller (SC-20/CL-100, Warner instruments) was used to control the bath temperature. The MetaFluor® system (MetaFluor, Visitron Systems) was used to monitor Fura-2AM ratio (F340/380 nm) and to acquire images (Brechbühl et al., 2011).

CHEMOSTIMULATION

The synthetic mouse alarm pheromone 2-*sec*-butyl-4,5-dihydrothiazole (SBT; Brechbühl et al., 2013b) as well as the synthetic rodent predator scents (Apfelbach et al., 2005) 2,4,5-trimethylthiazoline (TMT; #300000368, Contech), 2-propylthietane (2PT; #200000001, Contech) or the 2,3-dimetylpyrazine (Mamasuew et al., 2011a) (DMP; #W327107, Sigma) were used at 100 μM and prepared fresh before each experiment. Solution osmolarities in ACSF were between 285 and 300 Osm/L. A short perfusion of extracellular potassium (KCl; 20 mM) was used as a cellular viability test and was also used to standardize calcium responses. Intracellular calcium changes observed during the perfusion of ACSF were considered as baseline activity and increases twice larger than this baseline (corresponding to 10% of the KCl response) were considered as neuronal responses (Brechbühl et al., 2013b).

STATISTICS

A minimum of 3 animals and 6 slices per conditions were used for each experimental procedure. Values are expressed as mean ± s.e.m.

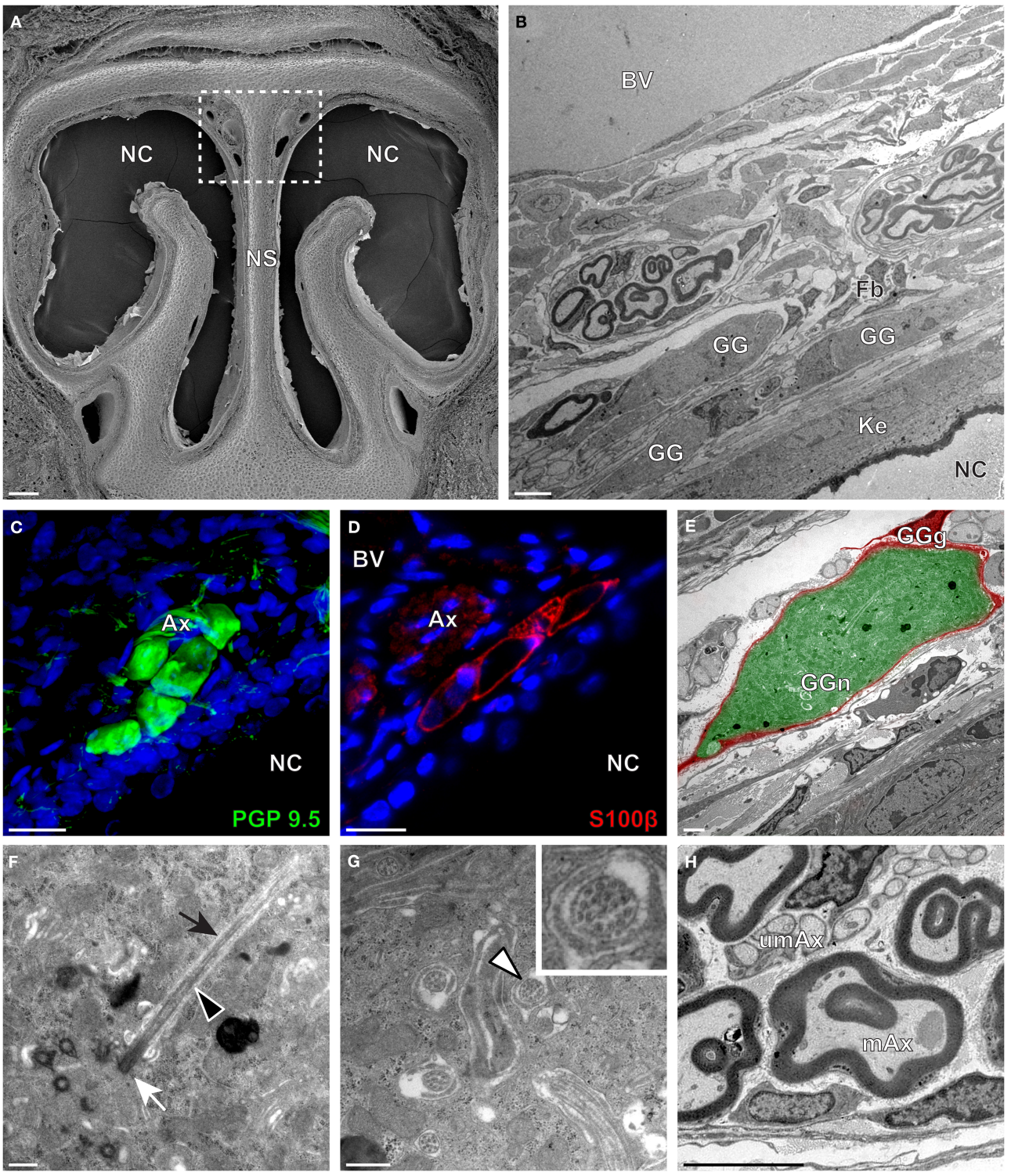

FIGURE 3 | Morphology and ultrastructural features of hamster GG. (A) General SEM view of a coronal slice performed in a hamster (P38) GG region. The nasal septum (NS) and the nasal cavities (NC) are shown. The white dashed rectangle highlights the GG region. **(B)** TEM observation of a group of hamster (P38) GG cells. The presence of a meshwork of fibroblasts (Fb) and a keratinized epithelium (Ke) separating the GG neurons from the NC, as well as the proximity of a large blood vessel (BV) can be observed. **(C,D)** Immunohistochemistry observations demonstrating the presence of both neuronal (**C**, PGP 9.5 in green, P40) and glial cells (**D**, slice view of S100β in red, P30) in the hamster GG. **(E)** High power pseudocolorized TEM view of one hamster (P36) GG neuron (GGn, in green) completely wrapped in a GG glial cell (GGg, in red). **(F,G)** Ultrastructural TEM view of hamster GGn cilia.

FIGURE 3 | Continued
(F) Sagittal observation of one hamster (P36) GGn ciliary process with its basal body (white arrow) corresponding to the beginning of the cilium as well as its long axoneme (black arrowhead). The GGn cell membrane (black arrow) shows the invagination of the cilium. **(G)** Coronal observation of a group of deeply invaginated hamster (P34) GGn cilia. A zoomed view of a single GGn cilium (white arrowhead) shows the particular distribution of the microtubular doublets (corresponding in hamster to $8+1$, $9+0$, or $>9+0$). **(H)** Coronal section of hamster (P38) GG axonal nerve bundles (Ax). A predominance of (mAx) myelinated fibers was observed. SEM, scanning electron microscopy; TEM, transmitted electron microscopy. A minimum of 4 animals (from P6 to P40) and 6 slices per conditions were used and observed for each SEM, TEM, or immunohistochemistry observations. **(C,D)** Nuclei are shown in blue (DAPI counterstain). Scale bars are 100 μm in **(A)**, 5 μm in **(B)**, 20 μm in **(C,D)**, 2 μm **(E)**, 0.5 μm in **(F,G)** and 3 μm in **(H)**.

RESULTS

COMPARATIVE NEUROANATOMY OF RODENTIAL GRUENEBERG GANGLIA REVEALS STRUCTURAL DIFFERENCES

The neuroanatomical structure of the GG was previously described in OMP-GFP transgenic mice (Brechbühl et al., 2008; Liu et al., 2009). Here, we first observed the GG neuroanatomy of non-transgenic C57BL/6J mice (**Figure 1** and **Table 1**) by scanning and transmitted electron microscopy (SEM and TEM, respectively) on coronal sections (**Figures 1A,B**). Morphologically, the GG was lacking direct contact with the nasal cavity (NC). It was situated near large BV and organized in clusters of round-ovoid cells found in fibroblast (Fb) meshworks between the nasal septum (NS) and a keratinized epithelium (Ke). The presence of the two cell populations, GG neurons (GGn) and GG glial cells (GGg), was further identified by immunohistochemistry, using specific neuronal (PGP 9.5; **Figure 1C**) and glial (S100β; **Figure 1D**) markers (Young et al., 2003) and was confirmed by high-power TEM view (**Figure 1E**). Cilia deeply invaginated in the neuronal soma (**Figure 1F**) and organized in discrete clusters with a particular microtubular doublet distribution of [proximal $(8+1)$ or distal $(9+0)$; (peripheral microtubular doublet + central microtubular doublet)] were observed (**Figure 1G**). We could differentiate, based on the high electron-density of the lamellate myelin sheaths wrapping the axonal fibers (Ax), bundles of numerous myelinated (mAx), and/or unmyelinated axons (umAx) emerging from the GG (**Figure 1H**). Thus, we were able to localize and characterize the presence of a GG in a non-transgenic mouse model. It displayed identical morphological features as the ones found in OMP-GFP mice (Brechbühl et al., 2008; Liu et al., 2009).

We then applied these technical approaches to look for the presence of a GG in the rat (**Figure 2**), hamster (**Figure 3**), and gerbil (**Figure 4**). Coronal slices of the tip of the noses were obtained and the putative localization of a GG was assessed using as a template the general anatomy of the nasal cavities found in the mouse, such as the enlargement of the nasal epithelium in the dorsal region of the nasal cavities (dashed white rectangles in **Figures 1A**, **2A**, **3A**, **4A**). Using these morphological criteria on the TEM preparations of different rodents, we found GG-like structures composed by cells of different shapes localized between the keratinized epithelium and the nasal septum (**Figures 2B**, **3B**, **4B**). They displayed relevant GG cellular and olfactory features as both neuronal and glial cell populations were found in these ganglion structures (**Figures 2C–E**, **3C–E**, **4C–E**) as well as the presence of numerous ciliary processes (**Figures 2F,G**, **3F,G**, **4F,G**). We thus demonstrate here neuroanatomically the presence of a GG in the rat, hamster and gerbil.

Interestingly, important species-dependent differences were observed in the structural morphologies of these GG (**Table 1**). By comparison, large grapes of GG cells were found in the mouse, rat, and gerbil while in hamster, only isolated or small groups of GG cells were sporadically distributed below the keratinized epithelium (**Figures 3B–D** and **Table 1**). Using a combination of electron microscopy and immunohistochemistry approaches, we also found that the glial-neuronal ratio (GGg/GGn) was not conserved between rodent species. In gerbils, this difference was particularly important as more than one GG neuron was often wrapped by a single glial cell (**Figures 4D,E** and **Table 1**). Interestingly, interspecies differences were also found at the ultrastructural level. For example, the long neuronal ciliary processes were different in their distribution and in their number. Indeed, in rats, only a single discrete cluster of ciliary processes was observed (**Figures 2F,G** and **Table 1**) whereas in other rodents more than one cluster could be found. The distribution of intraciliary microtubules also diverged between rodent species. While their typical doublet configuration of $(8+1)$ at the proximal part of the cilium and of $(9+0)$ along the distal axonem (Brechbühl et al., 2008) was always observed, an additional distal configuration of $(>9+0)$ was often found in hamsters (**Figure 3G** and **Table 1**). At the nerve level, the GG axonal bundles were also divergent (**Figures 1H**, **2H**, **3H**, **4H** and **Table 1**). Indeed, numerous myelinated and unmyelinated axons were found in mice, rats, and hamsters, while a predominance of lightly myelinated and/or unmyelinated fibers were observed in gerbils (**Figure 4H** and **Table 1**). In summary, we found a GG in each investigated rodent but divergent structural features were observed that might point to a species-dependent function of this olfactory subsystem.

RODENTIAL GRUENEBERG GANGLION NEURONS DISPLAY A DIFFERENTIAL EXPRESSION OF cGMP-RELATED SIGNALING PROTEINS

We then verified if the known signaling proteins expressed in mouse GG neurons were expressed in the GG of other rodents. We performed immunohistochemical investigations on coronal GG slices, focusing on cGMP-related signaling proteins reported to be implicated in mouse GG sensory transductions (Mamasuew et al., 2010, 2011b; Hanke et al., 2013). Thus, the expression of the particulate guanylyl cyclase G (GC-G), a potential transmembrane receptor and of the cyclic nucleotide-gated channel A3 (CNGA3) a non-selective cation channel, both expressed in the mouse GG (Fleischer et al., 2009; Liu et al., 2009; Brechbühl et al., 2013a), were examined (**Figure 5**). We found that these signaling proteins were expressed differently in the investigated rodents (**Table 2**). GC-G was clearly found in the GG ciliary processes

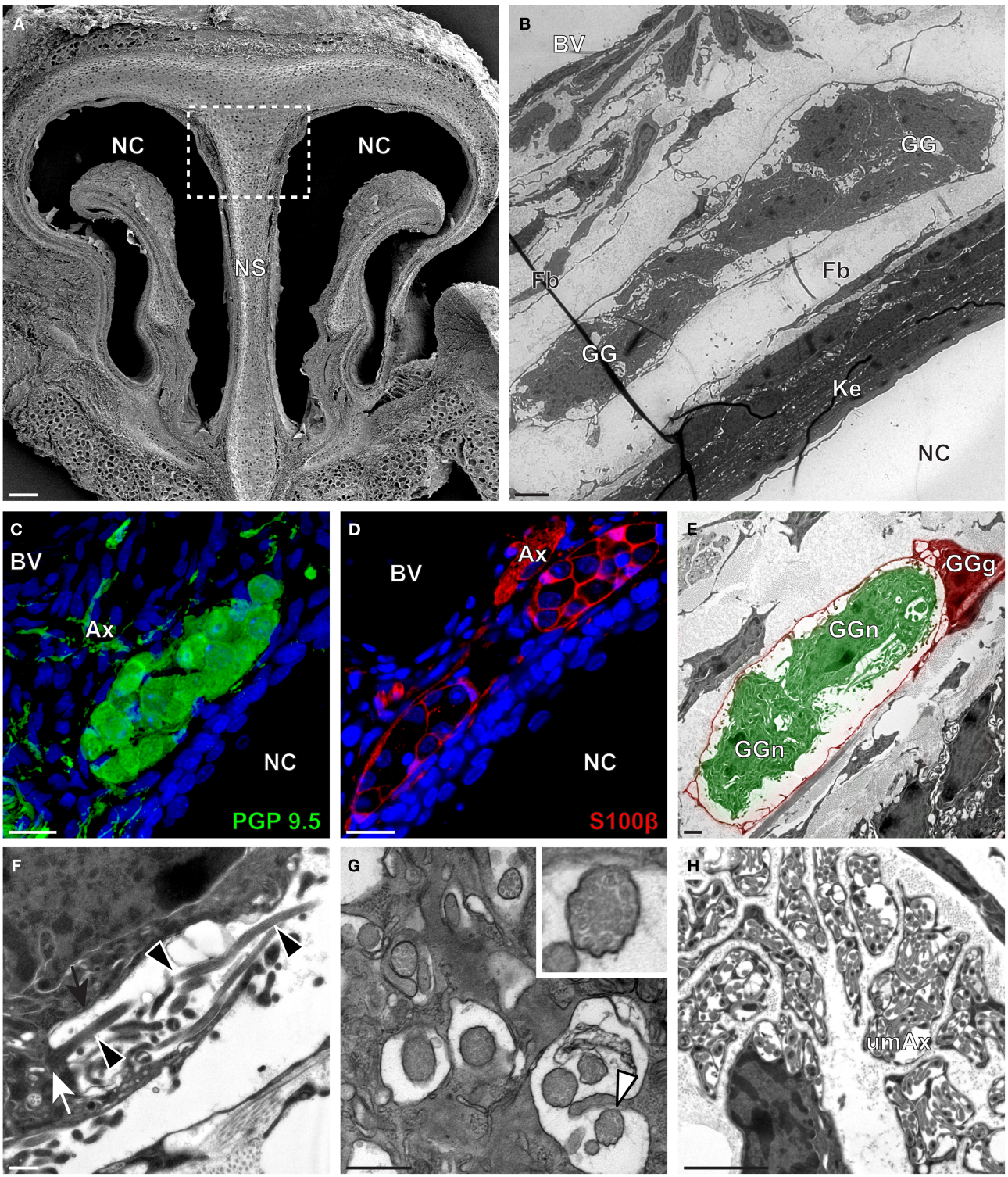

FIGURE 4 | Morphology and ultrastructural features of gerbil GG. (A) General SEM view of a coronal slice performed in the gerbil (P10) GG region. The nasal septum (NS) and the nasal cavities (NC) are shown. The white dashed rectangle highlights the GG region. **(B)** TEM observation of a group of gerbil (P10) GG cells. The presence of a meshwork of fibroblasts (Fb) and a keratinized epithelium (Ke) separating the GG neurons from the NC, as well as the proximity of a blood vessel (BV) can be observed. **(C,D)** Immunohistochemistry observations demonstrating the presence of both neuronal (**C**, PGP 9.5 in green, P40) and glial cells (**D**, slice view of S100β in red, P12) in the gerbil GG. **(E)** High power pseudocolorized TEM view of one gerbil (P10) GG neurons (GGn, in green) wrapped partially in a GG glial cell (GGg, in red). **(F,G)** Ultrastructural TEM view of gerbil GGn cilia. **(F)** Sagittal observation of one gerbil (P10) GGn ciliary process with basal body (white arrow) corresponding to the beginning of one cilium as well long observed axoneme (black arrowhead). The GGn cell membrane (black arrow) shows the invagination of the cilium.

FIGURE 4 | Continued
(G) Coronal observation of a group of deeply invaginated gerbil (P39) GGn cilia. A zoomed view of a single cilium (white arrowhead) shows the distribution of the microtubular doublets (corresponding in gerbil to 8 + 1 or 9 + 0). **(H)** Coronal section of a gerbil (P10) GG axonal nerve bundle (Ax). A predominance of (umAx) unmyelinated fibers was observed. SEM, scanning electron microscopy; TEM, transmitted electron microscopy. A minimum of 4 animals (from P10 to P40) and 6 slices per conditions were used and observed for each SEM, TEM, or immunohistochemistry observations. **(C,D)** Nuclei are shown in blue (DAPI counterstain). Scale bars are 100 μm in **(A)**, 5 μm in **(B)**, 20 μm in **(C,D)**, 2 μm **(E)**, 0.5 μm in **(F,G)** and 3 μm in **(H)**.

Table 2 | Physiological properties of the rodent GG.

Animal	Signaling proteins				Chemosensitivity								Thermosensitivity	
	GC-G		CNGA3		SBT		TMT		DMP		2PT		25–10°C	
Mouse	++	Cilia	++	Cilia, axon	+	21/23	++	33/33	+	23/24	++	17/17	+	11/14
Rat	++	Cilia	+	Widespread	(+)	3/12	++	27/29	+	12/16	+	34/41	+	10/14
Hamster	(+)	n.d	+	Widespread	+	9/9	+	12/16	++	13/13	+	6/9	(+)	4/11
Gerbil	++	Cilia	+	Widespread	–	2/14	(+)	21/57	(+)	28/32	–	2/14	++	11/14

Comparative table of the physiological criteria observed in the GG of mouse, rat, hamster, and gerbil. For the signaling proteins, the expressions (++, highly expressed; +, expressed; (+), residual expression) as well as the main identified subcellular-localization [cilia, axon, widespread, or n.d (not defined)] of both GC-G and CNGA3 are mentioned. For the chemo- and the thermo-sensitivity, the mean response intensity (++, highly sensitive; +, sensitive; (+), poorly sensitive; –, not sensitive) and the proportion of responding cells (n responding neurons/n tested and viable neurons) for SBT, TMT, DMP, 2PT at 100 μM and to cold temperature variation (from 25 to 10° C) are indicated. GC-G, particulate guanylyl cyclase G; CNGA3, cyclic nucleotide-gated channel A3.

of the mouse, rat and gerbil but only residual expression was found in hamster (**Figure 5A**). The expression of CNGA3 varied also (**Figure 5B**). In the mouse GG, CNGA3 was found to be principally expressed in cilia and axons with some somatic localization (Brechbühl et al., 2013a), while in the other rodents widespread distribution was detected. Thus, both the expression and the localization of these GG signaling proteins were found to be species-dependent, which may reflect neurosensory disparities.

CHEMO- AND THERMO-EVOKED SENSORY ACTIVITIES OF THE GRUENEBERG GANGLION ARE SPECIES-DEPENDENT

In the mouse, the GG is implicated both in chemo- and thermo-detection (Fleischer and Breer, 2010). Indeed, structurally similar thiazolic- and pyrazine-derived compounds (Mamasuew et al., 2011a; Brechbühl et al., 2013b) found for example in predator scents or emitted by stressed mice (Apfelbach et al., 2005; Brechbühl et al., 2013b) initiated, in the majority of GG neurons, strong reversible and physiological responses. Until now, the most potent molecules reported to generate neuronal activities are 2-*sec*-butyl-4,5-dihydrothiazole (SBT; a mouse alarm pheromone), 2,4,5-trimethylthiazoline (TMT; a red fox scent), 2-propylthietane (2PT; a stoat scent) (Brechbühl et al., 2013b), or 2,3-dimetylpyrazine [DMP (Mamasuew et al., 2011a); a molecule closely related to substances present in the urine of predators]. Temperature variations have also been reported to induce neuronal activities in the mouse GG (Mamasuew et al., 2008; Schmid et al., 2010; Stebe et al., 2013). For example, a cold environmental temperature initiated calcium elevations in most mouse GGn (Schmid et al., 2010; Brechbühl et al., 2013a). Here, we first established acute tissue slice preparations from GG regions of the rat, hamster, and gerbil to perform calcium imaging experiments (**Figure 6A**). The different rodent GG were identified by their specific morphologies and their Fura-2AM loading. We then compared chemo-evoked activities across species by perfusing GGn with SBT, TMT, DMP, or 2PT [100 μM; (Brechbühl et al., 2013b)] in a continuous oxycarbonated ACSF perfusion (**Figure 6B**). Thermo-evoked neuronal activities induced by a transient decrease in temperature from 25 to 10°C were also compared (**Figure 6C**). Neuronal calcium responses were measured and their intensities were normalized to a brief stimulation with KCl (**Figure 6D**). We found that GGn responded differently across rodents (**Figure 6D** and **Table 2**). As previously reported, in the mouse, strong neuronal responses were evoked by SBT, TMT, DMP, 2PT and by temperature stimuli in the majority of GGn (91, 100, 96, 100, and 79% of GGn, respectively; n total of viable recorded neurons = 81). In the rat, similar activities were recorded (25, 93, 75, 83, and 71%, respectively; $n = 58$), interestingly a reduction in the proportion of responsive neurons and in the calcium signals were observed for the mouse alarm pheromone SBT. In the hamster, chemo-evoked responses were also observed but a drastic decrease in thermo-evoked responses was found both for the number of temperature responding GGn and the mean normalized intensity of the responses (100, 75, 100, 67, and 36%, respectively; $n = 20$). On the contrary, in the gerbil chemo-evoked responses were considerably reduced but the thermo-evoked responses were present (14, 37, 88, 14, and 79%, respectively; $n = 64$). Thus, we show here that the acute tissue slice preparation first developed in the mouse could be applied in the rat, hamster and gerbil. Furthermore, this physiological model allowed the observation that species-dependent sensory activities occur in the different rodent Grueneberg ganglia.

DISCUSSION

Rodents have varied geographical distributions and live in different ecological niches. Across evolution, their senses have adapted to their habitats and they have therefore developed a series

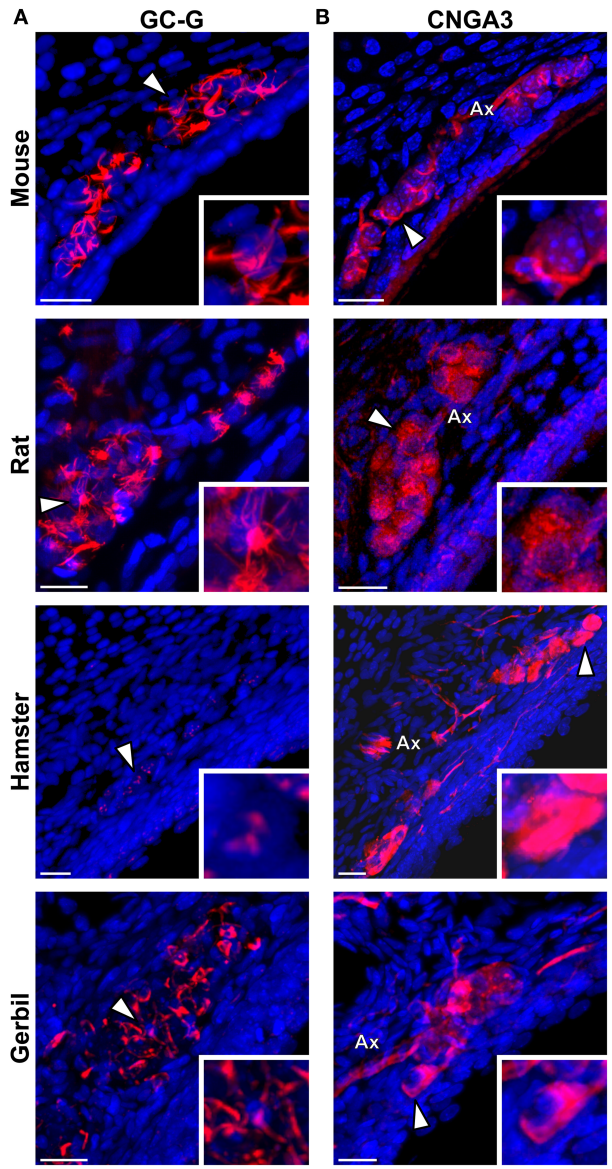

FIGURE 5 | Species-dependent expression of cGMP-associated signaling proteins in the rodential Grueneberg ganglia. Immunohistochemical investigations performed for GC-G and CNGA3 proteins in GG coronal slices from mouse, rat, hamster, and gerbil. **(A)** GC-G was found in mouse, rat, and gerbil GGn cilia. Residual expression was observed in hamster. **(B)** CNGA3 was found principally in GGn cilia and axon (Ax) with partial somatic expression in mouse, while in the other rodents widespread expressions were detected. **(A,B)** White arrowheads indicate the neuron illustrated in the high power view inset. A minimum of 3 animals (mouse: from P1 to P26; rat: from P3 to P29; hamster: from P2 to P16; gerbil: from P1 to P30) and 6 slices were used for each staining and species. Nuclei are shown in blue (DAPI counterstain). Scale bars, 20 μm.

of strategies and behaviors to survive in their environments (Kavaliers and Choleris, 2001). Detection of danger signals such as chemical warnings emitted by their conspecifics (alarm pheromones) or predator-produced cues (kairomones) takes place in the different olfactory subsystems present in their nasal cavities, which then convey multiple sensory informations (Ma, 2010). To increase their survival strategies and fitness, adaptation of the air-breathing pathway in nasal cavities as well as the general nose morphology itself have facilitated this specific olfactory detection (Negus, 1954; Harkema, 1991; Harkema et al., 2006; Rae et al., 2006). This environmental adaptation is especially significant for the most rostral part of the rodent wet-snout, the so-called rhinarium (Hill, 1948; Ade, 1999), which is implicated both in tactile and active olfactory sensing (sniffing behavior) (Wachowiak, 2011; Haidarliu et al., 2012, 2013) and is directly dependent of the environmental context such as temperature variations (Ade, 1999; Ince et al., 2012; Brechbühl et al., 2013a; Cilulko et al., 2013).

We here focused on the GG, an olfactory subsystem devoted to the detection of environmental stress (Brechbühl et al., 2008, 2013b), which is located in the rhinarium region (Haidarliu et al., 2012, 2013; Brechbühl et al., 2013a). We speculated that, due to this specific rostral localization and its temperature sensitivity, it has been influenced by the environmental pressure and has modified its structural morphology and physiological sensory abilities across species by an evolutionary process, conferring a putative ethological function to the GG. We therefore looked at the comparative anatomy and physiology of this olfactory subsystem in four different rodent models that live in distinctive ecological niches. We have first confirmed here by histological investigations the presence of a GG in the mouse, rat, and hamster (Grüneberg, 1973) and demonstrate its existence in the gerbil. We found that GG structural morphologies indeed vary; in particular in the hamster where the gross morphology of the GG was different compared to the other rodents. The hamster GGn have a flat-ovoid shape and are distributed sporadically in small groups of cells across the nasal epithelium at the tip of their noses. This morphological anatomical specificity might be a neuroanatomical adaptation, probably due to the large and flat hamster's nose that might limit the ganglion extension observed in the other investigated rodents. By these anatomical criteria, the hamster's rhinarium is closer to the center of the animal's body and thus should be less affected by external temperature variations than those of the rat and mouse (Sokoloff and Blumberg, 2002; Brechbühl et al., 2013a), a hypothesis reinforced here by the low-sensitivity of the hamster's GGn to temperature variations as observed by calcium imaging experiments. On the other hand, the high temperature sensitivity displayed by the gerbil GGn seems to be correlated with the environmental thermal stress of its desert habitat (extreme variations in day/night temperatures) that strongly influences the behaviors and the temperature of the body extremities (Thiessen, 1988; Klir et al., 1990). Furthermore, the chemosensitivity of GGn as observed by our calcium imaging experiments seems to be altered in gerbils compared to the other investigated rodents. This physiological particularity could similarly be linked to the precise morphology of the gerbil GG. Indeed in the gerbil, the GGg/GGn ratio is the lowest observed. As in our acute tissue-slice preparation the glial wrapping context of the neurons is preserved, we can therefore speculate that glial cells might thus interact with the chemosensitivity of the GGn. A situation also found in the olfactory system of other organisms such as the amphid neurons of *C. elegans* in which the genetic deletion of the wrapping glial cells drastically alter the chemo-sensory

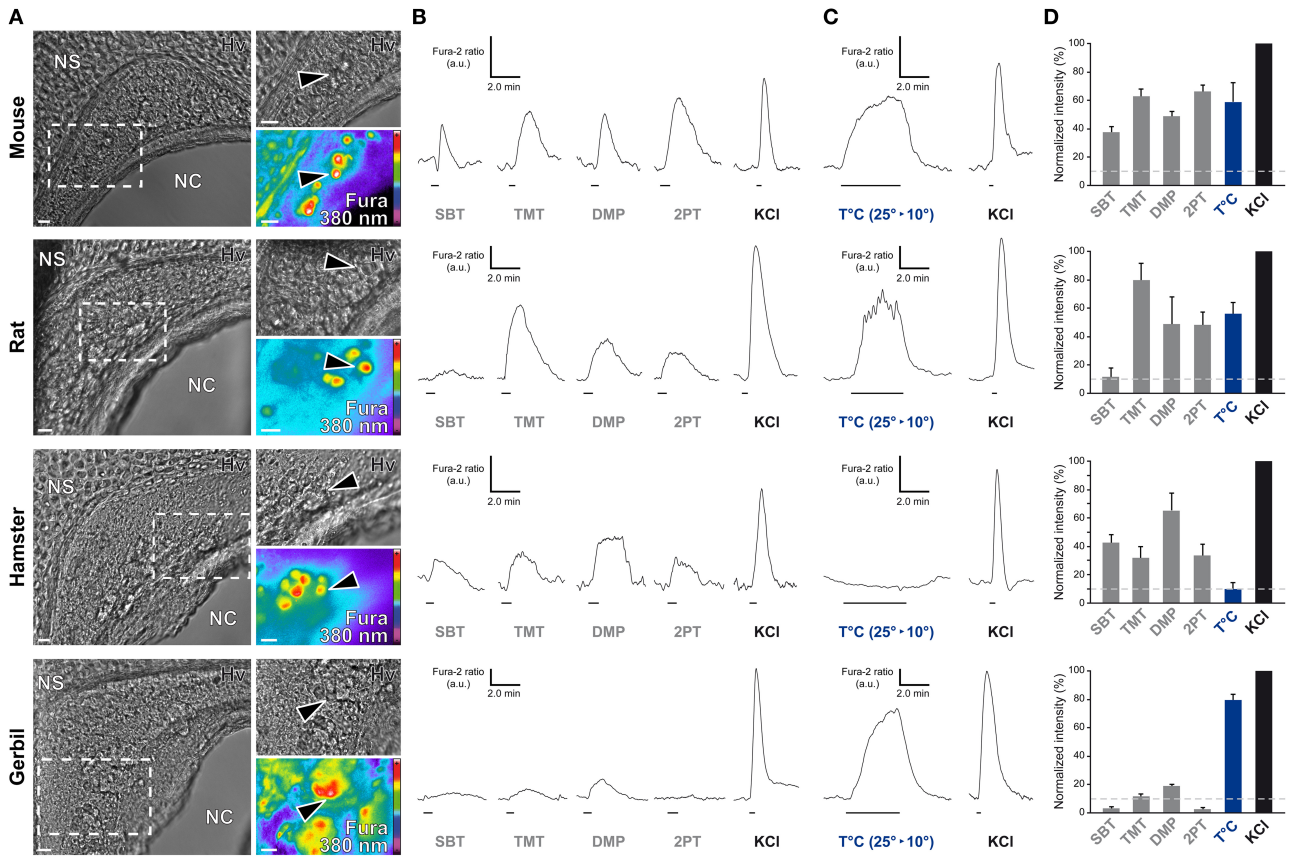

FIGURE 6 | Species-dependent characteristics of sensory responses in rodential Grueneberg ganglion neurons. (A) GG coronal slices from mouse, rat, hamster, and gerbil where GG neurons can be observed under Hoffman modulation view (Hv) between the nasal cavity (NC) and the nasal septum (NS). White dashed rectangles indicate the high power view regions used for recording neuronal activities. The fluorescence of Fura-2AM into GG neurons observed at 380 nm in a color encoded map for unbound Fura is illustrated here. Black arrowheads indicated GG neurons used for the traces found in **(B)** and/or in **(C)**. **(B)** Representative chemo-evoked responses observed at RT after the successive perfusion of SBT, TMT, DMP, or 2PT (100 μM) on the same GG neurons. **(C)** Representative thermo-evoked responses observed during a cold stimulation (T°C; decrease from 25 to 10°C). Here calcium increases are shown for mouse, rat and gerbil. In hamster, the illustrated chemo-responding neuron (in **B**) did not respond to the thermal stimulation. **(D)** Histograms summarizing Fura-2 ratio peak calcium responses intensity to chemo- and thermo-stimulations (respectively in gray and blue bars) normalized to KCl responses (20 mM; in black bars). 10% of KCl activity (gray dashed lines) was used as a limit for considering a neuronal response. Values are expressed as mean ± s.e.m. A minimum of 3 animals (mouse: from P0 to P6; rat: from P1 to P4; hamster: from P2 to P4; gerbil: from P0 to P3) and 6 slices were used for each species. Scale bars, 20 μm in **(A)**. Fluorescence intensity Fura-2 ratio = F340/F380 is indicated by arbitrary units (a.u.) in **(B)** and **(C)**. Perfusion times for chemo- and thermo-stimulations are indicated by horizontal bars in **(B)** and **(C)**.

function of the neurons (Bacaj et al., 2008). The apparent low responsiveness of the gerbils GGn could also be explained by a different repertoire of expressed receptors and affiliated chemical ligands, which could also be further investigated. Detailed morphological investigations, based on serial sections through the rodents GG and/or olfactory bulb, would also determine the longitudinal organization of the GG (number of GGn per individual) as well as the central projections (necklace glomeruli) in the different rodents and thus potentially be associated with the physiological differences observed.

In addition to the morphological properties, the species-dependent expression of cGMP-related signaling proteins in the GGn of the different rodents tested could also be correlated with the physiological responses observed. We cannot rule out that our immunostaining experiments might have been influenced by the antibody species-affinity. Nonetheless, we took advantage for example that the epitope of the GC-G antibody is at the C-terminal region of the protein, which shares approximately 95% identity between the mouse (gi: 124487301) and rat (gi: 404351639) or between the mouse and the predicted hamster GC-G sequence (gi: 524918444). We found, for example, that the expression of GC-G seems to be required for thermo- rather than for chemo-sensitivity. Indeed, only residual expression of the GC-G protein was found in the less temperature-sensitive hamster GG. Putative expression of other GC-members (Liu et al., 2009) could substitute for this GC chemo-related signaling function and explain the chemo-sensitivity found in hamster GGn. Other signaling proteins expressed in mice GGn, such as the V2r83 (member of the V2R class of olfactory receptors) (Fleischer et al., 2006b) or the cGMP-dependent protein

kinase of type II (cGKII) (Liu et al., 2009) were not investigated here. The signaling protein expression seem to be species-dependent, it could therefore be interesting to verify the expression of these proteins in the other rodent species and to further investigate their potential implication in the unknown transduction signaling cascades and physiological responses of GG neurons.

The mouse GG was shown to be involved in the recognition of volatile danger cues such as alarm pheromones and other structurally-related molecules involuntary released by rodents terrestrial predators (Brechbühl et al., 2008, 2013b). In mammals, alarm pheromones are complex and composed by more than one molecule (Kiyokawa et al., 2004). They have not been chemically identified in all rodent species. 2-heptanone has been proposed as a putative rat alarm pheromone (Gutierrez-Garcia et al., 2007). This pheromonal compound did not induce responses in the mouse GG (Brechbühl et al., 2008, 2013b; Mamasuew et al., 2011a) and in the GG of the other species tested (data not shown). This chemodetection seems to be mediated in the rat by another olfactory subsystem, the vomeronasal organ (VNO) (Kiyokawa et al., 2013) pointing out to the complexity of the detection of chemical danger cues. Interestingly, the identified mouse alarm pheromone SBT (Brechbühl et al., 2013b) was perfused on rodents GGn and its activation seems to be specific to the mouse and hamster confirming, at the molecular level, the hypothesis that alarm pheromones could be shared warning signals (Apfelbach et al., 2005).

For the other danger signaling chemicals, the predator cues, the GG-evoked responses observed were also different across species and were correlated with the predator-prey context. For example, the fox is a natural predator of rats. It is known to initiate in the rat important stereotypical fear-related behaviors and an increase of plasmatic stress-related hormones (Apfelbach et al., 2005; Kobayakawa et al., 2007; Ferrero et al., 2011). In our study, we used TMT as a fox scent in perfusion and it generated the highest observed calcium responses in rats GG, thus reinforcing the concept of a potential ethological function for this olfactory subsystem as well as the ecological notion of the predator-prey detection ability due to the habitat shift or learning process (Apfelbach et al., 2005; Kass et al., 2013). Based on this, it could be interesting to examine the presence of a GG and its sensitivities to kairomones in other species including mammals from other ecological niches that did not develop innate fear behaviors in the presence of terrestrial predator scents such as bats (Driessens and Siemers, 2010).

Taken together, the ability of the GG to detect a large array of danger cues with various efficacies in the same neuron and across rodents, raised the question of the potential expression of multiple olfactory receptors and/or multiple signaling pathways at the GG organ level (Fleischer et al., 2006b, 2007; Pyrski et al., 2007; Schmid et al., 2010; Liu et al., 2012; Stebe et al., 2013) but also at the single GG neuronal level (Brechbühl et al., 2013a). As demonstrated for another olfactory subsystem, the VNO (Salazar and Quinteiro, 2009), the presence of a sensory organ that shares gross morphological similarities may be taken into account with limitation to extrapolate physiological notions between species. Indeed, we show here that the GG has conserved a general similar morphology across the investigated rodent species nevertheless its sensory characteristics are strikingly species-dependent pointing to a probable evolutionary benefit for the survival of the species.

AUTHOR CONTRIBUTIONS

Julien Brechbühl and Marie-Christine Broillet designed research; Julien Brechbühl, Magali Klaey, Fabian Moine, Esther Bovay, Nicolas Hurni, Monique Nenniger-Tosato performed research; Julien Brechbühl, Magali Klaey, and Marie-Christine Broillet analyzed data; and Julien Brechbühl and Marie-Christine Broillet wrote the paper.

ACKNOWLEDGMENTS

We thank the Cellular Imaging Facility (CIF) of the University of Lausanne and its coordinator Jean-Yves Chatton for the confocal microscope resources; The Electron Microscopy Facility (EMF) of the University of Lausanne and in particular Antonio Mucciolo and Jean Daraspe for their excellent technical support, its coordinator Céline Loussert and its responsible Bruno Humbel; Ron Stoop and David Bovard for fruitful discussions on the manuscript. This work was supported by the Department of Pharmacology and Toxicology of the University of Lausanne and by a Swiss National Foundation Grant FNS 3100A0-125192 (to Marie-Christine Broillet).

REFERENCES

Ade, M. (1999). External morphology and evolution of the rhinarium of lagomorpha. with special reference to the glires hypothesis. *Zoosyst. Evol.* 75, 191–216. doi: 10.1002/mmnz.19990750203

Apfelbach, R., Blanchard, C. D., Blanchard, R. J., Hayes, R. A., and Mcgregor, I. S. (2005). The effects of predator odors in mammalian prey species: a review of field and laboratory studies. *Neurosci. Biobehav. Rev.* 29, 1123–1144. doi: 10.1016/j.neubiorev.2005.05.005

Bacaj, T., Tevlin, M., Lu, Y., and Shaham, S. (2008). Glia are essential for sensory organ function in *C. elegans*. *Science* 322, 744–747. doi: 10.1126/science.1163074

Brechbühl, J., Klaey, M., and Broillet, M. C. (2008). Grueneberg ganglion cells mediate alarm pheromone detection in mice. *Science* 321, 1092–1095. doi: 10.1126/science.1160770

Brechbühl, J., Luyet, G., Moine, F., Rodriguez, I., and Broillet, M. C. (2011). Imaging pheromone sensing in a mouse vomeronasal acute tissue slice preparation. *J. Vis. Exp.* 58:3311. doi: 10.3791/3311

Brechbühl, J., Moine, F., and Broillet, M. C. (2013a). Mouse Grueneberg ganglion neurons share molecular and functional features with *C. elegans* amphid neurons.*Front. Behav. Neurosci.* 7:193. doi: 10.3389/fnbeh.2013.00193

Brechbühl, J., Moine, F., Klaey, M., Nenniger-Tosato, M., Hurni, N., Sporkert, F., et al. (2013b). Mouse alarm pheromone shares structural similarity with predator scents. *Proc. Natl. Acad. Sci. U.S.A.* 110, 4762–4767. doi: 10.1073/pnas.1214249110

Cilulko, J., Janiszewski, P., Bogdaszewski, M., and Szczygielska, E. (2013). Infrared thermal imaging in studies of wild animals. *Eur. J. Wildl. Res.* 59, 17–23. doi: 10.1007/s10344-012-0688-1

Driessens, T., and Siemers, B. M. (2010). Cave-dwelling bats do not avoid TMT and 2-PT - components of predator odour that induce fear in other small mammals. *J. Exp. Biol.* 213, 2453–2460. doi: 10.1242/jeb.044743

Ferrero, D. M., Lemon, J. K., Fluegge, D., Pashkovski, S. L., Korzan, W. J., Datta, S. R., et al. (2011). Detection and avoidance of a carnivore odor by prey. *Proc. Natl. Acad. Sci. U.S.A.* 108, 11235–11240. doi: 10.1073/pnas.1103317108

Fleischer, J., and Breer, H. (2010). The Grueneberg ganglion: a novel sensory system in the nose. *Histol. Histopathol.* 25, 909–915.

Fleischer, J., Hass, N., Schwarzenbacher, K., Besser, S., and Breer, H. (2006a). A novel population of neuronal cells expressing the olfactory marker protein (OMP) in the anterior/dorsal region of the nasal cavity. *Histochem. Cell Biol.* 125, 337–349. doi: 10.1007/s00418-005-0077-x

Fleischer, J., Mamasuew, K., and Breer, H. (2009). Expression of cGMP signaling elements in the Grueneberg ganglion. *Histochem. Cell Biol.* 131, 75–88. doi: 10.1007/s00418-008-0514-8

Fleischer, J., Schwarzenbacher, K., Besser, S., Hass, N., and Breer, H. (2006b). Olfactory receptors and signalling elements in the Grueneberg ganglion. *J. Neurochem.* 98, 543–554. doi: 10.1111/j.1471-4159.2006.03894.x

Fleischer, J., Schwarzenbacher, K., and Breer, H. (2007). Expression of trace amine-associated receptors in the Grueneberg ganglion. *Chem. Senses* 32, 623–631. doi: 10.1093/chemse/bjm032

Fuss, S. H., Omura, M., and Mombaerts, P. (2005). The Grueneberg ganglion of the mouse projects axons to glomeruli in the olfactory bulb. *Eur. J. Neurosci.* 22, 2649–2654. doi: 10.1111/j.1460-9568.2005.04468.x

Grüneberg, H. (1973). A ganglion probably belonging to the N. terminalis system in the nasal mucosa of the mouse. *Z. Anat. Entwicklungsgesch.* 140, 39–52. doi: 10.1007/BF00520716

Gutierrez-Garcia, A. G., Contreras, C. M., Mendoza-Lopez, M. R., Garcia-Barradas, O., and Cruz-Sanchez, J. S. (2007). Urine from stressed rats increases immobility in receptor rats forced to swim: role of 2-heptanone. *Physiol. Behav.* 91, 166–172. doi: 10.1016/j.physbeh.2007.02.006

Haidarliu, S., Golomb, D., Kleinfeld, D., and Ahissar, E. (2012). Dorsorostral snout muscles in the rat subserve coordinated movement for whisking and sniffing. *Anat. Rec. (Hoboken)* 295, 1181–1191. doi: 10.1002/ar.22501

Haidarliu, S., Kleinfeld, D., and Ahissar, E. (2013). Mediation of muscular control of rhinarial motility in rats by the nasal cartilaginous skeleton. *Anat. Rec. (Hoboken)* 296, 1821–1832. doi: 10.1002/ar.22822

Hanke, W., Mamasuew, K., Biel, M., Yang, R. B., and Fleischer, J. (2013). Odorant-evoked electrical responses in Grueneberg ganglion neurons rely on cGMP-associated signaling proteins. *Neurosci. Lett.* 539, 38–42. doi: 10.1016/j.neulet.2013.01.032

Harkema, J. R. (1991). Comparative aspects of nasal airway anatomy: relevance to inhalation toxicology. *Toxicol. Pathol.* 19, 321–336. doi: 10.1177/019262339101900402

Harkema, J. R., Carey, S. A., and Wagner, J. G. (2006). The nose revisited: a brief review of the comparative structure, function, and toxicologic pathology of the nasal epithelium. *Toxicol. Pathol.* 34, 252–269. doi: 10.1080/01926230600713475

Hill, B. W. C. O. (1948). Rhinoglyphics: epithelial seulpture of the mammalian rhiarium. *Proc. Zool. Soc. Lond.* 118, 1–35. doi: 10.1111/j.1096-3642.1948.tb00364.x

Ince, C., Kuijen, A.-M. V., Milstein, D. M. J., Yürük, K., Folkow, L. P., Fokkens, W. J., et al. (2012). Why Rudolph's nose is red: observational study. *BMJ* 345:e8311. doi: 10.1136/bmj.e8311

Kass, M. D., Rosenthal, M. C., Pottackal, J., and McGann, J. P. (2013). Fear learning enhances neural responses to threat-predictive sensory stimuli. *Science* 342, 1389–1392. doi: 10.1126/science.1244916

Kavaliers, M., and Choleris, E. (2001). Antipredator responses and defensive behavior: ecological and ethological approaches for the neurosciences. *Neurosci. Biobehav. Rev.* 25, 577–586. doi: 10.1016/S0149-7634(01)00042-2

Kiyokawa, Y., Kikusui, T., Takeuchi, Y., and Mori, Y. (2004). Alarm pheromones with different functions are released from different regions of the body surface of male rats. *Chem. Senses* 29, 35–40. doi: 10.1093/chemse/bjh004

Kiyokawa, Y., Kodama, Y., Kubota, T., Takeuchi, Y., and Mori, Y. (2013). Alarm pheromone is detected by the vomeronasal organ in male rats. *Chem. Senses* 38, 661–668. doi: 10.1093/chemse/bjt030

Klir, J. J., Heath, J. E., and Bennani, N. (1990). An infrared thermographic study of surface temperature in relation to external thermal stress in the Mongolian gerbil, *Meriones unguiculatus*. *Comp. Biochem. Physiol. A Comp. Physiol.* 96, 141–146. doi: 10.1016/0300-9629(90)90055-W

Kobayakawa, K., Kobayakawa, R., Matsumoto, H., Oka, Y., Imai, T., Ikawa, M., et al. (2007). Innate versus learned odour processing in the mouse olfactory bulb. *Nature* 450, 503–508. doi: 10.1038/nature06281

Koos, D. S., and Fraser, S. E. (2005). The Grueneberg ganglion projects to the olfactory bulb. *Neuroreport* 16, 1929–1932. doi: 10.1111/j.1460-9568.2005.04468.x

Liu, C. Y., Fraser, S. E., and Koos, D. S. (2009). Grueneberg ganglion olfactory subsystem employs a cGMP signaling pathway. *J. Comp. Neurol.* 516, 36–48. doi: 10.1002/cne.22096

Liu, C. Y., Xiao, C., Fraser, S. E., Lester, H. A., and Koos, D. S. (2012). Electrophysiological characterization of Grueneberg ganglion olfactory neurons: spontaneous firing, sodium conductance, and hyperpolarization-activated currents. *J. Neurophysiol.* 108, 1318–1334. doi: 10.1152/jn.00907.2011

Ma, M. (2010). "Multiple olfactory subsystems convey various sensory signals," in *The Neurobiology of Olfaction,* ed A. Menini (Boca Raton, FL: Taylor and Francis Group, LLC), 225–240.

Mamasuew, K., Breer, H., and Fleischer, J. (2008). Grueneberg ganglion neurons respond to cool ambient temperatures. *Eur. J. Neurosci.* 28, 1775–1785. doi: 10.1111/j.1460-9568.2008.06465.x

Mamasuew, K., Hofmann, N., Breer, H., and Fleischer, J. (2011a). Grueneberg ganglion neurons are activated by a defined set of odorants. *Chem. Senses* 36, 271–282. doi: 10.1093/chemse/bjq124

Mamasuew, K., Hofmann, N., Kretzschmann, V., Biel, M., Yang, R. B., Breer, H., et al. (2011b). Chemo- and thermosensory responsiveness of Grueneberg ganglion neurons relies on cyclic guanosine monophosphate signaling elements. *Neurosignals* 19, 198–209. doi: 10.1159/000329333

Mamasuew, K., Michalakis, S., Breer, H., Biel, M., and Fleischer, J. (2010). The cyclic nucleotide-gated ion channel CNGA3 contributes to coolness-induced responses of Grueneberg ganglion neurons. *Cell. Mol. Life Sci.* 67, 1859–1869. doi: 10.1007/s00018-010-0296-8

Margolis, F. L. (1972). A brain protein unique to the olfactory bulb. *Proc. Natl. Acad. Sci. U.S.A.* 69, 1221–1224. doi: 10.1073/pnas.69.5.1221

Matsuo, T., Rossier, D. A., Kan, C., and Rodriguez, I. (2012). The wiring of Grueneberg ganglion axons is dependent on neuropilin 1. *Development* 139, 2783–2791. doi: 10.1242/dev.077008

Mombaerts, P., Wang, F., Dulac, C., Chao, S. K., Nemes, A., Mendelsohn, M., et al. (1996). Visualizing an olfactory sensory map. *Cell* 87, 675–686. doi: 10.1016/S0092-8674(00)81387-2

Negus, V. E. (1954). Introduction to the comparative anatomy of the nose and paranasal sinuses. *Ann. R. Coll. Surg. Engl.* 15, 141–171.

Potter, S. M., Zheng, C., Koos, D. S., Feinstein, P., Fraser, S. E., and Mombaerts, P. (2001). Structure and emergence of specific olfactory glomeruli in the mouse. *J. Neurosci.* 21, 9713–9723.

Pyrski, M., Koo, J. H., Polumuri, S. K., Ruknudin, A. M., Margolis, J. W., Schulze, D. H., et al. (2007). Sodium/calcium exchanger expression in the mouse and rat olfactory systems. *J. Comp. Neurol.* 501, 944–958. doi: 10.1002/cne.21290

Rae, T. C., Vidarsdottir, U. S., Jeffery, N., and Steegmann, A. T. (2006). Developmental response to cold stress in cranial morphology of Rattus: implications for the interpretation of climatic adaptation in fossil hominins. *Proc. Biol. Sci.* 273, 2605–2610. doi: 10.1098/rspb.2006.3629

Roppolo, D., Ribaud, V., Jungo, V. P., Luscher, C., and Rodriguez, I. (2006). Projection of the Grüneberg ganglion to the mouse olfactory bulb. *Eur. J. Neurosci.* 23, 2887–2894. doi: 10.1111/j.1460-9568.2006.04818.x

Salazar, I., and Quinteiro, P. S. (2009). The risk of extrapolation in neuroanatomy: the case of the Mammalian vomeronasal system. *Front. Neuroanat.* 3:22. doi: 10.3389/neuro.05.022.2009.

Schmid, A., Pyrski, M., Biel, M., Leinders-Zufall, T., and Zufall, F. (2010). Grueneberg ganglion neurons are finely tuned cold sensors. *J. Neurosci.* 30, 7563–7568. doi: 10.1523/JNEUROSCI.0608-10.2010

Sokoloff, G., and Blumberg, M. S. (2002). Contributions of endothermy to huddling behavior in infant Norway rats (*Rattus norvegicus*) and Syrian golden hamsters (*Mesocricetus auratus*). *J. Comp. Psychol.* 116, 240–246. doi: 10.1037/0735-7036.116.3.240

Stebe, S., Schellig, K., Lesage, F., Breer, H., and Fleischer, J. (2013). The thermosensitive potassium channel TREK-1 contributes to coolness-evoked responses of Grueneberg ganglion neurons. *Cell. Mol. Neurobiol.* 34, 113–122. doi: 10.1007/s10571-013-9992-x

Storan, M. J., and Key, B. (2006). Septal organ of Grüneberg is part of the olfactory system. *J. Comp. Neurol.* 494, 834–844. doi: 10.1002/cne.20858

Tachibana, T., Fujiwara, N., and Nawa, T. (1990). The ultrastructure of the ganglionated nerve plexus in the nasal vestibular mucosa of the musk shrew (*Suncus murinus*, insectivora). *Arch. Histol. Cytol.* 53, 147–156. doi: 10.1679/aohc.53.147

Thiessen, D. D. (1988). Body temperature and grooming in the Mongolian gerbil. *Ann. N.Y. Acad. Sci.* 525, 27–39. doi: 10.1111/j.1749-6632.1988.tb38593.x

Wachowiak, M. (2011). All in a sniff: olfaction as a model for active sensing. *Neuron* 71, 962–973. doi: 10.1016/j.neuron.2011.08.030

Young, H. M., Bergner, A. J., and Muller, T. (2003). Acquisition of neuronal and glial markers by neural crest-derived cells in the mouse intestine. *J. Comp. Neurol.* 456, 1–11. doi: 10.1002/cne.10448

Conflict of Interest Statement: The authors declare that the research was conducted in the absence of any commercial or financial relationships that could be construed as a potential conflict of interest.

Received: 25 June 2014; accepted: 11 August 2014; published online: 27 August 2014.

Citation: Brechbühl J, Klaey M, Moine F, Bovay E, Hurni N, Nenniger-Tosato M and Broillet M-C (2014) Morphological and physiological species-dependent characteristics of the rodent Grueneberg ganglion. Front. Neuroanat. ***8****:87. doi: 10.3389/fnana.2014.00087*

This article was submitted to the journal Frontiers in Neuroanatomy.

frontiers in
NEUROANATOMY

ORIGINAL RESEARCH ARTICLE
published: 21 November 2014
doi: 10.3389/fnana.2014.00134

Physiological characterization of formyl peptide receptor expressing cells in the mouse vomeronasal organ

***Tobias Ackels*[1]*, *Benoît von der Weid*[2], *Ivan Rodriguez*[2] *and Marc Spehr*[1]**

[1] *Department of Chemosensation, RWTH Aachen University, Aachen, Germany*
[2] *Department of Genetics and Evolution, University of Geneva, Geneva, Switzerland*

Edited by:
Pablo Chamero, University of Saarland, Germany

Reviewed by:
Diego Restrepo, University of Colorado Anschutz, USA
Xavier Grosmaitre, CNRS, France
Johannes Reisert, Monell Chemical Senses Center, USA

***Correspondence:**
Tobias Ackels, Department of Chemosensation, RWTH Aachen University, Worringerweg 3, 52074 Aachen, Germany
e-mail: t.ackels@sensorik.rwth-aachen.de

The mouse vomeronasal organ (VNO) is a chemosensory structure that detects both hetero- and conspecific social cues. Based on largely monogenic expression of either type 1 or 2 vomeronasal receptors (V1Rs/V2Rs) or members of the formyl peptide receptor (FPR) family, the vomeronasal sensory epithelium harbors at least three neuronal subpopulations. While various neurophysiological properties of both V1R- and V2R-expressing neurons have been described using genetically engineered mouse models, the basic biophysical characteristics of the more recently identified FPR-expressing vomeronasal neurons have not been studied. Here, we employ a transgenic mouse strain that coexpresses an enhanced variant of yellow fluorescent protein together with FPR-rs3 allowing to identify and analyze FPR-rs3-expressing neurons in acute VNO tissue slices. Single neuron electrophysiological recordings allow comparative characterization of the biophysical properties inherent to a prototypical member of the FPR-expressing subpopulation of VNO neurons. In this study, we provide an in-depth analysis of both passive and active membrane properties, including detailed characterization of several types of voltage-activated conductances and action potential discharge patterns, in fluorescently labeled vs. unmarked vomeronasal neurons. Our results reveal striking similarities in the basic (electro) physiological architecture of both transgene-expressing and non-expressing neurons, confirming the suitability of this genetically engineered mouse model for future studies addressing more specialized issues in vomeronasal FPR neurobiology.

Keywords: vomeronasal receptor, formyl peptide receptor, vomeronasal organ, sensory neurons, VNO, olfaction

INTRODUCTION

For mammals, the sense of smell is crucial to interact adequately with their environment. Fundamental information about hetero- and conspecifics, such as identity, social or reproductive state, is gathered by the olfactory system. In most mammals, this system consists of up to four anatomically and functionally distinct subsystems: the main olfactory system (Firestein, 2001; Mombaerts, 2004), the Grueneberg ganglion (Fuss et al., 2005; Koos and Fraser, 2005; Roppolo et al., 2006; Brechbühl et al., 2008; Schmid et al., 2010), the septal organ of Masera (Adams, 1992; Ma et al., 2003) and the vomeronasal organ (VNO). The VNO is a bilateral tubular structure located at the base of the nasal septum. Vomeronasal sensory neurons (VSNs) are highly sensitive chemoreceptors thought to primarily detect semiochemicals and other social cues (Leinders-Zufall et al., 2000; Dulac and Torello, 2003; Spehr et al., 2006; Ferrero et al., 2013). VSNs project single unbranched axons to the accessory olfactory bulb (AOB). To date, members of at least four chemoreceptor gene families are expressed in VSNs: the *V1r* (Dulac and Axel, 1995) and *V2r* (Herrada and Dulac, 1997; Matsunami and Buck, 1997; Ryba and Tirindelli, 1997) families, with more than 100 functional members each, a few odorant receptors (Lévai et al., 2006), and the recently discovered formyl peptide receptor (FPR)-related sequence (*Fpr-rs*) family of putative chemoreceptor genes. The *Fpr-rs* family comprises 7 members, 5 of which (*Fpr-rs1*, *rs3*, *rs4*, *rs6* and *rs7*) are predominantly or exclusively expressed in subsets of VSNs (Liberles et al., 2009; Rivière et al., 2009; Chamero et al., 2012). As key mediators of leukocyte chemotaxis, FPR1 and FPR-rs2 receptor proteins are expressed in immune cells such as granulocytes and monocytes (Rivière et al., 2009; He et al., 2013) where they serve crucial functions in host defense against pathogens by detecting microbe- and/or host-derived inflammation-associated metabolites (Migeotte et al., 2006; Le et al., 2007; Soehnlein and Lindbom, 2010). However, neither FPR1 nor FPR-rs2 was found transcribed in mouse VSNs (Liberles et al., 2009; Rivière et al., 2009).

Vomeronasal sensory neurons expressing members of the V1R family of G protein-coupled receptors are located in the more apical part of the vomeronasal sensory epithelium. These neurons co-express the G-protein α-subunit $G\alpha_{i2}$ and project to the anterior part of the AOB (Belluscio et al., 1999; Rodriguez et al., 1999). Functionally, V1R neurons respond to sulfated steroids and to a variety of other secreted ethologically relevant

small semiochemicals (Leinders-Zufall et al., 2000; Boschat et al., 2002; Novotny, 2003; Nodari et al., 2008; Isogai et al., 2011). By contrast, V2R expression is restricted to VSNs in the more basal $G\alpha_o$-positive layer (Martini et al., 2001; Matsuoka et al., 2001; Dulac and Torello, 2003). V2R neurons predominantly detect peptides/small proteins (Leinders-Zufall et al., 2004; Chamero et al., 2007; Kimoto et al., 2007; Ferrero et al., 2013; Kaur et al., 2014) and project to the posterior region of the AOB. For FPR-rs3 expressing neurons, we recently described axonal projections to the rostral AOB (Dietschi et al., 2013), the target region of V1R neurons.

The single *Fpr-rs* gene cluster is adjacent to a stretch of more than 30 *V1/2r* genes. However, neither *V1rs*, nor *V2rs* share significant sequence homology with vomeronasal *Fpr-rs* genes. Liberles and coworkers suggested that vomeronasal *Fpr*s evolved from recent gene duplications and positive selection in the rodent lineage (Liberles et al., 2009). Together with recent functional data obtained from recombinant FPR expression (Bufe et al., 2012), these considerations argue for a neofunctionalization of vomeronasal *Fpr-rs* genes. Their predicted seven-transmembrane topology, their selective, punctate and monogenic vomeronasal expression pattern, and their localization in microvillous dendritic VSN endings (Liberles et al., 2009; Rivière et al., 2009), however, strongly suggest a functional role of FPR-rs in vomeronasal chemosignaling. Interestingly, while *Fpr-rs1* is coexpressed with $G_{\alpha o}$ in basal sensory neurons, the remaining vomeronasal *Fpr-rs* genes all coexpress $G_{\alpha i2}$ in the apical layer of the VNO neuroepithelium (Liberles et al., 2009; Munger, 2009; Rivière et al., 2009). Vomeronasal sensory neurons are activated *in situ* by formylated peptides and various other antimicrobial/inflammatory modulators (Rivière et al., 2009; Chamero et al., 2011) and heterologously expressed FPR-rs proteins retain agonist spectra that share some similarities to immune system FPRs (Rivière et al., 2009). However, the exact biological role of vomeronasal FPRs remains to be determined.

To address the neurobiological function of vomeronasal FPRs experimentally, a detailed physiological characterization of *Fpr-rs* neurons in their native environment is mandatory. Genetically modified animals in which the receptor identity of a given chemosensory neuron is marked by coexpression of a fluorescent reporter have proven particularly fruitful in the analysis of olfactory signaling (Boschat et al., 2002; Bozza et al., 2002; Grosmaitre et al., 2006, 2009; Oka et al., 2006; Ukhanov et al., 2007; Leinders-Zufall et al., 2009; Pacifico et al., 2012). Here, we describe a transgenic mouse strain that expresses FPR-rs3 together with a fluorescent marker (Fpr-rs3-i-Venus). This mouse model allows optical identification and subsequent physiological analysis of FPR-rs3-expressing neurons in acute VNO tissue slices. Using single neuron patch-clamp recordings, we thus provide an in-depth electrophysiological characterization of the basic biophysical properties inherent to a prototypical member of the FPR-expressing subpopulation of VNO neurons. Our analysis spans several types of voltage-activated conductances as well as action potential discharge parameters in both fluorescently labeled and control VSNs. Our data reveal a number of physiological similarities between FPR-rs3-expressing and non-expressing neurons. Together, these results confirm the suitability of Fpr-rs3-i-Venus mice for future studies of vomeronasal FPR neurobiology and, in addition, these findings indicate that the FPR expression does not confer a distinct biophysical phenotype to the subpopulation of FPR-positive VSNs.

MATERIALS AND METHODS

ANIMALS

All animal procedures were in compliance with local and European Union legislation on the protection of animals used for experimental purposes (Directive 86/609/EEC) and with recommendations put forward by the Federation of European Laboratory Animal Science Associations (FELASA). Both C57BL/6 mice (Charles River Laboratories, Sulzfeld, Germany) and Fpr-rs3-i-Venus mice were housed in groups of both sexes at room temperature on a 12 h light/dark cycle with food and water available *ad libitum*. Experiments used young adults of either sex. We did not observe obvious gender-dependent differences.

TRANSGENIC MICE

The transgene (Fpr-rs3-i-Venus) contains the FPR-rs3 coding sequence followed by an internal ribosome entry site (IRES), and the coding sequence for tau-Venus, a fusion between the microtubule-associated protein tau and Venus yellow fluorescent protein (Nagai et al., 2002). These coding sequences are under the control of the H element followed by the MOR28 promoter (Serizawa et al., 2006; modified by and generously provided by P. Feinstein). The Fpr-rs3-i-Venus transgene was isolated on gel after BssHII digestion and purified using the QIAquick® Gel extraction kit (QIAGEN, Hilden, Germany). The transgene was injected into the pronuclei of fertilized C57BL6/DBA2 mouse oocytes following standard procedures. Four founders carrying the transgene were obtained. One of these founder animals expressed the transgene in VSNs and was, thus, used to start the colony. Backcrossed to C57BL/6J, mice were kept hemizygous. Wild type and transgenic mice had no obvious differences in size, weight, fertility, life expectancy or food consumption.

CHEMICALS AND SOLUTIONS

The following solutions were used: ($\mathbf{S}_1$) 4-(2-Hydroxyethyl)piperazine-1-ethanesulfonic acid (HEPES) buffered extracellular solution containing (in mM) 145 NaCl, 5 KCl, 1 $CaCl_2$, 1 $MgCl_2$, 10 HEPES; pH = 7.3 (adjusted with NaOH); osmolarity = 300 mOsm (adjusted with glucose). ($\mathbf{S}_2$) Oxygenated (95% O_2, 5% CO_2) extracellular solution containing (in mM) 125 NaCl, 25 $NaHCO_3$, 5 KCl, 1 $CaCl_2$, 1 $MgSO_4$, 5 BES; pH = 7.3; osmolarity = 300 mOsm. ($\mathbf{S}_3$) solution containing (in mM) 144 NaCl, 5 KCl, 1 TEACl, 1 $CaCl_2$, 1 $MgCl_2$, 10 HEPES, pH 7.3; osmolarity = 300 mOsm. ($\mathbf{S}_4$) solution containing (in mM) 134 NaCl, 5 KCl, 1 TEACl, 1 $CaCl_2$, 1 $MgCl_2$, 10 HEPES, 10 4-AP, pH 7.3; osmolarity = 300 mOsm. ($\mathbf{S}_5$) solution containing (in mM) 110 NaCl, 5 KCl, 25 TEACl, 1 $CaCl_2$, 1 $MgCl_2$, 10 HEPES, 10 4-AP, pH 7.3; osmolarity = 300 mOsm. ($\mathbf{S}_6$) solution containing (in mM) 115 NaCl, 25 TEACl, 1, 1 $MgCl_2$, 10 HEPES, 10 4-AP, pH 7.3; osmolarity = 300 mOsm. ($\mathbf{S}_7$) solution containing (in mM) 105 NaCl,

25 TEACl, 5 mM $BaCl_2$, 1 $MgCl_2$, 10 HEPES, 10 4-AP, pH 7.3; osmolarity = 300 mOsm. ($\mathbf{S_8}$) Pipette solution containing (in mM) 143 KCl, 2 KOH, 1 EGTA, 0.3 $CaCl_2$ (free Ca^{2+} = 110 nM), 10 HEPES, 2 MgATP, 1 NaGTP; pH = 7.1 (adjusted with KOH); osmolarity = 290 mOsm. ($\mathbf{S_9}$) Pipette solution containing (in mM) 133 CsCl, 10 NaCl, 2 CsOH, 1 EGTA, 0.3 $CaCl_2$ (free Ca^{2+} = 110 nM), 10 HEPES, 1 MgATP, 1 NaGTP; pH = 7.1 (adjusted with CsOH); osmolarity = 290 mOsm.

Free Ca^{2+} and Mg^{2+} concentrations were calculated using WEBMAXC STANDARD[1]. If not stated otherwise, chemicals were purchased from Sigma (Schnelldorf, Germany). ω-agatoxin IVa and ω-conotoxin GVIA were purchased from Biotrend (Zurich, Switzerland). Stimuli and pharmacological agents were applied from air pressure-driven reservoirs via an 8-in-1 multibarrel "perfusion pencil" (Science Products, Hofheim, Germany; Veitinger et al., 2011).

CRYOSECTIONS

For preparation of cryosections, the VNO was fixed in PBS containing 4% paraformaldehyde (2 h; 4°C), decalcified overnight in 0.5 M EDTA (4°C) and cryoprotected in PBS containing 30% sucrose (4°C). The dehydrated VNO was embedded in Tissue Freezing Medium and sectioned at 20 μm on a Leica CM1950 cryostat (Leica Biosystems, Nussloch, Germany).

VIBRATOME SECTIONS

Acute vomeronasal tissue sections were prepared as previously described (Hagendorf et al., 2009; Spehr et al., 2009). Briefly, mice were sacrificed by brief exposure to CO_2 followed by decapitation using sharp surgical scissors. The lower jaw and the soft palate were removed allowing access to the vomeronasal capsule. After removal of the cartilage, the dissected VNO was embedded in 4% low-gelling temperature agarose and coronal slices (150–200 μm) were cut in ice-cold oxygenated extracellular solution ($\mathbf{S_2}$) using a Leica VT1000S vibratome (speed: 3.5 a.u. = 0.15 mm/s; frequency: 7.5 a.u. = 75 Hz; amplitude: 0.6 mm; Leica Biosystems). Sections were transferred to a submerged, oxygenated ($\mathbf{S_2}$) and chilled storage chamber until use.

IMMUNOHISTOCHEMISTRY

Blocking was performed for 1 h in PBS containing 2% goat serum, 1% gelatine and 0.2% Triton X-100 (blocking solution). Sections were then incubated overnight at 4°C with primary antibody sera (1:500 rabbit anti-V2R2; 1:200 rabbit anti-FPR-rs3) in blocking solution, washed in PBS containing 0.05% Triton-X 100 (3 × 10 min, 1 × 30 min), and incubated for 1 h with Alexa®Fluor secondary antibodies (1:500). Excess antibodies were removed by washing in PBS containing 0.05% Triton-X 100 (3 × 10 min, 1 × 30 min). To control for nonspecific staining, experiments in which the primary antibodies were omitted were performed in parallel with each procedure.

ELECTROPHYSIOLOGY

Vomeronasal organ slices were transferred to a recording chamber (Luigs & Neumann, Ratingen, Germany) on an upright fixed-stage scanning confocal microscope (TCS SP5 DM6000CFS, Leica Microsystems) equipped with a 20x/1.0 NA water immersion objective (HCX APO L, Leica Microsystems) as well as a cooled a CCD-camera (DFC360FX, Leica Microsystems). Slices were continuously superfused with oxygenated $\mathbf{S_2}$ (∼3 ml/min; gravity flow; RT). Patch pipettes (4–7 MΩ) were pulled from borosilicate glass capillaries (1.50 mm OD/0.86 mm ID; Science Products) on a PC-10 micropipette puller (Narishige Instruments, Tokyo, Japan), fire-polished (MF-830 Microforge; Narishige Instruments) and filled with pipette solution ($\mathbf{S_8}$ or $\mathbf{S_9}$) depending on experimental design. An agar bridge (150 mM KCl) connected reference electrode and bath solution. An EPC-10 amplifier controlled by Patchmaster 2.67 software (HEKA Elektronik, Lambrecht/Pfalz, Germany) was used for data acquisition. We monitored and compensated pipette and membrane capacitance as well as series resistance. Only neurons exhibiting small and stable access resistances (≤3% of R_{input}; change <20%) were used for analysis. Liquid junction potentials were calculated using JPCalcW software (Barry, 1994) and corrected online. If not stated otherwise, signals were low-pass filtered (analog 3- and 4-pole Bessel filters (–3 dB); adjusted to $^1/_3$–$^1/_5$ of the sampling rate (5–10 kHz, depending on protocol)). Between recordings, holding potential (V_{hold}) was −60 mV. All electrophysiological data were recorded in whole-cell configuration at room temperature.

DATA ANALYSIS

All data were obtained from independent experiments performed on at least 3 days using at least three different animals. Individual numbers of cells/experiments (n) are denoted in figure legends. If not stated otherwise, results are presented as means ± SEM. Statistical analyses were performed using paired or unpaired t-tests or one-way ANOVA with Tukey's HSD *post hoc* test. Tests and corresponding p-values that report statistical significance are individually specified in figure legends. Drug sensitivity of voltage-gated K^+ (Kv) currents was examined based on an "additive" drug exposure regime, i.e., TEA (1 mM), 4-AP (10 mM), and TEA (25 mM) were sequentially applied and the inhibitor-sensitive currents were isolated by subsequent "offline" subtraction from each preceding recording.

Electrophysiological data were analyzed offline using PatchMaster 2.67 (HEKA Elektronik), IGOR Pro 6.3 (WaveMetrics, Lake Oswego, OR) and Excel (Microsoft, Seattle, WA) software. Activation curves were fitted by the Hill equation to calculate the membrane potential of half-maximal activation ($V_{1/2}$). Current activation time constants (τ) were calculated by fitting individual traces to monoexponential functions $I_{(t)} = I_1\ [\exp\ (-t/\tau)] + I_0$.

RESULTS

TRANSGENIC EXPRESSION OF Fpr-rs3-i-VENUS IN A SUBSET OF NEURONS IN THE MOUSE VNO

To analyze the biophysical properties inherent to a prototypical member of the FPR-expressing neurons, we engineered transgenic mice that express Fpr-rs3-i-Venus in a subset of olfactory sensory neurons (OSNs). Using standard transgenic techniques (see section materials and methods), we generated such a mouse strain in which FPR-rs3 is coexpressed with tau-Venus, an enhanced

[1]Available at http://www.stanford.edu/~cpatton/webmaxcS.htm

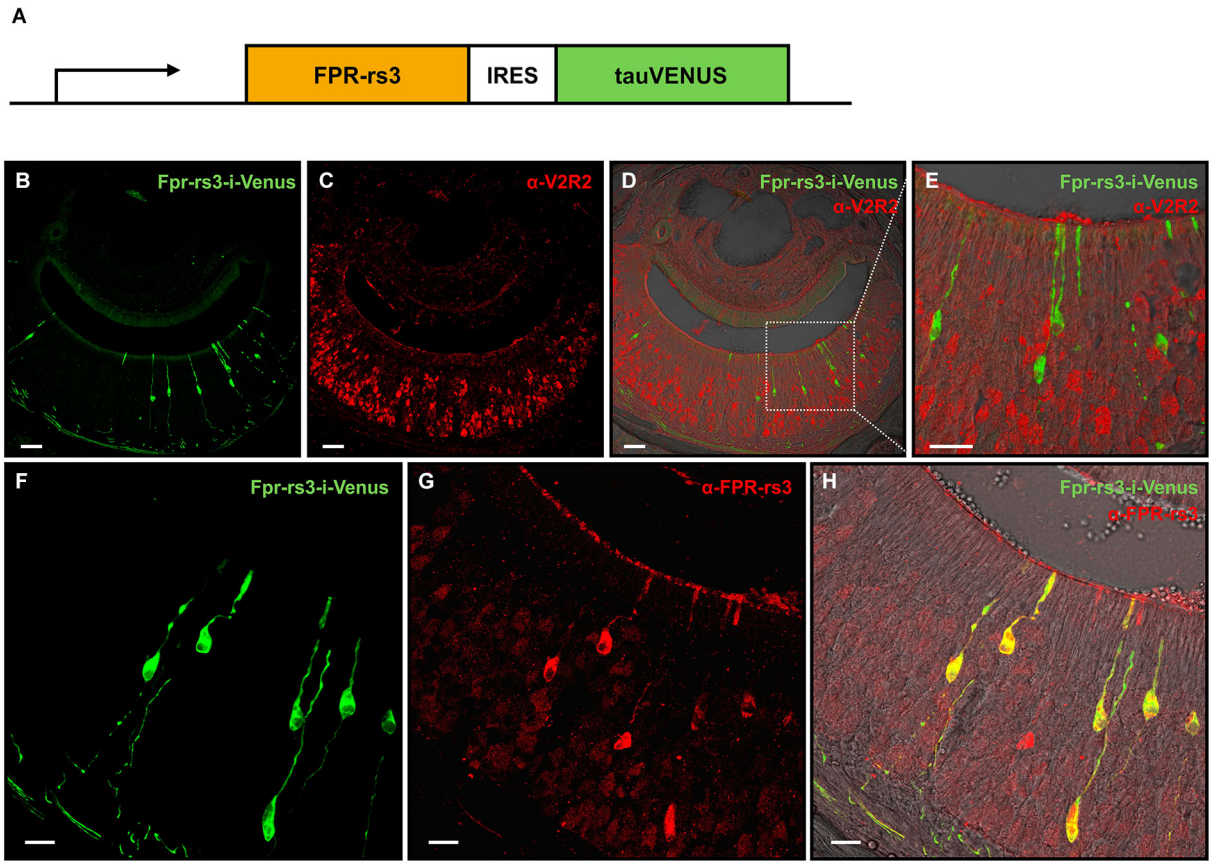

FIGURE 1 | Generation and characterization of the Fpr-rs3-i-Venus transgenic mouse line. **(A)** Schematic of the transgene that includes an OR promoter/enhancer, followed by the coding sequence of FPR-rs3 and a polycistron that drives the tau-Venus fluorophore. **(B)** Confocal image of a coronal VNO cryosection showing sparsely distributed fluorescently labeled FPR-rs3$^+$ VSNs (green) in the sensory neuroepithelium. **(C)** Confocal image displaying a coronal VNO cryosection immunostained with an antibody against V2R2 (red), a family-C V2R expressed in most basal VSNs. **(D)** Overlay of FPR-rs3 tau-Venus fluorescence and anti-V2R2 staining shows no co-localization of apically located FPR-rs3$^+$ and basal V2R2 expressing neurons. **(E)** Higher magnification of the boxed area in **(D)** illustrating the absence of overlapping fluorescence. **(F)** Confocal image of a VNO cryosection showing distinct green fluorescent FPR-rs3$^+$ sensory neurons (green). **(G)** Confocal image displaying the same area as in **(F)** stained against the FPR-rs3 protein (red). **(H)** Overlay of tau-Venus fluorescence and antibody staining against the FPR-rs3 protein. Note that all transgene-positive cells also express FPR-rs3 (yellow). Scale bars, 50 μm **(B–D)**, 10 μm **(E)** and 20 μm **(F–H)**.

variant of yellow fluorescent protein (Nagai et al., 2002) fused to the microtubule-associated protein tau (**Figure 1A**). Four founders were obtained. Two of them expressed the transgene in OSNs, and one of them in VSNs. We focused our attention on this latter line, given its exclusive vomeronasal expression pattern. Neither hemi-, nor homozygous Fpr-rs3-i-Venus mice from this line showed any obvious aberrant phenotype.

In coronal VNO tissue slices, a subpopulation of VSNs is fluorescently labeled (81 out of 11,416 neurons (∼0.7%); **Figures 1B,F**) indicating expression of the Fpr-rs3-i-Venus transgene. Fluorescent neurons are morphologically indistinguishable from unlabeled VSNs. Their somata appear to be predominantly located in the apical layer of the neuroepithelium (**Figure 1B**). Among the five vomeronasal FPRs, FPR-rs3, 4, 6 and 7 are expressed in the more apical $G_{\alpha i2}$-positive layer of the VNO sensory epithelium, whereas FPR-rs1 is located in more basal $G_{\alpha o}$-expressing neurons (Liberles et al., 2009; Rivière et al., 2009). To investigate layer-specific expression of the Fpr-rs3-i-Venus transgene we immunostained coronal VNO cryosections from hemizygous mice with an antibody against V2R2 (α-V2R2; specific for family-C V2Rs that are broadly expressed in the great majority of basal VSNs; **Figures 1C–E**; Martini et al., 2001; Silvotti et al., 2007). We never observed colabeling of transgene-expressing and V2R2-immunopositive VSNs ($n = 79$) confirming layer-specific expression of the FPR-rs3 transgene in apical VSNs. Immunostaining with an anti-FPR-rs3 antibody (Rivière et al., 2009; Dietschi et al., 2013) revealed 424 out of 53,284 FPR-rs3$^+$ VSNs (0.79%), an expression level within the previously reported range between 0.4% and 0.8% (Rivière et al., 2009; Dietschi et al., 2013). Moreover, all transgene-positive cells ($n = 225$) also express the FPR-rs3 protein (**Figures 1F–H**). Some FPR-rs3-immunopositive neurons (199 out of 424 cells) did not show detectable Venus fluorescence, consistent with the presence of VSNs endogenously expressing FPR-rs3.

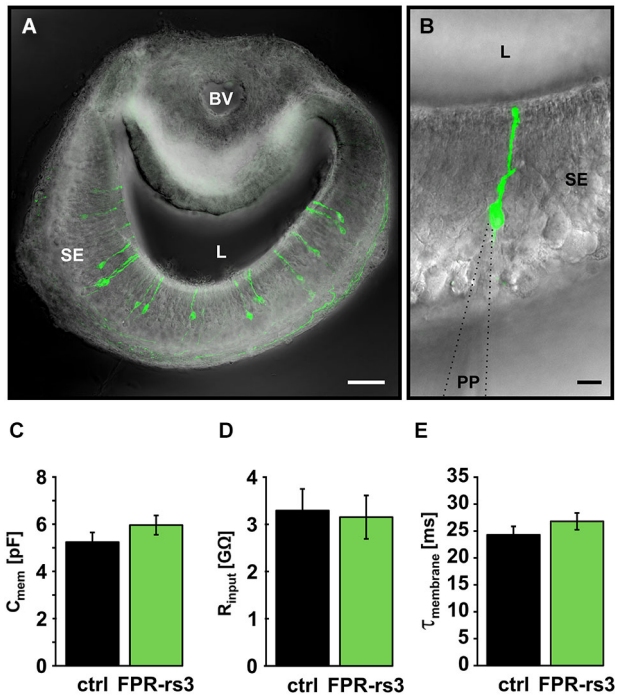

FIGURE 2 | Passive membrane properties of FPR-rs3$^+$ VSNs. **(A)** Confocal image (maximum projection) of a 150 μm acute coronal VNO tissue slice showing the distribution of fluorescent FPR-rs3 tau-Venus$^+$ neurons (green) in the vomeronasal sensory epithelium. Fluorescent axon bundles are visible within the basal lamina. **(B)** FPR-rs3 tau-Venus$^+$ neurons exhibit a single apical dendrite ending in a knob-like structure at the luminal border. Whole cell patch-clamp recordings were performed from the VSN soma. **(C)** Membrane capacitance and **(D)** input resistance (R_{input}) are similar for both control and FPR-rs3$^+$ neurons (n = 21). **(E)** Membrane time constant ($\tau_{membrane}$) of control neurons compared to FPR-rs3$^+$ cells shows no significant difference (n = 21). Data are mean ± SEM. Blood vessel (BV), lumen (L), patch pipette (PP), sensory epithelium (SE). Scale bars, 50 μm **(A)**, 10 μm **(B)**.

PASSIVE MEMBRANE PROPERTIES OF FPR-rs3$^+$ VSNs

The passive membrane properties of a neuron determine its basic electrophysiological characteristics and, thus, control its individual stimulus-response function. For FPR-rs expressing vomeronasal neurons, these critical physiological parameters are unknown. Using Fpr-rs3-i-Venus mice, we performed whole-cell patch-clamp recordings from optically identified, fluorescently labeled FPR-rs3-expressing neurons in acute VNO tissue slices (**Figures 2A,B**). For quantitative comparison, we additionally performed a series of control experiments in randomly chosen VSNs from C57BL/6 wild type mice.

Passive membrane properties (i.e., input resistance (R_{input}), membrane capacitance (C_{mem}), and membrane time constant (τ_{mem})) were obtained immediately after membrane rupture. Treated, to a first approximation, as a "biological constant" with a value of ∼1 μF/cm^2 (Gentet et al., 2000), C_{mem} was determined using a square pulse (5 mV, 10 ms) routine. Transgene-positive (FPR-rs3$^+$) neurons revealed an average C_{mem} value of 5.96 ± 0.49 pF (n = 21), similar to data obtained from control VSNs (5.24 ± 0.38 pF; n = 21; **Figure 2C**). We next determined R_{input} at the VSN soma by measuring the steady-state voltage response to a current step of defined amplitude. The average somatic R_{input} of FPR-rs3$^+$ neurons was 3.15 ± 0.49 GΩ (n = 21; **Figure 2D**). This large value resembles R_{input} measurements from control VSNs (3.29 ± 0.43 GΩ; n = 21), suggesting that FPR-rs3$^+$ neurons share the extraordinary sensitivity of V1/2R-expressing VSNs (Liman and Corey, 1996; Shimazaki et al., 2006; Hagendorf et al., 2009). Linear passive voltage responses were also used to estimate τ_{mem} from monoexponential fits to the voltage responses (from onset to steady state). We obtained relatively slow τ_{mem} values of 26.79 ± 2.25 ms (n = 21) in FPR-rs3$^+$ neurons vs. 24.29 ± 1.57 ms (n = 21) in control neurons (**Figure 2E**).

Together, these results describe different passive membrane parameters of FPR-rs3$^+$ neurons. Moreover, these data show that the passive electrical properties of FPR-rs3 expressing VSNs do not significantly differ from control neurons, suggesting (a) that FPR-rs expressing VSNs are not segregated or isolated from the "general" VSN population; and (b) that transgene expression *per se* does not perturb the passive biophysical properties of FPR-rs3$^+$ neurons.

ACTIVE MEMBRANE PROPERTIES OF FPR-rs3$^+$ NEURONS

Next, we examined the active membrane properties of FPR-rs3$^+$ neurons. A hallmark of VSNs is that depolarizing current injection of only a few picoamperes triggers repetitive action potential discharge (Liman and Corey, 1996; Shimazaki et al., 2006). This also holds true for FPR-rs3$^+$ neurons (**Figure 3A**). Current-clamp recordings from fluorescently labeled VSNs show repetitive spiking in response to depolarizing current steps of 2–24 pA. Spontaneous activity (measured at 0 pA current injection) was 2.37 ± 0.54 Hz (n = 19) for FPRrs3$^+$ neurons and 3.9 ± 1.08 Hz (n = 21) for control cells (**Figure 3B**, inset). By plotting mean instantaneous spike frequencies as a function of stationary current input (f-I curve; **Figure 3B**), response saturation at amplitudes >20 pA becomes apparent (maximum frequency f_{max} = 14.5 ± 0.88 Hz (n = 19; FPR-rs3$^+$ neurons) or 16.54 ± 1.17 Hz (n = 21; control VSNs)). Injection of negative current into FPR-rs3$^+$ neurons revealed a hyperpolarization-activated rebound depolarization ("sag"; **Figure 3A$_{iii}$**), indicative of I_h currents and, thus, HCN channel expression (Robinson and Siegelbaum, 2003; Dibattista et al., 2008). Plotting the sag potential amplitude (ΔV_{sag}; **Figure 3A$_{iii}$**) as a function of peak hyperpolarization reveals the threshold (< −75 mV) and voltage dependence of the sag (n = 5–23; **Figure 3C**), likely corresponding to an increase in HCN channel activation at more negative membrane potentials. A similar voltage dependence was observed for control cells (n = 5–32). In both FPR-rs3$^+$ and control VSNs, we frequently observed rebound spikes upon repolarization (**Figure 3A$_{iii}$**).

Next, we examined action potential discharge of FPR-rs3$^+$ neurons. **Figure 3D$_i$** depicts an averaged spike waveform and shows schematically how different spike parameters were analyzed: spike amplitude was measured as the threshold-to-peak distance, spike duration was calculated as the full duration at half-maximum (FDHM), spike generating kinetics was measured as the time-to-peak (TTP). All analyses were based on the first

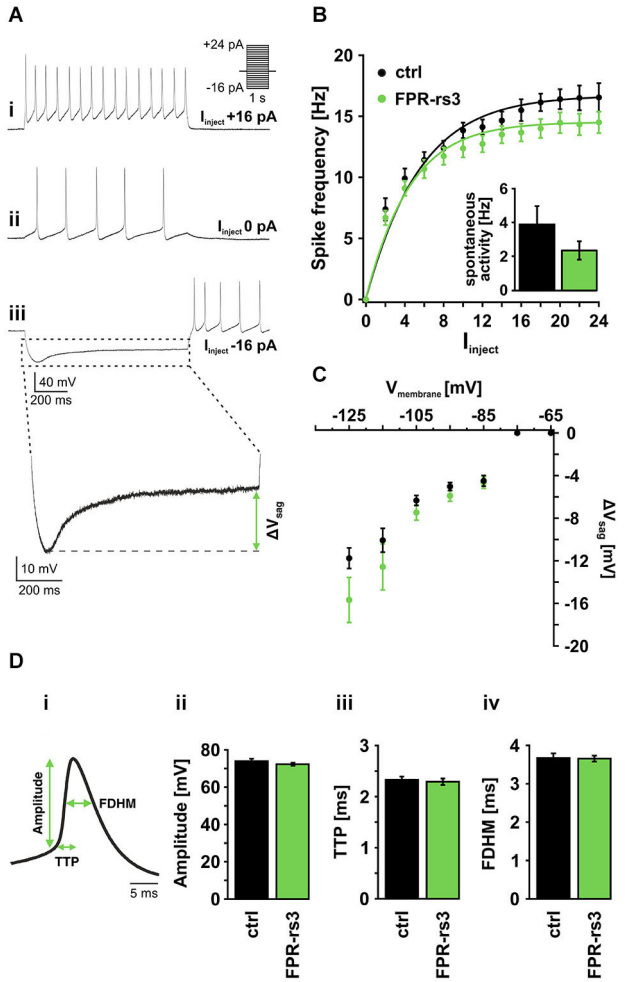

FIGURE 3 | Active membrane properties of FPR-rs3$^+$ VSNs.
(A) Representative current clamp traces showing de- / hyperpolarization and trains of (rebound) action potentials generated upon stepwise current injection. Note the spontaneous activity measured at 0 pA current injection **(A_{ii})**. Injection of negative current produces a prominent voltage "sag" most likely mediated by activation of HCN channels **(A_{iii})**. **(B)** Firing frequency of control (n = 21) and FPR-rs3$^+$ (n = 19) neurons as a function of the injected current (I_{inject}). The gradual increase in firing rate is comparable for control and FPR-rs3$^+$ VSNs. Inset: Spontaneous spiking frequency at 0 pA current injection. Note that f-I curves have been "background-corrected" using these values. **(C)** Voltage "sag" (ΔV_{sag}, n = 3–32) as a function of the peak membrane hyperpolarization (10 mV bins). ΔV_{sag} values of control and FPR-rs3$^+$ neurons show no statistical difference ($p > 0.01$, two-tailed Student's t-test). **(D)** Average spike waveform illustrating analysis parameters (amplitude, time-to-peak (TTP), full duration at half-maximum (FDHM; **D_i**). Amplitude analysis of the first action potential for each current injection step shows no difference between control and FPR-rs3$^+$ cells **(D_{ii})**. TTP analysis reveals values in the same range for both cell populations **(Diii)**. Spike width (FDHM) is not significantly different between control and FPR-rs3$^+$ VSNs **(D_{iv})**. Data are mean ± SEM.

spike of a given train of action potentials (see **Figure 3A$_i$**). Our results reveal an average amplitude of 72.24 ± 0.97 mV (n = 134) for FPR-rs3$^+$ neurons and 73.92 ± 0.87 mV (n = 172) for control neurons (**Figure 3D$_i$**). Average TTP values were 2.29 ± 0.06 ms (FPR-rs3$^+$ cells) and of 2.33 ± 0.09 ms (control neurons), while FDHM was 3.65 ± 0.08 ms (FPR-rs3$^+$ neurons) and 3.67 ± 0.12 ms (control VSNs), respectively.

These data show that FPR-rs3 expressing VSNs exhibit rather slow action potentials and, albeit an extraordinary sensitivity, show a relatively narrow spike frequency coding range. Together, these active membrane properties are shared by both FPR-rs3 expressing and control neurons.

VOLTAGE-GATED Na$^+$ CURRENTS OF FPR-rs3$^+$ NEURONS

In excitable cells, voltage-gated Na$^+$ (Na_V) channels are primarily responsible for action potential initiation and impulse propagation. Upon membrane depolarization, Na_V channels mediate the rapid Na$^+$ influx that underlies the upstroke of the action potential. However, the electrophysiological properties of the nine homologous members of the Na_V channel family ($Na_V1.1$ to $Na_V1.9$) are not identical and even small differences in Na_V channel expression can have profound effects on electrical excitability (Hille, 2001). Therefore, we next focused on macroscopic voltage-activated Na$^+$ currents (I_{Nav}) in FPR-rs3$^+$ neurons. Stepwise depolarizations from −120 mV to +70 mV (30 ms duration; 5 mV increment) in absence and presence of tetrodotoxin (TTX; **Figure 4A$_{i–ii}$**; Narahashi et al., 1966; Wu and Narahashi, 1988) allowed pharmacological isolation of the TTX-sensitive I_{Nav} (**Figure 4A$_{iii}$**). Plotting peak I_{Nav} density as a function of membrane depolarization, the current-voltage relationship (**Figure 4B**) reveals an activation threshold at approximately −65 mV and a maximum current density of −136.7 ± 14.1 pA/pF (n = 10). Similar values were recorded from control VSNs (maximum I_{Nav} = −157.5 ± 17.4 pA/pF; n = 20). **Figure 4C$_i$** illustrates the kinetics of channel gating during a single depolarizing step in membrane potential (−30 mV). As expected from relatively slow action potential firing in FPR-rs3$^+$ neurons (**Figure 3D**), TTP analysis of I_{Nav} reveals relatively slow activation kinetics (1.86 ± 0.10 ms; n = 10; **Figure 4C$_{ii}$**).

Next, we examined the voltage-dependence of TTX-sensitive I_{Nav} activation and inactivation in FPR-rs3$^+$ neurons (**Figures 4D,E**). Fitting normalized peak I_{Nav} amplitudes vs. voltage to a sigmoidal (Boltzmann) function demonstrates half-maximal current activation upon depolarization to approximately −50 mV ($V_{1/2}$ = 48.6 mV; n = 9; **Figure 4E$_i$**). Steady-state I_{Nav} inactivation was analyzed upon depolarization to +20 mV, preceded by prepulse steps to different potentials ranging from −120 mV to 0 mV (30 ms duration; 5 mV increment; **Figure 4D**). Again, offline subtraction of TTX-insensitive currents (**Figure 4D$_{ii}$**) from control recordings (**Figure 4D$_i$**) allowed pharmacological isolation of TTX-sensitive I_{Nav} (**Figure 4D$_{iii}$**). Steady-state inactivation curves are derived from inverse sigmoidal fits to normalized peak I_{Nav} amplitudes vs. prepulse voltage (**Figure 4E$_{ii}$**) and reveal half-maximal inactivation upon depolarization to $V_{1/2}$ = −25 mV (n = 10). Interestingly, at voltages ranging from approximately −60 mV to −5 mV, activation and inactivation curves overlap, suggesting coexpression of multiple Na_V channel isoforms and/or a substantial "window current".

Together, these results demonstrate that FPR-rs3$^+$ VSNs express one or more Na_V channel isoform(s) that exhibit relatively slow activation upon membrane depolarization >−65 mV

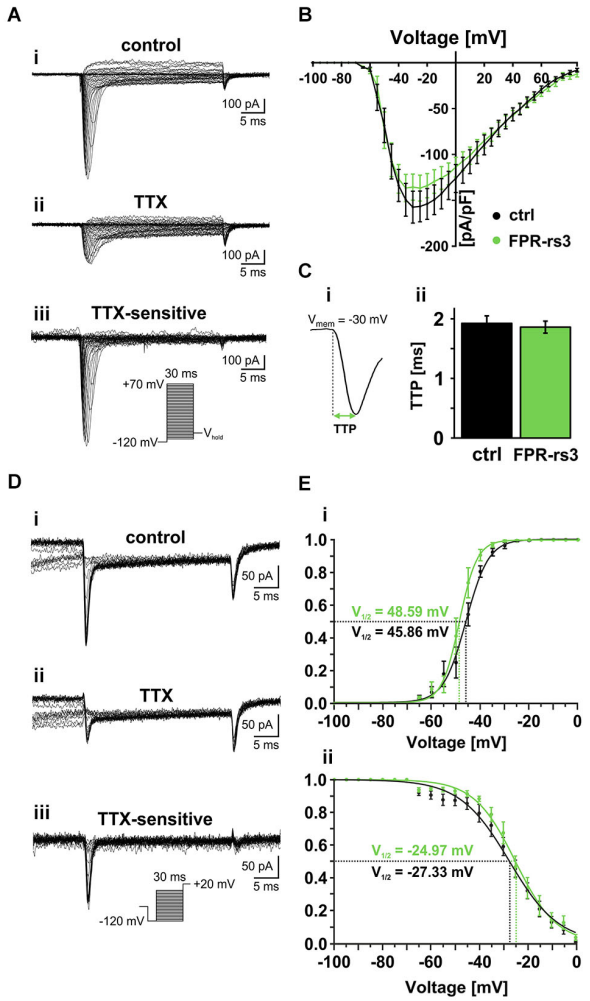

FIGURE 4 | Voltage-gated Na^+ currents. (A) Representative traces from whole-cell patch-clamp recordings of a TTX-sensitive fast activating Na^+ current in FPR-rs3$^+$ VSNs. **(A_i)** Voltage step recording under control conditions (extracellular solution S_1; intracellular solution S_9) reveals a voltage-dependent fast and transient inward current. **(A_{ii})** TTX treatment (1 μM) strongly diminishes the current. Digitally subtracted trace (control-TTX **(A_{iii})**) reveals the TTX-sensitive voltage-gated Na^+ current. **(B)** Current-voltage relationships of TTX-sensitive Na^+ currents isolated from control and FPR-rs3$^+$ neurons (control, $n = 20$; FPR-rs3$^+$, $n = 10$; $p > 0.01$, two-tailed Student's *t*-test). **(C)** Example of a voltage-clamp recording showing the fast activating transient inward current used for upstroke kinetics analysis **(C_i)**. TTP of the fast activating Na^+ current upon depolarization to −30 mV (control, $n = 20$; FPR-rs3$^+$, $n = 10$; **C_{ii}**). **(D)** Representative traces showing Na^+ channel steady-state inactivation under control conditions **(D_i)**, in presence of TTX **(D_{ii})**, and after digital subtraction (control-TTX **(D_{iii})**). Prepulse steps from −120 mV to 0 mV were applied to analyze inactivation (**D_{iii}**, inset). **(E)** Normalized activation **(E_i)** and steady-state inactivation **(E_{ii})** curves (peak current vs. pulse/prepulse voltage). Data points were fitted using a sigmoidal Boltzmann-type equation. Membrane voltage inducing half-maximal activation and inactivation ($V_{1/2}$) as indicated. Data are mean ± SEM.

with half-maximal and complete activation at ∼−50 mV and −30 mV, respectively. Moreover, the slope of the steady-state inactivation curve is relatively shallow, revealing that full channel inactivation only occurs at positive potentials. Since all measured parameters are similar to data recorded from control VSNs, our data further substantiate the notion that that FPR-rs expressing neurons do not constitute a biophysically segregated "outgroup" of VSNs.

VOLTAGE-GATED K^+ CURRENTS OF FPR-rs3$^+$ NEURONS

To a large extent, Kv channels control electrical signaling in excitable cells. Accordingly, the large and extended Kv channel family is functionally diversified by alternative splicing, oligomeric subunit assembly, and subcellular targeting (Jan and Jan, 2012). As Kv channels are involved in regulating a wide range of neuronal functions, such as setting the resting membrane potential, dictating the duration and/or frequency of action potentials, volume regulation, etc., we next characterized Kv channel-mediated currents (I_{Kv}) in FPR-rs3$^+$ neurons.

Activated by depolarization, outward flux of K^+ repolarizes the membrane and, thus, contributes to action potential termination and, in some neurons, afterhyperpolarization. To isolate different classes of I_{Kv} we used a pharmacological toolkit of several well-described Kv channel inhibitors (Alexander et al., 2013). Depending on concentration, tetraethylammonium (TEA) functions as a relatively selective inhibitor of big conductance Ca^{2+}-dependent K^+ (BK) channels at low millimolar concentrations (Yellen, 1984), whereas substantially higher concentrations (25 mM) serve as a nonselective "broadband" Kv channel blocker (Alexander et al., 2013). In addition, 4-aminopyridine (4-AP) specifically blocks A-type K^+ currents in various neurons (Mei et al., 1995; Amberg et al., 2003).

Under control conditions, stepwise depolarization from −100 to +85 mV (100 ms duration; 5 mV increment) triggered large outward currents that essentially showed no sign of inactivation (**Figure 5A**, inset). When steady-state currents were plotted as a function of depolarization, the resulting current-voltage relationship reveals I_{Kv} activation at approximately −30 mV (**Figure 5A**). Linear regression from data points corresponding to full activation (+60 mV – +85 mV) indicates I_{Kv} reversal at ∼−65 mV. When drug-sensitive currents were isolated by digital subtraction of blocker-insensitive from respective "control" recordings (**Figures 5B–D**, insets; see section materials and methods), the resulting current-voltage plots revealed no statistical differences between FPR-rs3$^+$ neurons and control VSNs (**Figures 5B–D**). Somewhat surprisingly, currents isolated by 4-AP treatment did not show a pronounced transient component typical for A-type K^+ currents. Interestingly, summation of the individual drug-sensitive I_{Kv} components added up to almost 100% of control currents (276.5 ± 31.1 pA/pF at +85 mV; $n = 13$; **Figure 5E**) showing that a "cocktail" of 4-AP (10 mM) and TEA (25 mM) is sufficient to block essentially all Kv channels in FPR-rs3$^+$ neurons. This pharmacological profile was statistically indistinguishable from control VSNs.

Next, we investigated how the pharmacologically different K_v channel populations shape action potential discharge in FPR-rs3$^+$ cells. Spikes were elicited and discharge parameters were analyzed as described (**Figures 3D**, **5F$_i$**). VSNs were challenged with either TEA (1 mM) or 4-AP (10 mM). Spike amplitude (**Figure 5F$_{ii}$**) was not altered by either drug. Both Kv channel

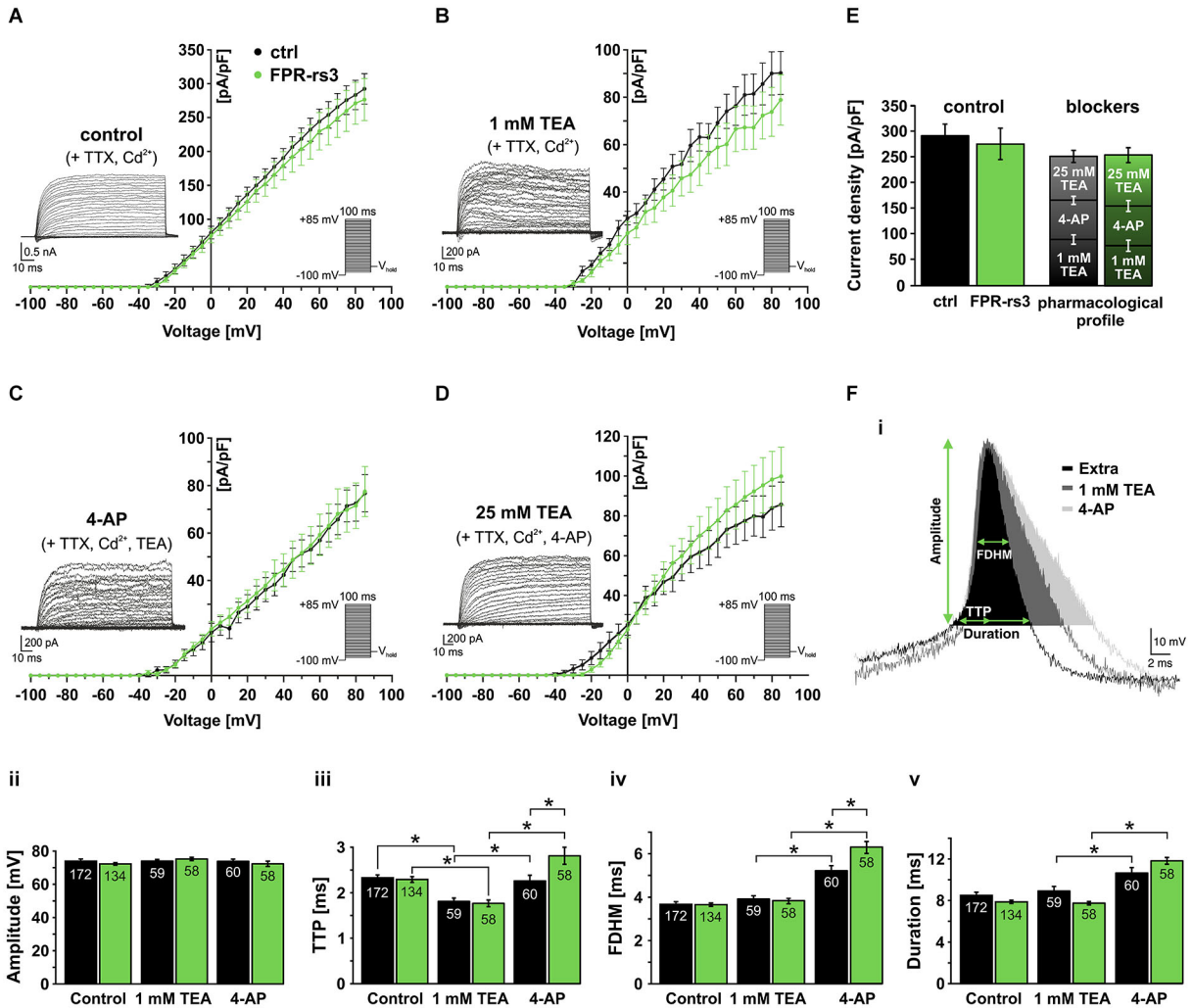

FIGURE 5 | Voltage-gated K^+ currents and their role in action potential firing. (A) Voltage-activated outward K^+ currents under control conditions (solution **S_1** including TTX (1 μM) and Cd^{2+} (200 μM) to isolate K^+ currents). Currents were induced by stepwise depolarization and measured during steady-state. Current densities were calculated and plotted against voltage (control, $n = 10$; FPR-rs3$^+$, $n = 13$). **(B)** Outward currents sensitive to 1 mM TEA (control-TEA; digital subtraction; $n = 10$). **(C)** Outward currents sensitive to 10 mM 4-AP (control/TEA-4-AP; digital subtraction; $n = 10$). **(D)** Outward currents sensitive to 25 mM TEA (control/TEA/4-AP-TEA; digital subtraction; $n = 10$). **(E)** Quantification of outward currents. Maximum current densities under control conditions (left bars; 292.5 ± 22.4 pA/pF at +85 mV, $n = 10$ (ctrl); 276.5 ± 31.1 pA/pF, $n = 13$ (FPR-rs3$^+$)) and added drug sensitive current densities (ctrl: 90.3 ± 9.1 pA/pF (1 mM TEA), 76.8 ± 7.9 pA/pF (10 mM 4-AP), 85.7 ± 11.2 pA/pF (25 mM TEA); FPR-rs3$^+$: 78.9 ± 10.6 pA/pF (1 mM TEA), 77.5 ± 10.5 pA/pF (10 mM 4-AP), 99.8 ± 14.6 pA/pF (25 mM TEA)). Data are mean ± SEM. **(F)** Representative spike waveform under control conditions (solution **S_1** (Extra)) and in presence of TEA (1 mM) and 4-AP (10 mM; **F_i**). Analysis parameters (amplitude, TTP, FDHM and spike duration) are depicted schematically. Bar graphs illustrate the quantification of discharge characteristics **($F_{ii–v}$)**. *$p < 0.01$; two-way ANOVA with Tukey's multiple comparisons test. Data are mean ± SEM, number of cells as depicted inside the bars.

inhibitors affected the upstroke dynamics (**Figure 5F$_{iii}$**). However, while block of putative BK channels by TEA (1 mM) accelerated the upstroke, inhibition of A-type currents prolonged the average TTP. 4-AP treatment also prolonged the spike width (FDHM) and, consequently, spike duration (**Figure 5F$_{iv–v}$**) whereas TEA did not elicit such effects. The effects of 4-AP are significantly more pronounced in FPR-rs3 expressing VSNs than in control neurons (**Figure 5F$_{iii–v}$**).

In summary, these data demonstrate that multiple Kv channel subunits are expressed in FPR-rs3$^+$ neurons. These different channel populations synergistically shape the firing properties of FPR-rs3 expressing VSNs. Moreover, with the notable exception of 4-AP-sensitive channel function during discharge, the Kv channel expression profile of FPR-rs3$^+$ neurons is largely comparable to control VSNs.

VOLTAGE-GATED Ca^{2+} CURRENTS OF FPR-rs3$^+$ NEURONS

Voltage-gated Ca^{2+} (Ca_V) channels are integral constituents of a neuron's Ca^{2+} signaling toolkit (Berridge et al., 2003). As such, they are key signal transducers that transform electrical

impulses (depolarization) into a biochemically relevant signal (Ca^{2+} influx) that regulates a wide variety of cellular events (Catterall, 2000b; Clapham, 2007). We therefore investigated Ca_V currents (I_{Cav}) in FPR-rs3$^+$ neurons.

The ten functional vertebrate Ca_V channel subunits are divided into three subfamilies (Ca_V1 to Ca_V3) that differ in function and regulation (Triggle et al., 2006). Both within and between subfamilies, individual Ca_V channel isoforms are identified by their distinct biophysical properties and pharmacological profiles (Catterall, 2000b; Alexander et al., 2013). Thus, we isolated transient (T-type) currents mediated by members of the Ca_V3 subfamily by digital subtraction of I_{Cav} recorded in response to depolarizing voltage steps (−100 mV to +45 mV; 100 ms duration; 5 mV increment) from two different prepulse potentials (−100 mV and −25 mV, respectively; **Figure 6A$_i$**, inset). Based on steady-state inactivation of Ca_V3 channels at −25 mV (Catterall et al., 2005), the fraction of low voltage activated (LVA) Ca^{2+} channels becomes readily apparent after subtraction (**Figure 6A$_i$**). As expected, these T-type currents rapidly inactivate and the underlying activation and inactivation kinetics become faster with increasing depolarization (Perez-Reyes et al., 1998). The resulting current-voltage relationship (**Figure 6A$_{ii}$**) and normalized I_{Cav} activation curve (sigmoidal fit; **Figure 6A$_{iii}$**) demonstrate an activation threshold of −60 mV and half-maximal current activation upon depolarization to −40 mV ($V_{1/2}$ = −40.27 mV; n = 9), values typical for T-type currents.

Next, we investigated functional expression of high voltage activated (HVA) Ca_V channels in FPR-rs3$^+$ neurons. All four members of the Ca_V1 subfamily are characterized by both long-lasting and large (L-type) Ca^{2+} currents and high sensitivity to dihydropyridines, such as nifedipine (Catterall et al., 2005). Therefore, to examine L-type I_{Cav}, we recorded responses to depolarizing voltage steps (−100 mV to +85 mV; 100 ms duration; 5 mV increment) and isolated nifedipine-sensitive currents by digital subtraction (**Figure 6B$_i$**). As expected for L-type currents, isolated I_{Cav} shows relatively slow, though lasting activation upon depolarization ≥−45 mV (**Figure 6B$_{ii}$**). Half-maximal activation is observed upon more pronounced depolarization ($V_{1/2}$ = −26.06 mV; n = 7; **Figure 6B$_{iii}$**).

Members of the Ca_V2 subfamily of HVA Ca^{2+} channels are selectively sensitive to peptide neurotoxins from spider and cone snail venoms (Catterall, 2000a). Using ω-conotoxin-GVIA, we next isolated conotoxin-sensitive N-type I_{Cav} from FPR-rs3$^+$ neurons (**Figure 6C$_i$**). N-type currents activate upon depolarizations ≥−40 mV (**Figure 6C$_{ii}$**). At approximately −25 mV, N-type I_{Cav} is half-maximally activated ($V_{1/2}$ = −25.46 mV; n = 7; **Figure 6C$_{iii}$**). Surprisingly, recordings from control VSNs reveal substantially larger conotoxin-sensitive currents (**Figure 6C$_{ii–iii}$**). While T- and L-type I_{Cav} in FPR-rs3$^+$ VSNs did not significantly differ from control neurons, maximum N-type current density was −24.05 ± 2.37 pA/pF in fluorescently labeled cells (n = 7), but −36.96 ± 6.50 pA/pF in control VSNs (n = 8). Moreover, half-maximal activation in controls was shifted to more positive values ($V_{1/2}$ = −19.24 mV; n = 8; **Figure 6C$_{iii}$**).

A slight, though also significant difference between FPR-rs3$^+$ and control neurons was observed for P/Q-type Ca^{2+} currents that were pharmacologically isolated using ω-agatoxin IVA (Randall and Tsien, 1995; Catterall, 2011). P/Q-type currents revealed relatively slow activation and slight inactivation. Compared to control recordings, both the current-voltage relationship (**Figure 6D$_{ii}$**) and the sigmoidal activation curve (**Figure 6D$_{iii}$**) of P/Q-type I_{Cav} in FPR-rs3$^+$ neurons was left-shifted to more negative potentials. Maximum current density, however, did not significantly differ between FPR-rs3$^+$ VSNs (−29.50 ± 3.31 pA/pF; n = 8) and control neurons (−31.46 ± 4.34 pA/pF; n = 5).

In summary, the above data show that FPR-rs3$^+$ neurons exhibit a variety of Ca_V currents, both LVA and HVA. Since both N- and P/Q-type currents show somewhat different properties in FPR-rs3 expressing VSNs, these two Ca_V2 channel isoforms might play distinct roles in FPR-rs3$^+$ neurophysiology.

DISCUSSION

For most mammals, the VNO is crucial for intra- and interspecific chemical communication. While the basic biophysical properties of both V1R- and V2R-expressing vomeronasal neurons have been described (Liman and Corey, 1996; Trotier and Døving, 1996; Fieni et al., 2003; Shimazaki et al., 2006; Ukhanov et al., 2007; Hagendorf et al., 2009), VSNs that express members of the recently discovered family of vomeronasal FPR-rs proteins (Liberles et al., 2009; Rivière et al., 2009) remain physiologically unexplored. Here, we describe a transgenic mouse model (Fpr-rs3-i-Venus) in which expression of one member of the FPR-rs family (FPR-rs3) is marked by Venus fluorescence. This mouse strain allows identification and electrophysiological analysis of FPR-rs3-expressing neurons in acute VNO tissue slices. Thus, we provide an in-depth analysis of both passive and active membrane properties, including detailed characterization of several types of voltage-activated conductances and action potential discharge patterns, in fluorescently labeled vs. unmarked vomeronasal neurons. Our results reveal a number of similarities, but also some differences in the basic (electro) physiological architecture of transgene-expressing vs. non-expressing neurons.

Vomeronasal transgene expression in Fpr-rs3-i-Venus mice faithfully recapitulates the punctate apical expression pattern of endogenous FPR-rs3 (Rivière et al., 2009; Dietschi et al., 2013). Furthermore, bicistronic expression of the tau-Venus fusion protein additionally targets the fluorescent marker to axons and axon terminals in the AOB. We therefore propose that Fpr-rs3-i-Venus mice not only provide a useful tool for physiological studies of FPR-rs3$^+$ neurons in the VNO (as described here), but also for studies of axon targeting and glomerular innervation in the AOB. While, based on the experimental strategy used here, we cannot exclude that FPR-rs3$^+$ VSNs additionally express other vomeronasal receptor genes, this appears unlikely since the negative feedback signal that ensures gene exclusion in apical VSNs is also maintained by exogenous expression of another receptor gene, even an OR (Capello et al., 2009).

The specific biophysical profile of FPR-rs3$^+$ VSNs is a critical determinant of their sensory input-output function. Passive membrane properties, such as R_{input}, C_{mem} and τ_{mem}, are therefore crucial functional descriptors of FPR-rs3$^+$ neuron physiology. C_{mem} and dendritic geometry together determine the amplitude of the receptor potential as well as, being inversely

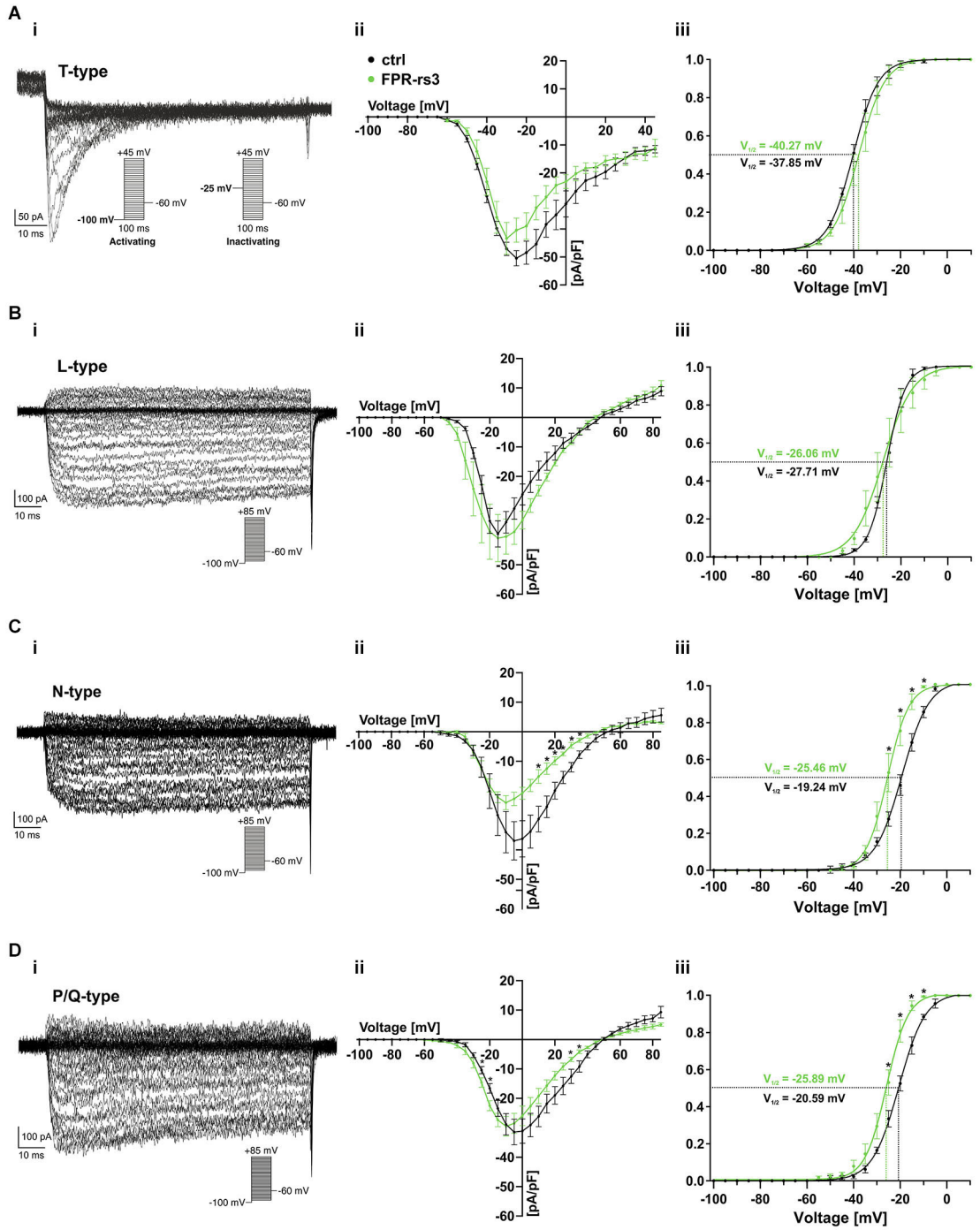

FIGURE 6 | Voltage-gated Ca^{2+} currents. (A–D) Representative Ca^{2+} current traces isolated either biophysically (prepulse inactivation protocol; **(A_i)**) or pharmacologically (nifedipine (10 μM; **B_i**); ω-conotoxin-GVIA (2 μM; **C_i**); ω-agatoxin IVA (200 nM; **D_i**). Step protocols as indicated. Absolute **(A_{ii}–D_{ii})** and normalized **(A_{iii}–D_{iii})** peak current densities are plotted as a function of membrane depolarization. Activation curves **(A_{iii}–D_{iii})** are fitted according to a sigmoidal Boltzmann-type equation. Membrane voltage inducing half-maximal activation ($V_{1/2}$) as indicated. Data are mean ± SEM; $^*p < 0.01$, two-tailed Student's *t*-test.

proportional, the speed of signal propagation along the dendrite (Gentet et al., 2000). C_{mem} values obtained for FPR-rs3$^+$ neurons are broadly consistent with previously reported data (Liman and Corey, 1996; Shimazaki et al., 2006; Ukhanov et al., 2007) and do not differ from values recorded from randomly chosen control VSNs from wild type C57BL/6 mice. The remarkably high input

resistance previously reported for VSNs (Liman and Corey, 1996; Fieni et al., 2003; Shimazaki et al., 2006; Dibattista et al., 2008; Sagheddu et al., 2010) is shared by FPR-rs3$^+$ neurons. Thus, FPR-rs3-dependent receptor currents of even a few picoamperes will be sufficient to trigger action potential discharge. We therefore propose that the primary signal transduction machinery in FPR-rs3$^+$ neurons must be balanced by proper gain/offset control mechanisms to avoid false-positive output. In this context, the rather narrow tuning range of the input-output function of FPR-rs3$^+$ neurons (and control VSNs) is noticeable. Frequency coding accommodates spike rates between 0 and ∼15 Hz that encode receptor currents ranging to a maximum of ∼25 pA (note that the "linear" dynamic range of the *f*-I curve is considerably more narrow). Similar values have previously been reported (Liman and Corey, 1996; Ukhanov et al., 2007). The relatively long τ_{mem} values (∼25 ms) we obtained for both FPR-rs3$^+$ and control neurons ensure that brief stimulatory events will not generate significant output, in line with the idea that stimulus exchange in the VNO is relatively slow probably allowing prolonged VSN receptor-ligand interaction.

Detailed spike waveform analysis revealed rather slow and broad action potentials in line with previously published results (Shimazaki et al., 2006; Hagendorf et al., 2009). Moreover, hyperpolarizing current injection triggers rebound depolarizations resulting in a pronounced "voltage sag" (Robinson and Siegelbaum, 2003; Dibattista et al., 2008). Mediated by HCN channels, we and others observed increasing "sag" amplitudes with membrane potentials becoming more hyperpolarized (Ukhanov et al., 2007; Dibattista et al., 2008). Thus, active membrane properties of FPR-rs3$^+$ neurons do not segregate these neurons from the "general" VSN population.

We used the pufferfish toxin TTX to isolate whole-cell currents mediated by voltage-gated Na_V channels. FPR-rs3$^+$ VSNs express one or more TTX-sensitive Na_V channel isoform(s), i.e., Nav1.1, 1.2, 1.3, 1.4, or 1.7 (Hille, 2001), which exhibit relatively slow activation upon membrane depolarization >-65 mV with half-maximal and complete activation at ~-50 mV and -30 mV, respectively. Notably, the slope of the steady-state inactivation curve is relatively shallow, revealing that full channel inactivation only occurs at positive potentials and, in addition, resulting in a substantial "window current" that ranges from approximately -60 mV to -5 mV.

Similar pharmacological approaches were used to isolate currents mediated by K_V and Ca_V channels, respectively. At least three different and probably heterogeneous populations of K_V channels were identified according to their sensitivity to 4-AP and different TEA concentrations, respectively (Liman and Corey, 1996). Interestingly, while 4-AP-sensitive currents lacked a prominent transient component typical for A-type K^+ currents (Mei et al., 1995; Amberg et al., 2003), this K_V channel population exerted considerable effects on action potential waveform. Moreover, these effects on upstroke kinetics (TTP) and spike width (FDHM/duration) where different between FPR-rs3$^+$ neurons and control VSNs. In addition to Na_V and K_V channels, several types of Ca_V channels were identified in FPR-rs3$^+$ neurons. T-, L-, N-, and P/Q-type I_{CaV} was isolated, either pharmacologically (L-, N-, P/Q-type) or by prepulse inactivation (T-type). While T- and L-type I_{Cav} in FPR-rs3$^+$ VSNs did not significantly differ from control neurons, we find that both N- and P/Q-type currents show somewhat different properties in FPR-rs3 expressing VSNs. We can only speculate about the mechanisms that might link FPR-rs3 expression to altered expression and/or functionality of either N- or P/Q-type Ca_V channels. The scope of possible explanations ranges from altered *Cacna1a*/*Cacna1b* transcription by random transgene insertion to direct binding of $G_{\beta/\gamma}$ to the α1 subunit of either Ca_V2 channel (Currie, 2010), complex co-regulation scenarios of, for example, accessory channel subunits (Neely and Hidalgo, 2014), or unknown intrinsic properties of a potential subpopulation of neurons that express FPR-rs3 instead of a "native" receptor. Whatever the mechanistic basis, the interpretation of future experiments will have to take potential physiological differences into account, which could arise from transgenic vs. endogenous expression.

The Fpr-rs3-i-Venus mouse model we introduce and the basic electrophysiological characterization we performed provide a foundation for future functional studies of FPR-rs neurophysiology. In analogy to FPR signaling in the immune system, current concepts of FPR-rs function suggest a role as chemoreceptors for inflammation-associated and pathogen-related compounds (Rivière et al., 2009; Chamero et al., 2011; Bufe et al., 2012). Immune system FPRs are broadly tuned detectors of either host- or pathogen-derived inflammatory signals (Le et al., 2002; Migeotte et al., 2006; He et al., 2014). Somewhat controversial results have been reported on the tuning profile(s) of recombinantly expressed vomeronasal FPR-rs proteins (Rivière et al., 2009; Bufe et al., 2012). Fpr-rs3-i-Venus mice will likely prove useful for studying FPR-rs3-ligand interaction in homologous cells.

ACKNOWLEDGMENTS

This work was funded by grants of the Volkswagen Foundation (I/83533), the Deutsche Forschungsgemeinschaft (SP724/6-1) and by the Excellence Initiative of the German federal and state governments and the Swiss National Science Foundation grants 31003A-149753 and 310030E-135910. MS is a Lichtenberg Professor of the Volkswagen Foundation. We thank Corinna H. Engelhardt and Susanne Lipartowski (RWTH-Aachen University) for excellent technical assistance.

REFERENCES

Adams, D. R. (1992). Fine structure of the vomeronasal and septal olfactory epithelia and of glandular structures. *Microsc. Res. Tech.* 23, 86–97. doi: 10.1002/jemt.1070230108

Alexander, S. P. H., Benson, H. E., Faccenda, E., Pawson, A. J., Sharman, J. L., Catterall, W. A., et al. (2013). The concise guide to pharmacology 2013/14: ion channels. *Br. J. Pharmacol.* 170, 1607–1651. doi: 10.1111/bph.12447

Amberg, G. C., Koh, S. D., Imaizumi, Y., Ohya, S., and Sanders, K. M. (2003). A-type potassium currents in smooth muscle. *Am. J. Physiol. Cell Physiol.* 284, C583–C595. doi: 10.1152/ajpcell.00301.2002

Barry, P. H. (1994). JPCalc, a software package for calculating liquid junction potential corrections in patch-clamp, intracellular, epithelial and bilayer measurements and for correcting junction potential measurements. *J. Neurosci. Methods* 51, 107–116. doi: 10.1016/0165-0270(94)90031-0

Belluscio, L., Koentges, G., Axel, R., and Dulac, C. (1999). A map of pheromone receptor activation in the mammalian brain. *Cell* 97, 209–220. doi: 10.1016/s0092-8674(00)80731-x

Berridge, M. J., Bootman, M. D., and Roderick, H. L. (2003). Calcium signalling: dynamics, homeostasis and remodelling. *Nat. Rev. Mol. Cell Biol.* 4, 517–529. doi: 10.1038/nrm1155

Boschat, C., Pélofi, C., Randin, O., Roppolo, D., Lüscher, C., Broillet, M.-C., et al. (2002). Pheromone detection mediated by a V1r vomeronasal receptor. *Nat. Neurosci.* 5, 1261–1262. doi: 10.1038/nn978

Bozza, T., Feinstein, P., Zheng, C., and Mombaerts, P. (2002). Odorant receptor expression defines functional units in the mouse olfactory system. *J. Neurosci.* 22, 3033–3043.

Brechbühl, J., Klaey, M., and Broillet, M.-C. (2008). Grueneberg ganglion cells mediate alarm pheromone detection in mice. *Science* 321, 1092–1095. doi: 10.1126/science.1160770

Bufe, B., Schumann, T., and Zufall, F. (2012). Formyl peptide receptors from immune and vomeronasal system exhibit distinct agonist properties. *J. Biol. Chem.* 287, 33644–33655. doi: 10.1074/jbc.m112.375774

Capello, L., Roppolo, D., Jungo, V. P., Feinstein, P., and Rodriguez, I. (2009). A common gene exclusion mechanism used by two chemosensory systems. *Eur. J. Neurosci.* 29, 671–678. doi: 10.1111/j.1460-9568.2009.06630.x

Catterall, W. A. (2000a). Structure and regulation of voltage-gated Ca^{2+} channels. *Annu. Rev. Cell Dev. Biol.* 16, 521–555. doi: 10.1146/annurev.cellbio.16.1.521

Catterall, W. A. (2000b). From ionic currents to molecular mechanisms: the structure and function of voltage-gated sodium channels. *Neuron* 26, 13–25. doi: 10.1016/S0896-6273(00)81133-2

Catterall, W. A. (2011). Voltage-gated calcium channels. *Cold Spring Harb Perspect. Biol.* 3:a003947. doi: 10.1101/cshperspect.a003947

Catterall, W. A., Perez-reyes, E., Snutch, T. P., and Striessnig, J. (2005). International union of pharmacology. XLVIII. Nomenclature and structure-function relationships of voltage-gated calcium channels. *Pharmacol. Rev.* 57, 411–425. doi: 10.1124/pr.57.4.5

Chamero, P., Katsoulidou, V., Hendrix, P., Bufe, B., Roberts, R. W., Matsunami, H., et al. (2011). G protein G(alpha)o is essential for vomeronasal function and aggressive behavior in mice. *Proc. Natl. Acad. Sci. U S A* 108, 12898–12903. doi: 10.1073/pnas.1107770108

Chamero, P., Leinders-Zufall, T., and Zufall, F. (2012). From genes to social communication: molecular sensing by the vomeronasal organ. *Trends Neurosci.* 35, 597–606. doi: 10.1016/j.tins.2012.04.011

Chamero, P., Marton, T. F., Logan, D. W., Flanagan, K., Cruz, J. R., Saghatelian, A., et al. (2007). Identification of protein pheromones that promote aggressive behaviour. *Nature* 450, 899–902. doi: 10.1038/nature05997

Clapham, D. E. (2007). Calcium signaling. *Cell* 131, 1047–1058. doi: 10.1016/j.cell.2007.11.028

Currie, K. P. M. (2010). G protein modulation of CaV2 voltage-gated calcium channels. *Channels (Austin)* 4, 497–509. doi: 10.4161/chan.4.6.12871

Dibattista, M., Mazzatenta, A., Grassi, F., Tirindelli, R., and Menini, A. (2008). Hyperpolarization-activated cyclic nucleotide-gated channels in mouse vomeronasal sensory neurons. *J. Neurophysiol.* 100, 576–586. doi: 10.1152/jn.90263.2008

Dietschi, Q., Assens, A., Challet, L., Carleton, A., and Rodriguez, I. (2013). Convergence of FPR-rs3-expressing neurons in the mouse accessory olfactory bulb. *Mol. Cell. Neurosci.* 56, 140–147. doi: 10.1016/j.mcn.2013.04.008

Dulac, C., and Axel, R. (1995). A novel family of genes encoding putative pheromone receptors in mammals. *Cell* 83, 195–206. doi: 10.1016/0092-8674(95)90161-2

Dulac, C., and Torello, A. T. (2003). Molecular detection of pheromone signals in mammals: from genes to behaviour. *Nat. Rev. Neurosci.* 4, 551–562. doi: 10.1038/nrn1140

Ferrero, D. M., Moeller, L. M., Osakada, T., Horio, N., Li, Q., Roy, D. S., et al. (2013). A juvenile mouse pheromone inhibits sexual behaviour through the vomeronasal system. *Nature* 502, 368–371. doi: 10.1038/nature12579

Fieni, F., Ghiaroni, V., Tirindelli, R., Pietra, P., and Bigiani, A. (2003). Apical and basal neurones isolated from the mouse vomeronasal organ differ for voltage-dependent currents. *J. Physiol.* 552, 425–436. doi: 10.1113/jphysiol.2003.052035

Firestein, S. (2001). How the olfactory system makes sense of scents. *Nature* 413, 211–218. doi: 10.1038/35093026

Fuss, S. H., Omura, M., and Mombaerts, P. (2005). The Grueneberg ganglion of the mouse projects axons to glomeruli in the olfactory bulb. *Eur. J. Neurosci.* 22, 2649–2654. doi: 10.1111/j.1460-9568.2005.04468.x

Gentet, L. J., Stuart, G. J., and Clements, J. D. (2000). Direct measurement of specific membrane capacitance in neurons. *Biophys. J.* 79, 314–320. doi: 10.1016/s0006-3495(00)76293-x

Grosmaitre, X., Fuss, S. H., Lee, A. C., Adipietro, K. A., Matsunami, H., Mombaerts, P., et al. (2009). SR1, a mouse odorant receptor with an unusually broad response profile. *J. Neurosci.* 29, 14545–14552. doi: 10.1523/jneurosci.2752-09.2009

Grosmaitre, X., Vassalli, A., Mombaerts, P., Shepherd, G. M., and Ma, M. (2006). Odorant responses of olfactory sensory neurons expressing the odorant receptor MOR23: a patch clamp analysis in gene-targeted mice. *Proc. Natl. Acad. Sci. U S A* 103, 1970–1975. doi: 10.1073/pnas.0508491103

Hagendorf, S., Fluegge, D., Engelhardt, C., and Spehr, M. (2009). Homeostatic control of sensory output in basal vomeronasal neurons: activity-dependent expression of ether-à-go-go-related gene potassium channels. *J. Neurosci.* 29, 206–221. doi: 10.1523/jneurosci.3656-08.2009

He, H.-Q., Liao, D., Wang, Z.-G., Wang, Z.-L., Zhou, H.-C., Wang, M.-W., et al. (2013). Functional characterization of three mouse formyl peptide receptors. *Mol. Pharmacol.* 83, 389–398. doi: 10.1124/mol.112.081315

He, H.-Q., Troksa, E. L., Caltabiano, G., Pardo, L., and Ye, R. D. (2014). Structural determinants for the interaction of formyl Peptide receptor 2 with Peptide ligands. *J. Biol. Chem.* 289, 2295–2306. doi: 10.1074/jbc.m113.509216

Herrada, G., and Dulac, C. (1997). A novel family of putative pheromone receptors in mammals with a topographically organized and sexually dimorphic distribution. *Cell* 90, 763–773. doi: 10.1016/s0168-9525(97)89832-0

Hille, B. (2001). *Ion Channels of Excitable Membranes.* 3rd Edn. ed B. Hille Sunderland, MA: Sinauer Associates, Inc.

Isogai, Y., Si, S., Pont-Lezica, L., Tan, T., Kapoor, V., Murthy, V. N., et al. (2011). Molecular organization of vomeronasal chemoreception. *Nature* 478, 241–245. doi: 10.1038/nature10437

Jan, L. Y., and Jan, Y. N. (2012). Voltage-gated potassium channels and the diversity of electrical signalling. *J. Physiol.* 590, 2591–2599. doi: 10.1113/jphysiol.2011.224212

Kaur, A. W. W., Ackels, T., Kuo, T.-H., Cichy, A., Dey, S., Hays, C., et al. (2014). Murine pheromone proteins constitute a context-dependent combinatorial code governing multiple social behaviors. *Cell* 157, 676–688. doi: 10.1016/j.cell.2014.02.025

Kimoto, H., Sato, K., Nodari, F., Haga, S., Holy, T. E., and Touhara, K. (2007). Sex- and strain-specific expression and vomeronasal activity of mouse ESP family peptides. *Curr. Biol.* 17, 1879–1884. doi: 10.1016/j.cub.2007.09.042

Koos, D. S., and Fraser, S. E. (2005). The Grueneberg ganglion projects to the olfactory bulb. *Neuroreport* 16, 1929–1932. doi: 10.1097/01.wnr.0000186597.72081.10

Le, Y., Murphy, P. M., and Wang, J. M. (2002). Formyl-peptide receptors revisited. *Trends Immunol.* 23, 541–548. doi: 10.1016/s1471-4906(02)02316-5

Le, Y., Wang, J. M., Liu, X., Kong, Y., Hou, X., Ruan, L., et al. (2007). Biologically active peptides interacting with the G protein-coupled formylpeptide receptor. *Protein Pept. Lett.* 14, 846–853. doi: 10.2174/092986607782110211

Leinders-Zufall, T., Brennan, P., Widmayer, P., S, P. C., Maul-Pavicic, A., Jäger, M., et al. (2004). MHC class I peptides as chemosensory signals in the vomeronasal organ. *Science* 306, 1033–1037. doi: 10.1126/science.1102818

Leinders-Zufall, T., Ishii, T., Mombaerts, P., Zufall, F., and Boehm, T. (2009). Structural requirements for the activation of vomeronasal sensory neurons by MHC peptides. *Nat. Neurosci.* 12, 1551–1558. doi: 10.1038/nn.2452

Leinders-Zufall, T., Lane, A. P., Puche, A. C., Ma, W., Novotny, M. V., Shipley, M. T., et al. (2000). Ultrasensitive pheromone detection by mammalian vomeronasal neurons. *Nature* 405, 792–796. doi: 10.1038/35015572

Lévai, O., Feistel, T., Breer, H., and Strotmann, J. (2006). Cells in the vomeronasal organ express odorant receptors but project to the accessory olfactory bulb. *J. Comp. Neurol.* 498, 476–490. doi: 10.1002/cne.21067

Liberles, S. D., Horowitz, L. F., Kuang, D., Contos, J. J., Wilson, K. L., Siltberg-Liberles, J., et al. (2009). Formyl peptide receptors are candidate chemosensory receptors in the vomeronasal organ. *Proc. Natl. Acad. Sci. U S A* 106, 9842–9847. doi: 10.1073/pnas.0904464106

Liman, E. R., and Corey, D. P. (1996). Electrophysiological characterization of chemosensory neurons from the mouse vomeronasal organ. *J. Neurosci.* 16, 4625–4637.

Ma, M., Grosmaitre, X., Iwema, C. L., Baker, H., Greer, C. A., and Shepherd, G. M. (2003). Olfactory signal transduction in the mouse septal organ. *J. Neurosci.* 23, 317–324.

Martini, S., Silvotti, L., Shirazi, A., Ryba, N. J. P., and Tirindelli, R. (2001). Co-expression of putative pheromone receptors in the sensory neurons of the vomeronasal organ. *J. Neurosci.* 21, 843–848.

Matsunami, H., and Buck, L. B. (1997). A multigene family encoding a diverse array of putative pheromone receptors in mammals. *Cell* 90, 775–784. doi: 10.1016/s0092-8674(00)80537-1

Matsuoka, M., Yoshida-Matsuoka, J., Iwasaki, N., Norita, M., Costanzo, R. M., and Ichikawa, M. (2001). Immunocytochemical study of Gi2alpha and Goalpha on the epithelium surface of the rat vomeronasal organ. *Chem. Senses* 26, 161–166. doi: 10.1093/chemse/26.2.161

Mei, Y. A., Louiset, E., Vaudry, H., and Cazin, L. (1995). A-type potassium current modulated by A1 adenosine receptor in frog melanotrophs. *J. Physiol.* 489, 431–442.

Migeotte, I., Communi, D., and Parmentier, M. (2006). Formyl peptide receptors: a promiscuous subfamily of G protein-coupled receptors controlling immune responses. *Cytokine Growth Factor Rev.* 17, 501–519. doi: 10.1016/j.cytogfr.2006.09.009

Mombaerts, P. (2004). Genes and ligands for odorant, vomeronasal and taste receptors. *Nat. Rev. Neurosci.* 5, 263–278. doi: 10.1038/nrn1365

Munger, S. D. (2009). Noses within noses. *Nature* 459, 521–522. doi: 10.1038/459521a

Nagai, T., Ibata, K., Park, E. S., Kubota, M., Mikoshiba, K., and Miyawaki, A. (2002). A variant of yellow fluorescent protein with fast and efficient maturation for cell-biological applications. *Nat. Biotechnol.* 20, 87–90. doi: 10.1038/nbt0102-87

Narahashi, T., Anderson, N. C., and Moore, J. W. (1966). Tetrodotoxin does not block excitation from inside the nerve membrane. *Science* 153, 765–767. doi: 10.1126/science.153.3737.765

Neely, A., and Hidalgo, P. (2014). Structure-function of proteins interacting with the α1 pore-forming subunit of high-voltage-activated calcium channels. *Front. Physiol.* 5:209. doi: 10.3389/fphys.2014.00209

Nodari, F., Hsu, F.-F., Fu, X., Holekamp, T. F., Kao, L.-F., Turk, J., et al. (2008). Sulfated steroids as natural ligands of mouse pheromone-sensing neurons. *J. Neurosci.* 28, 6407–6418. doi: 10.1523/jneurosci.1425-08.2008

Novotny, M. V. (2003). Pheromones, binding proteins and receptor responses in rodents. *Biochem. Soc. Trans.* 31, 117–122. doi: 10.1042/bst0310117

Oka, Y., Katada, S., Omura, M., Suwa, M., Yoshihara, Y., and Touhara, K. (2006). Odorant receptor map in the mouse olfactory bulb: in vivo sensitivity and specificity of receptor-defined glomeruli. *Neuron* 52, 857–869. doi: 10.1016/j.neuron.2006.10.019

Pacifico, R., Dewan, A., Cawley, D., Guo, C., and Bozza, T. (2012). An olfactory subsystem that mediates high-sensitivity detection of volatile amines. *Cell Rep.* 2, 76–88. doi: 10.1016/j.celrep.2012.06.006

Perez-Reyes, E., Cribbs, L. L., Daud, A., Lacerda, A. E., Barclay, J., Williamson, M. P., et al. (1998). Molecular characterization of a neuronal low-voltage-activated T-type calcium channel. *Nature* 391, 896–900.

Randall, A., and Tsien, R. (1995). Pharmacological dissection of multiple types of Ca^{2+} channel currents in rat cerebellar granule neurons. *J. Neurosci.* 15, 2995–3012.

Rivière, S., Challet, L., Fluegge, D., Spehr, M., and Rodriguez, I. (2009). Formyl peptide receptor-like proteins are a novel family of vomeronasal chemosensors. *Nature* 459, 574–577. doi: 10.1038/nature08029

Robinson, R. B., and Siegelbaum, S. A. (2003). Hyperpolarization-activated cation currents: from molecules to physiological function. *Annu. Rev. Physiol.* 65, 453–480. doi: 10.1146/annurev.physiol.65.092101.142734

Rodriguez, I., Feinstein, P., and Mombaerts, P. (1999). Variable patterns of axonal projections of sensory neurons in the mouse vomeronasal system. *Cell* 97, 199–208. doi: 10.1016/s0092-8674(00)80730-8

Roppolo, D., Ribaud, V., Jungo, V. P., Lüscher, C., and Rodriguez, I. (2006). Projection of the Grueneberg ganglion to the mouse olfactory bulb. *Eur. J. Neurosci.* 23, 2887–2894. doi: 10.1111/j.1460-9568.2006.04818.x

Ryba, N. J. P., and Tirindelli, R. (1997). A new multigene family of putative pheromone receptors. *Neuron* 19, 371–379. doi: 10.1016/s0896-6273(00)80946-0

Sagheddu, C., Boccaccio, A., Dibattista, M., Montani, G., Tirindelli, R., and Menini, A. (2010). Calcium concentration jumps reveal dynamic ion selectivity of calcium-activated chloride currents in mouse olfactory sensory neurons and TMEM16b-transfected HEK 293T cells. *J. Physiol.* 588, 4189–4204. doi: 10.1113/jphysiol.2010.194407

Schmid, A., Pyrski, M., Biel, M., Leinders-Zufall, T., and Zufall, F. (2010). Grueneberg ganglion neurons are finely tuned cold sensors. *J. Neurosci.* 30, 7563–7568. doi: 10.1523/jneurosci.0608-10.2010

Serizawa, S., Miyamichi, K., Takeuchi, H., Yamagishi, Y., Suzuki, M., and Sakano, H. (2006). A neuronal identity code for the odorant receptor-specific and activity-dependent axon sorting. *Cell* 127, 1057–1069. doi: 10.1016/j.cell.2006.10.031

Shimazaki, R., Boccaccio, A., Mazzatenta, A., Pinato, G., Migliore, M., and Menini, A. (2006). Electrophysiological properties and modeling of murine vomeronasal sensory neurons in acute slice preparations. *Chem. Senses* 31, 425–435. doi: 10.1093/chemse/bjj047

Silvotti, L., Moiani, A., Gatti, R., and Tirindelli, R. (2007). Combinatorial co-expression of pheromone receptors, V2Rs. *J. Neurochem.* 103, 1753–1763. doi: 10.1111/j.1471-4159.2007.04877.x

Soehnlein, O., and Lindbom, L. (2010). Phagocyte partnership during the onset and resolution of inflammation. *Nat. Rev. Immunol.* 10, 427–439. doi: 10.1038/nri2779

Spehr, J., Hagendorf, S., Weiss, J., Spehr, M., Leinders-Zufall, T., and Zufall, F. (2009). Ca^{2+}-calmodulin feedback mediates sensory adaptation and inhibits pheromone-sensitive ion channels in the vomeronasal organ. *J. Neurosci.* 29, 2125–2135. doi: 10.1523/jneurosci.5416-08.2009

Spehr, M., Spehr, J., Ukhanov, K., Kelliher, K. R., Leinders-Zufall, T., and Zufall, F. (2006). Parallel processing of social signals by the mammalian main and accessory olfactory systems. *Cell. Mol. Life Sci.* 63, 1476–1484. doi: 10.1007/s00018-006-6109-4

Triggle, D. J., Gopalakrishnan, M., Rampe, D., and Zheng, W. (2006). *Voltage-Gated Ion Channels as Drug Targets.* eds D. J. Triggle, M. Gopalakrishnan, D. Rampe and W. Zheng Weinheim: Wiley-VCH Verlag GmbH.

Trotier, D., and Døving, K. B. (1996). Direct influence of the sodium pump on the membrane potential of vomeronasal chemoreceptor neurones in frog. *J. Physiol.* 490, 611–621.

Ukhanov, K., Leinders-Zufall, T., and Zufall, F. (2007). Patch-clamp analysis of gene-targeted vomeronasal neurons expressing a defined V1r or V2r receptor: ionic mechanisms underlying persistent firing. *J. Neurophysiol.* 98, 2357–2369. doi: 10.1152/jn.00642.2007

Veitinger, S., Veitinger, T., Cainarca, S., Fluegge, D., Engelhardt, C. H., Lohmer, S., et al. (2011). Purinergic signalling mobilizes mitochondrial Ca^{2+} in mouse Sertoli cells. *J. Physiol.* 589, 5033–5055. doi: 10.1113/jphysiol.2011.216309

Wu, C. H., and Narahashi, T. (1988). Mechanism of action of novel marine neurotoxins on ion channels. *Annu. Rev. Pharmacol. Toxicol.* 28, 141–161. doi: 10.1146/annurev.pharmtox.28.1.141

Yellen, G. (1984). Ionic permeation and blockade in Ca^{2+}-activated K^+ channels of bovine chromaffin cells. *J. Gen. Physiol.* 84, 157–186. doi: 10.1085/jgp.84.2.157

Conflict of Interest Statement: The authors declare that the research was conducted in the absence of any commercial or financial relationships that could be construed as a potential conflict of interest.

Received: 29 August 2014; accepted: 01 November 2014; published online: 21 November 2014.

Citation: Ackels T, von der Weid B, Rodriguez I and Spehr M (2014) Physiological characterization of formyl peptide receptor expressing cells in the mouse vomeronasal organ. Front. Neuroanat. ***8****:134. doi: 10.3389/fnana.2014.00134*

This article was submitted to the journal Frontiers in Neuroanatomy.

frontiers in
NEUROANATOMY

MINI REVIEW ARTICLE
published: 26 November 2014
doi: 10.3389/fnana.2014.00135

Signaling mechanisms and behavioral function of the mouse basal vomeronasal neuroepithelium

Anabel Pérez-Gómez, Benjamin Stein, Trese Leinders-Zufall and Pablo Chamero*

Department of Physiology, University of Saarland School of Medicine, Homburg, Saarland, Germany

Edited by:
Ignacio Salazar, University of Santiago de Compostela, Spain

Reviewed by:
Michael Baum, Boston University, USA
Makoto Kashiwayanagi, Asahikawa Medical University, Japan

****Correspondence:***
Pablo Chamero, Department of Physiology, University of Saarland School of Medicine, Kirrbergerstrasse Building 45.2, Homburg, 66421 Saarland, Germany
e-mail: pablo.chamero@uks.eu

The vomeronasal organ (VNO) is a sensory organ that is found in most terrestrial vertebrates and that is principally implicated in the detection of pheromones. The VNO contains specialized sensory neurons organized in a pseudostratified neuroepithelium that recognize chemical signals involved in initiating innate behavioral responses. In rodents, the VNO neuroepithelium is segregated into two distinct zones, apical and basal. The molecular mechanisms involved in ligand detection by apical and basal VNO sensory neurons differ extensively. These two VNO subsystems express different subfamilies of vomeronasal receptors and signaling molecules, detect distinct chemosignals, and project to separate regions of the accessory olfactory bulb (AOB). The roles that these olfactory subdivisions play in the control of specific olfactory-mediated behaviors are largely unclear. However, analysis of mutant mouse lines for signal transduction components together with identification of defined chemosensory ligands has revealed a fundamental role of the basal part of the mouse VNO in mediating a wide range of instinctive behaviors, such as aggression, predator avoidance, and sexual attraction. Here we will compare the divergent functions and synergies between the olfactory subsystems and consider new insights in how higher neural circuits are defined for the initiation of instinctive behaviors.

Keywords: vomeronasal organ, olfaction, Gαo signaling, V2R, peptides, pheromone, behavior

INTRODUCTION

The mammalian olfactory system is composed of multiple chemosensory subsystems that differ in anatomical location, receptor types, and innervation within the central nervous system (Munger et al., 2009). The vomeronasal organ (VNO) is the sensory substructure of the accessory olfactory system that is specialized in the identification of specific chemosensory cues important for the display of socio-sexual behaviors. The VNO detects a range of molecules that can be both volatile and non-volatile, including peptides and small proteins. These molecules may be either pheromones secreted externally by conspecifics in urine, tears and saliva, as well as non-pheromones such as those from preys and predators (Wyatt, 2014). During olfactory investigation, chemosignals entering the nasal cavity are pumped into the VNO lumen, where they are detected by vomeronasal sensory neurons (VSNs). The mechanism of pumping consists in a distension-contraction of vascularized erectile tissue located in the lateral side of the VNO lumen (Trotier, 2011). Sympathetic stimulation triggers this vascular pump (Ben-Shaul et al., 2010) during exploratory behaviors, probably as a result of detection of other volatile stimuli by the main olfactory system (Martínez-García et al., 2009). Therefore, vomeronasal activity is unlikely to remain as an autonomous olfactory unit but instead requires intense interaction with other sensory inputs to transduce the stimulus information to downstream targets. Mature VSNs reside in the medial side within a pseudostratified sensory neuroepithelium formed by bipolar neurons, directed to the aqueous lumen, with an extended dendrite and cilia in which detection takes place. The VNO emerges in evolution on amphibians during adaptation to life on land (Trotier, 2011), and is present in many but not all mammals. It is missing in cetaceans, some bats and some primates (Mucignat-Caretta, 2010). In humans it appears to be vestigial (Trotier et al., 2000; Meredith, 2001). In the mouse, the VNO neuroepithelium is divided in non-overlapping apical and basal layers that express two different families of receptors, vomeronasal receptors 1 and 2 (V1Rs and V2Rs), respectively (Dulac and Axel, 1995; Herrada and Dulac, 1997; Matsunami and Buck, 1997; Ryba and Tirindelli, 1997). Furthermore, a subset of neurons in the VNO express five members of the formyl peptide receptor (FPR) family, four of them apical and one basal (Liberles et al., 2009; Riviere et al., 2009). The wiring logic of the VSN projection is maintained at the level of the accessory olfactory bulb (AOB): Apical VSNs connect with glomeruli in the rostral half of the AOB, whereas basal VSNs axons synapse in the caudal AOB. The implications of this neuronal segregation in the accessory olfactory system for the processing of chemosensory information are largely unknown. Moreover, certain species such as the goat, marmoset and tammar wallaby lack this anatomical segregation and display uniform-type vomeronasal epitheliums (Takigami et al., 2000, 2004; Schneider et al., 2012). Recent advances in the identification of subzone-specific ligands and ablation of sensory transduction components have now enabled a more detailed analysis of the molecular mechanisms controlled by each neural VNO pathway to initiate olfactory-mediated behaviors.

MOLECULAR AND FUNCTIONAL ORGANIZATION OF THE BASAL VNO

The spatial segregation in the VNO correlates with the differential expression of two G-protein subunits, Gαi2 and Gαo (Berghard and Buck, 1996; Jia and Halpern, 1996). These G-proteins are the initial step of a phospholipase C (PLC)-mediated signaling cascade to transduce sensory signals detected by V1Rs and V2Rs (Chamero et al., 2012). In the VNO, G-proteins form complexes identified as Gαoβ2γ8 in the basal and Gαi2β2γ2 in the apical neurons (Montani et al., 2013). The functional importance of the G-protein subunits in mediating sensory transduction responses was established by ablating genes in mice. VSNs from Gαo mutants display severe deficits to transduce chemosensory signals that result in a number of behavioral alterations including reduced olfactory-mediated aggression (Chamero et al., 2011). Furthermore, Gαo seems to be critical for the maintenance of the cellular homeostasis in the postnatal sensory neuroepithelium as Gαo mutant mice show a remarkable reduction in the size of the basal neuronal layer (Tanaka et al., 1999). Likewise, mutant mice lacking Gγ8 subunit display a similar cell loss in the VNO epithelium and a diminished aggressive response (Montani et al., 2013). Thus, Gαo and subsequent coupling with Gβ2γ8 represent the key candidate molecules to control PLC activation through specific olfactory stimuli in the basal VNO (Rünnenburger et al., 2002).

PLC activation produces inositol 1,4,5-trisphosphate and diacylglycerol, the only known activator of a member of the transient receptor potential family of ion channels, Trpc2. Trpc2 expressed in both apical and basal VNO layer is another key player in VNO signal transduction (Liman et al., 1999). Genetic ablation of *Trpc2* results in dramatic consequences in vomeronasal function in terms of VSNs responsiveness to urinary signals, cell survival, and socio-sexual behavior (Leypold et al., 2002; Stowers et al., 2002; Kimchi et al., 2007; Ferrero et al., 2013; Wu et al., 2014). The *Trpc2* gene, initially assumed to be exclusively expressed in the VNO, has been abundantly detected in the main olfactory epithelium (MOE) as well (Omura and Mombaerts, 2014). Therefore, the contribution of MOE-specific Trpc2 signaling to the described behavioral *Trpc2* null phenotype remains to be dissected. This may help to explain observed phenotypic discrepancies of *Trpc2* deletion (Leypold et al., 2002; Stowers et al., 2002; Kimchi et al., 2007) and surgical VNO removal (Clancy et al., 1984; Wysocki and Lepri, 1991; Pankevich et al., 2004; Martel and Baum, 2009) on ultrasonic vocalizations and sex-specific behaviors in both male and female mice. Additional signaling components expressed in both basal and apical VSNs are the discovered calcium-activated chloride and potassium channels, which seem to participate in the VNO sensory responses (Dibattista et al., 2008; Billig et al., 2011; Kim et al., 2011, 2012). A recent study using deep RNA sequencing identified nearly 800 novel, putative protein-coding, multi-exonic genes expressed in the whole VNO (Ibarra-Soria et al., 2014). Thus, new vomeronasal signaling components are expected to emerge in the near future.

The range and specificity of chemosignals detected by the VNO depend on the expression of particular vomeronasal receptors. Three families of vomeronasal receptor genes have been identified in the mouse VNO: V1Rs, V2Rs (also known as *Vmn1rs* and *Vmn2rs*) and *Fprs* (Tirindelli et al., 2009). VSNs in the basal layer of the VNO express V2Rs as well as a single FPR member, Fpr-rs1. The mouse genome contains 121 functional V2R genes and—curiously—even a larger number (158) of pseudogenes (Young and Trask, 2007). V2Rs evolved independently from V1Rs and differ in the type of chemosignals they detect, to date: peptides/proteins by V2Rs and small organic molecules by V1Rs, and in the expression logic: VSNs expressing V1Rs show a single-receptor type expression whereas basal VSNs expresses one V2R member of the subfamily C, along with an additional V2R gene from subfamily A, B or D in a non-random manner (**Figure 1**; Martini et al., 2001; Silvotti et al., 2007; Ishii and Mombaerts, 2011). Until now, only a handful of V2Rs have been deorphanized (**Table 1**) and all of them belong to the subfamily A, which represents nearly 85% of the V2R genes. Furthermore, V2R sequences of inbred mouse strains show high variation in subfamily A1, A5 and A8 while subfamilies B, C and D are highly conserved (Wynn et al., 2012). The importance of V2R subfamily expression for VSN pheromone specificity and detection still needs to be resolved. However, recent evidences suggest that expression of multiple receptors may have a role in the combinatorial activation logic of VSNs by overlapping specificities and concentrations (Leinders-Zufall et al., 2009; Kaur et al., 2014).

In addition to V2R expression, a subset of basal VSNs have been shown to express genes of the major histocompatibility complex (MHC) class 1b, also known as *H2Mv* molecules (Ishii et al., 2003; Loconto et al., 2003). This family comprises nine genes—M1, M9, M11 and six members of the M10 family—clustered in the genome. Most of the neurons express a single gene, but some seem to be able to express two or three. The proteins localize to the dendritic tips and microvilli of VSNs predicting a potential role in pheromone detection or signal transduction. *H2Mv* molecules have been proposed to form a protein complex together with V2Rs and β2-microglobulin necessary for the transport of the receptor to the plasma membrane (Loconto et al., 2003). Certainly, *H2Mv* molecules are dispensable for chemosignal detection but seem to be required to show high sensitivity to peptide ligands necessary for the display of aggressive and sexual behaviors (Leinders-Zufall et al., 2014). A fraction of Gαo-expressing VSNs do not co-express *H2-Mv* genes, for example sensory neurons expressing the Vmn2r26 receptor (also known as V2r1b), which are localized to the upper sublayer of the basal VNO. This spatial segregation is also maintained at the level of the AOB, defining a tripartite organization of the mouse vomeronasal system (**Figure 1**; Ishii and Mombaerts, 2008).

A third population of Gαo-expressing VSNs expresses Fpr-rs1 (**Figure 1**), an additional chemosensory G-protein coupled receptor (GPCR) that belongs to the FPR family (Liberles et al., 2009; Riviere et al., 2009). Fpr-rs1 neurons do not co-express V2Rs or other FPR members. Fpr-rs1 was found to display stereoselectivity for peptides with a D-amino acid in the C-terminal position, which are contained in pathogenic microorganisms

Table 1 | List of signaling molecules with proposed receptors located in the basal sensory epithelium.

Chemosignal	Source	Receptor	Gαo need	Behavioral effects	References
ESP1	Male mouse tears	V2Rp5 (Vmn2r116)	✓	-Lordosis	Kimoto et al. (2007), Haga et al. (2010)
ESP5	Mouse tears	V2Rp1 (Vmn2r112), V2Rp2 (Vmn2r111)	?	?	Kimoto et al. (2007), Dey and Matsunami (2011)
ESP6	Mouse tears	V2Rp1 (Vmn2r112)	?	?	Kimoto et al. (2007), Dey and Matsunami (2011)
ESP22	Juvenile mouse tears	?	?	-Inhibition of male sexual behavior	Ferrero et al. (2013)
HMW/MUPs	Mouse urine			-Male-male aggression -Maternal aggression	Chamero et al. (2007, 2011) Martín-Sánchez et al. (2014)
		?	✓	-Preference in females	Hurst et al. (2001), Cheetham et al. (2007), Sherborne et al. (2007), Roberts et al. (2010)
				-Urine countermarking behavior	Kaur et al. (2014)
				-Puberty acceleration -Ovulation	Mucignat-Caretta et al. (1995) Morè (2006)
MUP3		?	✓	-Male-male aggression -Countermarking	Kaur et al. (2014)
MUP20				-Attraction in females	Roberts et al. (2010, 2012),
		?	✓	-Conditioned place preference -Countermarking behavior -Maternal aggression	Kaur et al. (2014), Martín-Sánchez et al. (2014)
LMW	Mouse urine	?	*	-Male-male aggression -Maternal aggression	Chamero et al. (2007, 2011)
MHC class I peptides	Mouse urine	V2R1b (Vmn2r26) V2Rf2 (Vmn2r81)	✓	-Bruce effect	Leinders-Zufall et al. (2009, 2014)
N-formylated peptides	Bacteria or mitochondria	Fpr-rs1, V2Rf2 (Vmn2r81)	✓	?	Liberles et al. (2009), Riviere et al. (2009), Bufe et al. (2012) Leinders-Zufall et al. (2014)

*✓: Gαo expression needed to detect the chemosignal; *: partial detection by both apical and basal layers; ?: not determined; Brackets: alternative receptor names.*

(Bufe et al., 2012). This ligand detection profile raises the possibility of a pathogenic sensing role of the vomeronasal system to assess the health status of conspecifics during social communication.

SENSORY LIGANDS DETECTED BY THE BASAL VNO

Early functional experiments in the rat vomeronasal sensory epithelium described urine profile activation differences between the apical and basal VNSs (Inamura et al., 1999). Up to now, considerable evidence has shown that sensory neurons located in the basal VNO detect several families of nonvolatile peptide and protein chemosignals. The family of MHC class I peptides were the first identified sensory stimuli for V2R-positive VSNs (Leinders-Zufall et al., 2004). MHC peptides, that have been identified in mouse urine together with some other interesting species-specific peptide ligands (Sturm et al., 2013), are detected by VSNs at ultralow concentrations and require Gαo, but not Trpc2 (Leinders-Zufall et al., 2004; Kelliher et al., 2006; Chamero et al., 2011). Detection of MHC peptide ligands does not require or correlate with the expression of *H2Mv* molecules. Instead, vomeronasal receptors seem to be essential: genetic deletion experiments showed two V2Rs—Vmn2r26 (V2R1b) and Vmn2r81 (V2Rf2)—which are needed by their VSNs to respond to specific MHC peptides (Leinders-Zufall et al., 2009, 2014). Interestingly, MHC-independent peptides as well as formylated and non-formylated versions of mitochondrial peptides can also activate V2R positive VSNs (Sturm et al., 2013; Leinders-Zufall et al., 2014).

A second family of peptides—the exocrine-gland-secreting peptide (ESP) family—has been identified to be detected by V2R-expressing VSNs. The mouse genome contains 24 members of this family of 5–15 kDa peptides expressed in extraorbital, lacrimal, Harderian, and submaxillary glands (exocrine glands) in a sex- and strain-specific manner (Kimoto et al., 2007). Field potential recordings have shown that at least 16 ESPs elicit electrical responses in the VNO (Kimoto et al., 2007; Haga et al., 2010; Ferrero et al., 2013). Responses to ESP1, 5 and 6 have been linked with expression of a specific V2R subfamily (V2Rp) either by c-Fos activity measures, or by heterologous expression (Haga et al., 2010; Dey and Matsunami, 2011).

A third group of nonvolatile chemosignals functioning as stimuli of the basal VNO layer consist of the major urinary

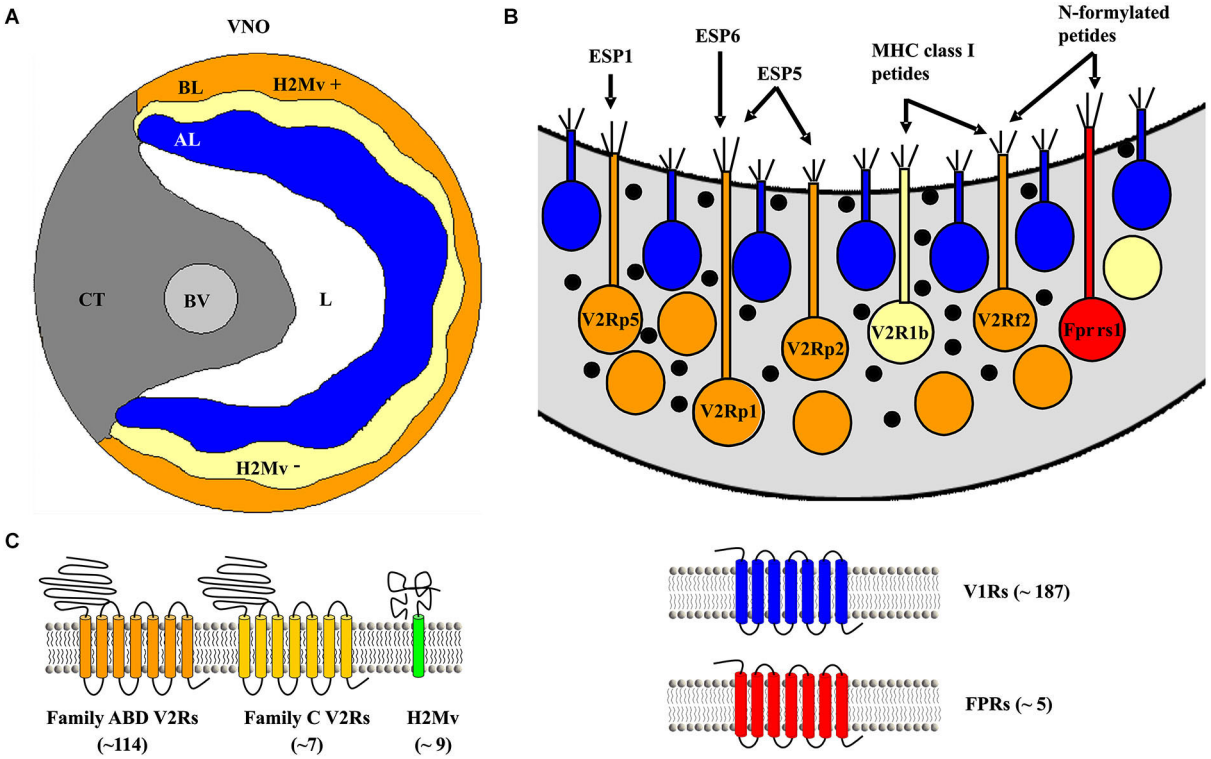

FIGURE 1 | The mouse vomeronasal organ (VNO) and established receptors located in the epithelium. (A) Schematic coronal section of the VNO. AL, apical layer of the sensory epithelium (*blue*); BL, basal layer (*yellow/orange*); BV, blood vessel; CT, cavernous tissue; *H2Mv+*, sensory epithelium cells lacking one of the nine known *H2-Mv* genes; *H2Mv−*, sensory neurons not expressing any of the nine *H2-Mv* genes; L, lumen. **(B)** Schematic drawing of sensory neurons showing their location in the basal sensory epithelium with their proposed ligands. **(C)** Schematic picture of the proposed receptors expressed in the basal part of the VNO sensory epithelium.

proteins (MUPs) and other related lipocalins. MUPs are abundantly expressed in urine, but are also found in other secretions, including saliva, milk, and even the olfactory epithelium (Ibarra-Soria et al., 2014). In the mouse, MUPs are encoded by a multigene family of 21 homologous, highly identical genes which are expressed in a sex- and strain-dependent manner (Logan et al., 2008; Mudge et al., 2008). MUPs evoke Ca^{2+} and electrophysiological responses on Gαo- and V2R-expressing VSNs using Trpc2/Gαo signaling (Chamero et al., 2007, 2011) and benefit of the presence of *H2Mv* molecules (Leinders-Zufall et al., 2014), but specific MUP receptors are yet to be described. Mouse VSNs detect conspecific MUPs utilizing a combinatorial strategy (Kaur et al., 2014) in addition to being activated by orthologous MUP proteins secreted by cats and rats (Papes et al., 2010), adopting a new chemosensory role as interspecific genetically encoded signals.

BEHAVIORAL RESPONSES

Odor-driven behaviors are reported to depend on the basal VNO layer largely relying on two main criteria: First, as result of gene knockout studies of specific signal transduction molecules or receptors from basal VSNs, and/or second, from experiments using chemosignals shown to (specifically) activate basal VSNs. Aggressive behavior toward intruder males was identified to require sensory transduction from basal VSNs. Ablation of either Gαo, Gγ8, and *H2Mv* genes severely reduced or eliminated male-male and maternal aggression (Chamero et al., 2011; Montani et al., 2013; Leinders-Zufall et al., 2014), both types of aggression shown to be partially elicited by MUPs (Chamero et al., 2007, 2011; Kaur et al., 2014). Gαo gene removal also resulted in a wide range of deficient reproductive behaviors in female mice, including defective puberty acceleration (Vandenbergh effect) and estrus induction (Whitten effect) in adult mice (Oboti et al., 2014). The identities of the pheromones that underlie the Vandenbergh and Whitten effects are still controversial. Molecules that activate either apical (Jemiolo et al., 1986; Novotny et al., 1999) and basal (Nishimura et al., 1989; Mucignat-Caretta et al., 1995; Morè, 2006) VSNs have been described to participate in these estrus-modulating effects. Nonetheless, it cannot be excluded that multiple olfactory subsystems are required to evoke certain behavioral responses triggered by odorant blends. Consistent with this view, apical and basal VNO subsystems are necessary and seem to interact in the generation of male and female aggression (Del Punta et al., 2002; Norlin et al., 2003; Chamero et al., 2011). In contrast, other pheromone-induced behavioral responses are controlled by single VNO receptor-ligand interactions. The sexual stance lordosis is enhanced by the tear peptide ESP1 that activates Vmn2r116 receptor, and mutant animals lacking this receptor

display a striking lordosis deficit (Haga et al., 2010). Consistent with these experiments, surgical lesions on the VNO and AOB (Keller et al., 2006; Martel and Baum, 2009) as well as deletion of Gαo and *H2Mv* genes (Leinders-Zufall et al., 2014; Oboti et al., 2014) also resulted in a drastic reduction of lordosis. Another member of the ESP peptide family has been implicated in the control of a different type of sexual behavior: ESP22, expressed in tears of prepubertal mice, was found to elicit a Trpc2-dependent inhibitory effect on adult male mating behavior (Ferrero et al., 2013).

MHC peptides have been shown to alter female reproductive function as detected in the Bruce effect test (Leinders-Zufall et al., 2004). Here, pregnancy is terminated in a recently mated female by the odor of a strange male. This test is frequently used as paradigm to assess genetic compatibility and individual recognition. MUPs are also proposed to operate as olfactory cues governing individual recognition, as they are genetically encoded and highly polymorphic (Cheetham et al., 2007). Hence, MUPs have been reported to mediate inbreeding avoidance, countermarking and female sexual attraction (Hurst et al., 2001; Sherborne et al., 2007; Roberts et al., 2010; Kaur et al., 2014). Related to this recognition capacity, MUP detection also plays an important role on aggression, conditioned learned spatial preference and detection of predators (Chamero et al., 2007, 2011; Papes et al., 2010; Roberts et al., 2012). Remarkably, single MUP ligands are able to evoke multiple behavioral responses depending on the gender and reproductive status of the receiving individual; MUP20—also known as darcin—may elicit sexual attraction and spatial learning in estrous females, maternal aggression in lactating females, and countermarking and aggression in adult males (Roberts et al., 2010, 2012; Kaur et al., 2014; Martín-Sánchez et al., 2014). Whether these responses are mediated by a single or multiple sensory neurons or receptor types remain to be elucidated.

These recent advances in the identification of specialized receptors, neural pathways and sensory ligands from the basal VNO layer provide the tools to stimulate, study, and determine the molecular mechanisms that trigger specific behavioral responses.

ACKNOWLEDGMENTS

This work was supported by grants from the Deutsche Forschungsgemeinschaft (CH 920/2-1), HOMFORexzellent (Pablo Chamero) and the VolkswagenFoundation (Trese Leinders-Zufall). Trese Leinders-Zufall is a Lichtenberg Professor of the Volkswagen Foundation.

REFERENCES

Ben-Shaul, Y., Katz, L. C., Mooney, R., and Dulac, C. (2010). In vivo vomeronasal stimulation reveals sensory encoding of conspecific and allospecific cues by the mouse accessory olfactory bulb. *Proc. Natl. Acad. Sci. U S A* 107, 5172–5177. doi: 10.1073/pnas.0915147107

Berghard, A., and Buck, L. B. (1996). Sensory transduction in vomeronasal neurons: evidence for G alpha o, G alpha i2 and adenylyl cyclase II as major components of a pheromone signaling cascade. *J. Neurosci.* 16, 909–918.

Billig, G. M., Pál, B., Fidzinski, P., and Jentsch, T. J. (2011). Ca2+-activated Cl− currents are dispensable for olfaction. *Nat. Neurosci.* 14, 763–769. doi: 10.1038/nn.2821

Bufe, B., Schumann, T., and Zufall, F. (2012). Formyl peptide receptors from immune and vomeronasal system exhibit distinct agonist properties. *J. Biol. Chem.* 287, 33644–33655. doi: 10.1074/jbc.m112.375774

Chamero, P., Katsoulidou, V., Hendrix, P., Bufe, B., Roberts, R., Matsunami, H., et al. (2011). G protein G(alpha)o is essential for vomeronasal function and aggressive behavior in mice. *Proc. Natl. Acad. Sci. U S A* 108, 12898–12903. doi: 10.1073/pnas.1107770108

Chamero, P., Leinders-Zufall, T., and Zufall, F. (2012). From genes to social communication: molecular sensing by the vomeronasal organ. *Trends Neurosci.* 35, 597–606. doi: 10.1016/j.tins.2012.04.011

Chamero, P., Marton, T. F., Logan, D. W., Flanagan, K., Cruz, J. R., Saghatelian, A., et al. (2007). Identification of protein pheromones that promote aggressive behaviour. *Nature* 450, 899–902. doi: 10.1038/nature05997

Cheetham, S. A., Thom, M. D., Jury, F., Ollier, W. E., Beynon, R. J., and Hurst, J. L. (2007). The genetic basis of individual-recognition signals in the mouse. *Curr. Biol.* 17, 1771–1777. doi: 10.1016/j.cub.2007.10.007

Clancy, A. N., Coquelin, A., Macrides, F., Gorski, R. A., and Noble, E. P. (1984). Sexual behavior and aggression in male mice: involvement of the vomeronasal system. *J. Neurosci.* 4, 2222–2229.

Del Punta, K., Leinders-Zufall, T., Rodriguez, I., Jukam, D., Wysocki, C. J., Ogawa, S., et al. (2002). Deficient pheromone responses in mice lacking a cluster of vomeronasal receptor genes. *Nature* 419, 70–74. doi: 10.1038/nature00955

Dey, S., and Matsunami, H. (2011). Calreticulin chaperones regulate functional expression of vomeronasal type 2 pheromone receptors. *Proc. Natl. Acad. Sci. U S A* 108, 16651–16656. doi: 10.1073/pnas.1018140108

Dibattista, M., Mazzatenta, A., Grassi, F., Tirindelli, R., and Menini, A. (2008). Hyperpolarization-activated cyclic nucleotide-gated channels in mouse vomeronasal sensory neurons. *J. Neurophysiol.* 100, 576–586. doi: 10.1152/jn.90263.2008

Dulac, C., and Axel, R. (1995). A novel family of genes encoding putative pheromone receptors in mammals. *Cell* 83, 195–206. doi: 10.1016/0092-8674(95)90161-2

Ferrero, D. M., Moeller, L. M., Osakada, T., Horio, N., Li, Q., Roy, D. S., et al. (2013). A juvenile mouse pheromone inhibits sexual behaviour through the vomeronasal system. *Nature* 502, 368–371. doi: 10.1038/nature12579

Haga, S., Hattori, T., Sato, T., Sato, K., Matsuda, S., Kobayakawa, R., et al. (2010). The male mouse pheromone ESP1 enhances female sexual receptive behaviour through a specific vomeronasal receptor. *Nature* 466, 118–122. doi: 10.1038/nature09142

Herrada, G., and Dulac, C. (1997). A novel family of putative pheromone receptors in mammals with a topographically organized and sexually dimorphic distribution. *Cell* 90, 763–773. doi: 10.1016/s0092-8674(00)80536-x

Hurst, J. L., Payne, C. E., Nevison, C. M., Marie, A. D., Humphries, R. E., Robertson, D. H., et al. (2001). Individual recognition in mice mediated by major urinary proteins. *Nature* 414, 631–634. doi: 10.1038/414631a

Ibarra-Soria, X., Levitin, M. O., Saraiva, L. R., and Logan, D. W. (2014). The olfactory transcriptomes of mice. *PLoS Genet.* 10:e1004593. doi: 10.1371/journal.pgen.1004593

Inamura, K., Matsumoto, Y., Kashiwayanagi, M., and Kurihara, K. (1999). Laminar distribution of pheromone-receptive neurons in rat vomeronasal epithelium. *J. Physiol.* 517(Pt. 3), 731–739. doi: 10.1111/j.1469-7793.1999.0731s.x

Ishii, T., Hirota, J., and Mombaerts, P. (2003). Combinatorial coexpression of neural and immune multigene families in mouse vomeronasal sensory neurons. *Curr. Biol.* 13, 394–400. doi: 10.1016/s0960-9822(03)00092-7

Ishii, T., and Mombaerts, P. (2008). Expression of nonclassical class I major histocompatibility genes defines a tripartite organization of the mouse vomeronasal system. *J. Neurosci.* 28, 2332–2341. doi: 10.1523/jneurosci.4807-07.2008

Ishii, T., and Mombaerts, P. (2011). Coordinated coexpression of two vomeronasal receptor V2R genes per neuron in the mouse. *Mol. Cell. Neurosci.* 46, 397–408. doi: 10.1016/j.mcn.2010.11.002

Jemiolo, B., Harvey, S., and Novotny, M. (1986). Promotion of the Whitten effect in female mice by synthetic analogs of male urinary constituents. *Proc. Natl. Acad. Sci. U S A* 83, 4576–4579. doi: 10.1073/pnas.83.12.4576

Jia, C., and Halpern, M. (1996). Subclasses of vomeronasal receptor neurons: differential expression of G proteins (Gi alpha 2 and G(o alpha)) and segregated projections to the accessory olfactory bulb. *Brain Res.* 719, 117–128. doi: 10.1016/0006-8993(96)00110-2

Kaur, A. W., Ackels, T., Kuo, T.-H., Cichy, A., Dey, S., Hays, C., et al. (2014). Murine pheromone proteins constitute a context-dependent combinatorial code governing multiple social behaviors. *Cell* 157, 676–688. doi: 10.1016/j.cell.2014.02.025

Keller, M., Pierman, S., Douhard, Q., Baum, M. J., and Bakker, J. (2006). The vomeronasal organ is required for the expression of lordosis behaviour, but not sex discrimination in female mice. *Eur. J. Neurosci.* 23, 521–530. doi: 10.1111/j.1460-9568.2005.04589.x

Kelliher, K. R., Spehr, M., Li, X. H., Zufall, F., and Leinders-Zufall, T. (2006). Pheromonal recognition memory induced by TRPC2-independent vomeronasal sensing. *Eur. J. Neurosci.* 23, 3385–3390. doi: 10.1111/j.1460-9568.2006.04866.x

Kim, S., Ma, L., Jensen, K. L., Kim, M. M., Bond, C. T., Adelman, J. P., et al. (2012). Paradoxical contribution of SK3 and GIRK channels to the activation of mouse vomeronasal organ. *Nat. Neurosci.* 15, 1236–1244. doi: 10.1038/nn.3173

Kim, S., Ma, L., and Yu, C. R. (2011). Requirement of calcium-activated chloride channels in the activation of mouse vomeronasal neurons. *Nat. Commun.* 2:365. doi: 10.1038/ncomms1368

Kimchi, T., Xu, J., and Dulac, C. (2007). A functional circuit underlying male sexual behaviour in the female mouse brain. *Nature* 448, 1009–1014. doi: 10.1038/nature06089

Kimoto, H., Sato, K., Nodari, F., Haga, S., Holy, T. E., and Touhara, K. (2007). Sex- and strain-specific expression and vomeronasal activity of mouse ESP family peptides. *Curr. Biol.* 17, 1879–1884. doi: 10.1016/j.cub.2007.09.042

Leinders-Zufall, T., Brennan, P., Widmayer, P., S, P. C., Maul-Pavicic, A., Jager, M., et al. (2004). MHC class I peptides as chemosensory signals in the vomeronasal organ. *Science* 306, 1033–1037. doi: 10.1126/science.1102818

Leinders-Zufall, T., Ishii, T., Chamero, P., Hendrix, P., Oboti, L., Schmid, A., et al. (2014). A family of nonclassical class I MHC genes contributes to ultrasensitive chemodetection by mouse vomeronasal sensory neurons. *J. Neurosci.* 34, 5121–5133. doi: 10.1523/jneurosci.0186-14.2014

Leinders-Zufall, T., Ishii, T., Mombaerts, P., Zufall, F., and Boehm, T. (2009). Structural requirements for the activation of vomeronasal sensory neurons by MHC peptides. *Nat. Neurosci.* 12, 1551–1558. doi: 10.1038/nn.2452

Leypold, B. G., Yu, C. R., Leinders-Zufall, T., Kim, M. M., Zufall, F., and Axel, R. (2002). Altered sexual and social behaviors in trp2 mutant mice. *Proc. Natl. Acad. Sci. U S A* 99, 6376–6381. doi: 10.1073/pnas.082127599

Liberles, S. D., Horowitz, L. F., Kuang, D., Contos, J. J., Wilson, K. L., Siltberg-Liberles, J., et al. (2009). Formyl peptide receptors are candidate chemosensory receptors in the vomeronasal organ. *Proc. Natl. Acad. Sci. U S A* 106, 9842–9847. doi: 10.1073/pnas.0904464106

Liman, E. R., Corey, D. P., and Dulac, C. (1999). TRP2: a candidate transduction channel for mammalian pheromone sensory signaling. *Proc. Natl. Acad. Sci. U S A* 96, 5791–5796. doi: 10.1073/pnas.96.10.5791

Loconto, J., Papes, F., Chang, E., Stowers, L., Jones, E. P., Takada, T., et al. (2003). Functional expression of murine V2R pheromone receptors involves selective association with the M10 and M1 families of MHC class Ib molecules. *Cell* 112, 607–618. doi: 10.1016/s0092-8674(03)00153-3

Logan, D. W., Marton, T. F., and Stowers, L. (2008). Species specificity in major urinary proteins by parallel evolution. *PLoS One* 3:e3280. doi: 10.1371/journal.pone.0003280

Martel, K. L., and Baum, M. J. (2009). Adult testosterone treatment but not surgical disruption of vomeronasal function augments male-typical sexual behavior in female mice. *J. Neurosci.* 29, 7658–7666. doi: 10.1523/jneurosci.1311-09.2009

Martínez-García, F., Martínez-Ricós, J., Agustín-Pavón, C., Martínez-Hernández, J., Novejarque, A., and Lanuza, E. (2009). Refining the dual olfactory hypothesis: pheromone reward and odour experience. *Behav. Brain Res.* 200, 277–286. doi: 10.1016/j.bbr.2008.10.002

Martini, S., Silvotti, L., Shirazi, A., Ryba, N. J., and Tirindelli, R. (2001). Co-expression of putative pheromone receptors in the sensory neurons of the vomeronasal organ. *J. Neurosci.* 21, 843–848.

Martín-Sánchez, A., McLean, L., Beynon, R. L., Hurst, J. L., Ayala, G., Lanuza, E., et al. (2014). From sexual attraction to maternal aggression: when pheromones change their behavioural significance. *Horm. Behav.* doi: 10.1016/j.yhbeh.2014.08.007. [Epub ahead of print].

Matsunami, H., and Buck, L. B. (1997). A multigene family encoding a diverse array of putative pheromone receptors in mammals. *Cell* 90, 775–784. doi: 10.1016/s0092-8674(00)80537-1

Meredith, M. (2001). Human vomeronasal organ function: a critical review of best and worst cases. *Chem. Senses* 26, 433–445. doi: 10.1093/chemse/26.4.433

Montani, G., Tonelli, S., Sanghez, V., Ferrari, P. F., Palanza, P., Zimmer, A., et al. (2013). Aggressive behaviour and physiological responses to pheromones are strongly impaired in mice deficient for the olfactory G-protein -subunit G8. *J. Physiol.* 591, 3949–3962. doi: 10.1113/jphysiol.2012.247528

Morè, L. (2006). Mouse major urinary proteins trigger ovulation via the vomeronasal organ. *Chem. Senses* 31, 393–401. doi: 10.1093/chemse/bjj043

Mucignat-Caretta, C. (2010). The rodent accessory olfactory system. *J. Comp. Physiol. A Neuroethol. Sens. Neural Behav. Physiol.* 196, 767–777. doi: 10.1007/s00359-010-0555-z

Mucignat-Caretta, C., Caretta, A., and Cavaggioni, A. (1995). Acceleration of puberty onset in female mice by male urinary proteins. *J. Physiol.* 486(Pt. 2), 517–522.

Mudge, J. M., Armstrong, S. D., McLaren, K., Beynon, R. J., Hurst, J. L., Nicholson, C., et al. (2008). Dynamic instability of the major urinary protein gene family revealed by genomic and phenotypic comparisons between C57 and 129 strain mice. *Genome Biol.* 9:R91. doi: 10.1186/gb-2008-9-5-r91

Munger, S. D., Leinders-Zufall, T., and Zufall, F. (2009). Subsystem organization of the mammalian sense of smell. *Annu. Rev. Physiol.* 71, 115–140. doi: 10.1146/annurev.physiol.70.113006.100608

Nishimura, K., Utsumi, K., Yuhara, M., Fujitani, Y., and Iritani, A. (1989). Identification of puberty-accelerating pheromones in male mouse urine. *J. Exp. Zool.* 251, 300–305. doi: 10.1002/jez.1402510306

Norlin, E. M., Gussing, F., and Berghard, A. (2003). Vomeronasal phenotype and behavioral alterations in G alpha i2 mutant mice. *Curr. Biol.* 13, 1214–1219. doi: 10.1016/s0960-9822(03)00452-4

Novotny, M. V., Ma, W., Wiesler, D., and Zidek, L. (1999). Positive identification of the puberty-accelerating pheromone of the house mouse: the volatile ligands associating with the major urinary protein. *Proc. Biol. Sci.* 266, 2017–2022. doi: 10.1098/rspb.1999.0880

Oboti, L., Pérez-Gómez, A., Keller, M., Jacobi, E., Birnbaumer, L., Leinders-Zufall, T., et al. (2014). A wide range of pheromone-stimulated sexual and reproductive behaviors in female mice depend on G protein Galphao. *BMC Biol.* 12:31. doi: 10.1186/1741-7007-12-31

Omura, M., and Mombaerts, P. (2014). Trpc2-expressing sensory neurons in the main olfactory epithelium of the mouse. *Cell Rep.* 8, 583–595. doi: 10.1016/j.celrep.2014.06.010

Pankevich, D. E., Baum, M. J., and Cherry, J. A. (2004). Olfactory sex discrimination persists, whereas the preference for urinary odorants from estrous females disappears in male mice after vomeronasal organ removal. *J. Neurosci.* 24, 9451–9457. doi: 10.1523/jneurosci.2376-04.2004

Papes, F., Logan, D. W., and Stowers, L. (2010). The vomeronasal organ mediates interspecies defensive behaviors through detection of protein pheromone homologs. *Cell* 141, 692–703. doi: 10.1016/j.cell.2010.03.037

Riviere, S., Challet, L., Fluegge, D., Spehr, M., and Rodriguez, I. (2009). Formyl peptide receptor-like proteins are a novel family of vomeronasal chemosensors. *Nature* 459, 574–577. doi: 10.1038/nature08029

Roberts, S. A., Davidson, A. J., McLean, L., Beynon, R. J., and Hurst, J. L. (2012). Pheromonal induction of spatial learning in mice. *Science* 338, 1462–1465. doi: 10.1126/science.1225638

Roberts, S. A., Simpson, D. M., Armstrong, S. D., Davidson, A. J., Robertson, D. H., McLean, L., et al. (2010). Darcin: a male pheromone that stimulates female memory and sexual attraction to an individual male's odour. *BMC Biol.* 8:75. doi: 10.1186/1741-7007-8-75

Rünnenburger, K., Breer, H., and Boekhoff, I. (2002). Selective G protein beta gamma-subunit compositions mediate phospholipase C activation in the vomeronasal organ. *Eur. J. Cell Biol.* 81, 539–547. doi: 10.1078/0171-9335-00277

Ryba, N. J., and Tirindelli, R. (1997). A new multigene family of putative pheromone receptors. *Neuron* 19, 371–379. doi: 10.1016/s0896-6273(00)80946-0

Schneider, N. Y., Fletcher, T. P., Shaw, G., and Renfree, M. B. (2012). Goalpha expression in the vomeronasal organ and olfactory bulb of the tammar wallaby. *Chem. Senses* 37, 567–577. doi: 10.1093/chemse/bjs040

Sherborne, A. L., Thom, M. D., Paterson, S., Jury, F., Ollier, W. E. R., Stockley, P., et al. (2007). The genetic basis of inbreeding avoidance in house mice. *Curr. Biol.* 17, 2061–2066. doi: 10.1016/j.cub.2007.10.041

Silvotti, L., Moiani, A., Gatti, R., and Tirindelli, R. (2007). Combinatorial co-expression of pheromone receptors, V2Rs. *J. Neurochem.* 103, 1753–1763. doi: 10.1111/j.1471-4159.2007.04877.x

Stowers, L., Holy, T. E., Meister, M., Dulac, C., and Koentges, G. (2002). Loss of sex discrimination and male-male aggression in mice deficient for TRP2. *Science* 295, 1493–1500. doi: 10.1126/science.1069259

Sturm, T., Leinders-Zufall, T., Maček, B., Walzer, M., Jung, S., Pömmerl, B., et al. (2013). Mouse urinary peptides provide a molecular basis for genotype discrimination by nasal sensory neurons. *Nat. Commun.* 4:1616. doi: 10.1038/ncomms2610

Takigami, S., Mori, Y., and Ichikawa, M. (2000). Projection pattern of vomeronasal neurons to the accessory olfactory bulb in goats. *Chem. Senses* 25, 387–393. doi: 10.1093/chemse/25.4.387

Takigami, S., Mori, Y., Tanioka, Y., and Ichikawa, M. (2004). Morphological evidence for two types of mammalian vomeronasal system. *Chem. Senses* 29, 301–310. doi: 10.1093/chemse/bjh032

Tanaka, M., Treloar, H., Kalb, R. G., Greer, C. A., and Strittmatter, S. M. (1999). G(o) protein-dependent survival of primary accessory olfactory neurons. *Proc. Natl. Acad. Sci. U S A* 96, 14106–14111. doi: 10.1073/pnas.96.24.14106

Tirindelli, R., Dibattista, M., Pifferi, S., and Menini, A. (2009). From pheromones to behavior. *Physiol. Rev.* 89, 921–956. doi: 10.1152/physrev.00037.2008

Trotier, D. (2011). Vomeronasal organ and human pheromones. *Eur. Ann. Otorhinolaryngol. Head Neck Dis.* 128, 184–190. doi: 10.1016/j.anorl.2010.11.008

Trotier, D., Eloit, C., Wassef, M., Talmain, G., Bensimon, J. L., Døving, K. B., et al. (2000). The vomeronasal cavity in adult humans. *Chem. Senses* 25, 369–380. doi: 10.1093/chemse/25.4.369

Wu, Z., Autry, A. E., Bergan, J. F., Watabe-Uchida, M., and Dulac, C. G. (2014). Galanin neurons in the medial preoptic area govern parental behaviour. *Nature* 509, 325–330. doi: 10.1038/nature13307

Wyatt, T. D. (2014). *Pheromones and Animal Behavior: Chemical Signals and Signature Mixes*. 2nd Edn. Cambridge: Cambridge University Press.

Wynn, E. H., Sánchez-Andrade, G., Carss, K. J., and Logan, D. W. (2012). Genomic variation in the vomeronasal receptor gene repertoires of inbred mice. *BMC Genomics* 13:415. doi: 10.1186/1471-2164-13-415

Wysocki, C. J., and Lepri, J. J. (1991). Consequences of removing the vomeronasal organ. *J. Steroid Biochem. Mol. Biol.* 39, 661–669. doi: 10.1016/0960-0760(91)90265-7

Young, J. M., and Trask, B. J. (2007). V2R gene families degenerated in primates, dog and cow, but expanded in opossum. *Trends Genet.* 23, 212–215. doi: 10.1016/j.tig.2007.03.004

Conflict of Interest Statement: The authors declare that the research was conducted in the absence of any commercial or financial relationships that could be construed as a potential conflict of interest.

Received: 16 September 2014; accepted: 03 November 2014; published online: 26 November 2014.

Citation: Pérez-Gómez A, Stein B, Leinders-Zufall T and Chamero P (2014) Signaling mechanisms and behavioral function of the mouse basal vomeronasal neuroepithelium. Front. Neuroanat. ***8****:135. doi: 10.3389/fnana.2014.00135*

This article was submitted to the journal Frontiers in Neuroanatomy.

frontiers in
NEUROANATOMY

ORIGINAL RESEARCH ARTICLE
published: 25 September 2014
doi: 10.3389/fnana.2014.00101

Lacrimal gland removal impairs sexual behavior in mice

Rosa Maria Cavaliere, Filippo Ghirardi and Roberto Tirindelli*

Department of Neuroscience, University of Parma, Parma, Italy

Edited by:
Pablo Chamero, University of Saarland, Germany

Reviewed by:
Alino Martinez-Marcos, Universidad de Castilla, Spain
Enrique Lanuza, Universidad de Valencia, Spain

****Correspondence:***
Roberto Tirindelli, Department of Neuroscience, University of Parma, Via Volturno, 39, 43125 Parma, Italy
e-mail: robertin@unipr.it

Exocrine gland-secreting peptides (ESPs) are a protein family involved in the pheromonal communication of rodents. ESP1 is a lacrimal peptide synthesized by the extraorbital glands of males of specific mouse strains that modulates the sexual behavior in females. Reportedly, BALB/c males, that produce high level of ESP1 in the tear fluid, were shown to enhance the lordosis behavior in C57BL/6 females during mating. In contrast, C57BL/6 and ICR males, both unable to express ESP1, failed to modulate this sexual behavior. Nonetheless, ICR males did become competent to enhance lordosis behavior in C57BL/6 females providing these were pre-exposed to ESP1. To exclude any strain differences, here, we investigated the pheromonal role of the extraorbital glands and indirectly of ESP1 in animals of the same strain. This was performed by applying the lordosis experimental paradigm in BALB/c mice before and after the surgical removal of these glands in males. The excision of the extraorbital glands reduced but did not abolish the production of ESP1 in the lacrimal fluid of BALB/c mice. An immunological analysis on soluble extracts of the glands that drain into the conjunctival sac revealed that the intraorbital glands (ILGs) are also responsible for the production of ESP1. The removal of both the extra and ILGs completely eliminated the tear secretion of ESP1. Extraorbital gland-deficient BALB/c mice were still able to induce lordosis behavior in sexually receptive females. In contrast, males with the removal of both the extra and ILGs failed to enhance lordosis behavior in females. Unexpectedly, C57BL/6 males did improve this sexual performance in BALB/c females. However, an analysis of the tear fluid of C57BL/6 males revealed low but detectable levels of ESP1. Overall, our study highlights the relevance of the orbital glands in modulating reproductive behavior and the sensitivity of the vomeronasal system to detect trace amount of ESP1.

Keywords: ESP1, lacrimal glands, vomeronasal, pheromones, lordosis behavior

INTRODUCTION

Mammals produce chemically different types of pheromones to mediate social behavior (Tirindelli et al., 2009). Small volatile pheromones diffuse in the air and mediate long distance communication. In contrast, peptide pheromones are dropped on the ground or even they remain on the body surface, allowing signal transmission between conspecifics but exclusively by direct contact.

In the mouse, peptide pheromones are reportedly excreted in the urine, vaginal smear and also through the tear fluid (Mucignat-Caretta et al., 1995; Hurst et al., 2001; Briand et al., 2004; Leinders-Zufall et al., 2004; Brennan and Kendrick, 2006; Chamero et al., 2007). The pheromonal components of salivary and lacrimal secretion include molecules belonging to a multigenic protein family named exocrine gland-secreting peptides (ESPs; Kimoto et al., 2005, 2007). ESP1 is a sex specific pheromone that is specifically expressed by the extraorbital glands (ELGs) of males of some mouse strains (including BALB/c) but not in others (including C57BL/6 and Slc:ICR) and released into tear fluids (Kimoto et al., 2005, 2007). ESP1 is detected by the chemosensory neurons of the vomeronasal organ of Jacobson (Kimoto et al., 2005), a secondary olfactory structure that lies underneath the nasal septum and opens into the anterior part of the nasal cavity. The vomeronasal organ expresses two groups of G- protein coupled receptors, namely V1Rs and V2Rs that sense both volatile and non volatile pheromones (Dulac and Axel, 1995; Herrada and Dulac, 1997; Matsunami and Buck, 1997; Ryba and Tirindelli, 1997). ESP1 is recognized by a specific V2R and the information is conveyed to brain centers where it elicits neuroendocrine and behavioral responses (Haga et al., 2010). In particular, ESP1 seems to modulate the lordosis behavior (Haga et al., 2010) which represents a sexual response of female mice to allow successful mating and it is characterized by a reflexive posture upon male mounting (Keller et al., 2006).

Haga et al. recorded the sexual behavior of a C57BL/6 receptive female mouse introduced into a cage housing either an ESP1-secreting male (BALB/c) or a male that does not produce ESP1 (C57BL/6). They found that females introduced to a BALB/c male showed a significant increase in lordosis response compared to females mated to a C57BL/6 male. To firmly establish the pheromonal role of ESP1, they also demonstrated that BALB/c females, pre-exposed to ESP1, displayed an increased lordosis behavior when challenged with a stud male of a non producing ESP1 strain as Slc:ICR (Haga et al., 2010).

These results provide strong evidence that ESP1 effectively enhances female sexual behavior. However, these studies did not entirely clarified whether the behavioral responses elicited by ESP1 would be influenced by the different mouse strains that were employed in these experiments. Mice are in fact able to selectively discriminate conspecifics of different strains (Leinders-Zufall et al., 2004; Cheetham et al., 2009; Kaur et al., 2014). Thus, we wanted to investigate if the lordosis behavior was not affected when tests were carried out on mice of the same strain (BALB/c). To accomplish this task, it was firstly necessary to remove the ELGs of male BALB/c mice in order to abolish the ESP1 production. Unexpectedly, we found that the excision of ELGs resulted in a reduced but still detectable level of ESP1 in the tear fluid. Analysis of the lacrimal glands that drain into the conjunctival sac showed that two small lateral glands, the intraorbital glands (ILGs), were responsible for the remaining production of ESP1. Removal of both ELGs and ILGs completely abolished any residual ESP1 immunoreactivity in the tear fluid. BALB/c males deprived of the ELGs and ILGs but not of ELGs alone failed to enhance lordosis behavior in BALB/c females. These findings establish the pheromonal role of the orbital glands in modulating sexual behavior most likely through the action of ESP1 and possibly other lacrimal secretions.

MATERIALS AND METHODS

ANIMALS

Mice of the BALB/c and C57BL/6 strain were purchased from Harlan and bred in our animal house. Mice were maintained on a 12 h dark, 12 h light cycle. For both immunological and behavioral studies, 2–4 month old mice were employed.

The experiments comply with the Principles of Animal Care of the National Institutes of Health and with the current law of the European Union and Italy. The present project was approved by the Ethical Committee of the University of Parma: approval ID: 17/14, date: 27/03/14.

SURGERY

For ovariectomy in BALB/c and C57BL/6, 1 month old female mice were anesthetized with a solution (0.1 ml/ 10 g weight) of xylazine (1 mg/ml) and ketamine (10 mg/ml).

Mice were placed ventrally and the dorsal surgical area was shaved and disinfected. A short dorsal midline skin and abdominal muscle incision was made halfway between the last dorsal rib and the base of the tail. The ovary and the oviduct were exteriorized. A sterile ligature was placed around the oviduct and the ovary was removed. The surgical plan was then closed with silk sutures.

For lacrimal gland surgery in BALB/c male mice, animals were anesthetized as above described. The main extraorbital lacrimal gland in the mouse is located just rostrally to the parotid gland and lies on the masseter muscle. The intraorbital gland is located rostrally to the extraorbital gland in proximity to the lateral commissure and lies on the supraorbital branch of the superficial temporal artery. The two glands are connected by the lacrimal duct that drains the fluid into the conjunctival sac. A skin incision was made between the lateral commissure of the eye and ear. After dissection of the subcutaneous tissue, the lacrimal gland was identified and exposed. By using forceps, the gland was easily separated from the parotid gland and exteriorized. The lacrimal duct was identified and closed with non-reabsorbable suture and the gland was removed. The lacrimal duct was then followed up to the junction with the intraorbital gland that, in turn, was removed making sure not to damage the superficial temporal vein (STV) and artery. Animals were left to recover for 2 weeks during which the eyes were lubricated and maintained aseptic with eye drops containing antibiotics and Celluvisc©.

BEHAVIORAL TESTS

For the *Courtship behavior test*, after ovariectomy, oestrus was induced in sexually naïve females by estradiol benzoate treatment (0.02 mg s.c. 24 h and 48 h before test) followed by a single progesterone injection (0.3 mg s.c.) 4 h before testing. Female mice were then caged individually and always tested in one assay.

Stud males were selected by training to mount oestrous females until they exhibit a number of mounts greater than 20 in 30 min. Each sexually experienced male mouse was isolated for 48 h before test without replacing the bedding.

In each experiment, a naive oestrus female was introduced into a cage housing an isolated stud male and their behavior was videotaped for 30 min. All experiments were performed in 17 × 25 cm Plexiglas transparent cages that allow the ventral view of the videotaping. The experiments were always carried out at the same time of day (3–5 p.m.).

For the analysis, the total numbers of stud male mounts, female lordosis behavior towards mounts and the intromission behavior towards females was scored according to Haga et al. (2010). Briefly, mount was defined as a stud male climbed onto a female for copulation. Lordosis response was positive when female, with all four paws on the cage floor, elevated the hind region while arching the back and tilting the head upwards. Intromission was defined as a repetitive male pelvic thrust during copulation. The experimenter analyzing behavior was blind to the experimental condition of the animals.

For the *Emergence* test, mice were placed inside a small dark box (15 × 14 × 12 cm), containing one exit door. The box was located in the middle of a large cage (33 × 55 × 18 cm). After 5 min habituation, the door was opened and the latency before emerging from the box, the number of walks out of the box and the time spent inside the box were measured in a 5 min trial. Locomotor activity was also observed during the period outside the box. The experiments were always carried out at the same time of day (3–5 p.m.).

Behavioral performances were analyzed by using "The Observer" software.

Statistical analysis was performed by ANOVA with Student's *t*-test and by Levene test (variance homogeneity) on SPSS 20.0 platform.

SAMPLE COLLECTION AND WESTERN BLOTTING

Tear fluids were collected twice a day for 2 weeks, washing the eye with 15 μl of a solution containing 5 mM sodium phosphate pH 7.4. The lacrimal fluids were then pooled, lyophilized and re-supended in water before electrophoresis.

Glandular soluble extract were obtained by homogenizing the collected glands in 10 mM Tris-HCl pH 7.5. The suspension was then ultracentrifuged for 30 min at 1000 g. The aqueous phase was harvested and the protein concentration was measured (Bio-Rad assay) before electrophoresis.

Polyacrylamide gel electrophoresis (SDS-PAGE) was run in Tricine buffer as previously described (Schägger, 2006). After run, proteins were transferred onto a nitrocellulose membrane for western analysis. The nitrocellulose membrane was first incubated with a blocking solution containing 3% non-fat dry milk (Bio-Rad) in Tris-HCl 10 mM, NaCl 150 mM, Tween 0.05% (TTBS) for 1 h and then the antibody anti-ESP1 (generous gift from Dr. Touhara) was added at a dilution of 1:20,000. After an overnight incubation, the membrane was washed for 1 h with TTBS and an HPR-conjugated secondary antibody (1:1000 in TTBS) was added for 3 h at room temperature. After washing, the membrane was developed with Super Signal West Pico Chemioluminescent Substrate according to the manufacturer's instruction (Pierce). Marker proteins (EzWay Protein-Blue marker, Komabiotech) were also run and transferred to identify the appropriate size of the immunoreactive product. Films were scanned and the immunoreactive bands were selected and subjected to densitometric analysis.

RT-PCR

RNA was extracted from fresh tissue and purified using Trizol reagent (Invitrogen Milano, Italy). About 2 μg of total DNAse treated RNA served as template for oligo-dT primed first strand cDNA synthesis with Im-Prom-II Reverse Transcriptase (Promega, Milano, Italy).

Specific PCR primers were designed to amplify ESP1: 5′-TGTTTGCCATGAAATAACATGTGC-3′, 5′-CTTGGTGAATTAG ACAAGTTGGTT-3′. The expected amplified sequence encompasses exon 2 between base 306 and 830 of the coding sequence.

PCR was performed in Mastercycler Personal (Eppendorf, Milano, Italy) using AmpliBiotherm DNA polymerase, 3 mM $MgCl_2$, 0.2 mM for each dNTPs and 200 pmol forward/reverse target-specific oligonucleotide primers. Cycling parameters consisted of an initial denaturation step (95°C, 2 min) followed by 35 cycles, each of these included a denaturation (95°C, 30 s), a primer annealing (53°C, 30 s), and an extension (72°C, 30 s) step. Reaction was completed by a final extension step at 72°C for 5 min. Semiquantitative analysis of RNA expression was performed on agarose gel after electrophoresis using the NIS-Elements Advanced Research software (Nikon, Firenze, Italy). Bands were excised and subcloned in pGEM-T vector and the plasmidic DNA was subjected to confirmatory sequencing.

RESULTS

To investigate if the lack of ESP1 expression in BALB/c male mice caused a reduction of the lordosis behavior in receptive females of the same strain, we identified and bilaterally excised the extraorbital glands (ELGs) which are reportedly known to produce this peptide. ELGs are pair structures that lie upon the masseter muscles orally to the parotid glands (**Figure 1A**). The lacrimal fluid produced by ELG is drained by a lacrimal duct

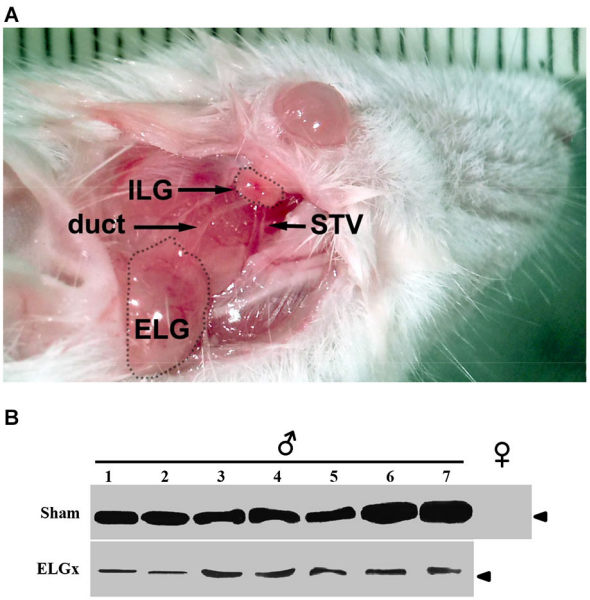

FIGURE 1 | ESP1-immunoreactivity in the tear fluid after removal of the extraorbital lacrimal glands. (A) The surgical area after the incision of the skin in the temporal region of the mouse is photographed. Shown are the extraorbital gland (ELG), the intraorbital gland (ILG), the lacrimal duct and the superficial temporal vein (STV). **(B)** The lacrimal fluid of seven BALB/c male mice, which underwent the removal of ELGs (ELGx), and of seven sham operated mice (control) was individually collected and analyzed by western blotting with an antibody against ESP1. Tear fluids were also pooled from five BALB/c female mice and used as a negative control. Arrowhead indicates the position of the molecular marker (aprotinin, 6.5 KDa).

that runs orally to open into the conjunctival sac in proximity to the lateral palpebral commissure. Although the removal of ELG always appeared complete, to make sure that any residual glandular tissues would not contribute in the ESP1 production, the duct was also closed with non absorbable suture. Control mice were also anesthetized and the surgical plan exposed before suturing. After 2 weeks of recovery, the lacrimal fluid of both operated (ELGx) and sham-operated (control) BALB/c mice was individually collected for 2 weeks and samples were run in a Tricine-SDS-PAGE for western analysis.

The immunological analysis with an antibody specific to ESP1 revealed that all ELGx mice still produced lower but detectable levels of ESP1 compared to controls (**Figure 1B**). This unexpected result led us to investigate the origin of residual production of ESP1 collected in the lacrimal fluid. Thus, we isolated all the lacrimal glands draining into the conjunctival sac and searched for ESP1 expression. The soluble extract of the glands was loaded onto a PAGE gel electrophoresis and the western blot analyzed for immunoreactivity against ESP1. As shown in **Figure 2A**, the ILGs were also found to produce ESP1. By densitometric analysis, we estimated a 80–100 times reduction of the ESP1 concentration in the lacrimal fluid of ELGx mice. Interestingly, ILGs share the same embryological origin as ELGs and their fluid drains into the ELG lacrimal ducts (Makarenkova et al., 2000; **Figure 1A**). To prove that ILGs produce ESP1 and to unequivocally exclude

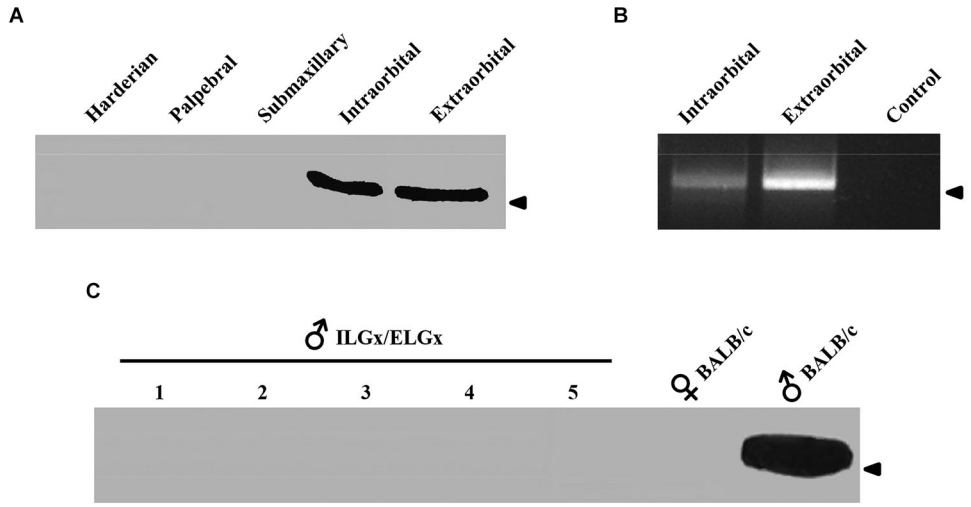

FIGURE 2 | ESP1 expression in lacrimal glands and tear fluid. (A) Soluble lacrimal gland extracts of BALB/c mice analyzed for ESP1 immunoreactivity by western blotting. Arrowhead indicates the position of the molecular marker (aprotinin, 6.5 KDa). **(B)** Expression pattern of the ESP1 gene in different lacrimal glands of BALB/c males, as determined by RT–PCR. PCR control without cDNA is also shown. Arrowhead indicates the position of the 500 bp DNA marker. **(C)** ESP1 immunoreactivity in tear fluids, analyzed by western blotting, in five BALB/c males after the removal of both ELGs and ILGs (ELGx/ILGx). Tear fluids of positive (BALB/c males) and negative (BALB/c females) controls were also tested for ESP1 immunoreactivity. Arrowhead indicates the position of the molecular marker (aprotinin, 6.5 KDa).

any cross reactivity with the anti-ESP1 antibody, ILG total RNA from BALB/c male mice was isolated and reverse-transcribed. RT-PCR of ILG cDNA with ESP1 specific primers indeed confirms that ESP1 is expressed by these glands that in turn are responsible for the remaining immunoreactivity in the tear fluid after removal of ELGs (**Figure 2B**). Thus, in order to completely abolish the ESP1 production in the BALB/c male mice, both ELGs and ILGs were removed. After ELG and ILG surgery, the tear fluid of individual BALB/c male mice was tested by western blotting for ESP1 immunoreactivity. The removal of both ELGs and ILGs (ELGx/ILGx) resulted in the complete loss of detectable levels of ESP1 in the tear fluid (**Figure 2C**). Moreover, ELGx and ILGx/ILGx male mice did not show any evident change in stress-related and locomotor behavior that might have been caused by surgery (**Table 1**). Therefore, we were able to investigate the effects of the orbital glands removal on sexual behavior in mice of the same strain (BALB/c).

Table 1 | Locomotor activity measured by the *Emergence Test* in BALB/c male mice after the bilateral removal of both the extra and intra orbital glands (ILGx/ELGx) ($n = 7$ for each group, Time trial, 300 s).

Locomotor activity	Sham	ELGx/ILGx	
Number of walks out	8 ± 1.8	7.4 ± 1	$F = 1.7$; $p = 0.79$
Latency (s)	9.4 ± 1.7	3.8 ± 1.2	$F = 1.51$; $p = 0.051$
Time outside the box (s)	235.9 ± 14.8	246.6 ± 8.8	$F = 1.56$; $p = 0.55$
Rearing (vertical exploration) (s)	26 ± 6.7	27.8 ± 4.4	$F = 1.37$; $p = 0.83$
Walking (horizontal exploration) (s)	110.1 ± 4.5	109.9 ± 7.6	$F = 0.94$; $p = 0.98$
Self-grooming (s)	2.7 ± 1.2	2.3 ± 1.8	$F = 0.25$; $p = 0.87$

Sexually naive BALB/c female mice were first ovariectomized and, after a recovery period, they were treated with estrogens and progesterone to induce estrous. When a BALB/c stud male (either control or operated) was introduced into a cage housing the receptive female, the male showed characteristic mounting behavior towards the female that includes mounting and penetration. Similarly, the oestrus female also showed a distinctive behavior which consisted in a reflexive posture upon male mounting. The number of mounting events and penetrations as well as female lordosis behavior was evaluated in a 30 min trial (**Figure 3A**).

The number of mounts carried out by ELGx, ELGx/ILGx and control mice ($n = 7$ for each group) on BALB/c females did not show any significant difference ($F = 2.36$, $\sigma = 0.16$, $p = 0.685$; $F = 0.57$, $\sigma = 0.47$, $p = 0.123$ respectively). The percentage of successful intromissions (out of the total mounts) of ELGx/ILGx males (21.9 ± 7.5 SE) towards receptive females was lower than in controls (49.2 ± 6.3 SE) and ELGx males (60.5 ± 15.4 SE) ($F = 011$, $\sigma = 0.75$, $p = 0.021$; $F = 1.09$, $\sigma = 0.33$, $p = 0.047$, respectively). We then analyzed the sexual behavior of BALB/c females in the same trial. BALB/c females introduced to an ELGx/ILGx male showed a threefold decrease in the percentage of lordosis response (out of the number of mounts) (13.9 ± 4.3 SE) compared to both ELGx (64.4 ± 3.5 SE) and control mice (48.7 ± 6.9 SE) ($F = 0.65$, $\sigma = 0.45$, $p < 0.0001$; $F = 0.64$, $\sigma = 0.45$, $p = 0.003$ respectively). No significant difference was observed in the lordosis behavior of BALB/c females challenged with either ELGx or control male mice ($F = 1.21$, $\sigma = 0.30$, $p = 0.12$).

To investigate whether the removal of ELGs and ILGs produced a similar behavioral response in a female of a different

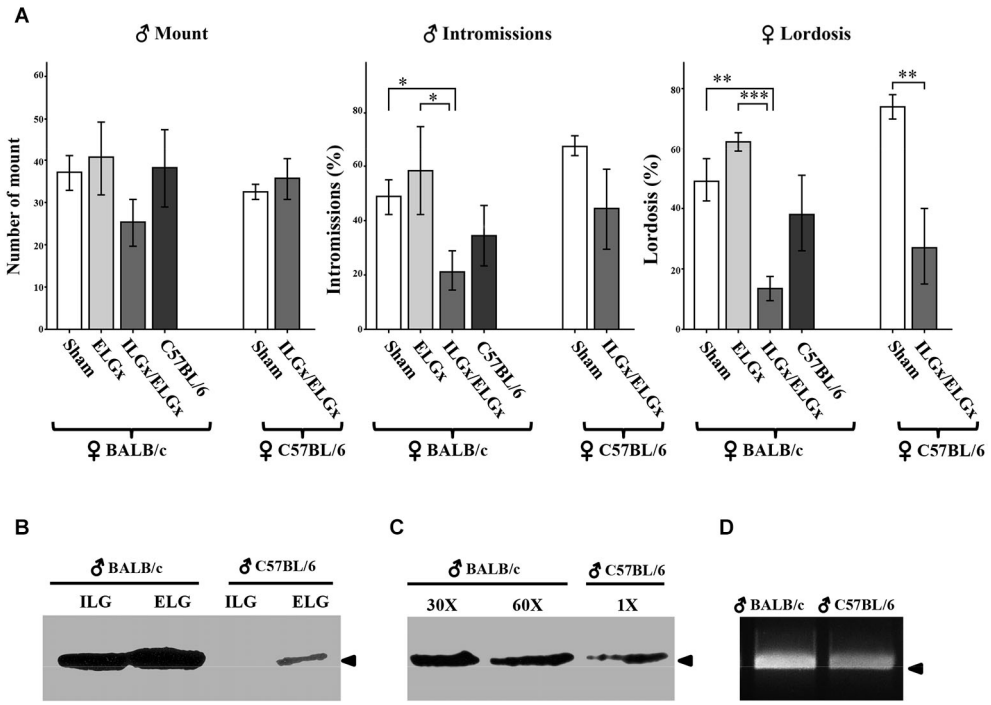

FIGURE 3 | Removal of the ESP1-expressing lacrimal glands impairs sexual behavior in BALB/c females. (A) BALB/c and C57BL/6 females were exposed to BALB/c males, which were deprived of the extraorbital glands (ELGx) or both the extraorbital and intraorbital glands (ELGx/ILGx), and to sham operated males (control). Histograms represent the number of male mounts, percentage of successful male intromissions per total mounts and percentage of female lordosis response per total mounts. Error bars represent SE; $n = 7$ for each animal group. * $P < 0.05$, ** $P < 0.01$, *** $P < 0.0001$. **(B)** ESP1 immunoreactivity in the extra and intraorbital gland soluble extracts of BALB/c and C57BL/6 male mice. **(C)** ESP1 immunoreactivity in the tear fluid of BALB/c and C57BL/6 male mice. BALB/c lacrimal fluid was diluted 30 and 60 times, respectively and the same volume of solution was loaded. Arrowhead indicates the position of the molecular marker (aprotinin, 6.5 KDa). **(D)** RT-PCR with ESP1 specific primers of cDNA synthesized from the mRNA of the extraorbital glands of BALB/c and C57BL/6 males. Arrowhead indicates the position of the 500 bp DNA marker.

mouse strain, we challenged C57BL/6 receptive females with ELGx/ILGx or BALB/c control mice ($n = 7$ for each group). As for BALB/c females, we found a significant reduction (but not abolishment) of the lordosis behavior of C57BL/6 females when mated to ELGx/ILGx mice (27.1 ± 14.7 SE) compared to controls (73.4 ± 4.5 SE) ($F = 11.6$, $\sigma = 0.08$, $p = 0.01$). In contrast, the percentage of intromissions ($F = 8.37$; $p = 0.14$) was not statistically significant as it was the case for the number of mounts ($F = 6.4$, $\sigma = 0.18$, $p = 0.35$).

To verify the reproducibility of our test with that of Haga et al. (2010), we wanted to assess if (sham operated) C57BL/6 males, that reportedly lack ESP1 expression, elicited the same behavioral responses as ELGx/ILGx on BALB/c females. Unexpectedly, we found no significant differences in both intromission ($F = 4.64$, $\sigma = 0.06$, $p = 0.27$) and lordosis ($F = 4.2$, $\sigma = 0{,}07$, $p = 0.46$) response of C57BL/6 males compared to controls ($n = 7$ for each group) (**Figure 3A**). Thus, we ask whether this result was due to behavioral differences related to the mouse strain which was employed (C57BL/6 vs. BALB/c) or whether our C57BL/6 males were able to produce ESP1. To answer this question we collected the tear fluid and the ELG-ILG soluble extracts of C57BL/6 males and tested them by SDS-PAGE and western analysis. Although at much lower concentration than in BALB/c mice, we detected ESP1 immunoreactivity in both the tear fluid and the glandular extract of our C57BL/6 males (**Figures 3B,C**). A densitometric analysis of the immunoreactive signals revealed that the concentration of ESP1 in the tear fluid of C57BL/6 males was approximately 90 times lower than in BALB/c and was comparable to that observed in ELGx males (not shown). This observation was confirmed by RT-PCR on reverse-transcribed mRNA extracted from ELGs and ILGs and amplified with ESP1-specific primers (**Figure 3D**).

DISCUSSION

In this work, we have analyzed the behavioral responses of oestrus BALB/c females elicited by BALB/c male mice that were surgically deprived of the extraorbital and intraorbital lacrimal glands that produce ESP1 (Kimoto et al., 2005). This peptide was shown to play a pheromonal role in the sexual communication of the mouse (Haga et al., 2010) since it was demonstrated that BALB/c mice that produce and secrete ESP1 into the conjunctival sac enhances lordosis behavior in receptive C57BL/6 females. In contrast, C57BL/6 males, that reportedly do not express ESP1, fail to induce such behavior in BALB/c females (Haga et al., 2010).

Our aim was to investigate if this behavioral response was independent of the mouse strain which is employed and whether

ELGs and ILGs are indeed important in mediating pheromonal communication.

In preliminary observations to this study, we found that ESP1, which was thought to be exclusively expressed in the extraorbital gland, is also produced by the ILGs. This pair glandular structure lies close to the lateral palpebral commissure and drains the fluid into the same duct as the extraorbital glands with which they share the same embryological origin (Makarenkova et al., 2000). Mice that underwent the bilateral surgery of ELGs and ILGs did not show any ESP1 immunoreactivity in the tear fluid whereas the removal of the ELGs alone did not abolish ESP secretion into the conjunctival sac.

In a behavioral context, BALB/c mice with the surgical ablation of both ELG and ILG (ELGx-ILGx) failed to enhance the lordosis behavior in BALB/c females confirming that this effect is not dependent on the strain which was employed (C57BL/6 or BALB/c). This is also confirmed by experiments where C57BL/6 females were paired with ELGx-ILGx males in a lordosis behavioral test. The surgical removal of the ELG alone in BALB/c mice (ELGx) was not sufficient to decrease lordosis behavior in BALB/c females. In fact, ELGx mice produce small but detectable amounts of ESP, thus suggesting that females are able to sense and respond to very low concentrations of ESP1 via the vomeronasal organ. This is consistent with what is observed in C57BL/6 males that also succeeded in enhancing lordosis behavior in BALB/c females. In C57BL/6 mice, we found levels of ESP1 in the tear fluid which were comparable to that observed in ELGx mice. Nevertheless, this result was unexpected as it disagrees with previous studies where C57BL/6 males were reportedly unable to produce ESP1 and therefore to enhance lordosis behavior in females (Haga et al., 2010). Thus, it is possible that variability in the ESP1 expression within the same strain may exist. This may be due to small genetic variations or caused by the different environments where these animals live. Overall, our results highlight the pheromonal role of the lacrimal glands and established that, ESP1, probably along with other pheromones, acts as a modulator of female lordosis behavior via the vomeronasal system. Lordosis, thus, appears to be a sexual performance largely, although not exclusively, modulated by ESP1 stimulation through the activation of the vomeronasal system. The modulation of lacrimal gland secretion on female behavior appears effective across different mouse strains providing they express, even at very low level, this peptide. This suggests that the neural pathways underlying the transmission of the lacrimal pheromone signal are preserved also in mouse strains that do not constitutively express ESP1. It is worth noting that the removal of ELGs and ILGs may also abolish the production of additional pheromones that are involved in other behavioral performances. The persistence of lordosis in mice deprived of both the extra and ILGs (see **Figure 3A**) also establishes that this sexual performance is only partially dependent on the secretion of these glands and that other chemical or physical stimuli are involved. Thus, the animal model which we have developed may be interesting to elucidate different aspects of the pheromonal communication in rodents. For example it was reportedly observed that ESP1 stimulation in BALB/c but not in C57BL/6 males does not induce cFos expression in the vomeronasal and accessory olfactory bulb neurons, as a result of desensitization caused by self-secreted ESP1(Haga et al., 2010). In this context, it might be interesting to investigate if desensitization is strain-specific (irreversible) or cFos responsiveness can be restored after lacrimal gland removal. Furthermore, ELGx/ILGx mice could be also successfully employed to investigate the behavioral responses in mice with the genetic ablation of the vomeronasal transduction molecules (Stowers et al., 2002; Norlin et al., 2003; Montani et al., 2013; Oboti et al., 2014).

AUTHOR CONTRIBUTION

Rosa Maria Cavaliere performed the experiments, collected and analyzed the data. Filippo Ghirardi performed the initial experiments and Roberto Tirindelli wrote the manuscript and directed the project.

ACKNOWLEDGMENTS

This work is supported by the Italian Ministry of Research (MIUR) and Italian Institute of Technology (IIT).

REFERENCES

Brennan, P. A., and Kendrick, K. M. (2006). Mammalian social odours: attraction and individual recognition. *Philos. Trans. R. Soc. Lond. B Biol. Sci.* 361, 2061–2078. doi: 10.1098/rstb.2006.1931

Briand, L., Trotier, D., and Pernollet, J. C. (2004). Aphrodisin, an aphrodisiac lipocalin secreted in hamster vaginal secretions. *Peptides* 25, 1545–1552. doi: 10.1016/j.peptides.2003.10.026

Chamero, P., Marton, T. F., Logan, D. W., Flanagan, K., Cruz, J. R., Saghatelian, A., et al. (2007). Identification of protein pheromones that promote aggressive behaviour. *Nature* 450, 899–902. doi: 10.1038/nature05997

Cheetham, S. A., Smith, A. L., Armstrong, S. D., Beynon, R. J., and Hurst, J. L. (2009). Limited variation in the major urinary proteins of laboratory mice. *Physiol. Behav.* 96, 253–261. doi: 10.1016/j.physbeh.2008.10.005

Dulac, C., and Axel, R. (1995). A novel family of genes encoding putative pheromone receptors in mammals. *Cell* 83, 195–206. doi: 10.1016/0092-8674(95)90161-2

Haga, S., Hattori, T., Sato, T., Sato, K., Matsuda, S., Kobayakawa, R., et al. (2010). The male mouse pheromone ESP1 enhances female sexual receptive behaviour through a specific vomeronasal receptor. *Nature* 466, 118–122. doi: 10.1038/nature09142

Herrada, G., and Dulac, C. (1997). A novel family of putative pheromone receptors in mammals with a topographically organized and sexually dimorphic distribution. *Cell* 90, 763–773. doi: 10.1016/S0092-8674(00)80536-X

Hurst, J. L., Payne, C. E., Nevison, C. M., Marie, A. D., Humphries, R. E., Robertson, D. H., et al. (2001). Individual recognition in mice mediated by major urinary proteins. *Nature* 414, 631–634. doi: 10.1038/414631a

Kaur, A. W., Ackels, T., Kuo, T. H., Cichy, A., Dey, S., Hays, C., et al. (2014). Murine pheromone proteins constitute a context-dependent combinatorial code governing multiple social behaviors. *Cell* 157, 676–688. doi: 10.1016/j.cell.2014.02.025

Keller, M., Pierman, S., Douhard, Q., Baum, M. J., and Bakker, J. (2006). The vomeronasal organ is required for the expression of lordosis behaviour, but not sex discrimination in female mice. *Eur. J. Neurosci.* 23, 521–530. doi: 10.1111/j.1460-9568.2005.04589.x

Kimoto, H., Haga, S., Sato, K., and Touhara, K. (2005). Sex-specific peptides from exocrine glands stimulate mouse vomeronasal sensory neurons. *Nature* 437, 898–901. doi: 10.1038/nature04033

Kimoto, H., Sato, K., Nodari, F., Haga, S., Holy, T. E., and Touhara, K. (2007). Sex- and strain-specific expression and vomeronasal activity of mouse ESP family peptides. *Curr. Biol.* 17, 1879–1884. doi: 10.1016/j.cub.2007.09.042

Leinders-Zufall, T., Brennan, P., Widmayer, P., S, P. C., Maul-Pavicic, A., Jäger, M., et al. (2004). MHC class I peptides as chemosensory signals in the vomeronasal organ. *Science* 306, 1033–1037. doi: 10.1126/science.1102818

Makarenkova, H. P., Ito, M., Govindarajan, V., Faber, S. C., Sun, L., McMahon, G., et al. (2000). FGF10 is an inducer and Pax6 a competence factor for lacrimal gland development. *Development* 127, 2563–2572.

Matsunami, H., and Buck, L. B. (1997). A multigene family encoding a diverse array of putative pheromone receptors in mammals. *Cell* 90, 775–784. doi: 10.1016/s0092-8674(00)80537-1

Montani, G., Tonelli, S., Sanghez, V., Ferrari, P. F., Palanza, P., Zimmer, A., et al. (2013). Aggressive behaviour and physiological responses to pheromones are strongly impaired in mice deficient for the olfactory G-protein -subunit G8. *J. Physiol.* 591, 3949–3962. doi: 10.1113/jphysiol.2012.247528

Mucignat-Caretta, C., Caretta, A., and Cavaggioni, A. (1995). Acceleration of puberty onset in female mice by male urinary proteins. *J. Physiol.* 486(Pt. 2), 517–522.

Norlin, E. M., Gussing, F., and Berghard, A. (2003). Vomeronasal phenotype and behavioral alterations in G alpha i2 mutant mice. *Curr. Biol.* 13, 1214–1219. doi: 10.1016/s0960-9822(03)00452-4

Oboti, L., Pérez-Gómez, A., Keller, M., Jacobi, E., Birnbaumer, L., Leinders-Zufall, T., et al. (2014). A wide range of pheromone-stimulated sexual and reproductive behaviors in female mice depend on G protein Gαo. *BMC Biol.* 12:31. doi: 10.1186/1741-7007-12-31

Ryba, N. J., and Tirindelli, R. (1997). A new multigene family of putative pheromone receptors. *Neuron* 19, 371–379. doi: 10.1016/s0896-6273(00)80946-0

Schägger, H. (2006). Tricine-SDS-PAGE. *Nat. Protoc.* 1, 16–22. doi: 10.1038/nprot.2006.4

Stowers, L., Holy, T. E., Meister, M., Dulac, C., and Koentges, G. (2002). Loss of sex discrimination and male-male aggression in mice deficient for TRP2. *Science* 295, 1493–1500. doi: 10.1126/science.1069259

Tirindelli, R., Dibattista, M., Pifferi, S., and Menini, A. (2009). From pheromones to behavior. *Physiol. Rev.* 89, 921–956. doi: 10.1152/physrev.00037.2008

Conflict of Interest Statement: The authors declare that the research was conducted in the absence of any commercial or financial relationships that could be construed as a potential conflict of interest.

Received: 04 July 2014; accepted: 05 September 2014; published online: 25 September 2014.

Citation: Cavaliere RM, Ghirardi F and Tirindelli R (2014) Lacrimal gland removal impairs sexual behavior in mice. Front. Neuroanat. ***8****:101. doi: 10.3389/fnana.2014.00101*

This article was submitted to the journal Frontiers in Neuroanatomy.

frontiers in
NEUROANATOMY

REVIEW ARTICLE
published: 12 December 2014
doi: 10.3389/fnana.2014.00153

The molecular evolutionary dynamics of the vomeronasal receptor (class 1) genes in primates: a gene family on the verge of a functional breakdown

Anne D. Yoder* and Peter A. Larsen

Department of Biology, Duke University, Durham, NC, USA

Edited by:
Ignacio Salazar, University of Santiago de Compostela, Spain

Reviewed by:
Alino Martinez-Marcos, Universidad de Castilla, Spain
Robert Anholt, North Carolina State University, USA

****Correspondence:***
Anne D. Yoder, Department of Biology, Duke University, Biological Science Building, Science Drive, Box 90338, Durham, 27708 NC, USA
e-mail: anne.yoder@duke.edu

Olfaction plays a critical role in both survival of the individual and in the propagation of species. Studies from across the mammalian clade have found a remarkable correlation between organismal lifestyle and molecular evolutionary properties of receptor genes in both the main olfactory system (MOS) and the vomeronasal system (VNS). When a large proportion of intact (and putatively functional) copies is observed, the inference is made that a particular mode of chemoreception is critical for an organism's fit to its environment and is thus under strong positive selection. Conversely, when the receptors in question show a disproportionately large number of pseudogene copies, this contraction is interpreted as evidence of relaxed selection potentially leading to gene family extinction. Notably, it appears that a risk factor for gene family extinction is a high rate of nonsynonymous substitution. A survey of intact vs. pseudogene copies among primate vomeronasal receptor Class one genes (V1Rs) appears to substantiate this hypothesis. Molecular evolutionary complexities in the V1R gene family combine rapid rates of gene duplication, gene conversion, lineage-specific expansions, deletions, and/or pseudogenization. An intricate mix of phylogenetic footprints and current adaptive landscapes have left their mark on primate V1Rs suggesting that the primate clade offers an ideal model system for exploring the molecular evolutionary and functional properties of the VNS of mammals. Primate V1Rs tell a story of ancestral function and divergent selection as species have moved into ever diversifying adaptive regimes. The sensitivity to functional collapse in these genes, consequent to their precariously high rates of nonsynonymous substitution, confer a remarkable capacity to reveal the lifestyles of the genomes that they presently occupy as well as those of their ancestors.

Keywords: olfaction, gene family evolution, positive selection, adaptation, lemurs, draft genomes

INTRODUCTION

Vomeronasal receptor (Class 1) genes (V1Rs) are one of five independently derived functional classes of chemoreceptor genes in the olfactory system of mammals. Together with vomeronasal receptor (Class 2) genes (V2Rs) and a small family of formyl peptide receptors (FPRs), V1Rs are found clustered within an anatomical structure referred to as the vomeronasal organ (VNO). The two additional classes of receptor, the odorant receptors (ORs) and trace amine-associated receptors (TAARs) are found in the nasal epithelium. All five are G-protein coupled receptors (GPCRs), and as such, have structural features that are shared with other chemosensory genes such as sweet and bitter taste receptors. All GPCRs are structured to detect an enormous variety of extracellular signals, including photons, ions, small organic molecules and entire proteins. The structure of a GPCR can be divided into three parts: the extracellular region, consisting of the N terminus and three extracellular loops, the transmembrane region (TM), consisting of seven α-helices; and the intracellular region, consisting of three intracellular loops and the C-terminal tail. ORs fall into Class A GPCRs wherein the TM regions comprise a consensus "ligand-binding cradle" that constitutes the bottom of the ligand-binding pocket within the TM bundle. The third TM helix (TM3) has a central role as a structural and functional hub (Venkatakrishnan et al., 2013), putatively placing it under very strong purifying selection given the essential nature of its structure and placement to the stability of the ligand-binding cradle (e.g., Herberger and Loretz, 2013). These insights into the structure-function relationships of the GPCRs have thus yielded new perspectives for molecular evolutionary investigations of the types and levels of selective forces as they act on V1R and other chemosensory genes within mammals generally, and in this review, primates specifically.

The olfactory system is divided into two general systems, the main olfactory system (MOS) and the vomeronasal system (VNS), which though derived from non-homologous evolutionary pathways, are intimately related both ontogenetically, sharing similar molecular and cellular processes, and evolutionarily,

showing similar adaptations to changing ecological scenarios. This system has been referred to as "dual olfaction" (Suárez et al., 2012) and thus lessons learned from one can reasonably be applied to the other. This view therefore differs from the so-called "differential tuning" hypothesis proposed by Grus and Zhang (2008) in which the authors make note of the fact that though functioning within a single morphological and behavioral system, the MOS and VNS are putatively under different selective regimes with the MOS tuned to environmental and volatile odorants and the VNS to non-volatile semiochemicals that govern many conspecific (e.g, mating) and heterospecific (e.g., predation) interactions. Evidence continues to accumulate that the VNS is finely tuned to social cues and thus under strong lineage-specific selection (e.g., Garrett and Steiper, 2014) and is changing more rapidly than the more conserved ORs (D'Oliveira Albanus et al., 2014). It has been further demonstrated that within the VNS, the two receptor types, V1Rs and V2Rs, derive from different evolutionary precursors with each receptive to different ligand types: V1Rs tuned to detect small chemicals and V2Rs to detect proteinaceous ligands (Giorgi et al., 2000; Leinders-Zufall et al., 2000, 2009; Pantages and Dulac, 2000; Rodriguez et al., 2000; Kouros-Mehr et al., 2001; Del Punta et al., 2002; Giorgi and Rouquier, 2002; Grus and Zhang, 2004; Grus et al., 2005, 2007; Nodari et al., 2008; Korsching, 2009; Haga et al., 2010; Isogai et al., 2011; Park et al., 2011; Wynn et al., 2012; Hohenbrink et al., 2012a, 2014; Haga-Yamanaka et al., 2014).

Though it has been proposed that a move from an aquatic to terrestrial lifestyle has driven an apparent shift from a predominantly V2R to V1R system in mammals, recent investigation of VR gene expression in snakes and lizards has overturned this hypothesis (Brykczynska et al., 2013). This study found that snakes and lizards retain an extremely limited number of V1R genes but exhibit a large number of V2R genes, including multiple lineages of reptile-specific and snake-specific expansions. Moreover, elegant *in vivo* work by Isogai et al. (2011) has shown that both receptor families are highly active in mice (Chamero et al., 2011). Collectively, the olfactory system allows for the detection of a multitude of odorants and pheromones that are environmentally transmitted and must be internally processed to identify everything from appropriate food sources to potential mates to predators. In short, this sensory system is critical for the survival of the individual and for the propagation of the species.

"THE DARK MATTER OF SOCIAL NEUROSCIENCE"

In a review of the role of oxytocin and vasopression in modulating social interactions and affilicative behavior among mammals, Insel (2010) adopted the term "dark matter" of social neuroscience to describe the "complex territory between perception and action" that governs social cognition. This conceptual framework also applies broadly to the olfactory system (Chamero et al., 2012). Olfaction is critical to an organism's ability to survive, though in primates, there are multiple clues from anatomy, behavior, and the genome to suggest that the sensitivity of the system has diminished over their evolutionary history (Heymann, 2006; Dong et al., 2009), especially within the anthropoid primates. This decay of the olfactory system in catarrhine primates specifically was initially thought to be linked to the acquisition of trichromatic vision in old world monkeys and apes. In large part, this conclusion was supported by the observation that the howler monkey, the only New World monkey to possess trichromatic vision, showed a much higher proportion of OR pseudogenes than other NW monkeys (Gilad et al., 2004). More complete characterization of the ratio of intact to pseudogene copies and their distributions in both OW and NW anthropoids has overturned this conclusion, however (Gilad et al., 2007; Matsui et al., 2010).

In mammals more generally, numerous studies have found a remarkable connection between organismal lifestyle and molecular evolutionary patterns among olfactory receptors within the MOS and the VNS (Chamero et al., 2012; Ibarra-Soria et al., 2014; Sánchez-Andrade and Logan, 2014). In the case of the VNS, the fit between organismal lifestyle and genomic repertoire is interpreted to relate to pheromonal communication between "emitter" and "receiver". Sex pheromones in particular play fundamental roles in mate choice in a system that is conserved across the animal kingdom (Gomez-Diaz and Benton, 2013; Petrulis, 2013a,b; Liberles, 2014). Recent studies in the mouse model have shown that both the VNO and MOS are key to mediating social behavior (Mandiyan et al., 2005; Chamero et al., 2012) with *in vivo* studies of specific receptor function revealing an extraordinary specificity of receptor response to specific stimuli (Isogai et al., 2011). The latter study in particular was able to characterize the stimulus-response profiles in 88 VNO receptors, finding a mix of conspecific and heterospecific associations. The results illustrate a fascinating combination of specificity and generality. Whereas some receptors were exquisitely tuned to stimuli from conspecifics (e.g., certain receptors responded only to stimuli from conspecific females) or to heterospecific cues (e.g., some showed a unique association with distinct classes of predators such as snakes, but not others, such as fox), others were much more generalized. Notably, Isogai et al. (2011) found fundamental functional differences between the two classes of VRs, with V1Rs being the more generalized and V2Rs the more specialized. Due to their ability to distinguish among distinct structural classes of steroids, the authors surmised that V1Rs are uniquely geared to detect the physiological status of an individual, whether conspecific or heterospecific. Taken as a whole, the increasing sophistication of studies focused on VNO function reveals a field poised for an explosive era of discovery by uniting and reciprocally illuminating the fields of neuroendrochrinology, neuroimmunology, neuroethology, and social behavior. This integrative approach holds tremendous promise for unlocking the secrets of what Insel (2010) has called "the dark matter of social neuroscience" (Chamero et al., 2012).

A MOLECULAR-EVOLUTIONARY LOCOMOTIVE

In a landmark study of the V1R genes in mammals, Young et al. (2010) found remarkable patterns of both inter- and intraspecific variability among mammalian genomes, as mined from draft genomes available at that time. They discovered patterns wherein species-specific subfamilies and "semi-private" alleles are common among the 37 mammals sampled with approximately 80% of V1R clades being species-specific. These molecular evolutionary complexities in the V1R gene family have been

repeatedly noted and hypothesized to differentially combine rapid rates of gene duplication, gene conversion, lineage-specific expansions, deletions, and/or pseudogenization (e.g., Rodriguez et al., 2002; Shi et al., 2005; Wynn et al., 2012; Brykczynska et al., 2013). This behavior is in keeping with patterns of gene family evolution in general. Demuth et al. (2006) has described the genomic "revolving door" of gene loss and gain that seems to characterize much of the human genome, as well as mammalian outgroups. In their comparison of human, chimp, mouse, rat, and dog, these authors found shifting patterns of expansions and contractions within the nearly 10,000 gene families compared by the study. Regarding primate evolution specifically, their study indicates that the human genome contains at least 1418 genes (6.4% of all known genes at that time) that do not have orthologs in the chimpanzee, with an even greater discrepancy found between mouse and rat. The authors raise the interesting point that duplication and losses within gene families have played a greater role than nucleotide substitution in generating evolutionary change across mammalian genomes, and in the human genome specifically.

The question thus arises: what are the forces that drive this molecular evolutionary locomotive? An obvious dichotomy to be considered is between neutral and adaptive processes (e.g., Demuth et al., 2006; Park et al., 2011; Wynn et al., 2012). The phylogenetic distribution within and among mammals for both ORs and VRs suggests a strong role for adaptation, both as individual gene classes (e.g., Shi et al., 2005; Verrelli et al., 2008; Luca et al., 2010; Matsui et al., 2010; Wang et al., 2010a,b; Yoder et al., 2014) and in concert with one another (Suárez et al., 2012). These patterns extend broadly across the animal kingdom. In a study that surveyed chemosensory signals and their receptors in the olfactory system of mice, insects, and nematodes, Ihara et al. (2013) review the current understanding of signaling molecules where the information stream from receptor to specific behavior has been characterized. They find an overarching pattern wherein each organism has evolved a chemosensory system that ideally suits its lifestyle or environmental conditions. Given their focus on model organisms, these authors were able to examine the precise molecular mechanisms that underlie the linkage from signaling mechanisms to behaviors. Another study of *in vitro* responses in the ORs of mouse and human found a high fidelity of OR orthologs in primates and rodents, demonstrating that amino acid changes can have dramatic functional consequences that are a reflection of niche and other species-specific demands (Adipietro et al., 2012). For non-model organisms, however, the correspondence among environment, genome, and behavior must be approximate and correlative.

In most cases, conclusions about relative adaptive fit of OR and VR repertoires have been drawn from the molecular characterization of intact vs. pseudogene copies within receptor classes (e.g., Lane et al., 2002; Rodriguez et al., 2002; Pfister and Rodriguez, 2005; Shi et al., 2005; Young et al., 2005; Liman, 2006; Niimura and Nei, 2006; Grus et al., 2007; Young and Trask, 2007; Olender et al., 2008, 2012; Johnstone et al., 2009; Nikaido et al., 2013). Specifically, when there is a large proportion of intact vs. pseudogene copies, the inference is made that a particular mode of chemoreception is critically linked to the organism's lifestyle and is thus under strong positive selection. Conversely, when the receptors in question are found to have a disproportionately large number of pseudogene copies, investigators interpret this as evidence of relaxed selection and concomitant drift in nucleotide substitutions. As a classic example of such inference, Gilad et al. (2004) interpreted the deterioration of the OR repertoire in Old World monkeys and apes (including humans) to have a functional correspondence with the acquisition of trichromatic vision in these but not other primates. Similarly, Zhao et al. (2011) interpreted the deterioration of the VNS in bats to be related to the acquisition of their novel communication and foraging system (although based on a limited sample). Numerous studies have noted a connection between nocturnality and a high proportion of intact VR genes (e.g., Wang et al., 2010a,b) based upon the assumption that nocturnal habits will place strong selective pressures on the olfactory system in lieu of the visual system.

Expansion and contraction in gene family evolution is likely universal in eukaryotes. In a detailed study of gene family histories in yeast, Ames et al. (2014) observed differential rates of both phenomena among and between gene families and species, finding that both appear to be correlated with species-specific adaptations. Moreover, this study found that gene families with highly specific functions (as would be the case with chemosensation) repeatedly and independently expanded in multiple species, thus suggesting common underlying adaptive pressures. Within the human lineage, at least 2.7% of the genome has been uniquely duplicated since the human-chimp divergence, undoubtedly reflecting many of the unique adaptations of the human lifestyle. Similarly, gene loss has also been proposed as an adaptive response to changing environmental conditions or adaptive strategies (Olson, 1999) though contraction has been more typically assumed to reflect a relaxation of selective pressure (e.g., Liman and Innan, 2003; Mundy and Cook, 2003; Mundy, 2006; Zhao et al., 2011).

The effects of positive selection are more easily conceived for expansion via gene duplication with subsequent amino acid changes to the newly duplicated gene. As an example, positive selection may be exerted on regions of a receptor gene where that receptor manifests its ligand-binding functions. If the sequence change expands the repertoire of chemosensory signals that can be detected, it follows that this will be advantageous to the organism and these changes will be fixed by positive selection. One possible example of this phenomenon can be inferred from a recent empirical study of the V1R gene family in strepsirrhine primates (the lemurs and lorises). In that study, the authors discovered a remarkable expansion of V1R genes in the strepsirrhines relative to other primates, finding a gene subfamily putatively unique to the strepsirrhine clade and designated as V1R*strep* (Yoder et al., 2014). Moreover, phylogenetic analysis of V1R*strep* revealed that a relatively ancient (>40 mya) gene duplication occurred within the lemur clade, resulting in two V1R*strep* subclades referred to as α and β. Presumably, this pattern of initial expansion followed by gene duplication and further expansion has conferred a functional advantage to the lemurs, a finding that is congruent with experimental work that has shown that orthologs are far more likely to correspond to a common odor than will paralogs within the same gene family (Adipietro et al., 2012).

V1Rs WITHIN THE PRIMATES: ON THE VERGE OF A FUNCTIONAL BREAKDOWN

As with most mammals, the phylogenetic relationships among primate V1Rs do not closely follow those of the species that carry them. In other words, there is a significant mismatch between the V1R gene tree and the primate species tree. Both **Table 1** and **Figure 1** illustrate the phylogenetic patterns among all primate V1Rs mined from (predominantly) draft genomes available in Ensembl as of 2010 (Young et al., 2010). The figure on the left (A) illustrates the accepted primate species phylogeny whereas that on the right (B) illustrates the primate V1R gene tree. **Figure 1** establishes both that the ancestral primate genome carried at least six subfamilies of V1R alleles, and that the strepsirrhines (illustrated in shades of blue) have a substantially higher number of copies than do the haplorrhines (all other colors). The figure thus illustrates differential patterns of expansion and contraction in the V1R system during primate evolutionary history.

Changes in gene family copy number among species can evolve at rapid rates (e.g., Cutler et al., 2007; She et al., 2008). Indeed, comparisons among inbred strains of laboratory mice have revealed similar patterns within the V1R complex, further supporting the idea that rates of change can be very high for chemosensory genes (Wynn et al., 2012). It is noteworthy that one of the common "symptoms" of gene family extinction is a high rate of nonsynonymous substitution (Nielsen et al., 2005). As a specific case, Wynn et al. (2012) observed that 57% of total single-nucleotide polymorphisms (SNPs) in the VRs of mice are nonsynonymous substitutions for both wild populations and for inbred laboratory strains. The relationship between nonsynonymous and synonymous substitution rates has long been used as a measure for estimating the strength and directionality of selection (i.e., purifying vs. positive). Referred to as the dN/dS rate ratio, this measure has served as a reliable (though approximate) method in studies across virtually all of metazoan life (Yang, 1998; Vamathevan et al., 2008; Yang et al., 2009; Yang and dos Reis, 2011) and is applicable to primate VRs (Shi et al., 2005; Hohenbrink et al., 2012b; Yoder et al., 2014). One consequence of this positive selection engine is that the pairwise genetic

Table 1 | Number of total and intact V1Rs identified by Young et al. (2010) in primate species.

Species	Total V1Rs*	Intact V1Rs
Macaque	60	0
Gibbon	110	2
Gorilla	115	3
Human	116	3
Baboon	94	3
Chimpanzee	106	4
Orangutan	178	5
Marmoset	63	8
Tarsier	266	42
Bushbaby	133	78
Mouse lemur	259	214

**Values are median estimates (Young et al., 2010).*

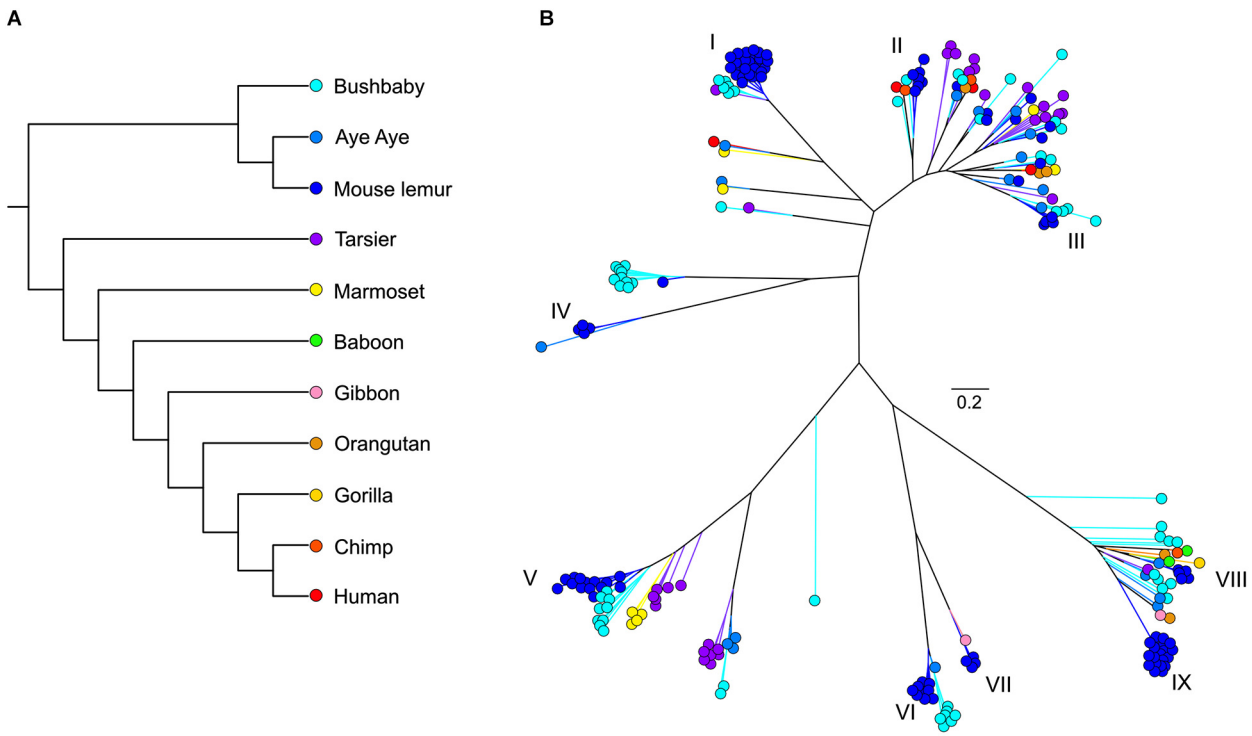

FIGURE 1 | (A) Phylogeny of primate species discussed herein. **(B)** Unrooted maximum likelihood tree generated from RAxML analyses of primate V1R amino acid sequences. Roman numerals identify mouse lemur V1R subfamilies described in Hohenbrink et al. (2012b).

distances among amino acids can be greater than their underlying nucleotide distances (e.g., see Table 1 in Yoder et al. (2014); whereas pairwise nucleotide distances tend to range up to a maximum of 13% in that study, those for amino acids can exceed 26%). It therefore stands to reason that these high rates of amino acid change must place VRs on the verge of functional collapse. Even the slightest relaxation of selective pressure can tip the balance towards pseudogenization and gene family contraction. In the words of Liman (2006, 2012) it is a "use it or lose it" system.

A survey of the number of intact copies among the primates appears to substantiate this hypothesis (**Figure 2**; **Table 1**). Whereas the two strepsirrhines (mouse lemur and bushbaby) for which draft genomes exist show a preponderance of intact copies, the converse is true for the haplorrhine primates surveyed. In some cases, the lack of intact copies is complete, as in the macque, which shows zero intact copies (**Table 1**). Notably, some of the haplorrhine primates show a high number of copies overall, though the vast majority are pseudogenes (e.g., orangutan). This overall pattern is both phylogenetically and anatomically correlated. The strepsirrhine/haplorrhine divergence occurred at least 60 mya (Yoder and Yang, 2000, 2004; Poux and Douzery, 2004; Wilkinson et al., 2011; Springer et al., 2012), and is also reflected in the very different anatomies of the olfactory apparatus in the two primate groups. Indeed, the word "strepsirrhine" refers to the sinuous or "comma-shaped" nostrils of lemurs and lorises while "haplorrhine" refers to the simple or "single-fold" nostrils of tarsiers, monkeys and apes.

THE EVOLUTIONARY FOOTPRINTS OF ANCESTORS AND THEIR DESCENDANTS

An intricate mix of phylogenetic footprints and current adaptive landscapes have left their mark on primate V1Rs suggesting that the primate clade offers an ideal model system for exploring the molecular evolutionary and functional properties of the VNS of mammals. The primate phylogeny is neatly divided into halves, with the haplorrhines on one side and the strepsirrhines on the other. And whereas the haplorrhines show anatomical and behavioral characteristics that reflect their reliance on vision over olfaction, the opposite is true of the strepsirrhines. Of all extant primates, the strepsirrhine primates are renowned for their

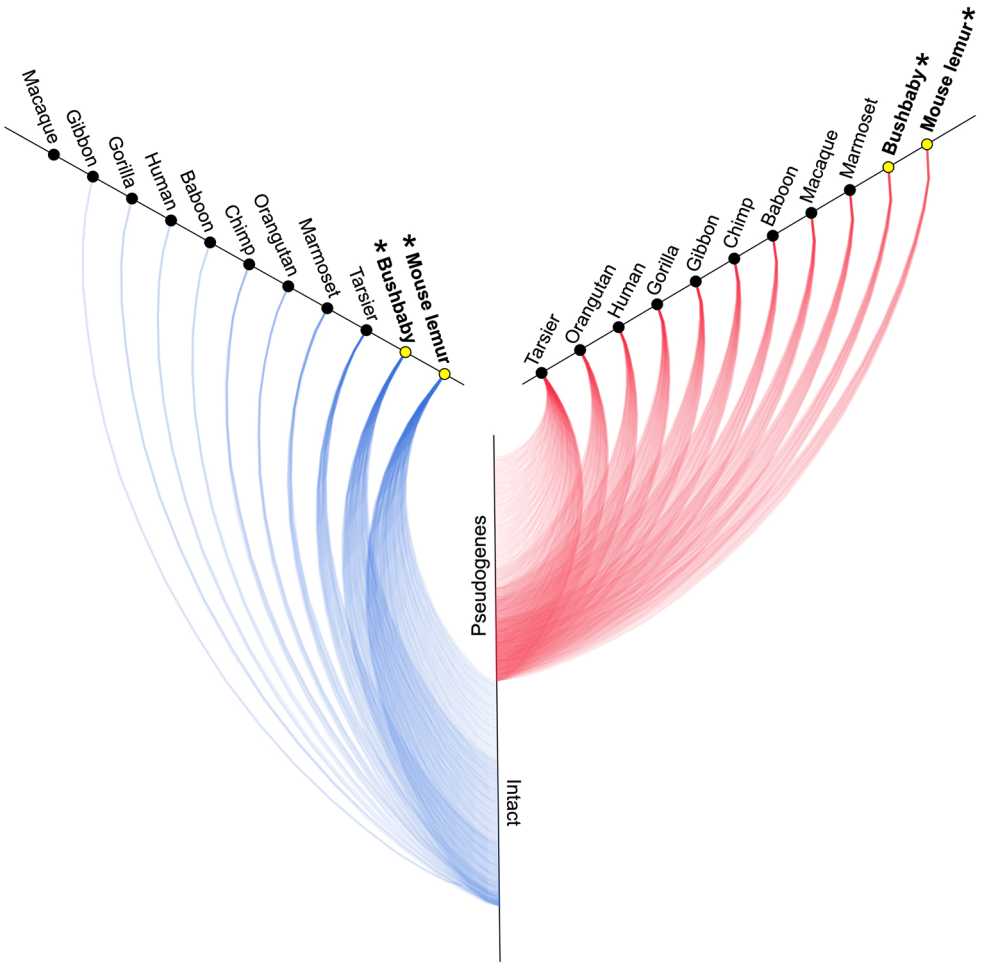

FIGURE 2 | Hive plot showing approximate number of intact (blue lines) and non-functional (red lines) V1R genes identified by Young et al. (2010) in primates (see Table 1). Asterisks and yellow circles identify strepsirrhine primates. See **Table 1** for exact counts of gene copies.

complex patterns of scent marking and other modes of olfactory communication (Schilling et al., 1990; Perret and Schilling, 1995; Perret, 1996, 2005; Kappeler, 1998; Perret et al., 2003; Suendermann et al., 2008; Boulet et al., 2010; Charpentier et al., 2010; Crawford et al., 2011; Delbarco-Trillo et al., 2011; Kappel et al., 2011; Rushmore et al., 2012). Moreover, all members of the Strepsirrhini retain the ancestral characteristic of a wet nose, typical of many mammals.

As might be predicted, haplorrhines show a V1R system that is notably diminished both in terms of copy number and in terms of intact vs. pseudogene copies with the converse being true of the strepsirrhines (**Figure 2**; **Table 1**). Though this functional anatomical division has often been attributed to a shift from a nocturnal lifestyle in the ancestral primate to a diurnal one in the vast majority of haplorrhine primates (excepting only the living tarsiers and the monotypic owl monkey, genus *Aotus*), causality is unlikely to be that simple. Not only are the circadian habits of the ancestral primate currently debated, the intensive study of V1Rs in strepsirrhine primates has revealed a system in which history (i.e., phylogeny) appears to trump present-day lifestyle. Namely, diurnal strepsirrhines were found to have V1R systems that are equally elaborate to those of nocturnal strepsirrhines (Yoder et al., 2014). It is here worth noting, however, that our survey of primate V1Rs as illustrated in **Figure 2** and **Table 1** depend in large part on, and by necessity, on bioinformatic mining from draft genomes (Young et al., 2010). When more targeted sequencing approaches are implemented, we find that allele counts in draft genomes may be dramatically underestimated (Larsen et al., 2014; **Figure 3**). These findings are consistent with those from other mammalian groups. For example, Wynn et al. (2012) expanded the number of known mouse VR alleles by more than nine fold by employing massively parallel sequencing methods for VR genomic characterization. Even so, these authors noted that even though these methods were capable of accurately resolving more than half of mouse VRs, they also concluded that copy number variation and non-specific short read mapping compromise complete repertoire analysis. Clearly, much remains to be learned about the genomic characterization of VRs in primates and other mammals.

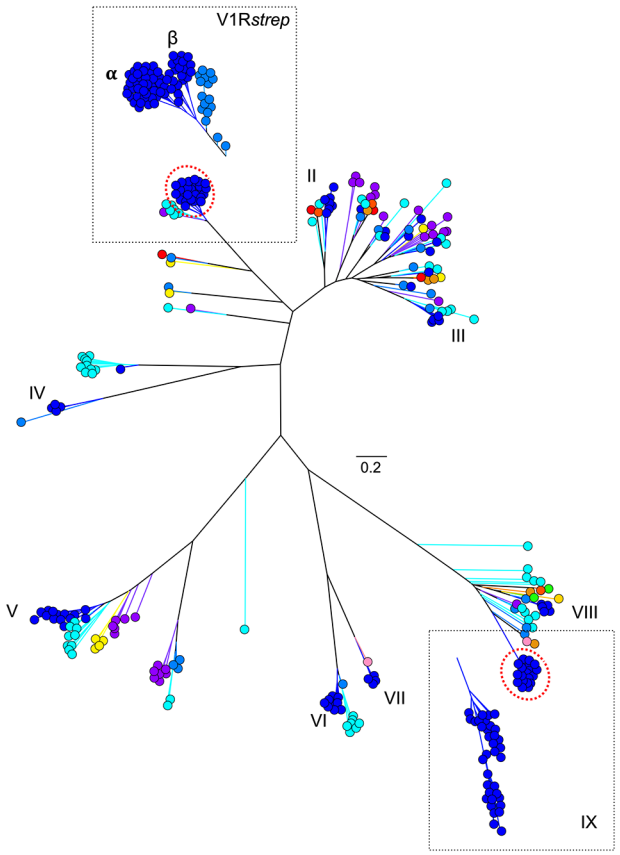

FIGURE 3 | Maximum likelihood tree (Figure 1B) with addition of novel V1R gene amino acid sequences identified from two V1R subfamilies by Yoder et al. (2014) and Larsen et al. (2014). Collectively, these analyses suggest the V1R*strep* and V1RIX repertoires within mouse lemur may be underestimated by approximately 25%. Refer to **Figure 1A** for color references.

CONCLUSIONS

In this review, we have synthesized information regarding gene family evolution across a broad phylogenetic expanse, spanning yeast to humans. Specifically, we have focused on the molecular-evolutionary dynamics of V1R genes in primates. As a result of these comparisons, we conclude that mammalian V1Rs are under extreme pressures for rapid evolution, both at the nucleotide and the amino acid levels. Moreover, these genes have been hypothesized to experience strong positive selection to maintain a diverse repertoire of functional copies when fine-scale and precise pheromonal communication is fundamental to species survival (e.g., predation) and/or propagation (e.g., mating behaviors). Alternatively, when other sensory systems such as vision are more dominant, positive selection is relaxed and the proportion of functional copies rapidly deteriorates, putatively due to the high rates of nonsynonymous substitution at the nucleotide level.

The distribution of intact to pseudogene copies in primates appears to bear out these assumptions. Whereas haplorrhine primates with their anatomically diminished olfactory systems show very few intact V1Rs, strepsirrhines with their ancestrally-retained and highly-developed olfactory anatomy show very large repertoires of intact V1Rs. Admittedly, limitations in available genomic resources for primates constrain our ability to draw definitive conclusions. In the near future, however, advancements in DNA sequencing technology (e.g., Pacific Biosciences *RS II*) will contribute to more robust primate genome assemblies (Chaisson et al., 2014) and, in turn, will provide more precise measures of gene family diversity, including V1Rs. In the meantime, we contend that the conservative nature of VR copy number estimates and the estimated ratios of intact to pseudogene copies yield patterns that will withstand further scrutiny with enhanced data. Primate V1Rs will likely persist in telling a story of ancestral function and divergent selection as species and clades have moved into ever diversifying adaptive regimes. The sensitivity to functional collapse in these genes, consequent to their precariously high rates of nonsynonymous substitution, confer a remarkable capacity to reveal the lifestyles of the genomes that they presently occupy as well as those of their ancestors.

ACKNOWLEDGMENTS

We thank Guest Associate Editors Pablo Chamero and Ignacio Salazar for their invitation to contribute to this special volume on the morphology, genetics and evolution of the mammalian olfactory subsystem. The manuscript was significantly improved thanks to comments from H. Matsunami and from two anonymous reviewers. Anne D. Yoder was supported by a travel grant from Burroughs Welcome during the preparation of this work.

REFERENCES

Adipietro, K. A., Mainland, J. D., and Matsunami, H. (2012). Functional evolution of mammalian odorant receptors. *PLoS Genet.* 8:e1002821. doi: 10.1371/journal.pgen.1002821

Ames, R. M., Money, D., and Lovell, S. C. (2014). Inferring gene family histories in yeast identifies lineage specific expansions. *PLoS One* 9:e99480. doi: 10.1371/journal.pone.0099480

Boulet, M., Crawford, J. C., Charpentier, M. J. E., and Drea, C. M. (2010). Honest olfactory ornamentation in a female-dominant primate. *J. Evol. Biol.* 23, 1558–1563. doi: 10.1111/j.1420-9101.2010.02007.x

Brykczynska, U., Tzika, A. C., Rodriguez, I., and Milinkovitch, M. C. (2013). Contrasted evolution of the vomeronasal receptor repertoires in mammals and squamate reptiles. *Genome Biol. Evol.* 5, 389–401. doi: 10.1093/gbe/evt013

Chaisson, M. J. P., Huddleston, J., Dennis, M. Y., Sudmant, P. H., Malig, M., Hormozdiari, F., et al. (2014). Resolving the complexity of the human genome using single-molecule sequencing. *Nature* doi: 10.1038/nature13907. [Epub ahead of print].

Chamero, P., Katsoulidou, V., Hendrix, P., Bufe, B., Roberts, R., Matsunami, H., et al. (2011). G protein G(alpha)o is essential for vomeronasal function and aggressive behavior in mice. *Proc. Natl. Acad. Sci. U S A* 108, 12898–12903. doi: 10.1073/pnas.1107770108

Chamero, P., Leinders-Zufall, T., and Zufall, F. (2012). From genes to social communication: molecular sensing by the vomeronasal organ. *Trends Neurosci.* 35, 597–606. doi: 10.1016/j.tins.2012.04.011

Charpentier, M. J. E., Crawford, J. C., Boulet, M., and Drea, C. M. (2010). Message 'scent': lemurs detect the genetic relatedness and quality of conspecifics via olfactory cues. *Anim. Behav.* 80, 101–108. doi: 10.1016/j.anbehav.2010.04.005

Crawford, J. C., Boulet, M., and Drea, C. M. (2011). Smelling wrong: hormonal contraception in lemurs alters critical female odour cues. *Proc. Biol. Sci.* 278, 122–130. doi: 10.1098/rspb.2010.1203

Cutler, G., Marshall, L. A., Chin, N., Baribault, H., and Kassner, P. D. (2007). Significant gene content variation characterizes the genomes of inbred mouse strains. *Genome Res.* 17, 1743–1754. doi: 10.1101/gr.6754607

Delbarco-Trillo, J., Burkert, B. A., Goodwin, T. E., and Drea, C. M. (2011). Night and day: the comparative study of strepsirrhine primates reveals socioecological and phylogenetic patterns in olfactory signals. *J. Evol. Biol.* 24, 82–98. doi: 10.1111/j.1420-9101.2010.02145.x

Del Punta, K., Leinders-Zufall, T., Rodriguez, I., Jukam, D., Wysocki, C. J., Ogawa, S., et al. (2002). Deficient pheromone responses in mice lacking a cluster of vomeronasal receptor genes. *Nature* 419, 70–74. doi: 10.1038/nature00955

Demuth, J. P., De Bie, T., Stajich, J. E., Cristianini, N., and Hahn, M. W. (2006). The evolution of mammalian gene families. *PLoS One* 1:e85. doi: 10.1371/journal.pone.0000085

D'Oliveira Albanus, R., Siqueira Dalmolin, R. J., Rybarczyk-Filho, J. L., Alves Castro, M. A., and Fonseca Moreira, J. C. (2014). Differential evolutionary constriants in the evolution of chemoreceptors: a murine and human case study. *ScientificWorldJournal* 2014:696485. doi: 10.1155/2014/696485

Dong, D., He, G., Zhang, S., and Zhang, Z. (2009). Evolution of olfactory receptor genes in primates dominated by birth-and-death process. *Genome Biol. Evol.* 1, 258–264. doi: 10.1093/gbe/evp026

Garrett, E. C., and Steiper, M. E. (2014). Strong links between genomic and anatomical diversity in both mammalian olfactory chemosensory systems. *Proc. Biol. Sci.* 281:20132828. doi: 10.1098/rspb.2013.2828

Gilad, Y., Wiebe, V., Przeworski, M., Lancet, D., and Pääbo, S. (2004). Loss of olfactory receptor genes coincides with the acquisition of full trichromatic vision in primates. *PLoS Biol.* 2:e5. doi: 10.1371/journal.pbio.0020005

Gilad, Y., Wiebe, V., Przeworski, M., Lancet, D., and Pääbo, S. (2007). Correction: loss of olfactory receptor genes coincides with the acquisition of full trichromatic vision in primates. *PLoS Biol.* 5:e148. doi: 10.1371/journal.pbio.0050148

Giorgi, D., Friedman, C., Trask, B. J., and Rouquier, S. (2000). Characterization of nonfunctional V1R-like pheromone receptor sequences in human. *Genome Res.* 10, 1979–1985. doi: 10.1101/gr.10.12.1979

Giorgi, D., and Rouquier, S. (2002). Identification of V1R-like putative pheromone receptor sequences in non-human primates. Characterization of V1R pseudogenes in marmoset, a primate species that possesses an intact vomeronasal organ. *Chem. Senses* 27, 529–537. doi: 10.1093/chemse/27.6.529

Gomez-Diaz, C., and Benton, R. (2013). The joy of sex pheromones. *EMBO Rep.* 14, 874–883. doi: 10.1038/embor.2013.140

Grus, W. E., Shi, P., and Zhang, J. (2007). Largest vertebrate vomeronasal type 1 receptor gene repertoire in the semiaquatic platypus. *Mol. Biol. Evol.* 24, 2153–2157. doi: 10.1093/molbev/msm157

Grus, W. E., Shi, P., Zhang, Y. P., and Zhang, J. (2005). Dramatic variation of the vomeronasal pheromone receptor gene repertoire among five orders of placental and marsupial mammals. *Proc. Natl. Acad. Sci. U S A* 102, 5767–5772. doi: 10.1073/pnas.0501589102

Grus, W. E., and Zhang, J. (2004). Rapid turnover and species-specificity of vomeronasal pheromone receptor genes in mice and rats. *Gene* 340, 303–312. doi: 10.1016/j.gene.2004.07.037

Grus, W. E., and Zhang, J. Z. (2008). Distinct evolutionary patterns between chemoreceptors of 2 vertebrate olfactory systems and the differential tuning hypothesis. *Mol. Biol. Evol.* 25, 1593–1601. doi: 10.1093/molbev/msn107

Haga, S., Hattori, T., Sato, T., Sato, K., Matsuda, S., Kobayakawa, R., et al. (2010). The male mouse pheromone ESP1 enhances female sexual receptive behaviour through a specific vomeronasal receptor. *Nature* 466, 118–122. doi: 10.1038/nature09142

Haga-Yamanaka, S., Ma, L., He, J., Qiu, Q., Lavis, L. D., Looger, L. L., et al. (2014). Integrated action of pheromone signals in promoting courtship behavior in male mice. *Elife* 3:e03025. doi: 10.7554/elife.03025

Herberger, A. L., and Loretz, C. A. (2013). Vertebrate extracellular calcium-sensing receptor evolution: selection in relation to life history and habitat. *Comp. Biochem. Physiol. Part D Genomics Proteomics* 8, 86–94. doi: 10.1016/j.cbd.2012.12.004

Heymann, E. W. (2006). The neglected sense-olfaction in primate behavior, ecology and evolution. *Am. J. Primatol.* 68, 519–524. doi: 10.1002/ajp.20249

Hohenbrink, P., Dempewolf, S., Zimmermann, E., Mundy, N. I., and Radespiel, U. (2014). Functional promiscuity in a mammalian chemosensory system: extensive expression of vomeronasal receptors in the main olfactory epithelium of mouse lemurs. *Front. Neuroanat.* 8:102. doi: 10.3389/fnana.2014.00102

Hohenbrink, P., Mundy, N. I., Zimmermann, E., and Radespiel, U. (2012a). First evidence for functional vomeronasal 2 receptor genes in primates. *Biol. Lett.* 9:20121006. doi: 10.1098/rsbl.2012.1006

Hohenbrink, P., Radespiel, U., and Mundy, N. I. (2012b). Pervasive and ongoing positive selection in the vomeronasal-1 receptor (V1R) repertoire of mouse lemurs. *Mol. Biol. Evol.* 29, 3807–3816. doi: 10.1093/molbev/mss188

Ibarra-Soria, X., Levitin, M. O., and Logan, D. W. (2014). The genomic basis of vomeronasal-mediated behaviour. *Mamm. Genome* 25, 75–86. doi: 10.1007/s00335-013-9463-1

Ihara, S., Yoshikawa, K., and Touhara, K. (2013). Chemosensory signals and their receptors in the olfactory neural system. *Neuroscience* 254, 45–60. doi: 10.1016/j.neuroscience.2013.08.063

Insel, T. R. (2010). The challenge of translation in social neuroscience: a review of oxytocin, vasopressin and affiliative behavior. *Neuron* 65, 768–779. doi: 10.1016/j.neuron.2010.03.005

Isogai, Y., Si, S., Pont-Lezica, L., Tan, T., Kapoor, V., Murthy, V. N., et al. (2011). Molecular organization of vomeronasal chemoreception. *Nature* 478, 241–245. doi: 10.1038/nature10437

Johnstone, K. A., Ciborowski, K. L., Lubieniecki, K. P., Chow, W., Phillips, R. B., Koop, B. F., et al. (2009). Genomic organization and evolution of the vomeronasal type 2 receptor-like (OlfC) gene clusters in Atlantic salmon, Salmo salar. *Mol. Biol. Evol.* 26, 1117–1125. doi: 10.1093/molbev/msp027

Kappel, P., Hohenbrink, S., and Radespiel, U. (2011). Experimental evidence for olfactory predator recognition in wild mouse lemurs. *Am. J. Primatol.* 73, 928–938. doi: 10.1002/ajp.20963

Kappeler, P. M. (1998). To whom it may concern: the transmission and function of chemical signals in lemur catta. *Behav. Ecol. Sociobiol.* 42, 411–421. doi: 10.1007/s002650050455

Korsching, S. (2009). The molecular evolution of teleost olfactory receptor gene families. *Results Probl. Cell Differ.* 47, 37–55. doi: 10.1007/400_2008_11

Kouros-Mehr, H., Pintchovski, S., Melnyk, J., Chen, Y. J., Friedman, C., Trask, B., et al. (2001). Identification of non-functional human VNO receptor genes provides evidence for vestigiality of the human VNO. *Chem. Senses* 26, 1167–1174. doi: 10.1093/chemse/26.9.1167

Lane, R. P., Cutforth, T., Axel, R., Hood, L., and Trask, B. J. (2002). Sequence analysis of mouse vomeronasal receptor gene clusters reveals common promoter motifs and a history of recent expansion. *Proc. Natl. Acad. Sci. U S A* 99, 291–296. doi: 10.1073/pnas.012608399

Larsen, P. A., Heilman, A. M., and Yoder, A. D. (2014). The utility of PacBio circular consensus sequencing for characterizing complex gene families in non-model organisms. *BMC Genomics* 15:720. doi: 10.1186/1471-2164-15-720

Leinders-Zufall, T., Ishii, T., Mombaerts, P., Zufall, F., and Boehm, T. (2009). Structural requirements for the activation of vomeronasal sensory neurons by MHC peptides. *Nat. Neurosci.* 12, 1551–1558. doi: 10.1038/nn.2452

Leinders-Zufall, T., Lane, A. P., Puche, A. C., Ma, W., Novotny, M. V., Shipley, M. T., et al. (2000). Ultrasensitive pheromone detection by mammalian vomeronasal neurons. *Nature* 405, 792–796. doi: 10.1038/35015572

Liberles, S. D. (2014). Mammalian pheromones. *Annu. Rev. Physiol.* 76, 151–175. doi: 10.1146/annurev-physiol-021113-170334

Liman, E. R. (2006). Use it or lose it: molecular evolution of sensory signaling in primates. *Pflugers Arch.* 453, 125–131. doi: 10.1007/s00424-006-0120-3

Liman, E. R. (2012). Changing senses: chemosensory signaling and primate evolution. *Adv. Exp. Med. Biol.* 739, 206–217. doi: 10.1007/978-1-4614-1704-0_13

Liman, E. R., and Innan, H. (2003). Relaxed selective pressure on an essential component of pheromone transduction in primate evolution. *Proc. Natl. Acad. Sci. U S A* 100, 3328–3332. doi: 10.1073/pnas.0636123100

Luca, F., Perry, G. H., and Di Rienzo, A. (2010). Evolutionary adaptations to dietary changes. *Annu. Rev. Nutr.* 30, 291–314. doi: 10.1146/annurev-nutr-080508-141048

Mandiyan, V. S., Coats, J. K., and Shah, N. M. (2005). Deficits in sexual and aggressive behaviors in Cnga2 mutant mice. *Nat. Neurosci.* 8, 1660–1662. doi: 10.1038/nn1589

Matsui, A., Go, Y., and Niimura, Y. (2010). Degeneration of olfactory receptor gene repertoires in primates: no direct link to full trichromatic vision. *Mol. Biol. Evol.* 27, 1192–1200. doi: 10.1093/molbev/msq003

Mundy, N. I. (2006). Genetic basis of olfactory communication in primates. *Am. J. Primatol.* 68, 559–567. doi: 10.1002/ajp.20252

Mundy, N. I., and Cook, S. (2003). Positive selection during the diversification of class I vomeronasal receptor-like (V1RL) genes, putative pheromone receptor genes, in human and primate evolution. *Mol. Biol. Evol.* 20, 1805–1810. doi: 10.1093/molbev/msg192

Nielsen, R., Bustamante, C., Clark, A. G., Glanowski, S., Sackton, T. B., Hubisz, M. J., et al. (2005). A scan for positively selected genes in the genomes of humans and chimpanzees. *PLoS Biol.* 3:e170. doi: 10.1371/journal.pbio.0030170

Niimura, Y., and Nei, M. (2006). Evolutionary dynamics of olfactory and other chemosensory receptor genes in vertebrates. *J. Hum. Genet.* 51, 505–517. doi: 10.1007/s10038-006-0391-8

Nikaido, M., Suzuki, H., Toyoda, A., Fujiyama, A., Hagino-Yamagishi, K., Kocher, T. D., et al. (2013). Lineage-specific expansion of vomeronasal type 2 receptor-like (OlfC) genes in cichlids may contribute to diversification of amino acid detection systems. *Genome Biol. Evol.* 5, 711–722. doi: 10.1093/gbe/evt041

Nodari, F., Hsu, F. F., Fu, X., Holekamp, T. F., Kao, L. F., Turk, J., et al. (2008). Sulfated steroids as natural ligands of mouse pheromone-sensing neurons. *J. Neurosci.* 28, 6407–6418. doi: 10.1523/JNEUROSCI.1425-08.2008

Olender, T., Lancet, D., and Nebert, D. W. (2008). Update on the olfactory receptor (OR) gene superfamily. *Hum. Genomics* 3, 87–97. doi: 10.1186/1479-7364-3-1-87

Olender, T., Waszak, S. M., Viavant, M., Khen, M., Ben-Asher, E., Reyes, A., et al. (2012). Personal receptor repertoires: olfaction as a model. *BMC Genomics* 13:414. doi: 10.1186/1471-2164-13-414

Olson, M. V. (1999). When less is more: gene loss as an engine of evolutionary change. *Am. J. Hum. Genet.* 64, 18–23. doi: 10.1086/302219

Pantages, E., and Dulac, C. (2000). A novel family of candidate pheromone receptors in mammals. *Neuron* 28, 835–845. doi: 10.1016/s0896-6273(00)00157-4

Park, S. H., Podlaha, O., Grus, W. E., and Zhang, J. (2011). The microevolution of V1r vomeronasal receptor genes in mice. *Genome Biol. Evol.* 3, 401–412. doi: 10.1093/gbe/evr039

Perret, M. (1996). Manipulation of sex ratio at birth by urinary cues in a prosimian primate. *Behav. Ecol. Sociobiol.* 38, 259–266. doi: 10.1007/s002650050241

Perret, M. (2005). Relationship between urinary estrogen levels before conception and sex ratio at birth in a primate, the gray mouse lemur. *Hum. Reprod.* 20, 1504–1510. doi: 10.1093/humrep/deh802

Perret, M., Aujard, F., Séguy, M., and Schilling, A. (2003). Olfactory bulbectomy modifies photic entrainment and circadian rhythms of body temperature and locomotor activity in a nocturnal primate. *J. Biol. Rhythms* 18, 392–401. doi: 10.1177/0748730403254248

Perret, M., and Schilling, A. (1995). Sexual responses to urinary chemosignals depend on photoperiod in a male primate. *Physiol. Behav.* 58, 633–639. doi: 10.1016/0031-9384(95)00112-v

Petrulis, A. (2013a). Chemosignals and hormones in the neural control of mammalian sexual behavior. *Front. Neuroendocrinol.* 34, 255–267. doi: 10.1016/j.yfrne.2013.07.007

Petrulis, A. (2013b). Chemosignals, hormones and mammalian reproduction. *Horm. Behav.* 63, 723–741. doi: 10.1016/j.yhbeh.2013.03.011

Pfister, P., and Rodriguez, I. (2005). Olfactory expression of a single and highly variable V1r pheromone receptor-like gene in fish species. *Proc. Natl. Acad. Sci. U S A* 102, 5489–5494. doi: 10.1073/pnas.0402581102

Poux, C., and Douzery, E. J. (2004). Primate phylogeny, evolutionary rate variations and divergence times: a contribution from the nuclear gene IRBP. *Am. J. Phys. Anthropol.* 124, 1–16. doi: 10.1002/ajpa.10322

Rodriguez, I., Del Punta, K., Rothman, A., Ishii, T., and Mombaerts, P. (2002). Multiple new and isolated families within the mouse superfamily of V1r vomeronasal receptors. *Nat. Neurosci.* 5, 134–140. doi: 10.1038/nn795

Rodriguez, I., Greer, C. A., Mok, M. Y., and Mombaerts, P. (2000). A putative pheromone receptor gene expressed in human olfactory mucosa. *Nat. Genet.* 26, 18–19. doi: 10.1038/79124

Rushmore, J., Leonhardt, S. D., and Drea, C. M. (2012). Sight or scent: lemur sensory reliance in detecting food quality varies with feeding ecology. *PLoS One* 7:e41558. doi: 10.1371/journal.pone.0041558

Sánchez-Andrade, G., and Logan, D. W. (2014). Deconstructing pheromone-mediated behavior one layer at a time. *BMC Biol.* 12:33. doi: 10.1186/1741-7007-12-33

Schilling, A., Serviere, J., Gendrot, G., and Perret, M. (1990). Vomeronasal activation by urine in the primate *Microcebus murinus*: a 2 DG study. *Exp. Brain Res.* 81, 609–618. doi: 10.1007/bf02423511

She, X., Cheng, Z., Zöllner, S., Church, D. M., and Eichler, E. E. (2008). Mouse segmental duplication and copy number variation. *Nat. Genet.* 40, 909–914. doi: 10.1038/ng.172

Shi, P., Bielawski, J. P., Yang, H., and Zhang, Y. P. (2005). Adaptive diversification of vomeronasal receptor 1 genes in rodents. *J. Mol. Evol.* 60, 566–576. doi: 10.1007/s00239-004-0172-y

Springer, M. S., Meredith, R. W., Gatesy, J., Emerling, C. A., Park, J., Rabosky, D. L., et al. (2012). Macroevolutionary dynamics and historical biogeogrphy of primate diversification inferred from a species supermatrix. *PLoS One* 7:e49521. doi: 10.1371/journal.pone.0049521

Suárez, R., García-González, D., and de Castro, F. (2012). Mutual influences between the main olfactory and vomeronasal systems in development and evolution. *Front. Neuroanat.* 6:50. doi: 10.3389/fnana.2012.00050

Suendermann, D., Scheumann, M., and Zimmermann, E. (2008). Olfactory predator recognition in predator-naive gray mouse lemurs *(Microcebus murinus)*. *J. Comp. Psychol.* 122, 146–155. doi: 10.1037/0735-7036.122.2.146

Vamathevan, J. J., Hasan, S., Emes, R. D., Amrine-Madsen, H., Rajagopalan, D., Topp, S. D., et al. (2008). The role of positive selection in determining the molecular cause of species differences in disease. *BMC Evol. Biol.* 8:273. doi: 10.1186/1471-2148-8-273

Venkatakrishnan, A. J., Deupi, X., Lebon, G., Tate, C. G., Schertler, G. F., and Babu, M. M. (2013). Molecular signatures of G-protein-coupled receptors. *Nature* 494, 185–194. doi: 10.1038/nature11896

Verrelli, B. C., Lewis, C. M., Stone, A. C., and Perry, G. H. (2008). Different selective pressures shape the molecular evolution of color vision in chimpanzee and human populations. *Mol. Biol. Evol.* 25, 2735–2743. doi: 10.1093/molbev/msn220

Wang, G. D., Shi, P., Zhu, Z. H., and Zhang, Y. P. (2010a). More functional V1R genes occur in nest-living and nocturnal terricolous mammals. *Genome Biol. Evol.* 2, 277–283. doi: 10.1093/gbe/evq020

Wang, G. D., Zhu, Z. H., Shi, P., and Zhang, Y. P. (2010b). Comparative genomic analysis reveals more functional nasal chemoreceptors in nocturnal mammals than in diurnal mammals. *Chinese Sci. Bull.* 55, 3901–3910. doi: 10.1007/s11434-010-4202-4

Wilkinson, R. D., Steiper, M. E., Soligo, C., Martin, R. D., Yang, Z., and Tavaré, S. (2011). Dating primate divergences through an integrated analysis of palaeontological and molecular data. *Syst. Biol.* 60, 16–31. doi: 10.1093/sysbio/syq054

Wynn, E. H., Sanchez-Andrade, G., Carss, K. J., and Logan, D. W. (2012). Genomic variation in the vomeronasal receptor gene repertoires of inbred mice. *BMC Genomics* 13:415. doi: 10.1186/1471-2164-13-415

Yang, Z. (1998). Likelihood ratio tests for detecting positive selection and application to primate lysozyme evolution. *Mol. Biol. Evol.* 15, 568–573. doi: 10.1093/oxfordjournals.molbev.a025957

Yang, Z., and dos Reis, M. (2011). Statistical properties of the branch-site test of positive selection. *Mol. Biol. Evol.* 28, 1217–1228. doi: 10.1093/molbev/msq303

Yang, Z., Nielsen, R., and Goldman, N. (2009). In defense of statistical methods for detecting positive selection. *Proc. Natl. Acad. Sci. U S A* 106:E95. doi: 10.1073/pnas.0904550106

Yoder, A. D., Chan, L. M., dos Reis, M., Larsen, P. A., Campbell, C. R., Rasoloarison, R., et al. (2014). Molecular evolutionary characterization of a V1R subfamily unique to Strepsirrhine primates. *Genome Biol. Evol.* 6, 213–227. doi: 10.1093/gbe/evu006

Yoder, A. D., and Yang, Z. H. (2000). Estimation of primate speciation dates using local molecular clocks. *Mol. Biol. Evol.* 17, 1081–1090. doi: 10.1093/oxfordjournals.molbev.a026389

Yoder, A. D., and Yang, Z. (2004). Divergence dates for Malagasy lemurs estimated from multiple gene loci: geological and evolutionary context. *Mol. Ecol.* 13, 757–773. doi: 10.1046/j.1365-294x.2004.02106.x

Young, J. M., Kambere, M., Trask, B. J., and Lane, R. P. (2005). Divergent V1R repertoires in five species: amplification in rodents, decimation in primates and a surprisingly small repertoire in dogs. *Genome Res.* 15, 231–240. doi: 10.1101/gr.3339905

Young, J. M., Massa, H. F., Hsu, L., and Trask, B. J. (2010). Extreme variability among mammalian V1R gene families. *Genome Res.* 20, 10–18. doi: 10.1101/gr.098913.109

Young, J. M., and Trask, B. J. (2007). V2R gene families degenerated in primates, dog and cow, but expanded in opossum. *Trends Genet.* 23, 212–215. doi: 10.1016/j.tig.2007.03.004

Zhao, H., Xu, D., Zhang, S., and Zhang, J. (2011). Widespread losses of vomeronasal signal transduction in bats. *Mol. Biol. Evol.* 28, 7–12. doi: 10.1093/molbev/msq207

Conflict of Interest Statement: The authors declare that the research was conducted in the absence of any commercial or financial relationships that could be construed as a potential conflict of interest.

Received: 16 October 2014; accepted: 25 November 2014; published online: 12 December 2014.

Citation: Yoder AD and Larsen PA (2014) The molecular evolutionary dynamics of the vomeronasal receptor (class 1) genes in primates: a gene family on the verge of a functional breakdown. Front. Neuroanat. ***8****:153. doi: 10.3389/fnana.2014.00153*

This article was submitted to the journal Frontiers in Neuroanatomy.